PB-231 265

HYPOLIMNION AERATION WITH COMMERCIAL OXYGEN. VOLUME I. DYNAMICS OF BUBBLE PLUME

R. E. Speece, et al

Texas University

Prepared for:

Environmental Protection Agency

December 1973

DISTRIBUTED BY:

NTIS

National Technical Information Service
U. S. DEPARTMENT OF COMMERCE
5285 Port Royal Road, Springfield Va. 22151

PB 231 265

SELECTED WATER RESOURCES ABSTRACTS
INPUT TRANSACTION FORM

1. Report No.

W 74-06525

5. Report Date

6.

8. Performing Organization Report No.

Hypolimnion Aeration with Commercial Oxygen -
Vol. I - Dynamics of Bubble Plume,

Speece, R.E.; Rayyan, F; Murfee, G.

Texas University,
~~The University of Texas at Austin~~
Austin, ~~Texas 78712~~

EPA Project
16080 FYW

13. Type of Report and Period Covered

12. Sponsoring Organization

Environmental Protection Agency, Technology Series report ~~number~~
EPA-660/2-73-025a, December 1973. 184p, 86 fig, 7 tab, 47 ref

This study deals with a proposed scheme for restoration and maintenance of dissolved oxygen in the hypolimnion of stratified impoundments without disturbing the stratification. Commercial oxygen is an economical alternative to air as an oxygen source for hypolimnion aeration. In addition, it possesses many other advantages, the main one being avoidance of nitrogen gas supersaturation and its related toxicity to fish.

Laboratory and lake studies were conducted to demonstrate the gas transfer dynamics of a bubble plume generated by the injection of pure oxygen bubbles within the hypolimnion. The experimental results verified the practicality of the original concept - hypolimnion aeration which preserves stratification. Efficient oxygen absorption was achieved within the hypolimnion.

Mathematical models were formulated and calibrated by experimental data. The calibrated model was then used to predict the oxygen transfer and hydrodynamic characteristics of the bubble plume for various oxygen injection rates and injection depths. The sensitivity of the model to the various input parameters was shown. (EPA)

(See also W74-06526)

17a. Descriptors

Water Quality, ~~Modeling,~~ *Hypolimnion, *Aeration, Stratification, Water Quality Control, *Texas, *Oxygenation, *Bubbles, Model studies, Dissolved oxygen, ~~Stratification,~~ Absorption

17b. Identifiers

*Lake Travis (Tex.), Bubble plumes

05D, 05G

ia

Copy Available from GPO Sup Doc, as EP1.23:660/2-73-025a, $2.05; microfiche from NTIS as PB $1.45

Reproduced by
NATIONAL TECHNICAL
INFORMATION SERVICE
U S Department of Commerce
Springfield VA 22151

19. Security Class. (Report)

20. Security Class. (Page)

21. No. of Pages

22. Price

Send To:
WATER RESOURCES SCIENTIFIC INFORMATION CENTER
U S DEPARTMENT OF THE INTERIOR
WASHINGTON D C 20240

R. E. Speece	The University of Texas at Austin

RESEARCH REPORTING SERIES

Research reports of the Office of Research and Monitoring, Environmental Protection Agency, have been grouped into five series. These five broad categories were established to facilitate further development and application of environmental technology. Elimination of traditional grouping was consciously planned to foster technology transfer and a maximum interface in related fields. The five series are:

1. Environmental Health Effects Research
2. Environmental Protection Technology
3. Ecological Research
4. Environmental Monitoring
5. Socioeconomic Environmental Studies

This report has been assigned to the ENVIRONMENTAL PROTECTION TECHNOLOGY series. This series describes research performed to develop and demonstrate instrumentation, equipment and methodology to repair or prevent environmental degradation from point and non-point sources of pollution. This work provides the new or improved technology required for the control and treatment of pollution sources to meet environmental quality standards.

EPA-660/2-73-025a
December 1973

HYPOLIMNION AERATION
WITH
COMMERCIAL OXYGEN

VOLUME I
DYNAMICS OF BUBBLE PLUME

By

R. E. Speece
Fawzi Rayyan
The University of Texas at Austin

Project 16080 FYW
Program Element 1B2045

Project Officer

Lowell E. Leach
Robert S. Kerr Environmental Research Laboratory
Ada, Oklahoma 74820

Prepared for
OFFICE OF RESEARCH AND DEVELOPMENT
U.S. ENVIRONMENTAL PROTECTION AGENCY
WASHINGTON, D.C. 20460

ic

For sale by the Superintendent of Documents, U.S. Government Printing Office, Washington, D.C. 20402 - Price $2

EPA Review Notice

This report has been reviewed by the Environmental Protection Agency and approved for publication. Approval does not signify that the contents necessarily reflect views and policies of the Environmental Protection Agency, nor does mention of trade names or commercial products constitute endorsement or recommendation for use.

ABSTRACT

The characteristics of a bubble-water plume, as used in hypolimnion aeration, were studied. The major factor introduced in the study of these characteristics was the effect of mass transfer.

A mathematical model was developed for this case and compared with a mathematical model which neglects the effect of mass transfer. Both the case of slip velocity and zero slip velocity were considered and a comparison is presented. The model calculates the diameter of the bubble, the diameter of the plume, the velocity of plume rise, the water flow rate, and the momentum and energy flux for the rising plume at any level above the diffuser. It also calculates the amount of oxygen absorbed at any level and the increase of the dissolved oxygen concentration in the plume for any oxygen flow rate.

The model was verified by field measurements. A description of the field experiment and the techniques used are presented.

This report was submitted in fulfillment of Project Number 16080 FYW under the partial sponsorship of the Office of Research and Monitoring, Environmental Protection Agency.

CONTENTS

Section		Page
I	CONCLUSIONS	1
II	RECOMMENDATIONS	3
III	INTRODUCTION	5
IV	OBJECTIVE AND SCOPE	9
V	BACKGROUND	11
VI	EQUIPMENT AND TECHNIQUES	31
VII	MATHEMATICAL FORMULATION	43
VIII	EXPERIMENTAL OBSERVATIONS	59
IX	DISCUSSION	65
X	ACKNOWLEDGMENTS	105
XI	REFERENCES	106
XII	LIST OF PUBLICATIONS	110
XIII	APPENDICES	111

Preceding page blank

FIGURES

No.		Page
1	THERMAL STRATIFICATION PHENOMENON	6
2	PROPOSED MECHANISM OF BUBBLE FORMATION (KUMAR (31))	13
3	TERMINAL VELOCITY OF AIR BUBBLES IN TAP WATER AS A FUNCTION OF BUBBLE SIZE (HABERMAN (17))	19
4	RELATIONSHIP BETWEEN LIQUID FILM COEFFICIENT AND BUBBLE DIAMETER (MODIFICATION OF BARNHART (31))	23
5	RELATIONSHIP OF INITIAL AND FINAL VOLUME OF BUBBLE FOR DIFFERENT COLUMN HEIGHTS (DATTA (10))	24
6	VOLUME OF BUBBLE VS. HEIGHT ABOVE OUTLET AND CORRESPONDING VELOCITY (DATTA (10))	24
7	POSSIBLE FLOW REGIMES WITH A BUBBLE SCREEN IN A TWO-LAYER DENSITY SYSTEM (CEDERWALL (8))	26
8	VELOCITY PROFILES ABOVE A SINGLE ORIFICE (KOBUS (20))	30
9	RATE OF SPREAD OF VELOCITY PROFILES (KOBUS (20))	30
10	FIELD EXPERIMENTAL SET-UP	35
11	FLUOROMETER CALIBRATION CURVES	36
12	FLOW METER CALIBRATION CURVE	38
13	MAP OF TEST SITES	40

FIGURES

No.		Page
14	DEFINITION SKETCH	45
15	THE COEFFICIENT OF ENTRAINMENT AS A FUNCTION OF THE AIR FLOW RATE FOR TWO- AND THREE- DIMENSIONAL AIR BUBBLE PLUMES (CEDERWALL (8))	51
16	AVERAGE RISING SPEED OF BUBBLE STREAM FROM A SINGLE ORIFICE (KOBUS (20))	54
17	DYE CONCENTRATION AT VARIOUS DEPTHS AND DISTANCES AWAY FROM THE DIFFUSER	62
18	DYE MOVEMENT AT A DEPTH OF 75 FEET (40 FEET AWAY FROM THE DIFFUSER)	62
19	TEMPERATURE PROFILE - LAKE TRAVIS MAY 14,1972	63
20	MEASURED AND PREDICTED CENTER LINE VELOCITY FOR 0.75 and 2.0 L./Min. O_2 FLOW RATE AND INJECTION DEPTH OF 60 FEET	67
21	MEASURED AND PREDICTED CENTER LINE VELOCITY FOR 1 AND 2 L./Min. O_2 FLOW RATE AND INJECTION DEPTH OF 30 FEET	68
22 to 24	PREDICTION CONSIDERING THE EFFECT OF ENTRAINMENT COEFFICIENT ON HALF-WIDTH OF PLUME, CENTER LINE VELOCITY AND WATER FLOW RATE RESPECTIVELY	70-72
25	PREDICTED BUBBLE DIAMETER AS A FUNCTION OF DEPTH FOR 2 AND 0.2 MM. BUBBLES	73
26 to 31	COMPARISON OF PREDICTIONS OF MODEL ONE (0.2 and 2.0 MM. BUBBLE) AND MODEL TWO FOR CENTER LINE VELOCITY, HALF-WIDTH OF THE PLUME, WATER FLOW RATE, MOMENTUM FLUX AND KINETIC ENERGY FLUX FOR AN OXYGEN FLOW RATE OF 1 L. /Min. AND INJECTION DEPTH OF 45 METERS	75-80

FIGURES

No.		Page
32	DEFINITION SKETCH	82
33 to 37	PREDICTION CONSIDERING THE EFFECT OF INJECTION DEPTH ON CENTER LINE VELOCITY, HALF-WIDTH, WATER FLUX, MOMENTUM FLUX, AND KINETIC ENERGY FLUX FOR INJECTION DEPTHS OF 75 AND 45 METERS	83-87
38 to 41	PREDICTION CONSIDERING THE EFFECT OF FLOW RATE ON HALF-WIDTH OF THE PLUME, CENTER LINE VELOCITY, AND WATER FLOW RATE FOR 1 AND 3 L./MIN. AND 0.2 and 2.0 MM. BUBBLE	89-92
42 to 43	PREDICTION OF MODEL ONE (0.2 MM. BUBBLE) AND TWO OF THE HALF-WIDTH OF THE PLUME AND CENTER LINE VELOCITY CONSIDERING NON ZERO SLIP VELOCITY AND COMPARED WITH PREDICTIONS FOR ZERO SLIP VELOCITY	94-95
44 to 45	PREDICTION OF MODEL ONE (2.0 MM. BUBBLE) OF THE CENTER LINE VELOCITY AND HALF-WIDTH OF PLUME CONSIDERING NON ZERO SLIP VELOCITY AND COMPARED TO ZERO SLIP VELOCITY	96-97
46	INCREASE IN OXYGEN CONCENTRATION VS. HEIGHT ABOVE DIFFUSER FOR A FLOW RATE OF 1 L./MIN. AND BUBBLES OF 0.2 AND 2.0 MM. AS PREDICTED BY MODEL ONE	98
47	RELATIONSHIP BETWEEN LIQUID FILM COEFFICIENT AND BUBBLE DIAMETER AT 20°C	112
48	MG. OF O_2 AS A FUNCTION OF DEPTH	113
49	MG. OF N_2 AS A FUNCTION OF DEPTH	114
50	FRACTION OF ORIGINAL AMOUNT OF O_2 REMAINING AS A FUNCTION OF DEPTH	115

FIGURES

No.		Page
51	FRACTION OF BUBBLE GAS WHICH IS O_2	116
52	NITROGEN/OXYGEN RATIO AS A FUNCTION OF DEPTH	117
53	RELATIVE AMOUNT OF O_2 IN BUBBLE NORMALIZED TO CONSTANT RELEASE DEPTH	118
54	CSATO (Mg/mm^3) VS. DEPTH	
55	MG. OF CO_2 IN BUBBLE AS A FUNCTION OF DEPTH	120
56	CSATO VS. DEPTH	121
57 to 86	MODEL PREDICTIONS FOR CENTER LINE VELOCITY, HALF-WIDTH OF PLUME, WATER FLOW RATE AND THE INCREASE IN D.O. FOR INJECTION DEPTHS OF 25, 50, 75, 100 METERS AND FLOW RATES OF 1 AND 2 L./MIN.	122 151

TABLES

No.		Page
1	MEASURED CENTER LINE VELOCITY OF RISE	60
2	MEASURED AND COMPUTED CENTER LINE VELOCITY OF RISE	66
3	MODEL PREDICTIONS FOR 1 L./MIN. AND DEPTH OF INJECTION OF 25 AND 50 METERS	100
4	MODEL PREDICTIONS FOR 1 L./MIN. AND DEPTH OF INJECTION OF 75 AND 100 METERS	101
5	MODEL PREDICTIONS OF 2 L./MIN. AND DEPTH OF INJECTION OF 25 AND 50 METERS	102
6	MODEL PREDICTION FOR 2 L./MIN. AND DEPTH OF INJECTION OF 75 AND 100 METERS	103
7	ILLUSTRATIVE EXAMPLE	104

SECTION I

CONCLUSIONS

1. The proposed mathematical model for the dynamics of plumes incorporating mass transfer is in good agreement with the field measurements.

2. The effect of mass transfer on the various dynamic characteristics of the bubble plume cannot be neglected.

3. Slip velocity as a function of diameter has a negligible effect on plumes of small bubbles but an increasing effect with larger bubbles.

4. With larger bubbles, the bubble-water plume exhibits a higher final center line velocity, a higher water flow rate, a higher momentum flux, a higher kinetic energy, but a smaller half-width as compared to smaller bubbles.

5. An increase in the oxygen flow rate from one to three l /min did not lead to a noticeable corresponding increase in the water flow rate.

6. A deeper injection depth led to a lower center line velocity, momentum flux, and kinetic energy flux, but to a larger plume and a higher water flow rate, at any height above the diffuser.

7. The energy left in a plume generated by 0.2 mm diameter bubbles was very small at the metalimnion and did not measurably cause any disturbance of the stratification.

SECTION II

RECOMMENDATIONS

It is recommended that the plume dynamics from a line source diffuser be experimentally and mathematically verified. The factors which control "uncoupling" of the bubble plume at the metalimnion need to be quantitatively defined. The entrainment coefficient, α, was taken from the literature for this study and should be evaluated in the field. The spatial zone of influence for a point source and line source diffuser needs to be defined. A number of these recommendations are presently under study in the author's laboratory. Finally, a full scale demonstration of hypolimnion aeration with commercial oxygen is in order.

Preceding page blank

SECTION III

INTRODUCTION

The phenomenon of temperature stratification of lakes and reservoirs has been observed for several years. Thermal regimes in impoundments in temperate climates include a period in the summer during which vertical temperature gradients become large. Such a stratification persists until the Fall when temperature becomes uniform throughout the impoundment and the "Fall overturn" occurs. Stratification of the impoundment leads to the formation of three distinct layers, as shown in Figure 1. The epilimnion (the warmer layer on top) with almost a uniform temperature and density throughout; the metalimnion, (the middle layer), with a steep temperature gradient; and finally the hypolimnion (the bottom, cold layer of water), with a slight temperature gradient throughout. Temperature and density are not the only differences between these three layers. The epilimnion has a good quality water except for the high temperature. This of course includes a near saturation level of dissolved oxygen. The hypolimnion, on the other hand, is a good source of cold water, but unfortunately becomes poor water quality when the dissolved oxygen is depleted. Depending on the depth of the impoundment and the level of nutrients, the dissolved oxygen concentration in that layer drops to zero. This fact limits the withdrawal of water from this nutrient-rich low-quality layer. Literature is abundant on the water quality of hypolimnetic water and will not be discussed here.

Several remedies for this problem have been suggested; a brief discussion of such methods will be presented here.

Destratification

In order to avoid anaerobic conditions in the hypolimnion, the impoundment is mixed to provide D.O. in the bottom waters. Some of the methods used are mechanical mixing, air pumping, water pumping, etc. Regardless of the benefits achieved by such action, certain disadvantages are also attached to it. Such disadvantages are; the loss of the cold water resource, the increase in productivity due to recycling nutrients and the economical loss associated with the loss of cold water fisheries in the impoundment.

Preceding page blank

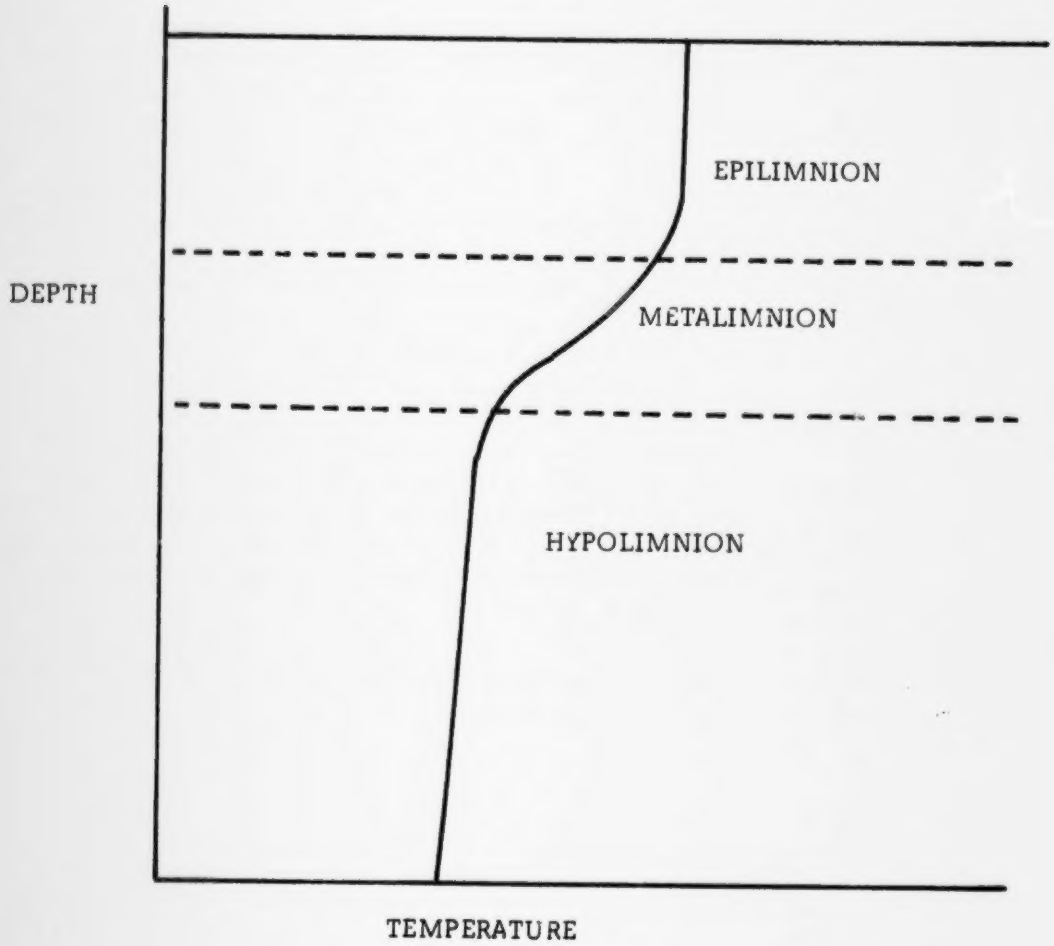
EPILIMNION
METALIMNION
HYPOLIMNION
DEPTH
TEMPERATURE

Fig. 1 THERMAL STRATIFICATION PHENOMENON

Selective Withdrawal

This method which requires gates at various depths, besides being expensive, could lead to deteriorating the water quality down-stream by releasing water of high nutrient content, thus increasing its productivity. In addition, temperature and D.O. cannot be independently regulated.

Hypolimnion Aeration

Aeration of the hypolimnion water by use of pure oxygen without destroying the stratification has certain engineering merits (38). Some of the advantages of such a process are:

1. Preservation of the cold water resource;
2. Nutrients are not recycled and are kept entrapped in the hypolimnion away from the euphotic zone; and
3. Cold water fisheries could be sustained below the reservoir.

SECTION IV

OBJECTIVE AND SCOPE

Aeration of the hypolimnion by the use of pure oxygen in the form of very fine bubbles generates a gas-water jet and the hydro-dynamic characteristics of air bubble plumes have been studied before by several investigators (1, 2, 8, 11, 14, 25, 27, 47). However, the effect of mass transfer on the hydro-dynamics of this system has not yet been considered. This work will consider the effect of the phenomenon of mass transfer in conjunction with the velocity of rise, the size of the gas-water jet, water flow, and finally the momentum and kinetic energy flux for such a rising plume. Mathematical expressions describing this plume along with computer programs for the solution of the governing equations will be developed.

This mathematical model solves for the bubble diameter, the center line velocity of rise and the diameter of the plume at any height above the injection point. Using these computed values, the water flow, momentum flux, and kinetic energy at any level are calculated. The model calculates the change in D.O. concentration at any level for a given oxygen flow rate and bubble diameter.

To show the effect of the mass transfer phenomenon on the behavior of the plume, a comparison with the case of no mass transfer will be carried out. Consideration of zero and non zero slip velocity will also be investigated.

Field measurements to verify the model were carried out, the description of which is shown in Section VI.

The experimental works also included a study of the mixing and circulation generated by the rising plume. Associated diffusion of this plume was studied experimentally and described in Section VI.

Preceding page blank

SECTION V

BACKGROUND

Air bubble systems have been used extensively and for a variety of purposes. They have been used in industrial processes such as distillation, evaporation, direct contact heat exchange, etc. They have also been used for pneumatic breakwaters, prevention of ice formation and destratification and quality control management of lakes and reservoirs (2, 14, 15, 21, 23, 32).

Numerous papers have been written on the advances in this area ranging from fundamental studies to descriptions of several new processes and equipment designs. The purpose of this section is to present a comprehensive review of those references that are related to this study. It will cover the following topics.

1. Bubble formation
2. Shape of bubbles
3. Path of rising bubbles
4. Velocity of rise of single bubbles and swarms of bubbles
5. Gas-liquid mass transfer
6. Induced mixing and energy consideration

Bubble Formation

Several papers have been written describing bubble formation from a single orifice and from porous plates submerged in different liquids. Kumar and his colleagues (6, 19, 31, 35) have reviewed the literature in this area and published a series of articles on the basic aspects of bubble formation from single submerged nozzles and porous plates. Their work included bubble formation under constant flow conditions (31) and under constant pressure (35). In their analysis they assumed that the bubble formation takes place in two stages, the expansion stage and the detachment stage, Figure 2. The final volume of the bubble is the sum of the volumes pertaining to the two stages. This in equation form is

Preceding page blank

$$V_F = V_E + Qt_c \quad (1)$$

where:
V_F = final volume
V_E = volume from first stage
Q = flow rate
t_c = time of detachment

At vanishingly small flow rates, the bubble volume can be directly obtained by equating the surface tension force with the buoyancy force. However, at a finite flow rate, forces associated with the expansion also exert their influences. The bubbles expand at a definite rate, thereby giving rise to the inertial force and the viscous drag, both of which add to the surface tension force.

The first stage is assumed to end when the downward forces are equal to the upward forces. The quantitative expressions for various forces are;

buoyancy force = $V(\rho_1 - \rho_g)\,g$ (2)
viscous drag = $6\pi\, r_e \mu v_e$ (3)
surface tension = $\pi D \gamma (\cos \theta)$ (4)
inertial force = $(d/dt_e)\,(Mv_e)$ (5)

where:
V = volume of bubble in cm^3
ρ_1 = density of liquid, g/cm^3
ρ_g = density of gas, g/cm^3
D = orifice diameter, cm
v_e = velocity of center of bubble in first stage, cm /sec
γ = surface tension, dyn /cm
M = virtual mass of bubbles, g

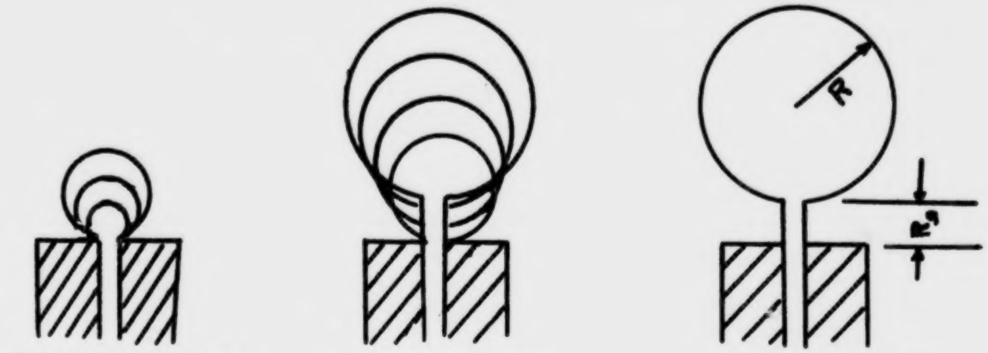

EXPANSION STAGE

DETACHMENT STAGE

CONDITION OF DETACHMENT

Fig. 2 PROPOSED MECHANISM OF BUBBLE FORMATION (KUMAR (31))

Kumar et al. (31) considered the virtual mass of the bubble to be the sum of the mass of gas and that of 11/16 of its volume of the liquid surrounding it.

A mathematical formulation for calculating the final volume of the bubble is presented. The effect of various parameters, viscosity, surface tension, liquid density, flow rate and orifice diameter on the bubble formation and its volume is covered in these studies. Bowonder and Kumar (6) have also presented studies on bubble formation on porous plates submerged in liquids of various physical properties. They found that the number of effective sites for bubble formation was much smaller than the total potentially available sites. The number of effective sites was found to be a function of surface tension, liquid density and gas flow rate. Pattle (29) has studied the factors in the production of small bubbles less than 1 mm. in diameter. Some of these are grease, low surface tension, and availability of organic or inorganic solute.

Datta and his colleagues (10) presented a correlation of the bubble size and the orifice diameter which is represented in the equation

$$R = (3r\gamma/2\rho g)^{1/3} \qquad (6)$$

where: R = bubble radius

r = orifice radius

γ = surface tension of liquid

ρ = density of liquid

Various techniques have been used to measure the radius of the rising bubble. They varied from photography to weighing by means of an analytical balance (17, 41).

Shape of Bubble

Haberman and Morton (17) observed three types of bubble shapes. Small bubbles are spherical, larger bubbles are ellipsoidal, and the largest bubbles assume a spherical cap shape. They attributed this to the surface tension, viscous and hydrodynamic forces. For small bubbles surface tension is the governing force and tends to make the surface of the bubble as small as possible. For large bubbles the viscous and the hydrodynamic forces govern and flattening of the surface occurs.

Datta (10) has also summarized the shape of the bubbles formed at circular orifices of different sizes oriented vertically upward and progressively increasing in diameter:

1. For circular orifices up to 0.04 cm diameter, the bubbles are substantially spherical.

2. For orifices between 0.04 and 0.4 cm diameter, the bubbles are spherical at the orifice, but on release rapidly assume an ellipsoidal shape with the larger axis horizontal.

3. With orifice diameter exceeding 0.4 cm, the bubble becomes unstable. They may assume a symmetrical saucer shape.

Path of Rising Bubbles

Haberman and Morton (17) observed three types of motion of bubbles;

a. rectilinear motion,

b. motion in a helical path, and

c. rectilinear motion with rocking.

Spherical bubbles followed either a rectilinear or helical path while ellipsoidal and spherical cap bubbles followed all three types of motion. They associated the type of motion of the bubble with the Reynolds number. For a Reynolds number of approximately 300, the motion is rectilinear. With an increase in the Reynolds number, spiraling begins and increases in amplitude and frequency until a maximum is reached. At Reynolds numbers of approximately 3,000, the spiraling disappears and only rectilinear motion with rocking is obtained.

Datta (10) reported that the spherical bubbles follow a vertical path, the ellipsoidal bubbles follow a zigzag, while the spherical-cap shaped bubbles followed an irregular path.

Haberman (17) as well as Datta (10) have observed the effect of the liquid viscosity on the path the bubble follows. For a very viscous liquid, the bubbles tend to preserve symmetrical shapes up to much larger size than is the case with water and their path tends to remain vertical.

Velocity of Rise of Bubbles in Liquid

Single Bubble

The complexity of the rise of the bubble and the many variables involved makes it impossible to describe the bubble motion theoretically. Data dealing with the rise of gas bubbles are scarce and often conflicting. Most of the experimental results reported are represented by imperical equations. In general, the equation of motion (16) of gaseous bodies is

$$\text{drag force} + \text{pressure force} + \text{weight} = (\text{mass} + \text{added mass}) \times \text{acceleration} \qquad (7)$$

This equation can be solved if the total mass of the bubble and all the forces acting on it are known.

The drag of the bubble in liquid is in general a very complicated function of its geometry, its velocity, and the physical properties of the medium. The shape of the bubble in turn is a complex function of the hydrodynamics, viscous, and inertial forces exerted. In addition, such effects as the container walls and bottom and the free surface of the liquid may also have a strong influence on the drag of a bubble.

As mentioned earlier, small bubbles can be considered and have been observed to act as rigid spheres. The earliest work on the motion of rigid spherical bodies was that of Stokes (40).

At large Reynolds numbers (R) and for spherical gas bubbles, Moore (24) derived an equation for the velocity of rise which has been also arrived at by other investigators. His conclusion was that the drag coefficient is equal to 48/R. For non-spherical bubbles several equations are available, such as that presented by Haberman (17).

$$U = 1.02 \, (g r_e)^{1/2} \qquad (8)$$

Haberman (17) as well as Datta (10) have observed the effect of the liquid viscosity on the path the bubble follows. For a very viscous liquid, the bubbles tend to preserve symmetrical shapes up to much larger size than is the case with water and their path tends to remain vertical.

Velocity of Rise of Bubbles in Liquid

Single Bubble

The complexity of the rise of the bubble and the many variables involved makes it impossible to describe the bubble motion theoretically. Data dealing with the rise of gas bubbles are scarce and often conflicting. Most of the experimental results reported are represented by imperical equations. In general, the equation of motion (16) of gaseous bodies is

$$\text{drag force} + \text{pressure force} + \text{weight} = (\text{mass} + \text{added mass}) \times \text{acceleration} \qquad (7)$$

This equation can be solved if the total mass of the bubble and all the forces acting on it are known.

The drag of the bubble in liquid is in general a very complicated function of its geometry, its velocity, and the physical properties of the medium. The shape of the bubble in turn is a complex function of the hydrodynamics, viscous, and inertial forces exerted. In addition, such effects as the container walls and bottom and the free surface of the liquid may also have a strong influence on the drag of a bubble.

As mentioned earlier, small bubbles can be considered and have been observed to act as rigid spheres. The earliest work on the motion of rigid spherical bodies was that of Stokes (40).

At large Reynolds numbers (R) and for spherical gas bubbles, Moore (24) derived an equation for the velocity of rise which has been also arrived at by other investigators. His conclusion was that the drag coefficient is equal to 48/R. For non-spherical bubbles several equations are available, such as that presented by Haberman (17).

$$U = 1.02\ (g r_e)^{1/2} \qquad (8)$$

where: U = the terminal velocity

r_e = the equivalent radius of the bubble

g = acceleration due to gravity

Davies and Taylor (11) are the earliest in the field of experimentation and analysis dealing with bubble rise velocities. They proposed the behavior of bubbles rising through actual liquid could be approximated by the hypothetical case of a bubble rising through an inviscid liquid when surface tension effects are important. With the additional assumption of constant pressure within the bubble, they proceeded to obtain the velocity which satisfied Bernoulli's equation at the frontal stagnation point. They gave the velocity of spherical-cap bubbles in an infinite liquid as

$$U = 2/3\ (gr_e)^{1/2} \tag{9}$$

Maneri and Mendelson (22), using the wave theory arrived at a similar expression for the velocity of rise between infinite parallel plates.

$$U = 0.486\ (gr_e)^{1/2} \tag{10}$$

Dumiterscu's analysis (13) is considered a better approximation. He obtained the potential function for the flow in a tube and assumed a spherical nose for the bubble. Solving simultaneously he obtained the bubble velocity and the frontal radius of curvature. His result for the velocity is

$$U = 0.495\ (gr_e)^{1/2} \tag{11}$$

Uno and Kintner (44) experimentally investigated the behavior of bubbles rising in tubes. A literature review on solid spheres led them to conclude that the presence of the tube wall could be accounted for by the general equation

$$U/U_\infty = \phi\,(1 - d/D)^n \tag{12}$$

where: U = rise of velocity of bubble in bounded liquid

U_∞ = rise of velocity of bubble in infinite media

d = diameter of bubble (sphere)

D = diameter of tube

By assuming that the above equation applies equally well to bubbles, they were able to correlate their data and evaluate n and ϕ to obtain

$$U/U_{\infty} = [1/\beta(1 - d/D)]^{0.765} \tag{13}$$

where β is a factor which depends on tube diameter and surface tension. This dependence was presented in a graphical form.

Haberman and Morton (17) have carried out an extensive study on bubbles moving in various liquids. They have noticed that below a diameter of 1 cm, bubble velocity is highly dependent upon the purity of the liquid. An impure liquid like tap water gave results tending more towards rigid spheres. Figure 3 summarizes their findings of the velocity of rise of bubbles in tap and filtered water. As seen from the figure, the critical radius at which the bubbles have maximum velocity in pure water was found to be approximately 1.5 mm with a rise velocity of 25 cm/sec. This radius corresponds to the largest one at which the bubble is still spherical. They also observed that proximity of sequential bubbles might have large effects on the rise of the bubble. One of their tests showed that bubbles of an equivalent radius of 0.17 cm and rising through mineral oil show an increase of 9% and 39% for spacing of 7.7 cm and 3.2 cm respectively.

In the derivation of Stoke's equation, it is assumed that there is no slip at the surface of a solid sphere falling through water. In the case of gas bubbles rising through liquid there will, in general, be a finite velocity of the liquid on the outside of the boundary envelope due to entrainment and this will result in an increased value of the terminal velocity. Hadamard and Rybezynski (18, 34) showed that this leads to a terminal velocity given by

$$V_t = 2/9\, R^2 g\, (\rho - \rho') /\eta\, [(3\eta' + 3\eta)/(3\eta' + 2\eta)] \tag{14}$$

where the liquid and gas being considered are isotropic media of viscosities η, η', respectively. ρ' is the density of the gas and R is the radius of the bubble. The expression in square brackets corrects for the effect on velocity of internal circulation due to viscous drag, and has a value of approximately 1.5 when η/η' is small and is independent of the bubble radius. Bouissinesq (5), starting with the assumption that the viscosities of the gas and liquid are not isotropic in the neighborhood of the boundary envelope and there there is a surface viscosity, η_s, which

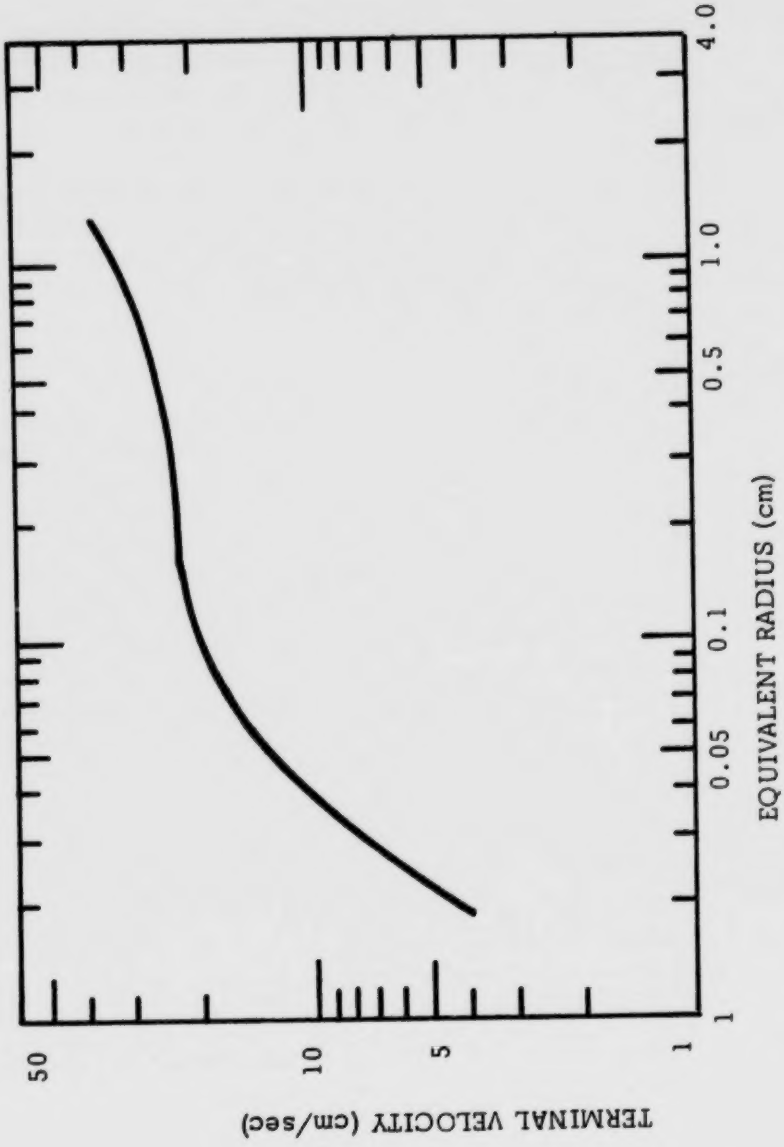

Fig. 3 TERMINAL VELOCITY VS. RADIUS

causes a resistance to motion in the surface deduced the equation

$$V_t = 2/9\, R^2 g(\rho - \rho')/\eta\ [(\eta_s + R/\eta_s + R)\ (3\eta' + 3\eta/3\eta' + 2\eta)] \qquad (15)$$

The expression in square brackets will change with increasing R from 1.0 to 1.5. The effect of surface viscosity would be to cause a thin boundary layer of water to travel upwards with the bubble and in the case of small bubbles would prevent relative motion in the boundary layer.

All the above experiments and corresponding expressions have been done on a single bubble in a confined boundary and did not account for the change of velocity of rise due to change in flow rate nor did they account for the change in velocity due to a change in bubble volume caused by mass transfer.

Swarm of Bubbles

The literature available on the motion of swarms of gas bubbles in a liquid column is found to be rather scanty. Schmidt and his co-workers (36) dealt with the motion of swarms of gas bubbles through liquid. Their interest was concentrated on the motion of steam bubbles in water pipes of steam boilers. O'Brien and Gosline (28) have given some data on the speed of air bubbles rising in a swarm through water and two mineral oils in a 6" tube. Nicklin (27) presented a theory on the motion of the bubbles in a two phase flow which showed that the velocity of the bubbles consists of a component equal to the superficial liquid velocity and a component due to buoyancy.

His analysis included two cases: one where there is no liquid flow and his results are summerized by

$$U = U_R = G/\varepsilon A = U_o/(1 - \varepsilon) = U_o + G/A \qquad (16)$$

where: U = bubble velocity when gas is bubbled steadily through stagnant liquid.

U_R = average relative velocity of the phases in two phase flow

U_o = velocity of bubble due to buoyancy

G = volume flow rate of gas

A = cross section of area of tube

ϵ = voidage fraction = number of bubbles x volume of bubble.

The second case was that of a finite liquid flow and his results are summarized by

$$U_R = G/\epsilon A - L/(1 - \epsilon)A \tag{17}$$

where L is volume flow rate of liquid. Nicklin (27) also derived an equation describing the energy losses associated with the process.

In all of the above analyses no consideration has been given to the change in bubble volume due to mass transfer and thus there is a change in velocity associated with this phenomena. Since this aspect is very important and directly associated with this study, a brief review will be given below.

Mass Transfer

The extent of change in bubble volume is dependent on the concentration of the bubble gas in the liquid, the solubility of the gas and the time of contact, i.e. velocity, of rise and the height of the liquid column. If the deficit is great and the gas is soluble, and the liquid column is sufficiently long, all bubbles will go into solution and therefore dissolve completely before reaching the surface. Otherwise, it will rise at such a velocity corresponding to the size of the residual bubble. The governing equation for mass transfer is

$$dm/dt = k_1 A(C_s - C_a) \tag{18}$$

where:

dm = the mass of gas transferred to the liquid (mg)

dt = the time of contact (sec)

k_1 = over-all diffusion coefficient based on liquid film resistance (mm/sec)

A = total interfacial area between liquid and gas (mm^2)

C_s = saturation concentration under specific partial pressure of gas in contact with liquid (mg/l)

C_a = actual concentration (mg/l)

In this equation k_1 is a function of the bubble diameter and temperature. Figure 4 shows clearly this dependence.

A in the above equation, which is the interfacial area, is the sum of the surface areas of all bubbles, thus a function of bubble diameter. And finally dt, or the contact time, is related to the velocity of rise of the bubble which in turn is a function of the bubble diameter.

Datta and his colleagues (10) carried out an experiment to study the reduction of bubble volume with height due to mass transfer. Figures 5 and 6 summarize their results. Figure 5 shows the effect of column height and Figure 6 shows the volume change and corresponding velocity of rise. Results of observation by Pattle (29) on the terminal height of small bubbles showed that over a range of bubble volume from 3×10^{-6} ml to 30×10^{-6} ml the terminal height was roughly proportional to the volume.

Induced Mixing and Energy Consideration

The use of air bubbling systems as pneumatic breakwaters and for the elimination of ice on the surface of reservoirs, ponds, and similar bodies of water, or for complete mixing of stratified waters has led several investigators to study the properties of this system more thoroughly. Several papers (14, 21) are available on the properties of the system when used as pneumatic breakwater. The interest in this case is centered on the induced surface currents. The use of the system for elimination of ice on the water surface has been used successfully but not studied in detail. It has been suggested that bubbles transport warmer water from the lower regions to the surface.

Other investigators have studied the use of the system for mixing stratified bodies of water. Gay and Hagedorn (16) found that in additon to the induced surface current, a strong bottom current toward the outlet exists. Zieminski et al. (47) studied experimentally the properties of this system in mixing stratified waters and found that the circulation pattern undergoes random changes caused by the randomness of the bubble motion. They also found that the mixing time decreased slowly with an increased air flow rate. They concluded that in decreasing the rate of flow a critical value is reached beyond which the currents generated are not sufficiently strong to establish a circulation of an appreciable magnitude in the whole body of water. Their report included photographic evidence of the induced circulation.

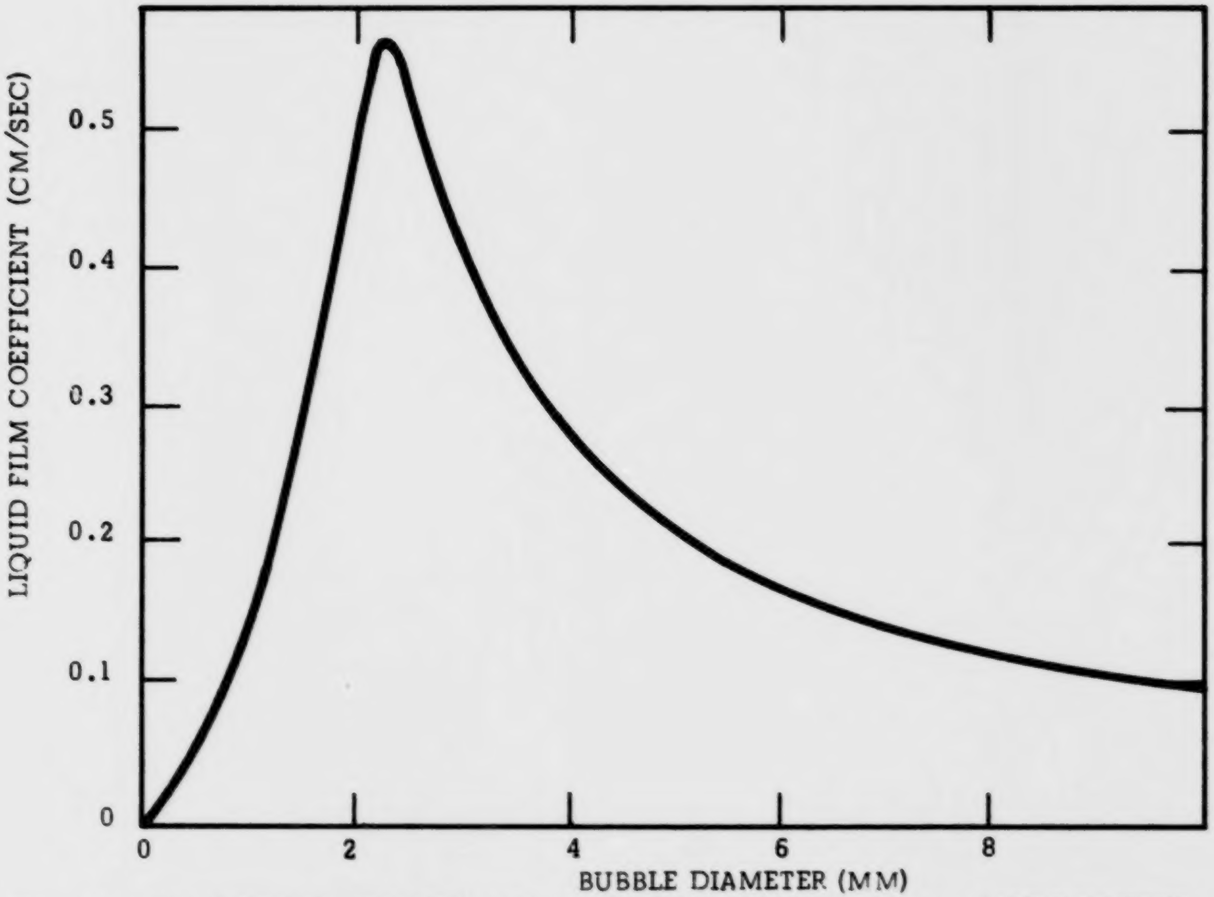

Fig. 4 RELATIONSHIP BETWEEN LIQUID FILM COEFFICIENT AND BUBBLE DIAMETER (MODIFICATION OF BARNHART (31))

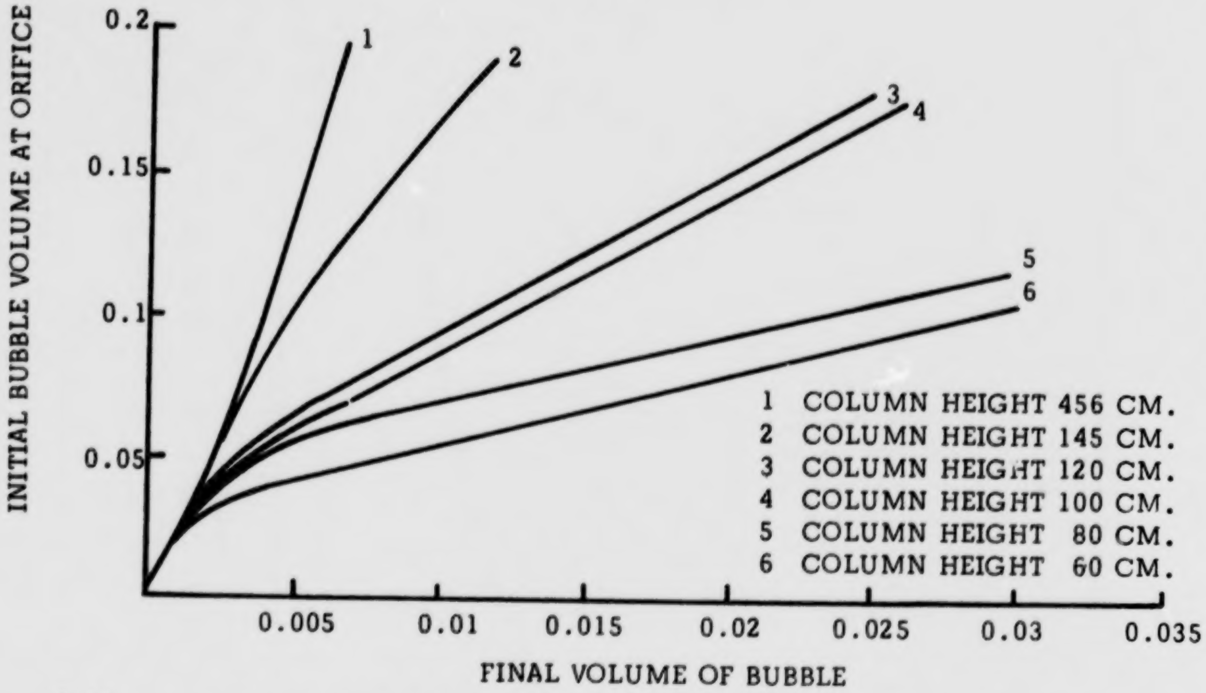

Fig. 5 RELATIONSHIP OF INITIAL AND FINAL VOLUME OF BUBBLE FOR DIFFERENT COLUMN HEIGHTS (DATTA (10))

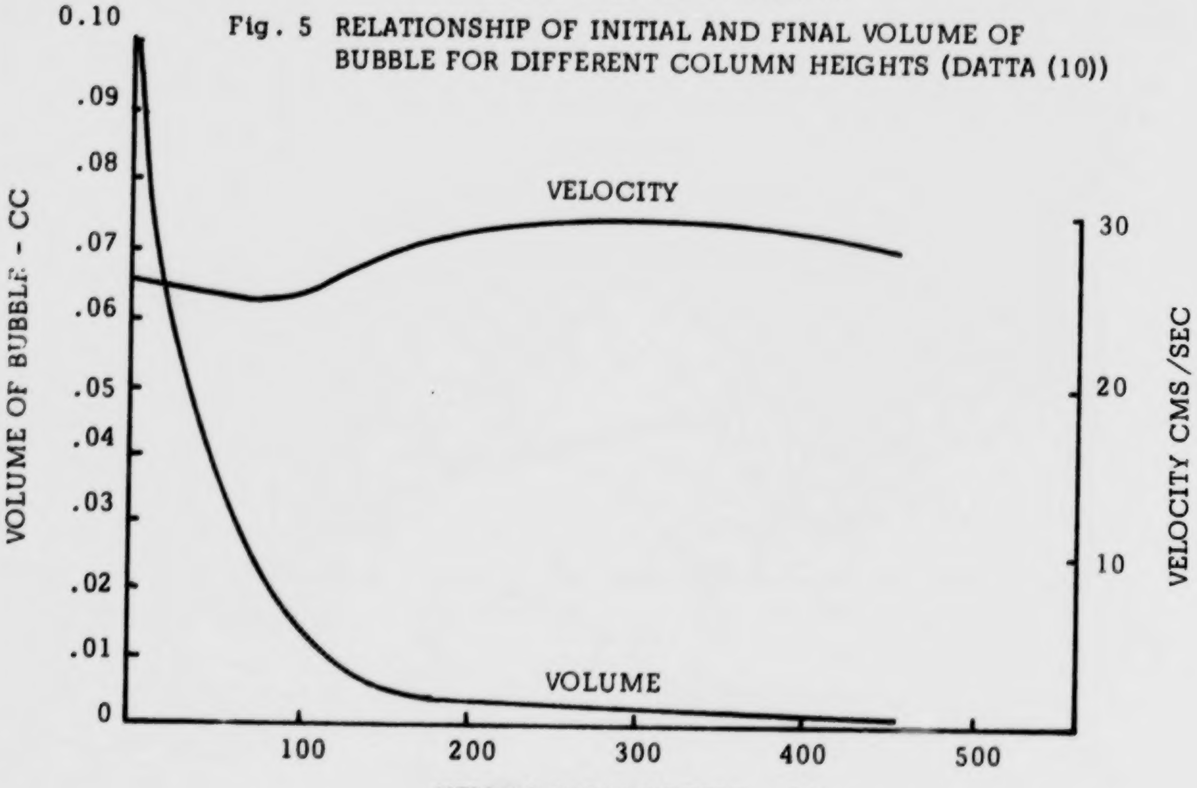

Fig. 6 VOLUME OF BUBBLE VS HEIGHT ABOVE OUTLET AND CORRESPONDING VELOCITY (DATTA (10))

Ditmars et al. (8) hypothesized that air bubbling in a stratified body of water could lead to an uncoupling effect between the water flow and the air bubbles as shown in Figure 7.

One of the earliest experiments in this area was conducted by Siemes and Weises (37) who described the mixing effect using the concept of effective diffusivity. Their results were reported in a graphical form in which the effective diffusivity was plotted against superficial gas velocity. They discussed the variation of effective diffusivity with a gas flow rate which seemed to be a linear function of gas velocity at a low gas flow rate. The results of Tadaki and Maeda (42) showed that the effective diffusivity D_e increased with gas flow rate although the liquid flow rate had no significant effect. Reith (32) in his recent work, noted that at very large gas flow rates the longitudinal mixing could be characterized by a constant Peclet number (product of Prandtl and Reynolds numbers) of 3.0. The Peclet number was based on the tube diameter, gas velocity, and effective diffusivity.

Subramanian and Chi Tien (41) studied the effective longitudinal mixing due to single bubbles and a swarm of bubbles and described it by the diffusion equation using the effective diffusivity. The following expression for the velocity of flow in the liquid phase in the whole system was derived.

$$V = 2\gamma \beta f \tag{19}$$

where: γ = the bubble density

f = the frequency of bubble formation

β = the amount of liquid carried upward by a single gas bubble.

β was considered to be of two components, the volume of the liquid entrained by the boundary layer of bubbles up to the separation point and the volume of the liquid entrained by the wake behind the bubble which is assumed to form from the separation point. Mathematical expressions to calculate these values are derived. Their equation of the effective diffusivity is

$$D_e = 4.5 \times 10^5 V^2 \tag{20}$$

and the velocity of entrained liquid is given by

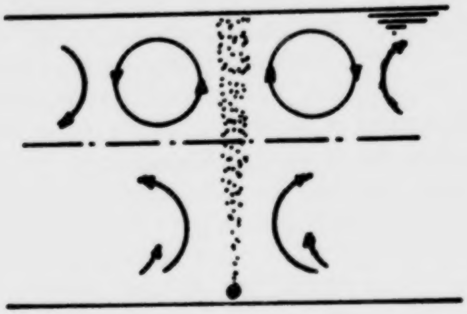

a. COMPLETE UNCOUPLING BETWEEN PLUME WATER AND AIR-BUBBLES AT THE INTERFACE.

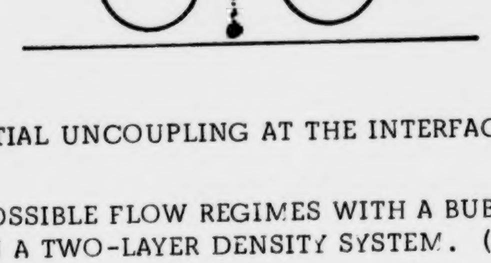

b. PARTIAL UNCOUPLING AT THE INTERFACE.

Fig. 7 POSSIBLE FLOW REGIMES WITH A BUBBLE SCREEN IN A TWO-LAYER DENSITY SYSTEM. (CEDERWALL (8))

$$V = 0.019375\beta f \qquad (21)$$

De Nevers (12) has studied fluid circulation by bubbles in baffled and unbaffled systems. His mathematical model is summarized by

$$h = W/(\rho_1 g \ \epsilon/2 \ (-dp/dl)) - 1 \qquad (22)$$

where:
h = the height of circulation
W = the width of circulation
ρ_1 = liquid density
g = the acceleration of gravity
ϵ = the volume fraction of gas-liquid mixture occupied by gas.

The limitation of this model is that it assumes that liquid continues to circulate around the same closed loop while gas enters at the bottom and leaves at the top. However, this is not the case since at the top, some of the liquid continues to move with the gas which is leaving the circulation, this other liquid must flow in somewhere to replace it. The above model does not account for such a condition.

The convective currents which rise from heated bodies have been discussed first by Schmidt (36). He studied the behavior of convective plumes of air above a steady point and line source of heat in a uniform, incompressible atmosphere. He observed that plumes of hot air rising from small sources tend to be confined within conical regions where the flow is turbulent (just as in the case of forced jets). Using this fact he discussed the dynamics of such cases by supposing that the distribution of temperature and velocity can be found by balancing the horizontal turbulent transfer of heat and momentum against the vertical transfer by convection, allowance being made for the effect of buoyancy. Some assumptions have to be made to connect the horizontal turbulent transfer and the mean vertical flow before the analysis can be carried out. Schmidt (36) assumed that there is geometrical and mechanical similarity of the process in horizontal sections of the plume, and used the mixture length theories of turbulence to find the complete form of velocity and temperature profiles for both point and line sources of heat in an atmosphere at uniform temperature. His calculated results for the point source were verified by experiment using small electrically heated grids of air. His experimental measurements fitted quite well a normal distribution profile, exp. $(-45r^2/x^2)$.

More recently, Yih and Rouse, and Yih and Humphreys (46, 33) have given the results of measurements of temperature and vertical velocity above a single gas burner and above a line of gas burners in air. Those measurements were taken at a variety of source strengths. The results were combined in non-dimensional form to give a vertical velocity profile and buoyancy profile for each of the two types of sources. For a point source they chose the profile exp. $(-96r^2/x^2)$ for the vertical velocity and the profile exp. $(-71r^2/x^2)$ for the buoyancy as giving the best fit with the quoted experimental results.

With the exception of some comments by Batchelor (4) on convective plumes in unstably stratified fluids, little attention has been given to cases in which there is a density gradient in the ambient fluid or atmosphere.

Taylor and his colleagues (25) were among the earliest to mathematically describe the gravitational convection from maintained and instantaneous sources of buoyancy in uniform and stratified fluid. The assumptions they followed in their derivation are:

1. The profiles of vertical velocity and buoyancy are similar, at all heights.

2. The rate of entrainment of fluid at any height is proportional to a characteristic velocity at that height.

3. The fluids are incompressible and do not change volume on mixing and that local variations in density throughout the motion are small compared to a reference density.

Their governing equations are:

$$d/dx\,(\pi b^2 U) = 2\pi b\alpha U \qquad (23)$$

$$d/dx\,(\pi b^2 \rho) = \pi b^2 g\,(\rho_o - \rho) \qquad (24)$$

$$d/dx\,\pi b^2 U\,(\rho_1 - \rho) = 2\pi b\alpha U\,(\rho_1 - \rho_o) \qquad (25)$$

where:
b = the width of the plume (m.)
U = the velocity of rise (m./sec.)
α = the entrainment coefficient relating the inflow velocity at the edge of the plume to the vertical velocity within the plume.

ρ = the fluid density inside the plume

ρ_o = the fluid density outside the plume

ρ_1 = the reference density.

The above three equations represent conservation of volume, conservation of momentum, and conservation of density deficiency.

Solution of the above equations for constant flow rate and uniform fluid yields

$$b = 6\alpha/5 \; x \tag{26}$$

$$U = 5/6\alpha \; (9/10\alpha Q)^{1/3} \; x^{-1/3} \tag{27}$$

Theoretical treatment of point source in a stratified fluid using the above equation of conservation and assuming that the velocity and buoyancy profiles are normal distribution curves centered about the axis of symmetry, led to a prediction of the final height to which a plume of light fluid will rise in stably stratified fluid.

Kobus (20) in his analysis of the flow induced by air bubble systems and from his experiments found that the vertical velocity profile can be represented by a Gaussian distribution curve with a linear spread in the vertical. His analytical treatment included the momentum flux increase due to the buoyancy of the air.

Figure 8 shows the observed velocity profile above a single orifice and Figure 9 shows the rate of spread of the velocity profiles. The analytical origin was found to be dependent on the local orifice geometry and especially to vary with the orifice elevation above the floor, and was found for his test arrangement to be equal to 0.8 meters. He also noticed that this value seems to increase slightly with depth.

Cederwall and Ditmars (8) in their analysis of air bubble plumes followed the analysis of Taylor with the assumption of compressible fluid rather than incompressible. They assumed Gaussian velocity distribution profiles. Their analysis included points and line sources in homogenous ambient fluid with some attempt at the analysis in stratified fluid. They used the experimental data of Kobus to test their model.

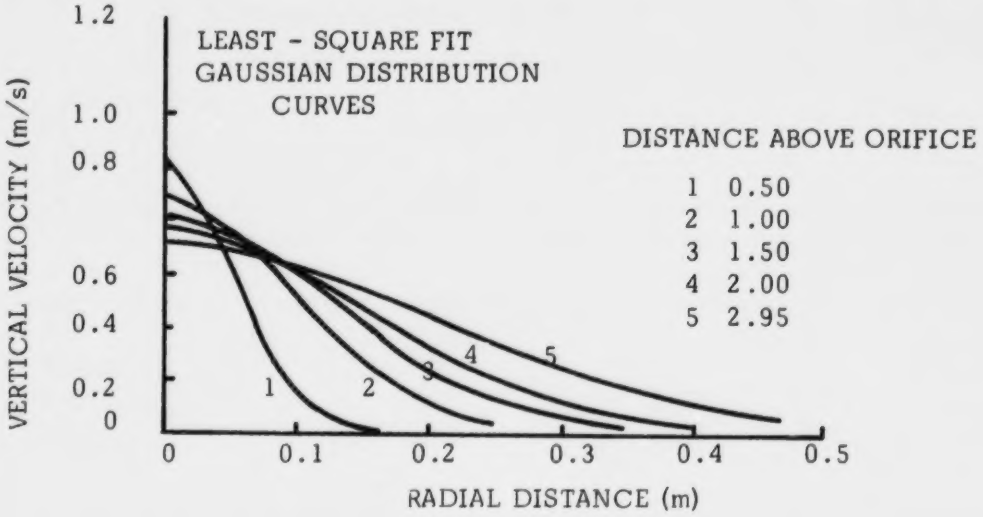

Fig. 8 VELOCITY PROFILES ABOVE A SINGLE ORIFICE. (KOBUS (20))

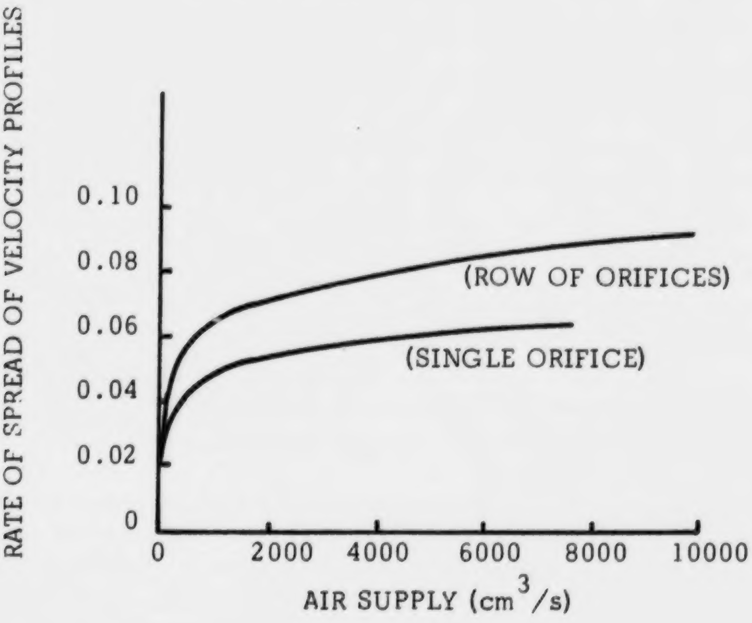

Fig. 9 RATE OF SPREAD OF VELOCITY PROFILES. (KOBUS (20))

SECTION VI

EQUIPMENT AND TECHNIQUES

Several laboratory techniques have been reported to be used in measuring the velocity of rise and the induced mixing due to buoyant jets. These techniques varied from photography to use of radio-isotopes. In this study a dye was used as a tracer. A fluorescent dye was chosen so that its concentration could be measured with a fluorometer. The following sections will describe the dye selected, the fluorometer, and other equipment used as well as the techniques employed.

Tracer

The tracer to be used should respond perfectly well to the water movement. To do so, its specific gravity, viscosity, and other physical characteristics should match those of the water it is dispersed into. It should be easy to handle, cheap, non-toxic to human beings and harmless to aquatic biota, and above all should be easily detected quantitatively. Rhodamine B, a fluorescent tracer of a commercial organic pigment, is an excellent tracer. It is available commercially in powder form or in a 40% by weight solution in acetic acid at a cost of approximately $5.00 per pound. It is quite soluble in water and is also readily soluble in methanol. This property makes it possible to adjust the solution density to match that of the water in which it is to be dispersed. It is non-toxic if used at a low concentration. The FDA has established as a pro tem allowance limit for Rhodamine B in drugs and proprietary products a continuing ingestion rate not to exceed 0.75 mg per day.

This tracer is easily detected by its fluorescence which reaches a maximum at 570 mμ. To avoid any interference with naturally occuring substances which usually peak at a shorter wave length, selection of the primary and secondary filter is very important.

Pritchard and Carpenter (30) found that Rhodamine B is not seriously affected by bacterial action and that it decomposes only slowly on exposure to light. Its fluorescence remains constant over a pH range of 4 - 10. They tested the adsorption properties of this dye on living matter and found that a sample containing 0.4 ppb of Rhodamine B and a large algae population showed no decrease in fluorescence after four days. However, this dye is very sensitive to temperature. Pritchard and Carpenter found that the fluorescence of this dye decreases with increasing temperature at the rate of 2 - 3% per degree centigrade.

Feuerstein and Selleck (15) found the response to temperature change to be:

$$F = F_o e^{nt} \tag{28}$$

where:
F = the fluorescence reading in units
F_o = the corresponding reading at 0^oC
n = constant = -0.027
t = the sample temperature (^oC)

Therefore, for accurate work, the temperature of the samples must be taken and correction applied.

Fluorometer

Rhodamine B can be easily detected quantitatively with a fluorometer. The Turner Model III flourometer is commonly used and this was used in this study. The fluorometer is basically an optical bridge which is analogous to the accurate wheatstone bridge used in measuring electrical resistance (43). The optical bridge measures the difference between light emitted by the sample and that from a calibrated rear light path. A single photomultiplier surrounded by a mechanical light interrupter sees light alternately from the sample and the rear light path. The photomultiplier output is alternating current, permitting a drift-free AC amplifier to be used for the first electronic stages. The second stage is a phase-sensitive detector whose output is either positive or negative, depending on whether there is an excess of light in the forward (sample) or rear light path respectively. Output of the phase detector drives a servo amplifier which is in turn connected to a servo motor. The servo motor drives the light cam (and the fluorescence dial) until equal amounts of light reach the photomultiplier from the sample and the rear light path. The quantity of light required in the rear path to balance that from the sample is indicated by the fluorescence dial.

The fluorometer may be equipped with a variety of sample doors. Two types were used in this study; namely the discrete sample cuvette door and the continuous sample door. It also has four operating ranges and different levels of sensitivity.

Fundamentally, fluorescence is the emission of radiation from a molecule or atom following absorption of radiation. From an analytical standpoint, the intensity of fluorescent light emitted by a sample under constant input light intensity is directly proportional to the concentration of the fluorescent compound. Many investigators have agreed with the manufacturer that at low concentration of the fluorescent material, the response of the fluorometer is linear with the concentration of tracer. The operating and service manual (1964) lists three reasons for deviation from linearity:

1. Extremely high concentration of the fluorescent material, leading to self-absorption of light. This concentration quenching effect frequently occurs at concentrations above about one ppm and should be checked.

2. High concentration of a material in the reagents which absorbs either the exciting ultraviolet light, or the emitted light.

3. Non-linearity in a chemical reaction which is used to convert the unknown to a fluorescent material, or non-linear recoveries.

None of these reasons were applicable in this study.

Feuerstein and Selleck (15) reported that the response of Rhodamine B is not linear in the Turner Model III fluorometer, but has the relationship:

$$C = KF^n \tag{29}$$

where: C = the concentration

F = the fluorescence reading

K, n = constants

Wilson's (45) findings agreed with the findings of Feuerstein and Selleck, as well as this study.

Diffusers

Two types of diffusers were used and tested.

1. Porous PVC diffuser with a bubble of approximately 2 mm in diameter

2. Porous ceramic diffuser which produces bubbles in the range of 0.2 - 0.3 mm in diameter and a maximum of 0.5 mm. For best results and to minimize coalescence this diffuser should be horizontal. This was achieved by strapping the diffuser to a metal rack and balancing it by four ropes tied to the oxygen line.

Other Equipments

1. Gear type, small size, model 7012 positive displacement pump with a capacity of approximately 42 ounces of water per minute. This pump was used for the sample collection.

2. Submersible pump.

3. Buoys (floats) shown in Figure 10. They are made of four foot by four foot by two foot deep plywood and are filled with stryofoam. They house two 55 gallon drums to accomodate four oxygen cylinders, a pressure regulator, and a flow meter.

4. Flow meter

5. Boat and motor

Calibration of Equipment

A laboratory study was conducted to calibrate the fluorometer and to determine the characteristics of the fluorescence phonomena of Rhodamine B in the aquatic environment of the experiment.

A ten-liter sample of lake water was collected and left to come to room temperature (21°C). Rhodamine B solutions of various concentrations were made to use in constructing a standard calibration curve. Using those solutions, corresponding fluorescence readings on the four scales were recorded. These fluorescence readings are plotted against the concentration of Rhodamine B in Figure 11. The fluorescence was found to be non-linear with concentration. This agreed with the results of Feuerstein and Selleck (15), and Wilson (45).

The following equations express the concentration-fluorescence relationships on the four sensitivity ranges.

$$1\text{x} \quad C = 1.95\,(F)^{0.89} \qquad (30)$$

$$3\text{x} \quad C = 0.55\,(F)^{0.92} \qquad (31)$$

$$10\text{x} \quad C = 0.195\,(F)^{0.92} \qquad (32)$$

$$30\text{x} \quad C = 0.048\,F(F)^{0.95} \qquad (33)$$

where: C = concentration of Rhodamine B in micrograms/liter
F = fluorescence reading at 21°C

No attempt was made to make temperature corrections, since all readings were done at room temperature, which was 21 ± 0.5°C. Calibration of the instrument as well as later readings were made in a dim room, to avoid light leakage which would affect the fluorescence readings.

Experimental Method

General Procedure Outline

1. Set the oxygen flow at a predetermined flow rate and wait for a

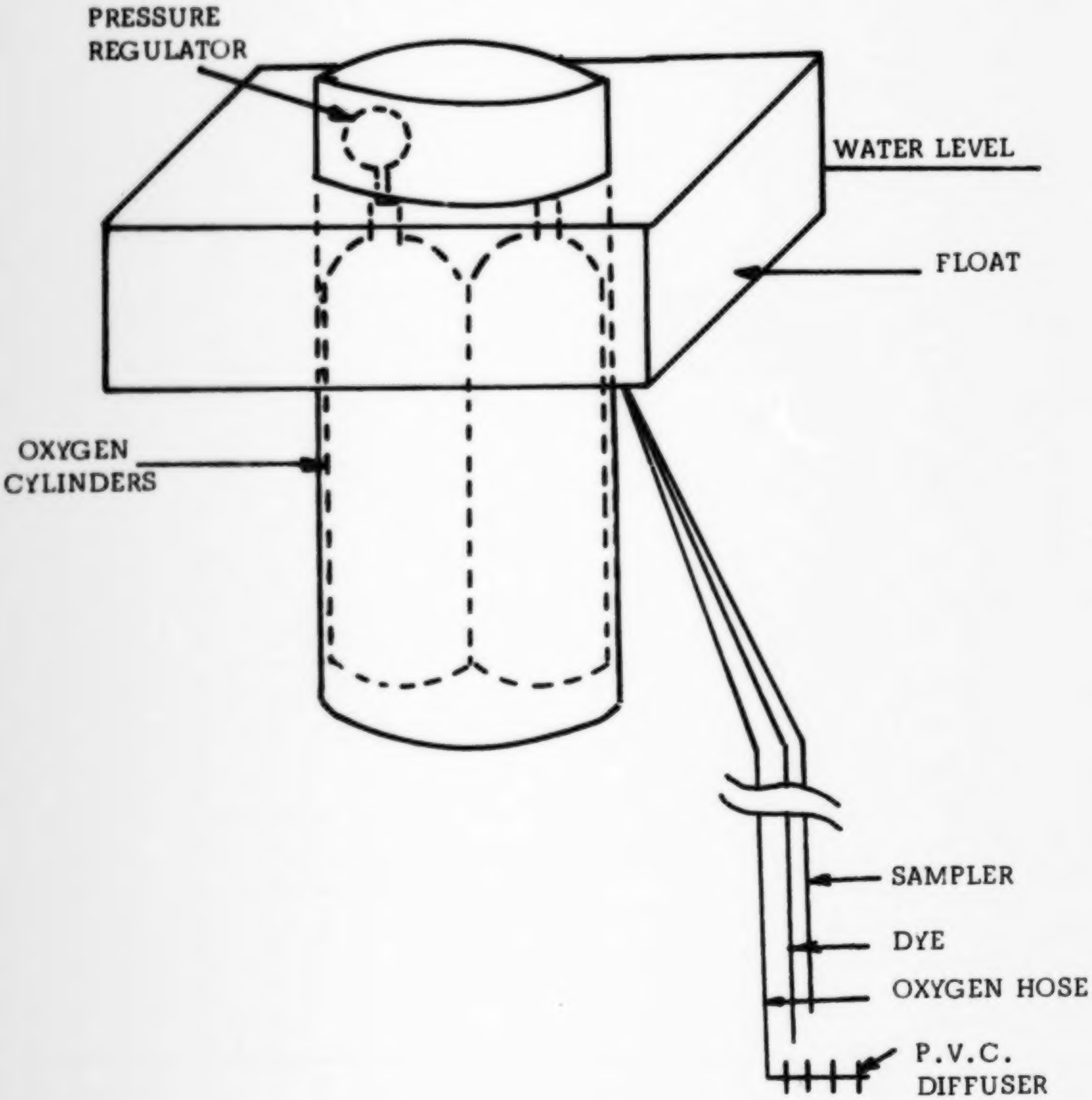
PRESSURE REGULATOR
WATER LEVEL
FLOAT
OXYGEN CYLINDERS
SAMPLER
DYE
OXYGEN HOSE
P.V.C. DIFFUSER

Fig. 10 FIELD EXPERIMENTAL SET-UP

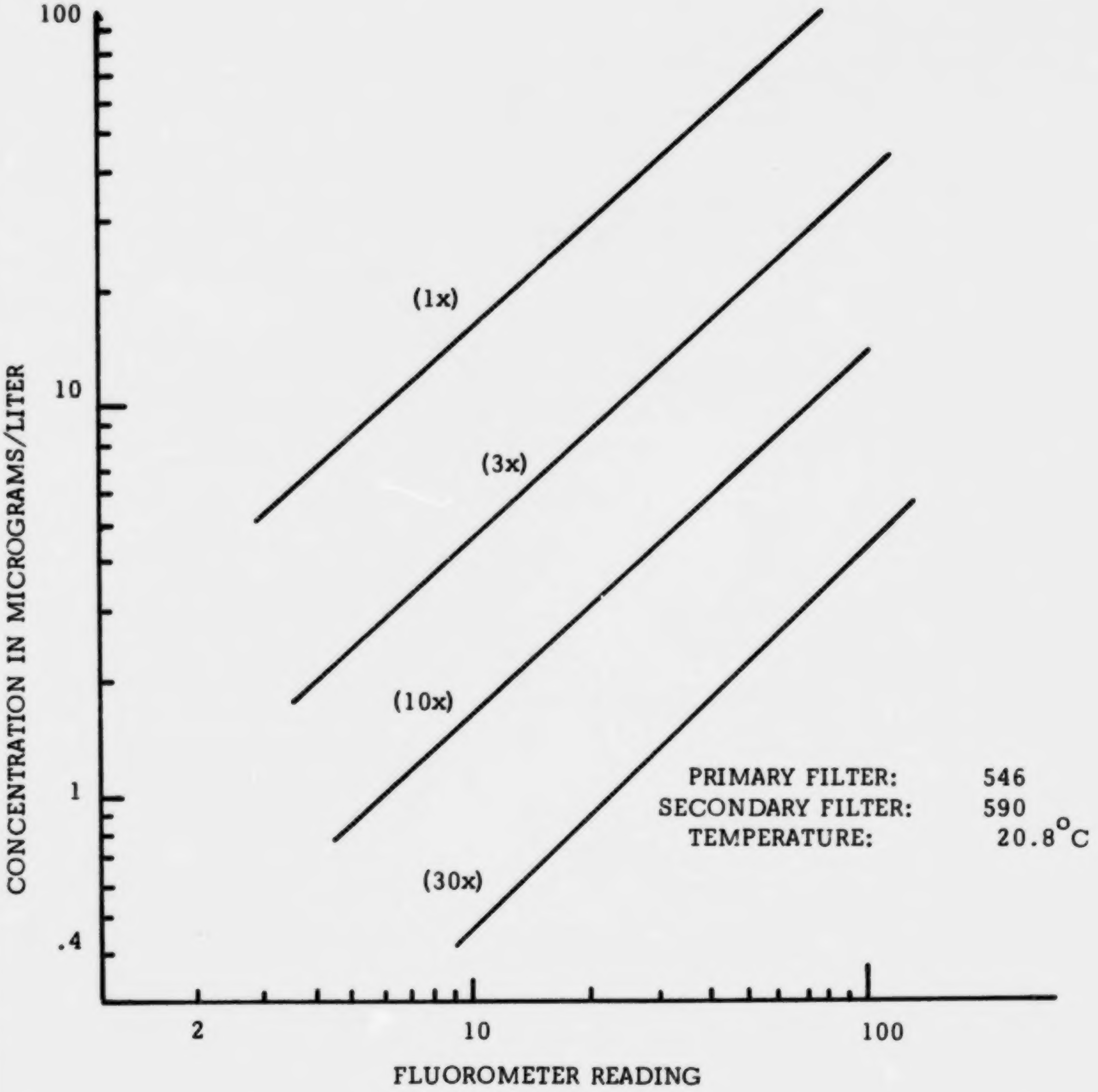

Fig. 11 FLUOROMETER CALIBRATION CURVES

minimum of half an hour to establish the flow field and have steady state conditions.

2. Inject dye.
3. Sample at the center of the plume at known intervals and depths for determining the center line velocity.
4. Sample at known intervals and depths at known distances from the diffuser, (point sample or continuous sample), for determining mixing patterns.
5. Read collected samples on the fluorometer and reduce data.

Setting the Flow

As indicated in the experimental set-up, the oxygen cylinders adapted with pressure regulators and flow meters described earlier were used. The following equations and the calibration curve shown in Figure 12 were used in setting the flow meter at the desired rate.

$$q^{o}_{G} = q^{o}_{A}\, 0.0181/\mu^{o}_{G} \tag{34}$$

$$q'_{G} = q^{o}_{G}\, P/760 \tag{35}$$

where: q^{o}_{A} = standard air flow as read from graph

q^{o}_{G} = standard gas flow in same units

q'_{G} = gas flowing at P but volume reduced to measurement at standard condition

μ^{o}_{G} = viscosity of gas in centipoises at standard condition

P = absolute pressure in mm of Hg

Injection of Dye

Method I

Forty to 50 ml of 40% by weight of Rhodamine B is diluted with lake water to approximately $\frac{1}{2}$ liter volume and poured into the dye container. The outlet of the submersible pump is then connected to the dye container and power is turned on. This forces the dye down the hose which is approximately five inches above the diffuser. Enough water was pumped to insure that the dye had discharged. This is considered to be equal to the volume of the dye hose.

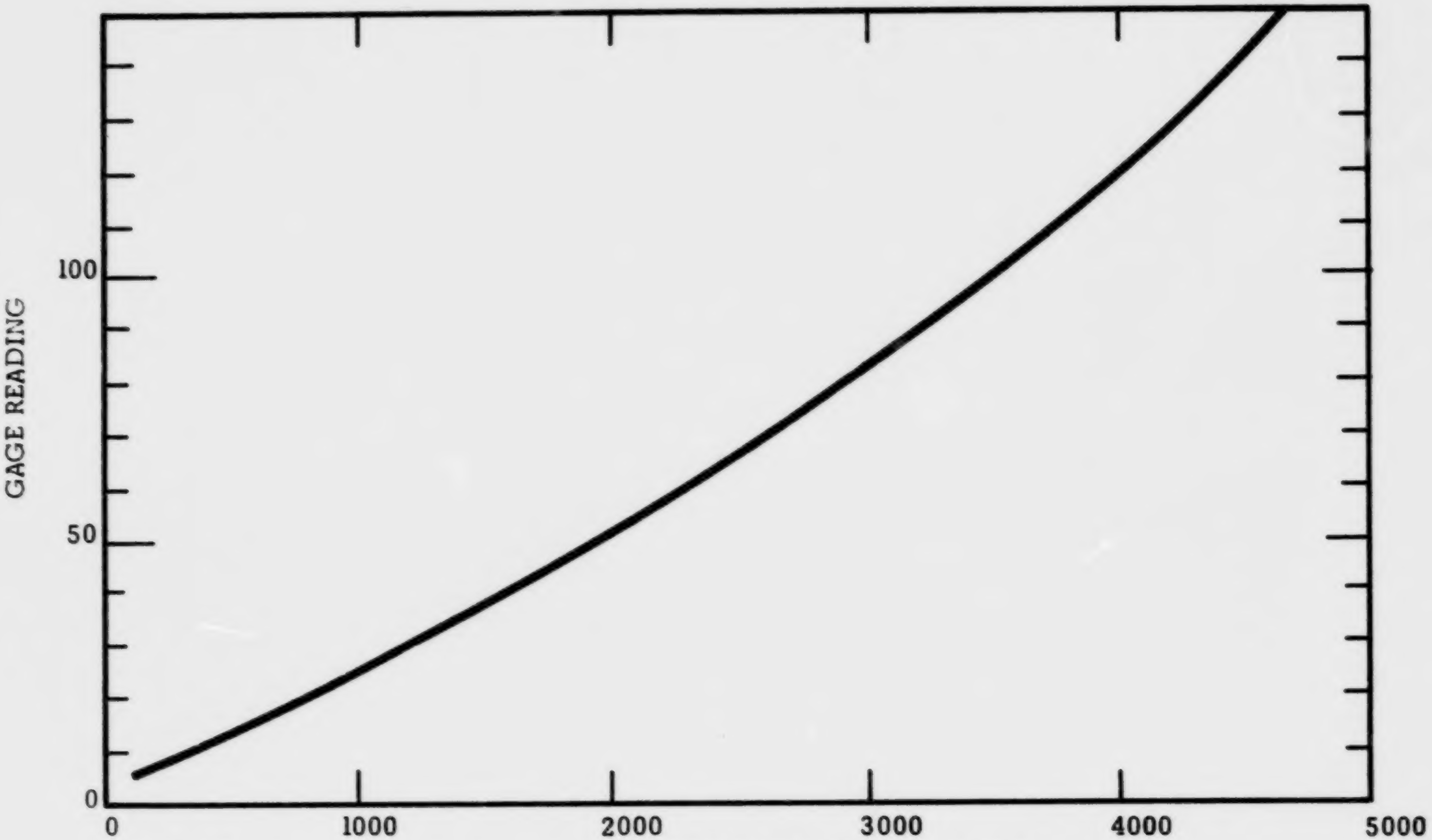

Fig. 12

FLOW METER CALIBRATION CURVE

Method II

The dye solution is made into a two-liter bottle with an outlet near the bottom. This is connected to a small gear pump to force the dye into a stiff plastic hose five to ten inches above the diffuser.

Sampling

The most critical part of the sampling was determining the instant that the dye reached the diffuser. To determine this instant, a sampling stiff plastic hose was attached to the dye hose and ended one inch beyond it. The other end of this hose was connected to one of the small gear pumps.

The dye was injected with close monitoring of the stiff plastic hose that was connected to the gear pump. As soon as the dye was detected in the hose (i.e. at the surface) the pump was turned off (to avoid spilling of dye on the surface which would lead to erroneous results) and the time was recorded. With the known pump flow rate and the volume of the hose, the lag time was calculated and the instant the dye hit the diffuser was set. For velocity measurements three or four stiff plastic hoses varying in length were suspended in the center of the plume (or as closely as possible) and connected to the gear pumps. Samples of ten to 20 ml volume are collected into BOD bottles from all sampling hoses and at recorded intervals of time. The time interval between each sample and the next was ten seconds reduced to five seconds around the time the dye was expected to hit that sampling line. The determination of this time was based on a trial run with sampling at intervals of 15 - 20 seconds.

For measurements of the circulation pattern and the dye diffusion, samples were collected using stiff plastic hoses and the gear pumps. The samples were collected at known depths and distances away from the diffuser at recorded time intervals.

Test Sites

The test sites were located in Lake Travis, the largest of the Highland Lakes of Central Texas. Lake Travis is impounded by Mansfield Dam, which was constructed by the United States Bureau of Reclamation in 1934. It serves for flood control, irrigation, and power generation. The lake is 65 miles long with 270 miles of shoreline and a maximum depth of 225 feet. The surface is 42,000 acres and the capacity is two million acre feet.

Figure 13 shows the three test sites where the experiments were conducted.

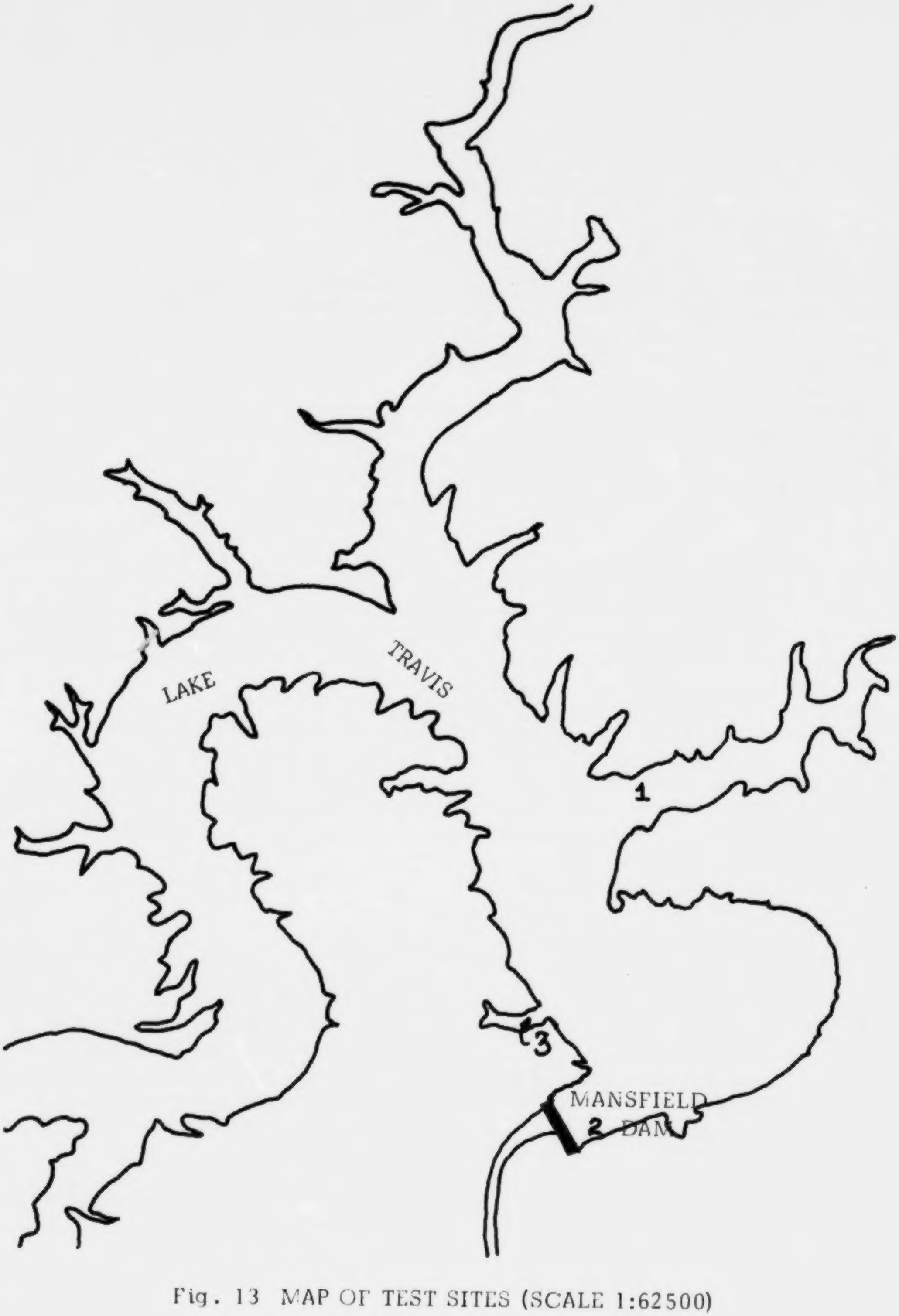
LAKE
TRAVIS
1
3
2
MANSFIELD
DAM

Fig. 13 MAP OF TEST SITES (SCALE 1:62500)

Difficulties Encountered

This study was carried out in three separate sites on Lake Travis in Texas. The first of these sites utilized the set-up shown in Figure 10 and the use of the boat. The boat with sampling instruments used to be tied to the buoy on the side of the diffuser. However, surface currents induced by wind and passing motor boats caused oscillation and rotating of the boat and the buoy which in turn caused movement of the diffuser. This movement along with surface surges caused an unstable plume to exist. The movement of the plume, as would be expected, did not follow the movement of the buoy nor the diffuser and sampling lines attached to it for measurement of the center line velocity. Thus, regardless of the many runs made, no reliable results were obtained. The alternative was to conduct this part of the study on a more stable base and thus the second and third areas were chosen.

The quantity and concentration of dye used along with the instability of the plume limited the number of runs carried out. The dye concentration was still detectable in the plume vinicity after two hours and at different levels of concentration which made it difficult to establish a base line and start a second run. The reason for this was attributed to the random motion of the bubble plume, for the above mentioned causes, such that no definite circulation patterns were defined.

Another problem encountered later on at the second and third sites was the entrapment of bubbles in the velocity measurement sampling lines. The quantity of those air bubbles was sometimes of such a magnitude that discontinuity of flow in the sampling lines was brought about. Restarting the flow in them, although timed, caused in most instances missing the right interval for sampling at that depth. Such a condition used to happen most often in the timing hose, the closest to the diffuser, used for setting the zero time for sampling. Although the hose end was turned upward away from the diffuser, bubbles were sucked into it and caused the discontinuity of flow. Such an incident caused the failure of the whole run, due to lack of knowledge of the lag period.

SECTION VII

MATHEMATICAL FORMULATION

Detailed analysis of an air bubble plume is virtually impossible due to the many variables associated with it. Taylor and his colleagues (25), as mentioned earlier, presented the first thorough description of the plume. Cederwall (8) adopted the techniques of Taylor with the assumption of compressible fluid rather than incompressible fluid assumed by Taylor. However, neither of the above authors nor other investigators have attempted to consider an important variable, which is the mass transfer and the associated changes in the plume's characteristic parameters; i.e. velocity or rise, radius of the plume, and energy.

Most bubble plume mathematical formulations have been made in conjunction with high intensity air injection rates where gas transfer was minor. The concept of hypolimnion aeration with commercial oxygen of necessity incorporates significantly lower oxygen injection rates and essentially complete absorption. Therefore, mass transfer must be incorporated into the plume hydrodynamics.

This work will adopt the techniques of Taylor and Cederwall (25, 8) and the following assumptions.

1. All bubbles produced are of the same volume and no coalescence takes place.
2. At any cross section, change in volume of each bubble due to mass transfer is the same regardless of its location in the plume.
3. No mass transfer occurs between the mathematical source and the actual source.
4. The number of bubbles produced per unit time is constant.
5. The rate of entrainment is constant, not proportional to center line velocity.
6. Vertical velocity and buoyancy force in a horizontal cross-section are of similar form at all heights and assumed Gaussian.
7. Water density is constant (no density gradient).

Preceding page blank

8. The bubbles are compressible and their expansion is isothermal.

Governing Equations

Zero Slip Velocity

The governing equations for a three-dimensional symmetrical bubble plume in ambient fluid are:

Rate of water discharge $= Q = \int_A V dA$ (36)

Water momentum flux $= M = \int_A \rho_m V^2 dA$ (37)

Air-water buoyancy flux $= B = \int_A (\rho_w - \rho_m) V dA$ (38)

Water kinetic energy (K.E.) flux $= \int_A (\rho_w V^3)/2 dA$ (39)

where:

V = local plume velocity

ρ_w = ambient water density, (surrounding the plume)

ρ_m = air-water mixture density

A = cross-sectional area

Since no measurements of the velocity or density distribution across the plume were made, the assumption used by other investigators (8, 25, 20) i.e. Gaussian will be used here.

$$V = V_c e^{-r^2/b^2} \quad (40)$$

$$(\rho_w - \rho_m) = \Delta\rho_m e^{-r^2/(\lambda b)^2} \quad (41)$$

where:

V_c = center line velocity of the plume

r = lateral co-ordinate

b = nominal half-width of the plume related to the deviation of the velocity distribution by $2\sigma = \sqrt{2}\, b$

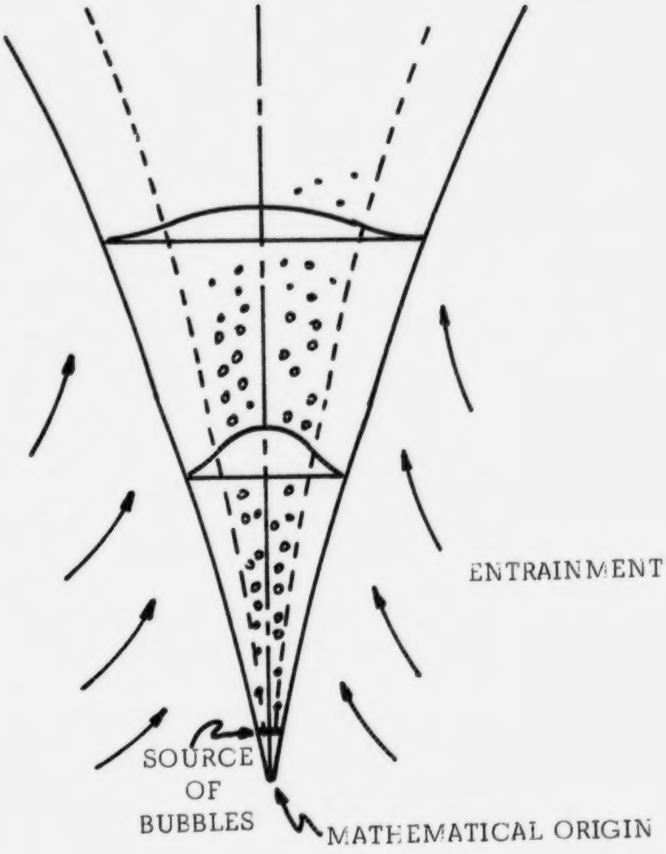
ENTRAINMENT
SOURCE OF BUBBLES
MATHEMATICAL ORIGIN

Fig. 14 DEFINITION SKETCH

λ = a non-dimensional parameter representing the ratio of sideway spread between the velocity and the density profile.

Solution of Equations 36 through 39 using the velocity and density distribution assumed above leads to

$$\text{water flow} = Q = \int_o^\infty 2\pi V r dr = 2\pi \int_o^\infty V_c e^{-r^2/b^2} rdr$$

$$= 2\pi \int_o^\infty V_c\, e^{-r^2/b^2} rdr = \pi V_c b^2 \qquad (42)$$

$$\text{air-water jet momentum flux} = M = \int_A \rho_m V^2 dA$$

$$= 2\pi\rho_m \int_o^\infty (V_c e^{-r^2/b^2})^2\ rdr = \pi V_c^{\,2} \rho_m b^2/2 \qquad (43)$$

Making the Boussinesq assumption that density difference may be neglected except in buoyancy terms, $\rho_m \simeq \rho_w$ in Equation 43; thus

$$M = \pi V_c^{\,2} \rho_w b^2/2 \qquad (44)$$

The buoyancy equation for a zero slip velocity is

$$B = \int_o^\infty 2\pi (V)\ (\rho_w - \rho_m)\ rdr = 2\ V_c \Delta\rho_m \int_o^\infty e^{-r^2/b^2} \cdot e^{-r^2/(\lambda b)^2} \qquad (45\ a)$$

$$B = \pi V_c \Delta\rho_m\ (\lambda^2 b^2/1 + \lambda^2) \qquad (45\ b)$$

The kinetic energy flux is

$$\int_o^\infty \pi\, (V_c e^{-r^2/b^2})^3\ \rho_w rdr \qquad (46\ a)$$

$$= \pi\ V_c^3\ \rho_w \int_o^\infty (e^{-r^2/b^2})^3\ rdr = \pi V_c^3\ \rho_w b^2/6 \qquad (46\ b)$$

In all the above equations V_c, $\Delta\rho_m$, and b (the radius) are the unknowns.

However, considering a small segment of the plume of a thickness dx, the water flux is

$$dQ = 2\pi b\, dx(V_H) \qquad (47)$$

where V_H is the horizontal flow velocity related to the vertical center line velocity by a constant such that $V_H = \alpha V_C$ where α is constant and equal to the entrainment coefficient. Thus equation 47 becomes

$$dQ/dx = 2\pi b(\alpha V_c) \qquad (48)$$

The driving force of the plume is the buoyancy and the momentum flux is

$$dm/dx = \int_o^\infty 2\pi(\rho_w - \rho_m)grdr$$

$$dm/dx = \pi b^2 g\Delta\rho_m \lambda^2 \qquad (49)$$

The buoyancy at any level x above the diffuser is

$$B = q_o(\rho_w - \rho_a)\, H_o/(H_o + H - x) \qquad (50\ a)$$

where:

H_o = piezometric head equivalent to the atmospheric pressure

H = depth above diffuser

q_o = air flow rate at atmospheric pressure

since $\rho_a << \rho_w$

$$B = q_o\,(\rho_w)\, H_o/(H_o + H - x) \qquad (50\ b)$$

equating equations 45 and 50 gives

$$\pi V_c \Delta\rho_m\,(\lambda^2 b^2)/(1 + \lambda^2) = q_o(\rho_w)\, H_o/(H_o + H - x) \qquad (51)$$

and equating equations 49 and 44 yields

$$d/dx(\pi V_c^2 \rho_w b^2/2) = \pi b^2 g\Delta\rho_m \lambda^2$$

or

$$d/dx\,(V_c^2\,b^2) = 2b^2 g\,(\Delta\rho_m/\rho_w)\,\lambda^2 \qquad (52)$$

which upon rearrangement yields

$$\Delta\rho_m/\rho_w = d/dx\,(V_c^2\,b^2)\,/2b^2 g\lambda^2 \qquad (53)$$

but from 51

$$\Delta\rho_m/\rho_w = q_o\left(\frac{H_o}{H_o + H - x}\right)/\pi V_c\,\lambda^2 b^2/(1 + \lambda^2) \qquad (54)$$

equation 53 and 54 yields

$$d/dx\,(V_c^2 b^2)\,/2b^2 g\lambda^2 = \frac{q_o\left(\dfrac{H_o}{H_o+H-x}\right)}{\pi V_c\left(\dfrac{\lambda^2 b^2}{1+\lambda^2}\right)}$$

$$d/dx\,(V_c^2 b^2) = \frac{2gq_oH_o}{(H_o+H-x)\dfrac{\pi V_c}{1+\lambda^2}} = \frac{2gq_oH_o\,(1+\lambda^2)}{\pi(H_o+H-x)V_c} \qquad (55)$$

also from 42 and 48

$$\frac{d(\pi V_c b^2)}{dx} = 2\pi b(\alpha V_c)$$

$$d/dx\,(V_c b^2) = 2b\alpha V_c \qquad (56)$$

In equations 55 and 56, assuming that values could be assigned for α and λ the only two unknowns are b and V_c. However, the above two equations cannot be solved in a close form but rather a step - by - step integration must be used to solve them for the unknowns.

The first step is to reduce the equations in the following form.

$$\frac{d(b)}{dx} = 2\alpha - \frac{gq_oH_o(1+\lambda^2)}{\pi(H_o+H-x)bV_c^3} \qquad (57)$$

$$\frac{d(V_c)}{dx} = \frac{2gq_oH_o(1+\lambda^2)}{\pi(H_o+H-x)\,b^2V_c^2} - 2\alpha\frac{V_c}{b} \qquad (58)$$

The term q_o in equations 57 and 58 is the gas flow rate which is equivalent to the number of bubbles of known volume produced per unit time, i.e.

$$q_o = n\pi D^3/6 \qquad (59)$$

where: n = number of bubbles produced per unit time

D = diameter of bubbles produced

However, the diameter due to mass transfer is a function of x, (D_x). Thus substituting this equality in equations 57 and 58 yields

$$\frac{d(b)}{dx} = 2\alpha - \frac{g\left(\frac{n\pi D_x^3}{6}\right)H_o(1+\lambda^2)}{\pi(H_o+H-x)\,bV_c^3} \qquad (60)$$

$$\frac{dV_c}{dx} = \frac{2g\left(\frac{n\pi D_x^3}{6}\right)H_o(1+\lambda^2)}{\pi(H_o+H-x)\,b^2V_c^2} - 2\,\alpha\,\frac{V_c}{b} \qquad (61)$$

Cederwall and Ditmars (8) normalized equations 57 and 58 and used numerical integration to solve for the unknowns. Solution of equations 60 and 61 was also by numerical integration. However, the introduction of the new variable D_x and calculating its changes with depth for each step used in the numerical integration was found best to be done by setting up a computer program to solve first for the diameter at each step and supply that to equations 60 and 61 to solve for the other two variables.

Before proceeding in describing this computer program, a comment on some of the assumptions and determing the values of α and λ seems to be necessary.

Bubble size is uniform

The diffusers used in this study which were described earlier and according to manufacturers' claims and visual observation do seem to produce uniform initial bubbles and almost no coalescence. This assumption was necessary to simplify the solution and any other assumption would have been impossible to verify.

Bubble volume due to mass transfer is reduced

It is true that the bubbles at the side of the plume will be reduced in volume at a faster rate than those at the center and any distribution like Gaussian could be adopted, but again the verification of this is very difficult, if not impossible. However, considering the fact that there is hardly any variation in deficit across the plume, this assumption is acceptable.

No mass transfer occurs between the mathematical origin and the actual source

The mathematical origin which is a function of the properties of the diffuser is considered here a constant = 1.0 meter. This increase in depth is incorporated in the solution of the differential equations. However, the injection depth is considered to be the actual diffuser depth and mass transfer calculation is based on that assumption. Thus no mass transfer was considered to take place in that region.

The number of bubbles produced per unit time is constant

Control of the flow rate and equal distribution of flow across the diffuser makes this assumption acceptable.

The rate of entrainment is constant

There is no way to verify this assumption or even to measure it under the experimental conditions on the lake. The coefficient used in this analysis is that derived by Cederwall (8) as illustrated in Figure 15, based on the experimental observation of Kobus (20).

The velocity and buoyancy force distribution at all levels is similar

Difficulties encountered in running the experiment made it impossible to verify this assumption. However, Kobus (20) did measure the velocity

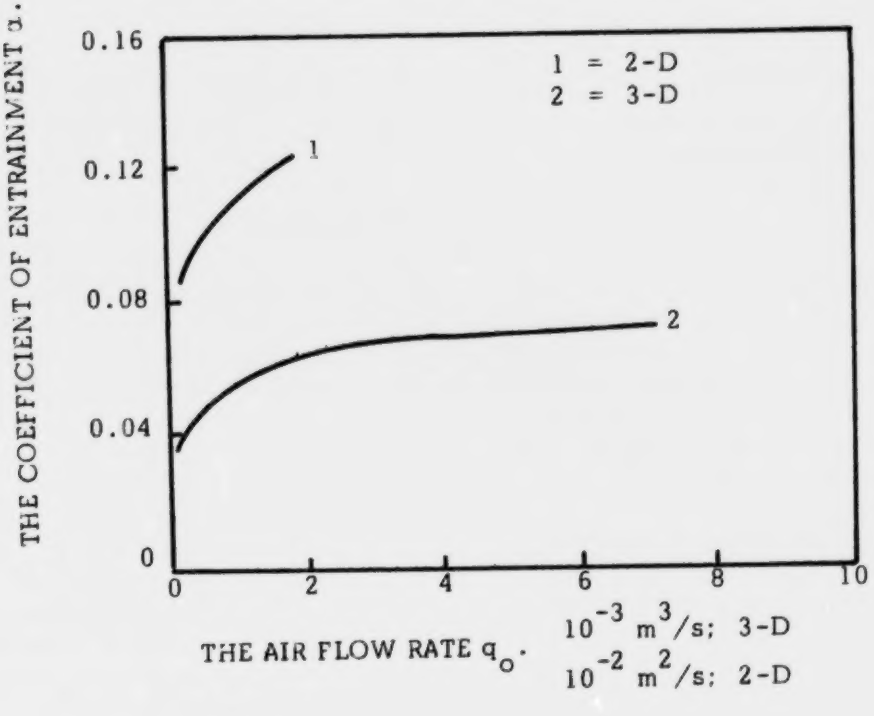

Fig. 15 THE COEFFICIENT OF ENTRAINMENT AS A FUNCTION OF THE AIR FLOW RATE FOR TWO- AND THREE-DIMENSIONAL AIR BUBBLE PLUMES (CEDERWALL (8))

distribution in a small scale lab experiment and found it to be Gaussian. Other investigators (8, 15, 33) also used this assumption.

The ambient water condition is uniform

A study of a typical temperature profile of a deep stratified reservoir, Figure 1, and the almost constant temperature below the metalimnion makes this assumption acceptable.

The bubbles are compressible

Expansion of rising air bubbles is neither adiabatic nor truly isothermal. However, for the sake of simplicity the assumption of isothermal conditions is adopted.

The spreading ratio (λ) is constant

Cederwall et al. (8), in a photographical recording of air bubble plumes found that the lateral spreading of the air bubbles is slow relative to the expansion of the plume. They concluded that the λ is fairly constant throughout the rise of the plume and of a magnitude of about 0.2. This value was used in this work. Other values of 0.1 and 0.3 were also tested by Cederwall and in this work, but showed practically no difference in results.

Slip Velocity Consideration

The previous mathematical formulation of the governing equations of the water-bubble plume, considered the velocity of the bubbles relative to the surrounding water (slip velocity) to be zero. This section will incorporate the slip velocity and present the differential equations governing this consideration. Essentially the governing equations are the same except in equation 45 a, the conservation of buoyancy. The velocity term is of two components; local plume velocity (V), and the velocity of the rising bubbles relative to the water (V_b). This consideration leads to

$$B = \int 2\pi (V+V_b)(\rho_w - \rho_m)\, r dr \tag{62}$$

$$= V_c \Delta\rho_m \frac{\lambda^2 b^2}{1+\lambda^2} + V_b \Delta\rho_m \lambda^2 b^2 \tag{63}$$

which is equal to the buoyancy flux at any level (equation 50), thus

$$\pi V_c \Delta\rho_m \frac{\lambda^2 b^2}{1+\lambda^2} + \pi V_b \Delta\rho_m \lambda^2 b^2 = q_o \rho_m \frac{H_o}{H_o+H-x} \qquad (64)$$

continuing the solution in the fashion presented earlier for zero slip gives the final two equations to be solved:

$$\frac{d(V_c b^2)}{dx} = 2\alpha V_c b \qquad (65)$$

$$\frac{d(V_c^2 b^2)}{dx} = \frac{2gH_o(n\pi D^3/6)}{\pi(H_o+H-x)\left(\frac{Vc+Vb}{1+\lambda^2}\right)} \qquad (66)$$

which yield

$$\frac{db}{dx} = 2\alpha - \frac{g\left(\frac{n\pi D^3}{6}\right) H_o}{\pi V_c^2\, b(H_o+H-x)\left(\frac{V_c}{1+\lambda^2} + V_b\right)} \qquad (67)$$

$$\frac{dV_c}{dx} = \frac{2g\left(\frac{n\pi D^3}{6}\right) H_o}{\pi V_c b^2(H_o+H-x)\left(\frac{V_c}{1+\lambda^2} + V_b\right)} - \frac{2\alpha V_c}{b} \qquad (68)$$

Equations 67 and 68 cannot be solved in a closed form and thus a numerical integration has to be used to solve for the unknowns.

Cederwall and Ditmars (8) in their solution assumed that at x = 0 $V_c >> V_b$ and reduced the equations accordingly. They also used the value of V_b = constant = 0.3 meters per second based on Kobus' (20) observation reproduced in Figure 16. The values presented by Kobus are a function of the air flow rate. It also shows that the orifice diameter is not a factor in the velocity of rise. Haberman and Morton (17) observed that proximity could affect the speed of the rising bubbles. But they did not pursue this fact and no measurement was taken.

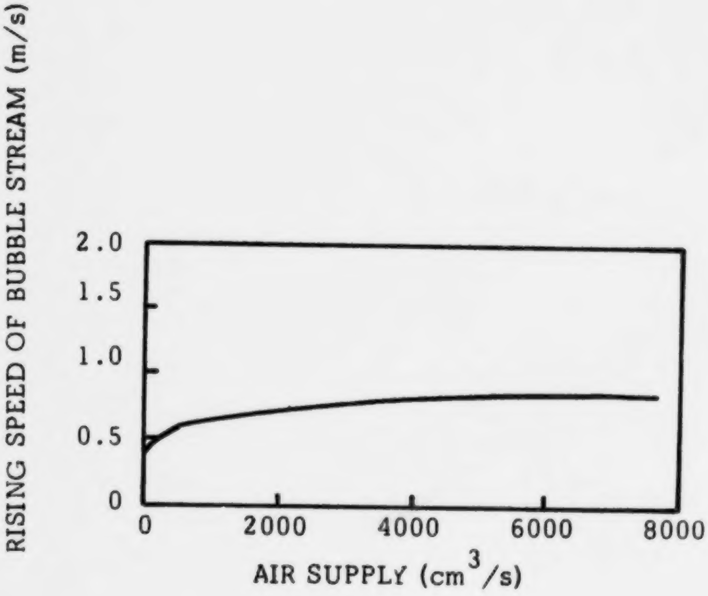

Fig. 16 AVERAGE RISING SPEED OF BUBBLE STREAM FROM A SINGLE ORIFICE. (KOBUS (20))

Since no measurement of the velocity of rise of the bubble column relative to the water as a function of the bubble diameter, which is an important factor, was made in this study, the results of the measurement of Haberman and Morton (17), although for single bubbles, will be used here. These results are presented in Figure 3 and approximated by the equations

$$V_b = 24.4 \times D \text{ in cm/sec for } 0.0 < D < 0.72 \text{ mm.}$$

$$V_b = 17.6 + \frac{(D - 0.72)}{0.03 + 0.156\,(D - 0.72)} \quad \text{for } 0.72 < D < 5 \text{ mm.}$$

where D is the bubble diameter. Thus V_b is a function of the bubble diameter and will be used as such in solving the differential equations.

Description of Computer Model

This program consists of a main program and three sub-programs which will be described below.

Program HYPO

This program, which is based on the oxygen mass transfer equation,

$$dM/dt = k_1 A\,(c_s - c_a)$$

calculates the mass of oxygen transferred from the bubbles to the surrounding water for a given increment of time or a given height of rise. It also calculates the new volume of the bubble after mass transfer has taken place. The program accounts for bubble expansion due to reduction in hydrostatic head and accounts for transfer of nitrogen gas from the water to the rising bubbles. The program was developed by Speece (39) and was verified with actual field data in connection with this project, Hypolimnion Aeration. This program calls HYDRO, the first sub-program, and supplies it with the calculated diameter values.

Sub-program HYDRO

This program, which acts as the main program if no mass transfer was considered, is to supply the next sub-program with the initial conditions and other parameters before it calls the next sub-program RKAM. With the values of the variables being calculated and stored it solves for the water flow rate, momentum, kinetic energy flux and increase in D.O.

Sub-program RKAM

This sub-program, which is a general routine for solving up to ten simultaneous first - order differential equations, is written by the computation center at U.T. at Austin, but was modified to suit the new conditions. This program uses the Runge - Kutta procedure which is a self-starting single step method, and the Adams - Maulton procedure which is a multistep method which requires a self-starting method (Runge - Kutta) together with a predictor formula (Adams - Bashforth). The program carries out error analysis and doubles or halves the size of the step if necessary to keep the results within certain bounds of error set by the user. However, this program was forced to use only the indicated step value with no halving or doubling of the step size so as to match the step used in HYPO. This program calls the next sub-program F.

Sub-program F

This is a listing of the differential equations to be solved.

Sub-program VELB (DYAM)

This sub-program is added in case of slip velocity considerations and equations 67 and 68 will replace 60 and 61 in sub-program F.

Thus the program HYPO solves for the diameter at each step and supplies HYDRO with those values to solve the two differential equations. The final output is either in the form of listing or a plot by calling a system routine (PLOTT). This routine won't be described here nor will listing of it be included in the listing of the program in Appendix. However, a write-up on that routine is available from the computation center at U.T. at Austin.

To start the integration process of equations 60 and 61, initial values of the two dependent variables for a corresponding value of the independent variable should be specified. Solution of the simple plume equations was used in predicting the initial velocity of rise.

$$V_c = \left[\frac{25\, g q_o H_o\, (1+\lambda^2)}{24\, \alpha^2\, \pi (H_o + H)} \right]^{1/3} x^{-1/3} \qquad (69)$$

where x corresponds to the height above the mathematical source. This value, which is a function of the properties of the source used, was found by Kobus (20) to be 0.8 meter. In this study this depth was considered to be equal to 1.0 meter, and thus the velocity was calculated accordingly. The corresponding radius of the plume was considered to be equal to the actual source.

Integration Step Length

To carry out the numerical integration of the two differential equations, a step size should be indicated. As mentioned earlier, the program can vary the step size to keep the error within a set limit. However, this was not possible in considering the mass transfer, so the step size was taken to be fixed at a value of 0.1 meter. The single step error associated with this step size was of the order of 10^{-10} - 10^{-13} which is a negligible error. Larger steps could be used at a larger error. However, for small bubble size, e.g. 0.2 mm., the step should be as small as possible to account for the time of contact. Thus it is up to the user to indicate the step size required.

SECTION VIII

EXPERIMENTAL OBSERVATIONS

As mentioned previously, the general purpose of this investigation was to measure the velocity of rise of the buoyant plume, and the circulation pattern generated by such a plume through measurement of the dispersion of the Rhodamine B dye.

Velocity of Rise

Measurement of the velocity of rise of the water-bubble column was taken by the procedure outlined earlier. In spite of the frequent runs made (over 50 runs), only a few meaningful results were obtained. The run was considered successful if the lag time was established accurately and the results obtained were duplicated in at least two more runs under the same conditions. Table 1 shows the experimental results obtained for the velocity of rise using the P.V.C. (2 mm bubbles) at three flow rates and different injection depths. Two measurements at 1.0 and 2.0 l/min at a depth of injection of 30 feet using the ceramic diffuser (0.2 mm bubbles) yielded a velocity of rise of 0.042 and 0.06 m/sec at 20 feet above the diffuser. The latter reported observations were duplicated once. Other results are not reported as they were not possible to duplicate and were considered unreliable.

General

At quiescent conditions and at gas flows of 1.0 and 2.0 l/min the bubble plume showed good stability and was observed at the surface directly above the diffuser. Measurements of the water-bubble column radius were not possible under the conditions of the experiment. The bubble column at shallow injections (low mass transfer) showed quite a spread and was symmetrical. However, at higher injection depths, the observed diameter of the bubble plume at the surface was much less. Bubble size associated with deep injections was at least an order of magnitude less than those for shallow injection depths. Many bubbles from the P.V.C. diffuser (2 mm) did surface from an injection depth of 90 feet, and a flow

Preceding page blank

TABLE 1

Measured Center Line Velocity of Rise Using P.V.C. Diffuser (2 mm Bubbles)

Flow Rate 1 / min	Injection Depth	Distance of Rise (ft)	Measured Velocity cm /sec
0.75	60	20	10.4
0.75	60	60	9.3
2.0	60	20	15.4
2.0	60	40	11.4
2.0	60	60	10.8
1.0	30	30	12.2
2.0	30	30	17.8

rate of 2 l/min but at a much smaller volume than when generated at the diffuser. Most of the bubbles from the ceramic diffuser were absorbed before reaching the surface. Only a very minor number of larger bubbles surfaced. These large bubbles were attributed in part to coalescence due to the presence of the bands strapped around the diffuser and the balancing lines (Figure 10), and in part attributed to not having the diffuser perfectly horizontal. No measurement of bubble diameters were made.

Induced Mixing and Circulation

In this work, an attempt was made to study experimentally the induced mixing and circulation. The experimental procedure is covered in Section VI.

The sampling was carried out at several points away from the diffuser. The farthest was 110 feet away. The dye was detectable at that distance from the diffuser more than two hours from injection time. Typical results are shown in Figure 17.

Since almost no movement exists in the hypolimnion, one could reason that the only way that the dye reached that distance is the induced mixing and turbulence generated by the rising plume. In an attempt to measure the diffusion coefficient for such a case, the continuous sampling gate was used on the fluorometer and continuous sampling 40 feet away from the diffuser was conducted. A plot, for this observation, of concentration vs. time at a sampling depth of 75 feet and an injection depth of 90 feet is shown in Figure 18. During the sampling period, tests for concentration at other depths were carried out. The concentration of dye from the surface to a depth of 55 - 60 feet was almost zero and increased suddenly beyond that level. This observation and consideration of the temperature profile (Figure 19) for the lake during that period, substantiate the complete uncoupling hypothesized by Cederwall et al. (8) and shown graphically in Figure 7.

Another thing that was noticed and is shown in Figure 18 was that after going down, the dye concentration started going up again and stayed almost at the last level for over half an hour before starting to go down again. This impulse-like behavior was so often observed that the idea of calculating a diffusion coefficient for this system was dropped. However, a listing of the collected data on the induced mixing and circulation is included in the Appendix (Part A).

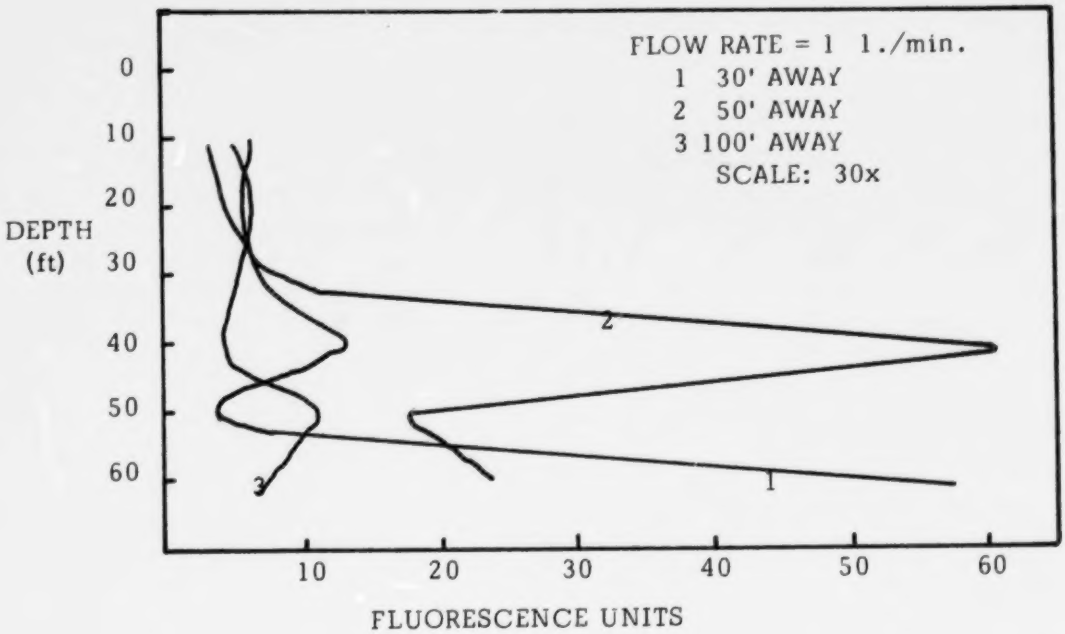

Fig. 17 DYE CONCENTRATION AT VARIOUS DEPTHS AND DISTANCES AWAY FROM THE DIFFUSER.

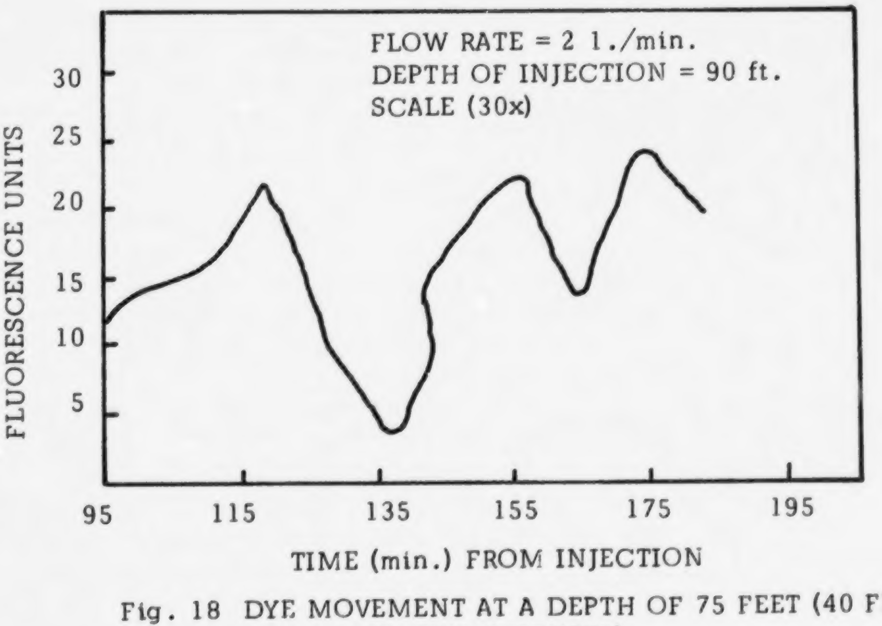

Fig. 18 DYE MOVEMENT AT A DEPTH OF 75 FEET (40 FEET AWAY FROM THE DIFFUSER).

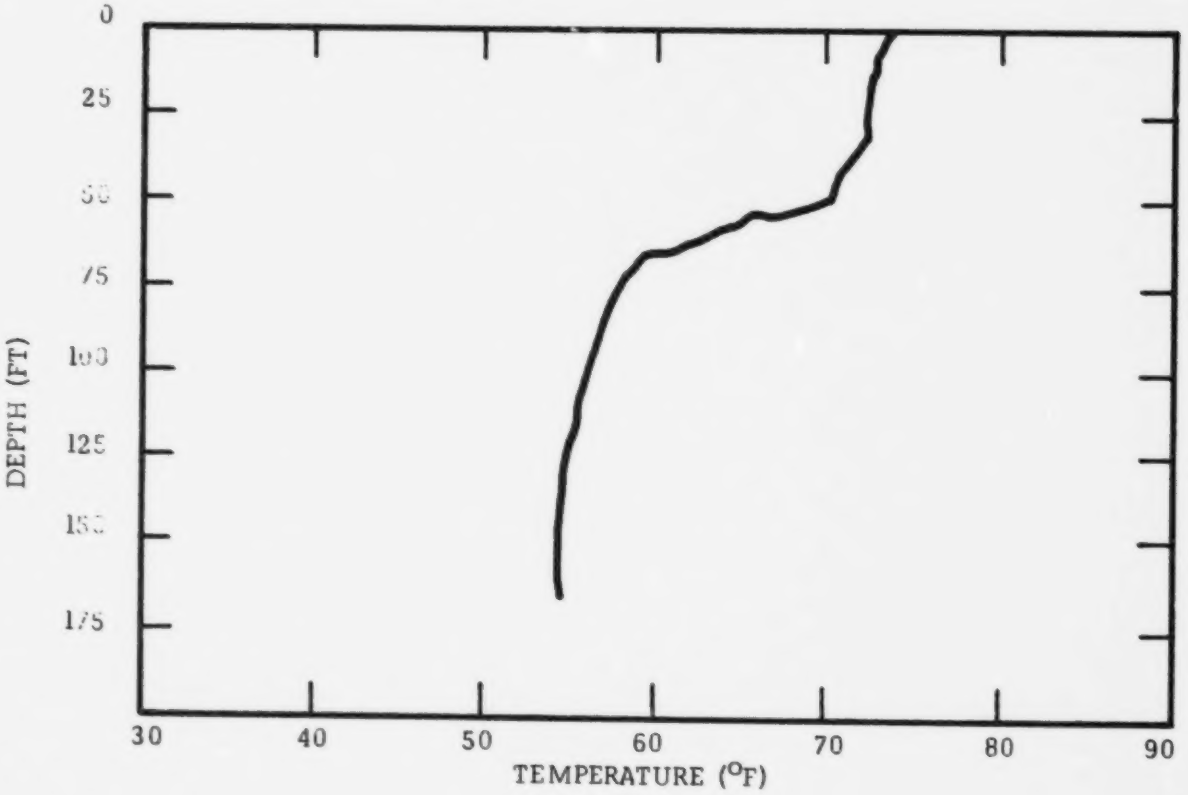

Fig. 19 TEMPERATURE PROFILE OF LAKE TRAVIS - MAY 14, 1972

SECTION IX

DISCUSSION

In the following discussion the model with mass transfer will be referred to as Model One and the model with no mass transfer will be referred to as Model Two.

Comparison With Experimental Results

Center line velocity was the only variable measured experimentally. Thus comparison with the model prediction will be only for this variable. Table 2 lists the field observations and the model prediction with mass transfer as compared with the no mass transfer case. Graphical comparison is also shown in Figures 20 and 21. This prediction is based on zero slip velocity and an entrainment coefficient of 0.03. As can be seen from the table and the graphical representation, the prediction of the model with mass transfer is in very good agreement with the field observation. For an oxygen flow rate of 0.75 l/min at an injection depth of 60 feet, the model prediction was within 5.8% and 9.7% of the measured velocity at two sampling depths. Moreover, for a flow rate of 2 l/min at an injection depth of 60 feet, the model prediction was within 0% to 7.5% of the measured velocity at three different levels. The model prediction for a flow rate of 1.0 l/min at a depth of 30 feet is within 13% of the measured velocity, but was within 2.5% for a flow rate of 2 l/min at the same injection depth.

Since consideration of slip velocity means less entrainment, the model prediction with mass transfer and non-zero slip velocity fit the field data at an entrainment coefficient of approximately 0.02.

Thus the model is in excellent agreement with the field observation at the three oxygen flow rates used as demonstrated above.

Effect of Entrainment Coefficient

To demonstrate the effect of the value of the entrainment coefficient on the prediction of the dynamic characteristics of the plume, three different

TABLE 2

Measured and Computed Velocity of Rise for a 2.0 mm Bubble Plume

Flow Rate l/min	Injection Depth	Distance of Rise	Measured Velocity cm/sec	Computed* Velocity with mass transfer cm/sec	Computed* Velocity without mass transfer cm/sec
0.75	60	20	10.4	11.0	13.0
0.75	60	60	9.3	8.4	11.96
2.0	60	20	15.4	15.3	18.04
2.0	60	40	11.4	12.2	16.5
2.0	60	60	10.8	11.6	16.5
1.0	30	30	12.2	13.8	16.2
2.0	30	30	17.8	17.36	20.45

*Computed velocities considering zero slip and an entrainment coefficient of 0.03

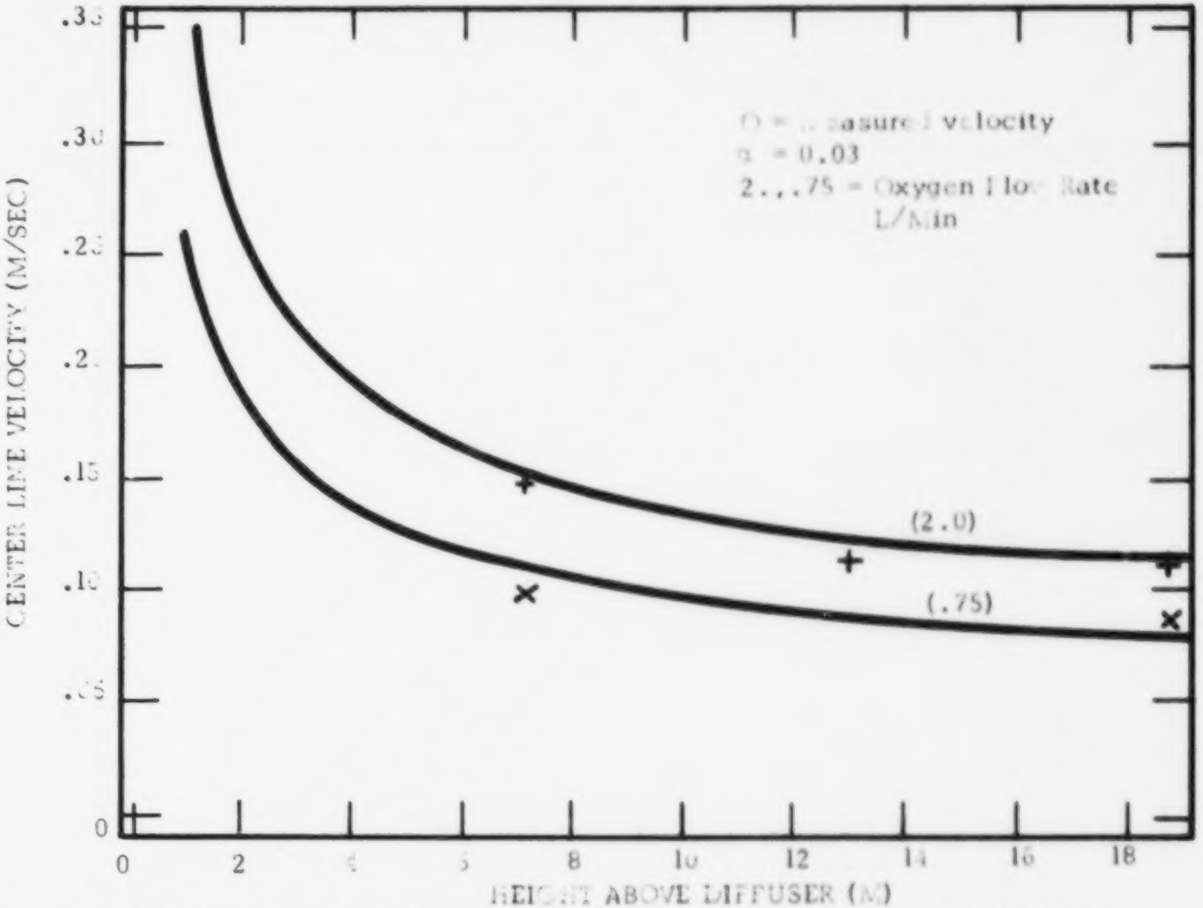

Fig. 20 MEASURED AND PREDICTED CENTER LINE VELOCITY FOR 0.75 AND 2.0 L/MIN OXYGEN FLOW RATE AND AN INJECTION DEPTH OF 60 FEET (2 MM BUBBLE)

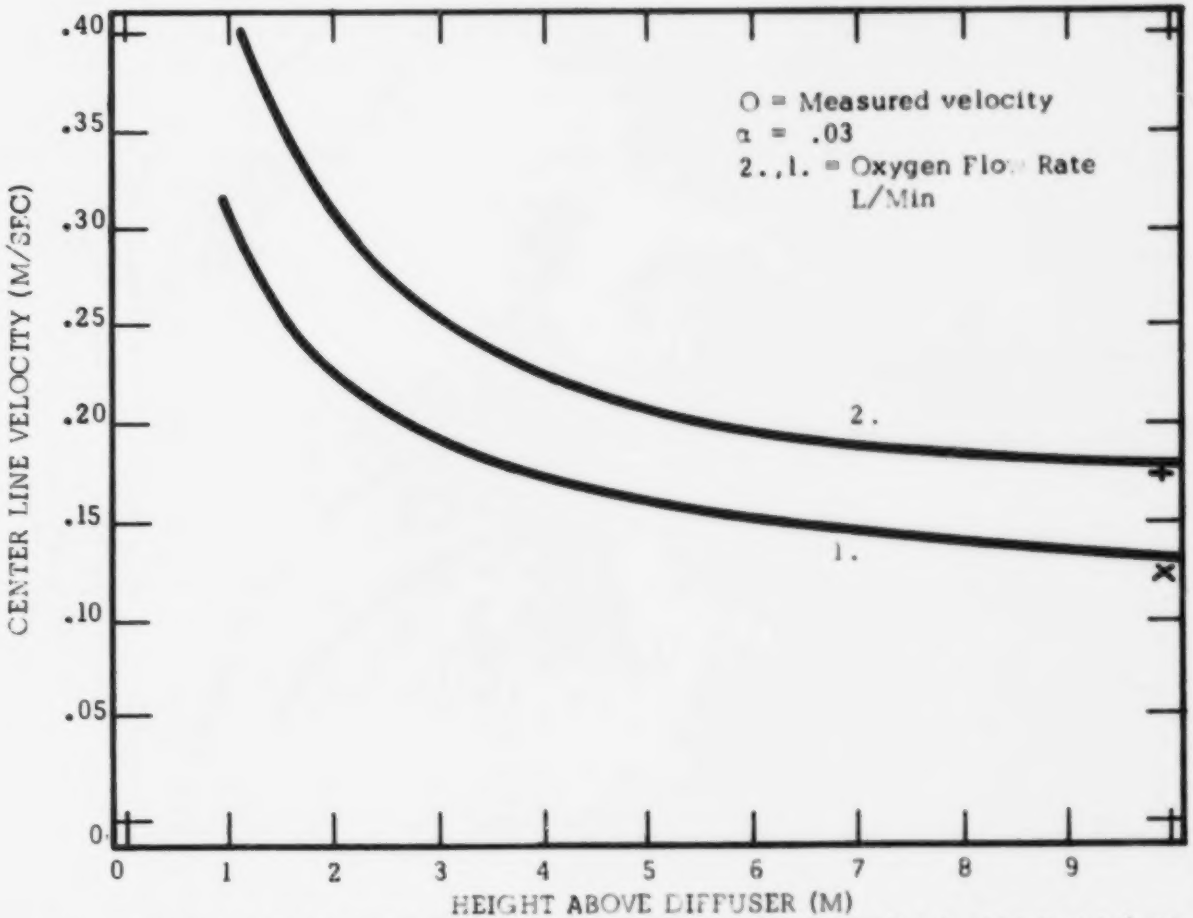

Fig. 21 MEASURED AND PREDICTED CENTER LINE VELOCITY FOR 1.0 AND 2.0 L/MIN AND AN INJECTION DEPTH OF 30 FEET (2.0 MM BUBBLE)

values of 0.01, 0.03, and 0.05 for a constant oxygen flow rate were used. For an oxygen flow rate of 1 l/min, the results are shown graphically in Figures 22 and 24, for the half-width of the plume, velocity of rise, and water flow, respectively. The initial velocity was calculated based on Equation 69 and the initial half-width was assumed equal to 0.1 meter, and the initial bubble diameter was equal to 0.2 mm. A higher entrainment coefficient led to a lower velocity (Figure 23), but to a larger plume (Figure 22), and higher water flow rate, (Figure 24).

Thus the choice of the entrainment coefficient is very critical and more studies need to be made to evaluate this constant for more reliable prediction.

Comparison of the Two Models

Illustration of the prediction of Model One and comparison with the prediction of Model Two was found to be best done by an example.

Assume an impoundment 150 feet (46 m) deep with a metalimnion approximately 50 feet (15 m) below the surface. Using a 0.1 meter radius diffuser that produces 0.2 mm bubbles and an oxygen flow rate of 1.0 l/min, it is required to know the velocity, width, water flow rate, momentum flux, and kinetic energy flux at the metalimnion for an injection depth of 45 m. Compare the results to the case of no mass transfer. Compare the results if a 2.0 mm bubble diffuser was used instead of a 0.2 mm bubble one. Assume an entrainment coefficient of 0.03 for all cases and zero slip velocity. The models' predictions are shown graphically in Figure 25 through Figure 31.

Figure 25 shows that a 0.2 mm bubble was absorbed after rising a distance of 6.5 m while the 2.0 mm bubble had a residual size at the metalimnion of .87 mm. Of course, the model with no mass transfer did not account for such a condition. After the bubbles disappeared the two differential equations took the form

$$db/dx = 2\alpha \tag{70}$$

$$dV_c/dx = -2\alpha\,(V_c/b) \tag{71}$$

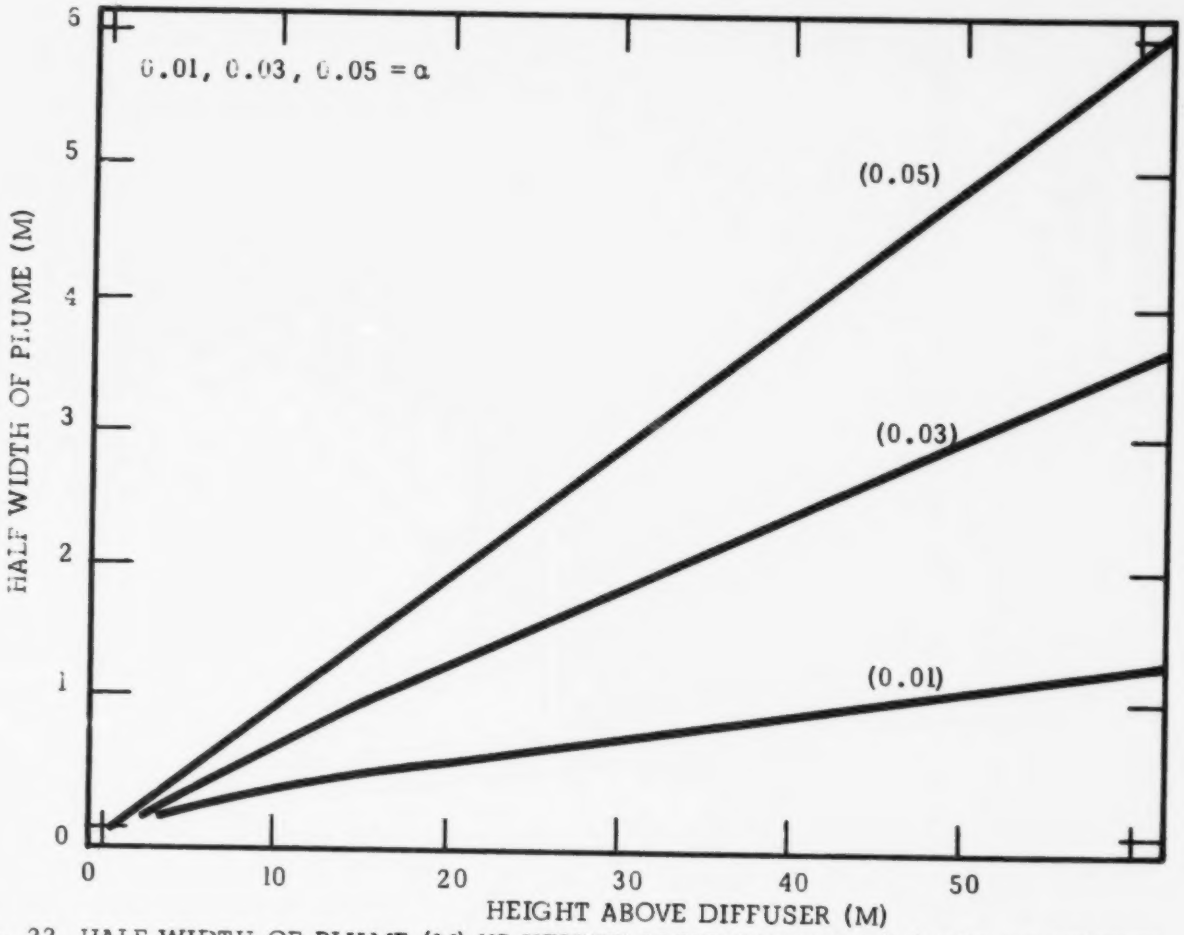

Fig. 22 HALF WIDTH OF PLUME (M) VS HEIGHT ABOVE DIFFUSER (M) FOR AN OXYGEN FLOW RATE OF 1 L/MIN AND AN INJECTION DEPTH OF 75 M AND AN ENTRAINMENT COEFFICIENT OF 0.01, 0.03, AND 0.05

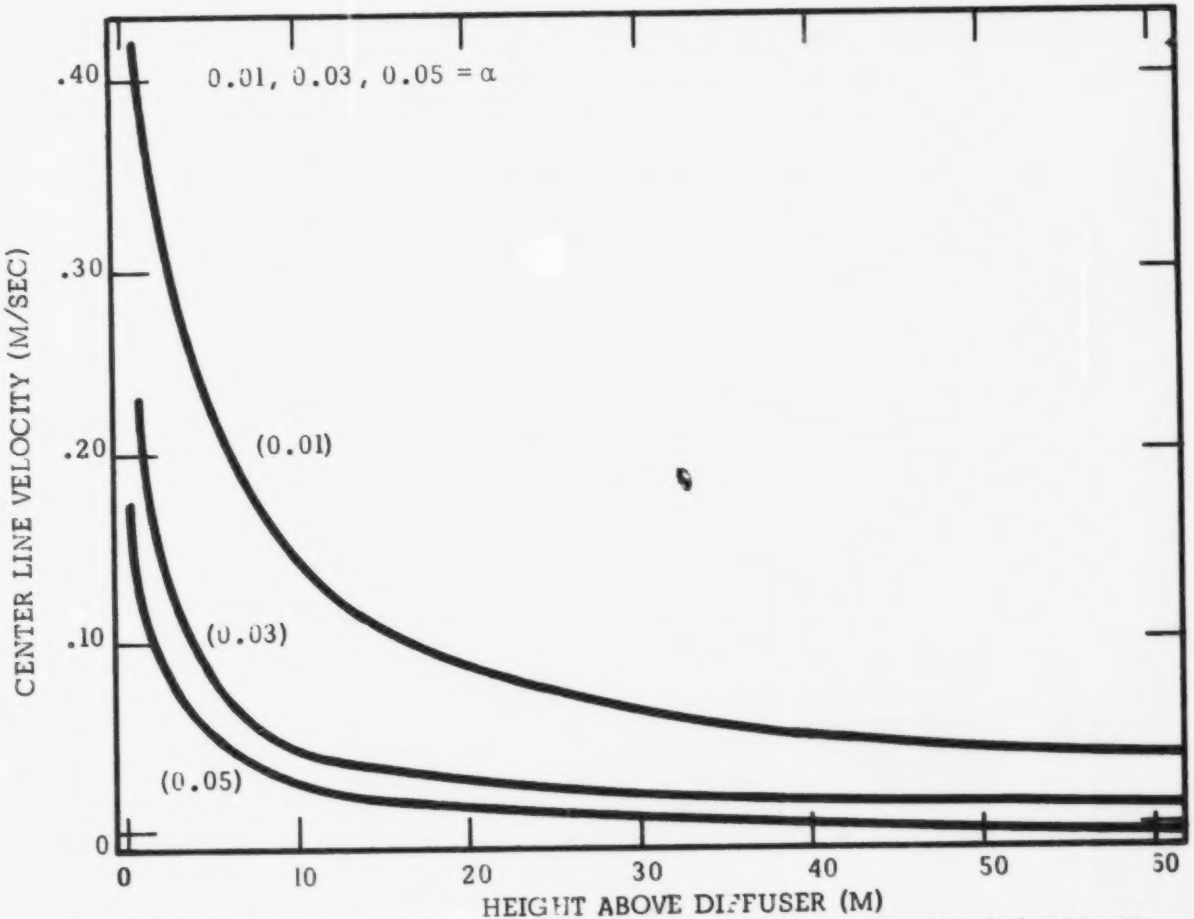

Fig. 23 CENTER LINE VELOCITY (M/SEC) VS HEIGHT ABOVE DIFFUSER (M) FOR AN OXYGEN FLOW RATE OF 1 L/MIN AND AN INJECTION DEPTH OF 75 M AND AN ENTRAINMENT COEFFICIENT OF 0.01, 0.03, AND 0.05

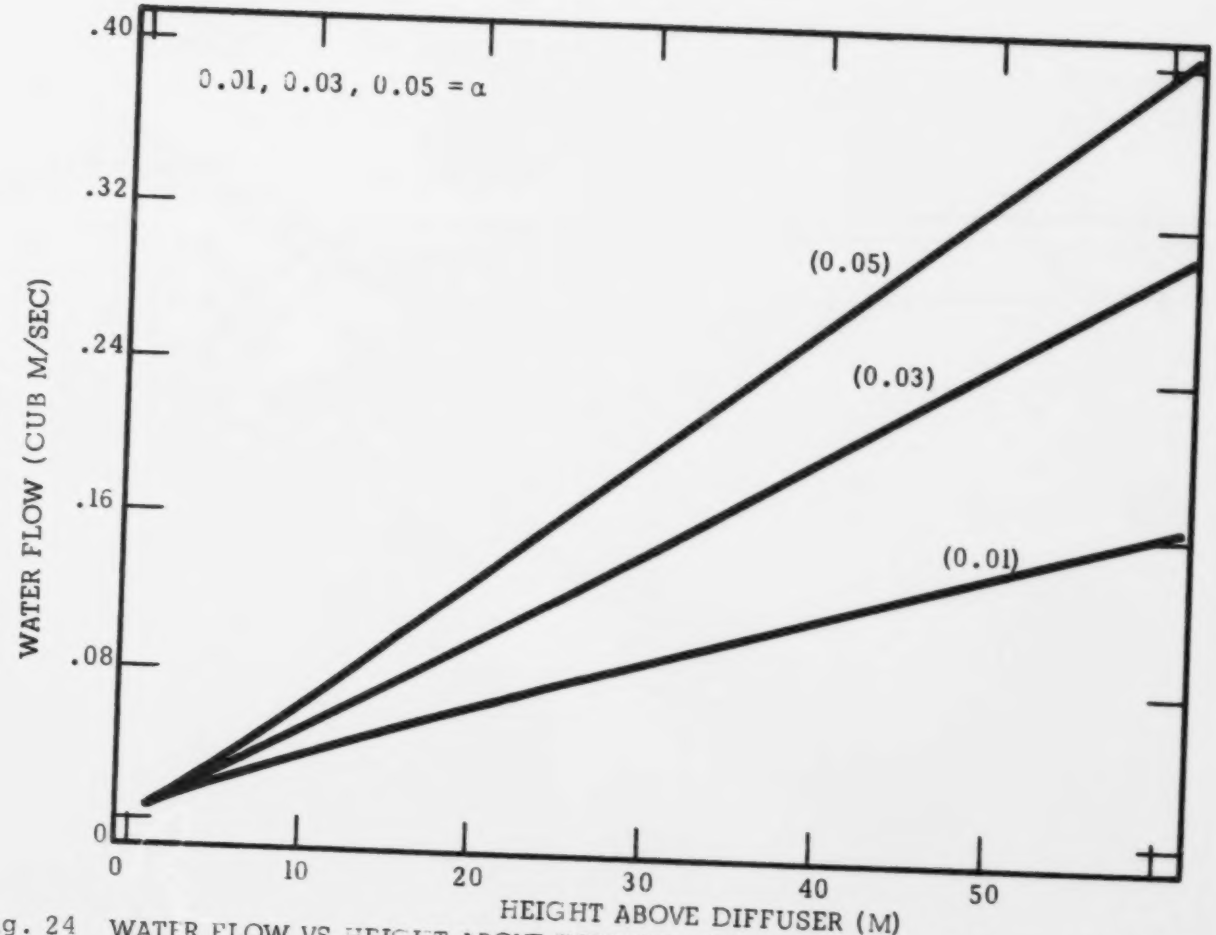

Fig. 24 WATER FLOW VS HEIGHT ABOVE DIFFUSER (M) FOR AN OXYGEN FLOW RATE OF 1 L/MIN AND AN INJECTION DEPTH OF 75M AND AN ENTRAINMENT COEFFICIENT OF 0.01, 0.03, AND 0.05

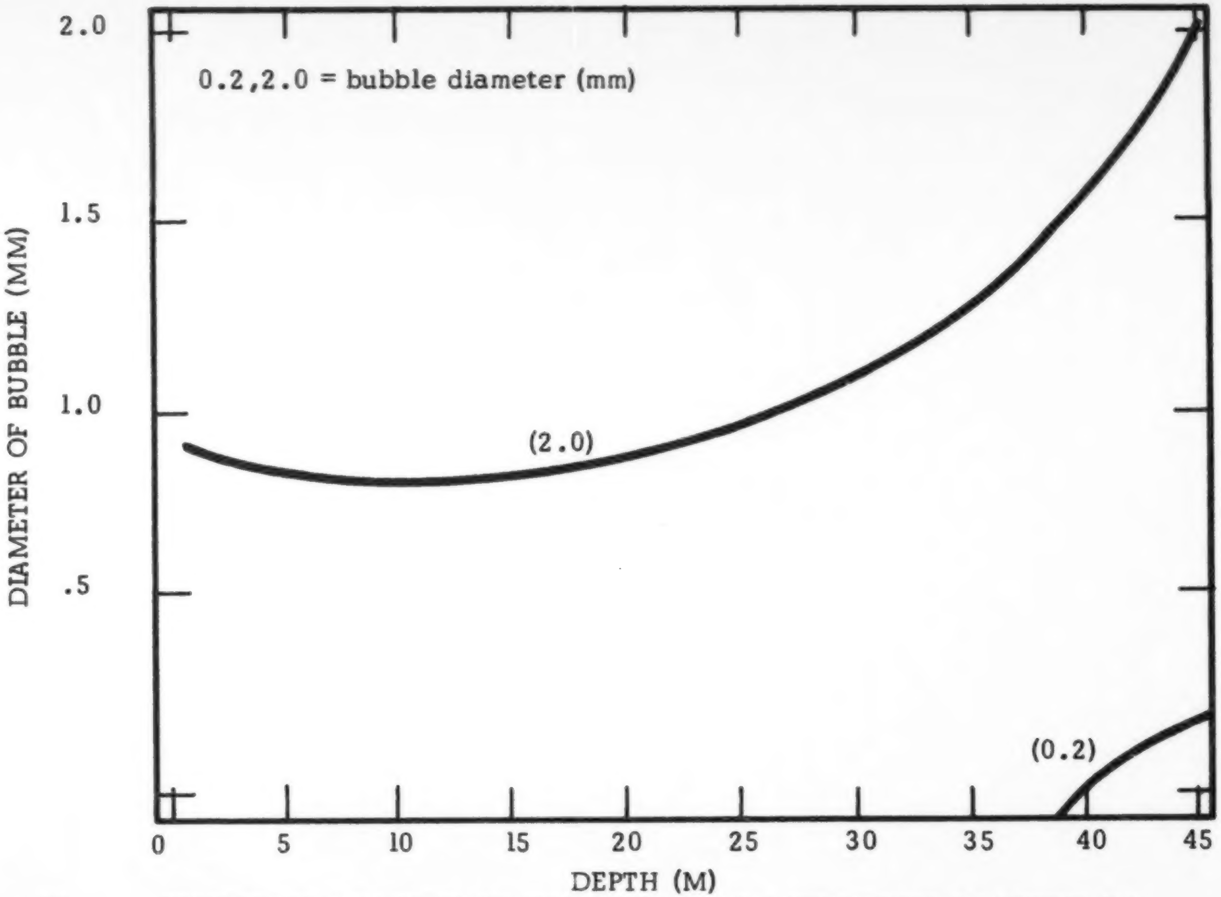

Fig. 25 PREDICTED DIAMETER OF BUBBLE (MM) AS A FUNCTION OF DEPTH (M) FOR 2.0 AND 0.2 MM BUBBLES AT AN INJECTION DEPTH OF 45 M

and the plume continued to rise driven by its momentum. The effect of the vanished buoyancy caused a faster deceleration of the 0.2 mm bubble plume compared to the 2.0 mm bubble or the no mass transfer case, Figure 26. The deceleration of the plume was considered by Albertson et al. (1) to be coupled with an acceleration of the surrounding fluid and an increase of the half-width of the plume causing the total flow rate of the flow past successive sections to increase with distance above the outlet. Such an increase in the diameter of the plume and the increased flow rate of the plume of the 0.2 mm bubble which continued to expand as a direct function of height (Equation 70) would be larger than the radius of the plume due to the 2.0 mm bubble and the no mass transfer case. Regardless of the larger radius, the water flow which is a function of the radius to the second power and the center line velocity, the water flow rate of the 0.2 mm bubble was the smallest of the two cases, while the no mass transfer was the largest, Figure 28. This demonstrates the effect of the high reduction in the velocity of rise of the plume for small bubbles. This effect was demonstrated also in the momentum flux of the plume, Figure 29. The momentum flux of the 0.2 mm bubble increased to the point where the bubbles were absorbed and then continued at a constant rate as shown to a larger scale in Figure 30. However, the momentum flux due to the 2.0 mm bubble plume continued to increase with height but still at a lower rate than the no mass transfer case. This was also demonstrated in the kinetic energy flux which is a function of the velocity to the third power. This led to a decrease in the kinetic energy flux with height for the 0.2 mm bubble plume and a slight increase for the 2.0 mm bubble but caused a high increase in the no mass transfer case as shown in Figure 31. Thus Model One can predict the point at which buoyancy has completely vanished (as in the case of 0.2 mm bubbles) and shows its effect on the characteristics of the plume. This effect is well demonstrated in the low center line velocity of the plume compared to the no mass transfer case. Although this work assumed constant water density in the hypolimnion, the effect of the mass transfer was very significant. However, if we consider a very small density gradient and couple it with the effect brought about by the mass transfer, and consider again the center line velocity of the plume predicted by Model One, one can assume that the plume could have come to a stop before reaching the metalimnion.

Effect on Metalimnion

Regardless of the argument presented above that the plume might come to a stop before reaching the metalimnion, this work will consider it to

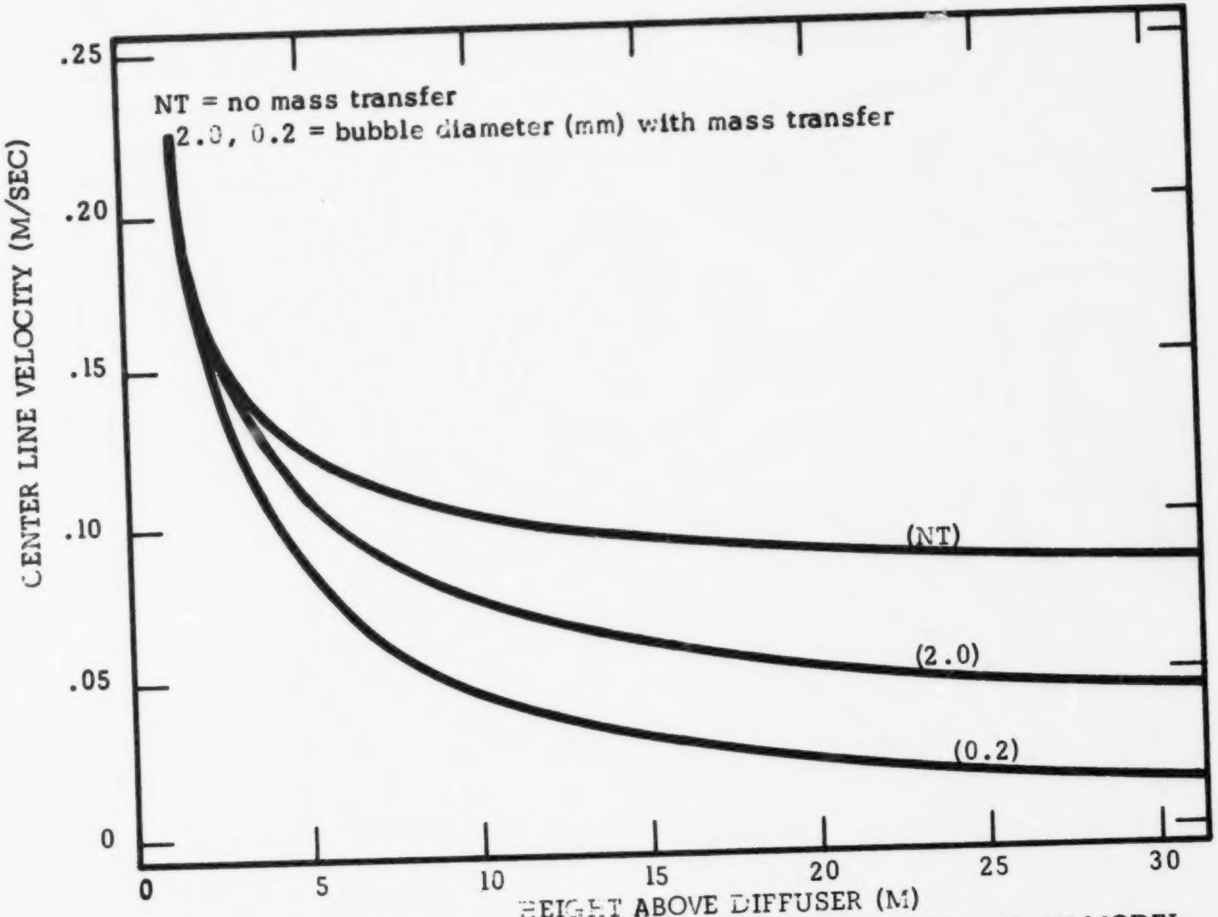

Fig. 25 CENTER LINE VELOCITY VS HEIGHT ABOVE DIFFUSER PREDICTED BY MODEL ONE AND MODEL TWO FOR AN INJECTION DEPTH OF 45 M AND AN OXYGEN FLOW RATE OF 1 L / MIN

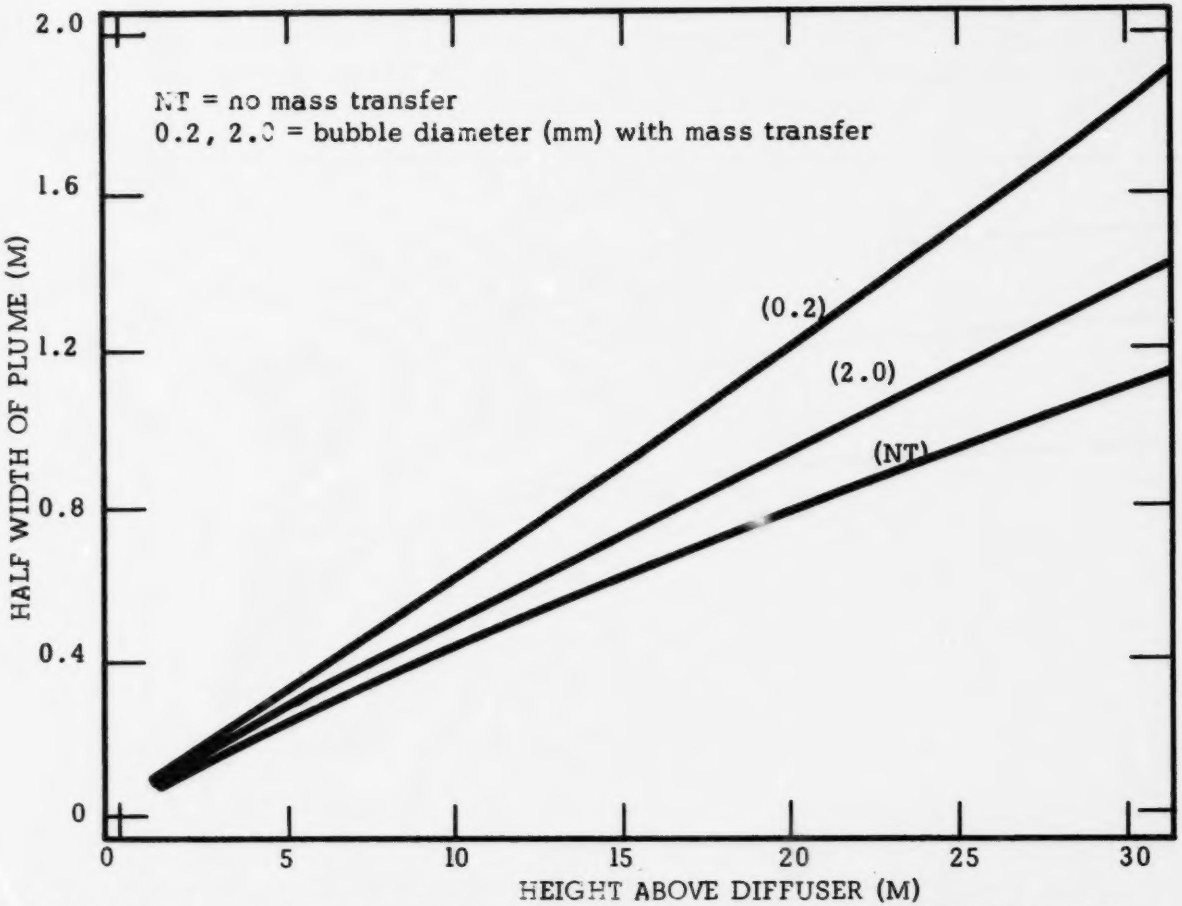

Fig. 27 HALF WIDTH OF PLUME VS HEIGHT ABOVE DIFFUSER PREDICTED BY MODEL ONE (0.2 AND 2.0MM BUBBLE PLUME) AND MODEL TWO FOR AN INJECTION DEPTH OF 45 M AND AN OXYGEN FLOW RATE OF 1 L/MIN

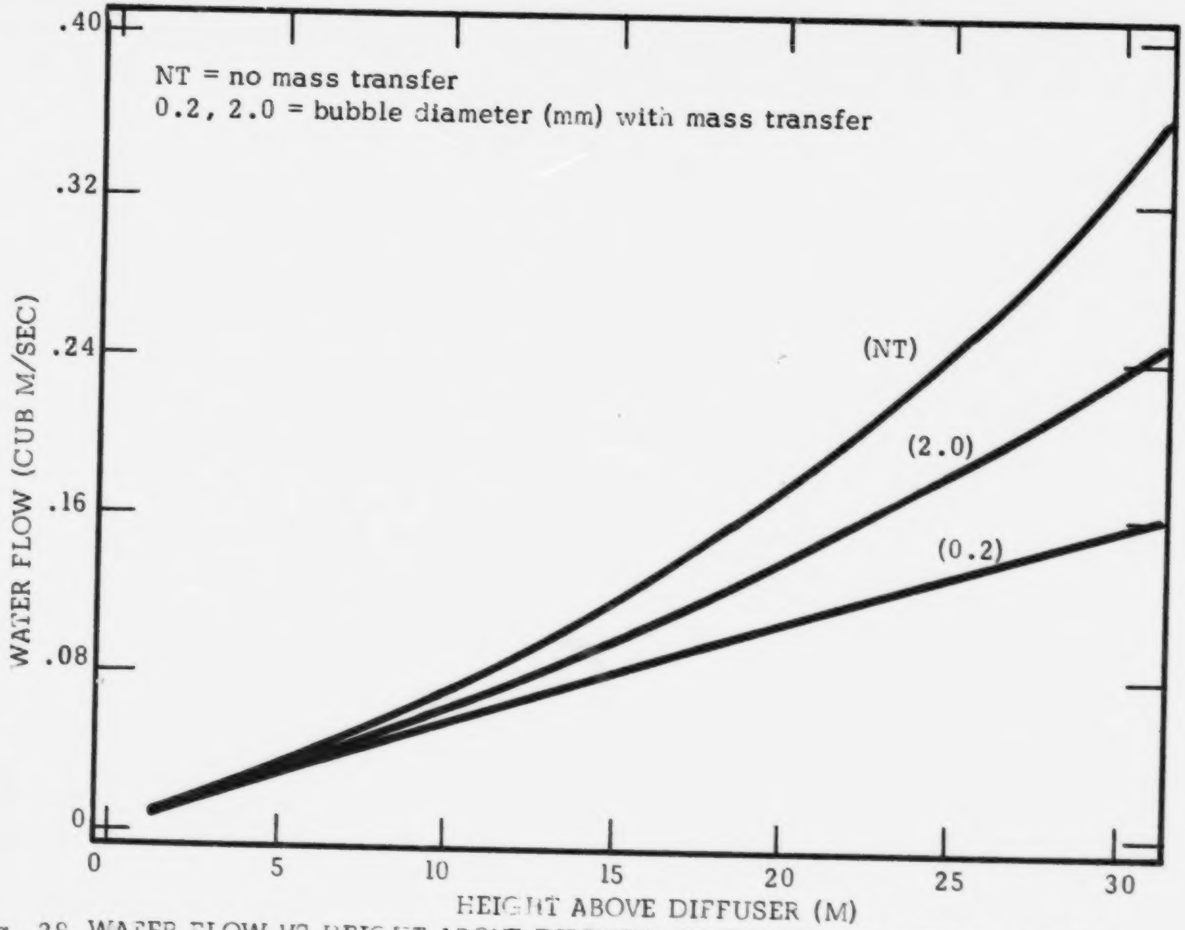

Fig. 28 WATER FLOW VS HEIGHT ABOVE DIFFUSER PREDICTED BY MODEL ONE (0.2 AND 2.0MM BUBBLE PLUME) AND MODEL TWO FOR AN INJECTION DEPTH OF 45M AND AN OXYGEN FLOW RATE OF 1 L/MIN

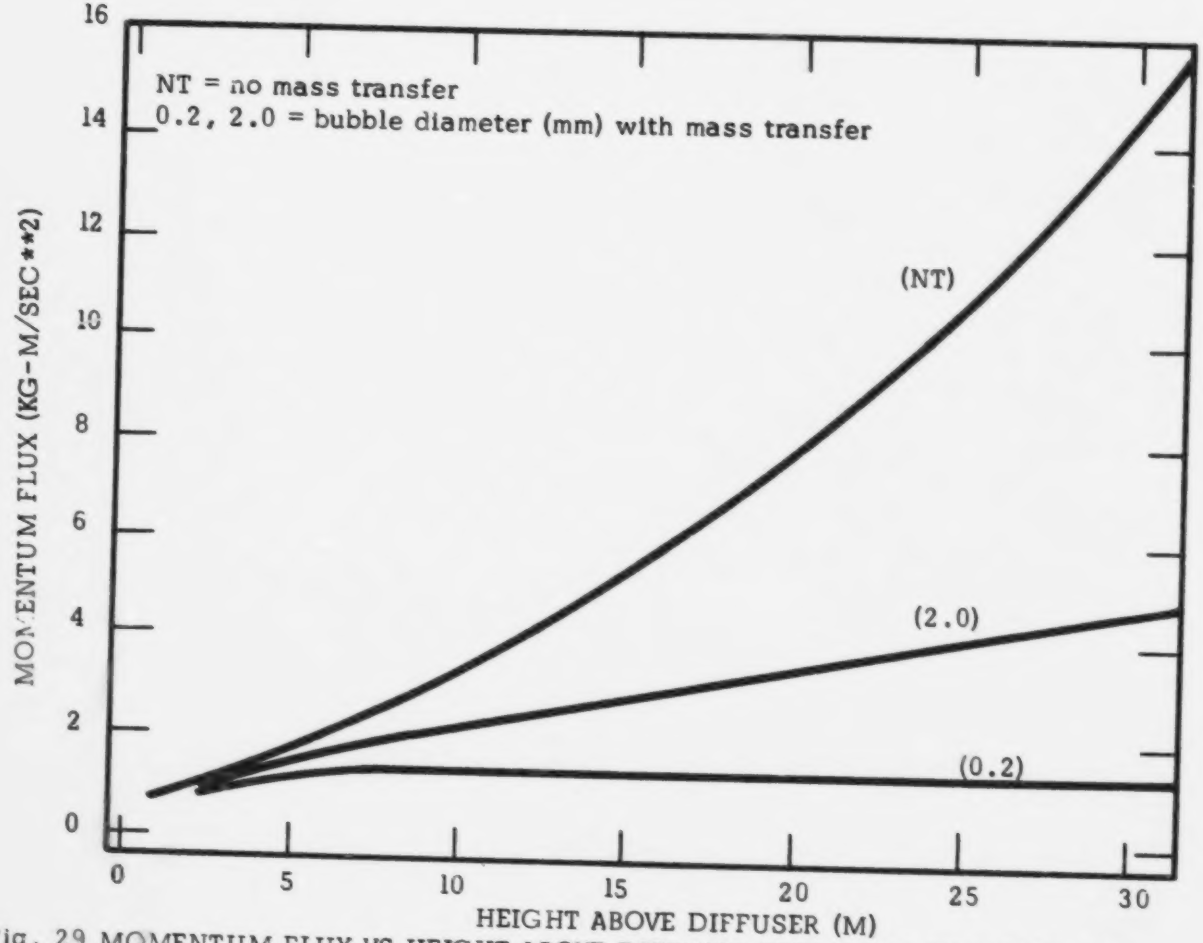

Fig. 29 MOMENTUM FLUX VS HEIGHT ABOVE DIFFUSER PREDICTED BY MODEL ONE (0.2 AND 2.0 MM BUBBLE PLUME) AND MODEL TWO FOR AN INJECTION DEPTH OF 45M AND AN OXYGEN FLOW RATE OF 1 L/MIN

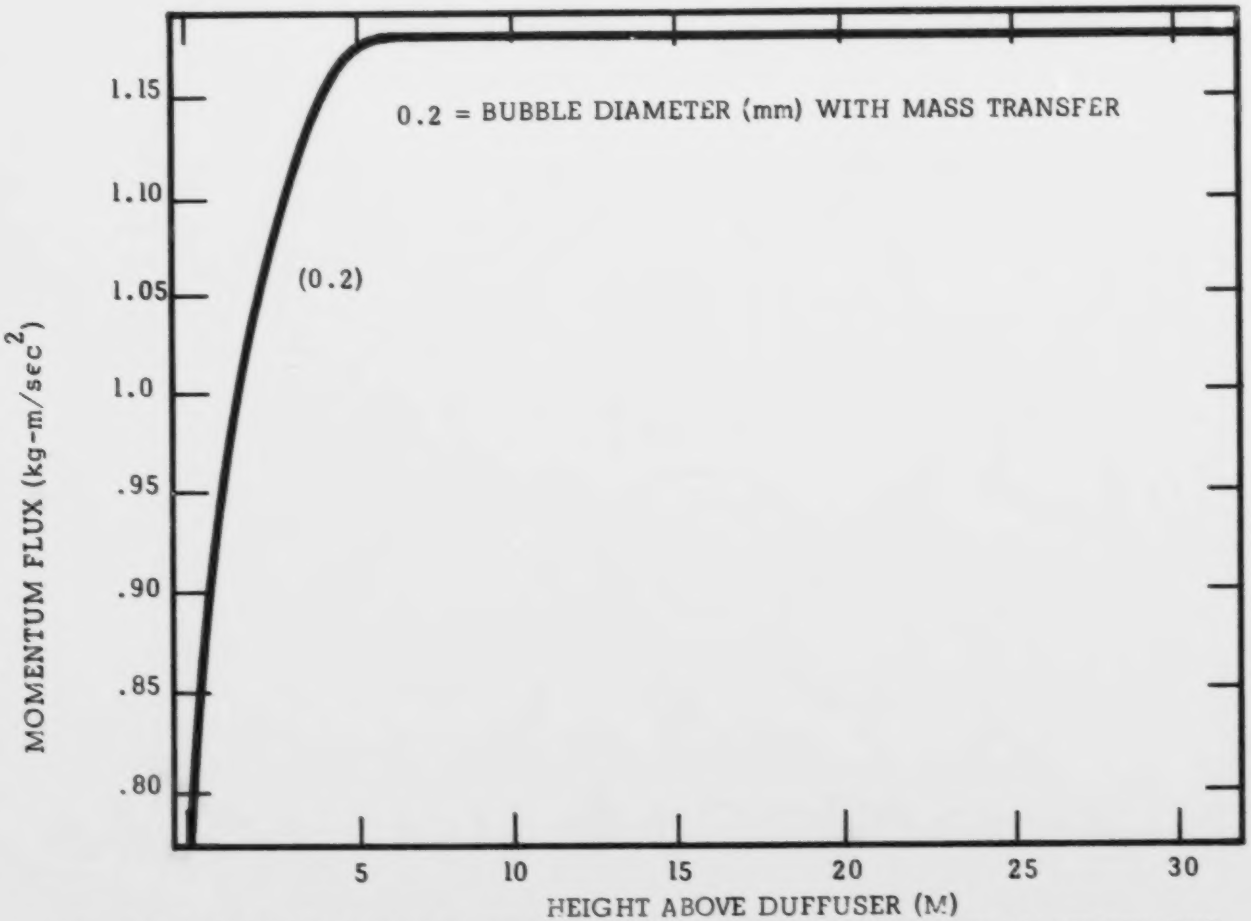

Fig. 30 MOMENTUM FLUX VS HEIGHT ABOVE DIFFUSER PREDICTED BY MODEL ONE FOR A 0.2 MM BUBBLE PLUME AT A DEPTH OF INJECTION OF 45M AND FLOW RATE OF 1 L/MIN

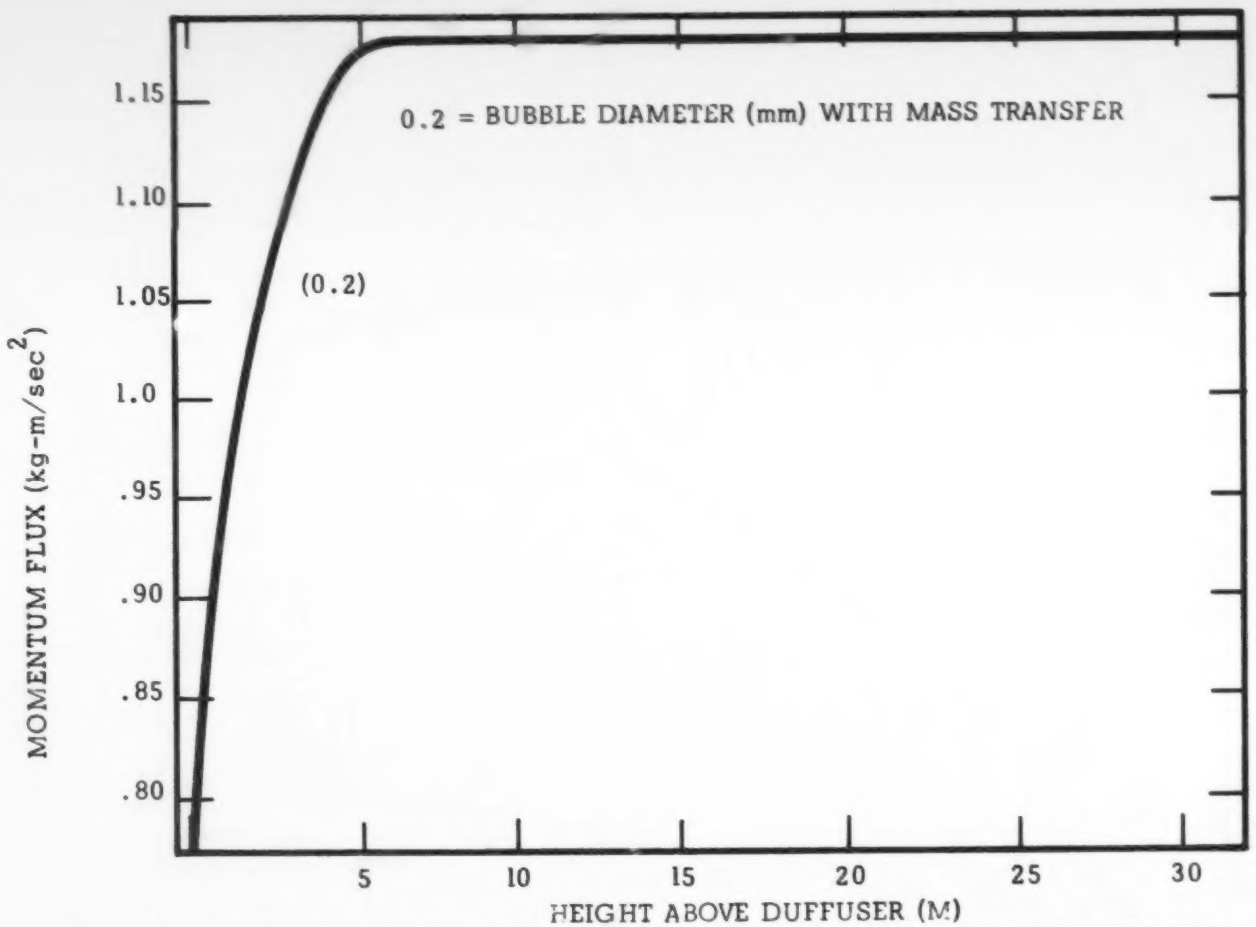

Fig. 30 MOMENTUM FLUX VS HEIGHT ABOVE DIFFUSER PREDICTED BY MODEL ONE FOR A 0.2 MM BUBBLE PLUME AT A DEPTH OF INJECTION OF 45M AND FLOW RATE OF 1 L/MIN

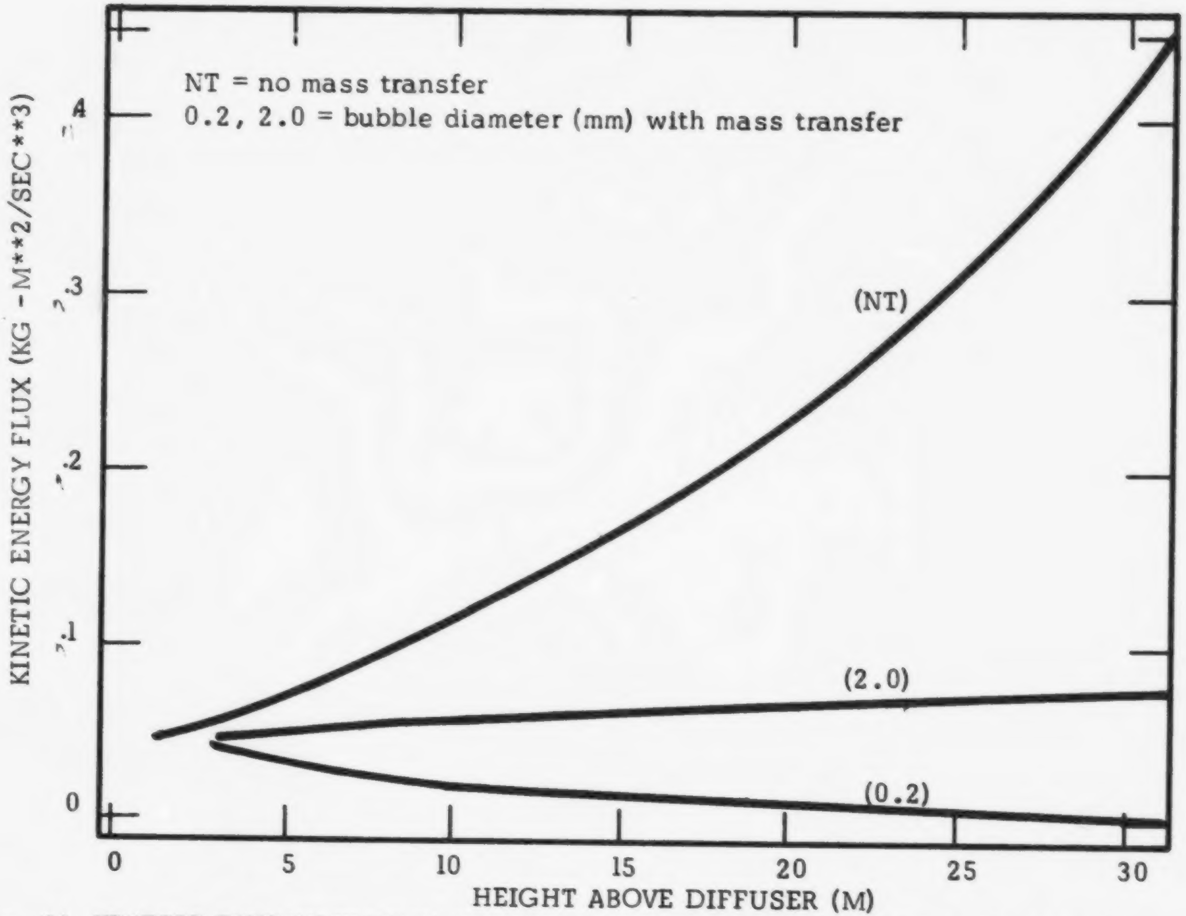

Fig. 31 KINETIC ENERGY FLUX VS HEIGHT ABOVE DIFFUSER PREDICTED BY MODEL ONE (0.2 AND 2.0 MM BUBBLE PLUME) AND MODEL TWO FOR AN INJECTION DEPTH OF 45M AND AN OXYGEN FLOW RATE OF 1 L/MIN

continue to rise and show that its effect on the metalimnion is negligible.

As the plume rises it will expand and entrain more and more water, causing it to decelerate. This rising water jet will raise the layer above it or penetrate through it depending on the energy left in it. When this plume hits the metalimnion, the difference in density coupled with a low energy could bring this plume to a stop. This phenomenon was shown to exist as indicated in Section VIII - Induced Mixing and Circulation. The configuration for this condition is shown in Figure 32, where the plume will cause a rise in the metalimnion (Δh). Analysis of this condition on a three-dimensional basis is rather complicated. However, a one-dimensional analysis could lead to a rough measure of this rise (Δh):

$$\rho_1 V_c^2 = \Delta h(\rho_1 - \rho_T)\, g \qquad (72)$$

Using this equation, the plume of the example in Section IX - Comparison of the Two Models, Model One for which the velocity at the metalimnion is 1.4 cm/sec will cause a h = 1.06 cm for a temperature difference of 20°F. On the other hand, Model Two will cause a h = 37 cm for the same condition.

Effect of Injection Depth

To demonstrate the effect of the injection depth on the various characteristics of the plume, the model was run for an injection depth of 45 meters and an injection depth of 75 meters for an impoundment with a metalimnion 15 meters below the surface. The diffuser was assumed to be 0.1 meter in radius and to produce 0.2 mm bubbles. The flow rate was considered 1 l/min and the entrainment coefficient 0.03. The results are shown in Figure 33 through Figure 37. The initial velocity was calculated according to Equation 69 and the final velocity at the metalimnion is shown in Figure 33. The increase in depth will lead to an increase in the half-width of the plume, Figure 34, and in the water flow rate, Figure 35. However, the effect of the smaller initial velocity and the earlier disappearance of bubbles for a 75 meter injection depth caused the momentum flux to be less than that for a 45 meter injection depth, Figure 36. The kinetic energy flux, Figure 37, shows also the effect of the above mentioned factors.

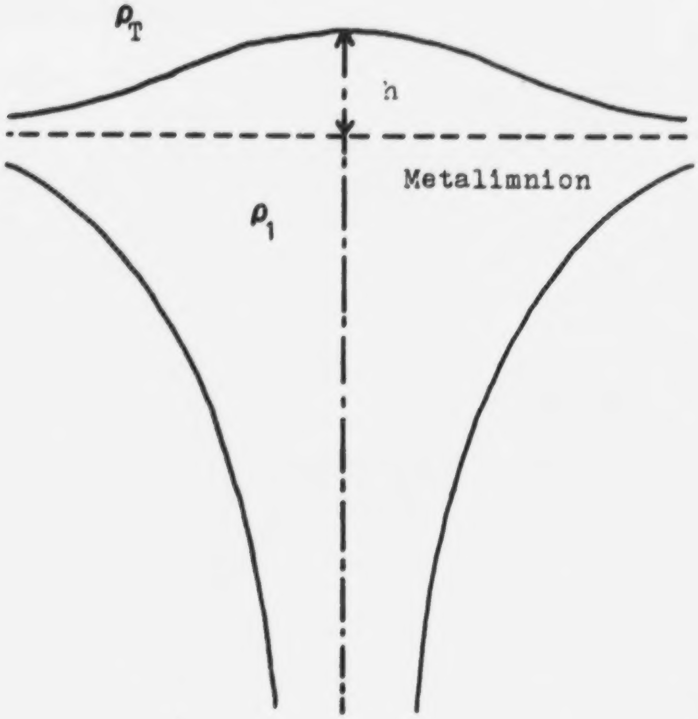
ρ_T
h
Metalimnion
ρ_1

Fig. 32 DEFINITION SKETCH

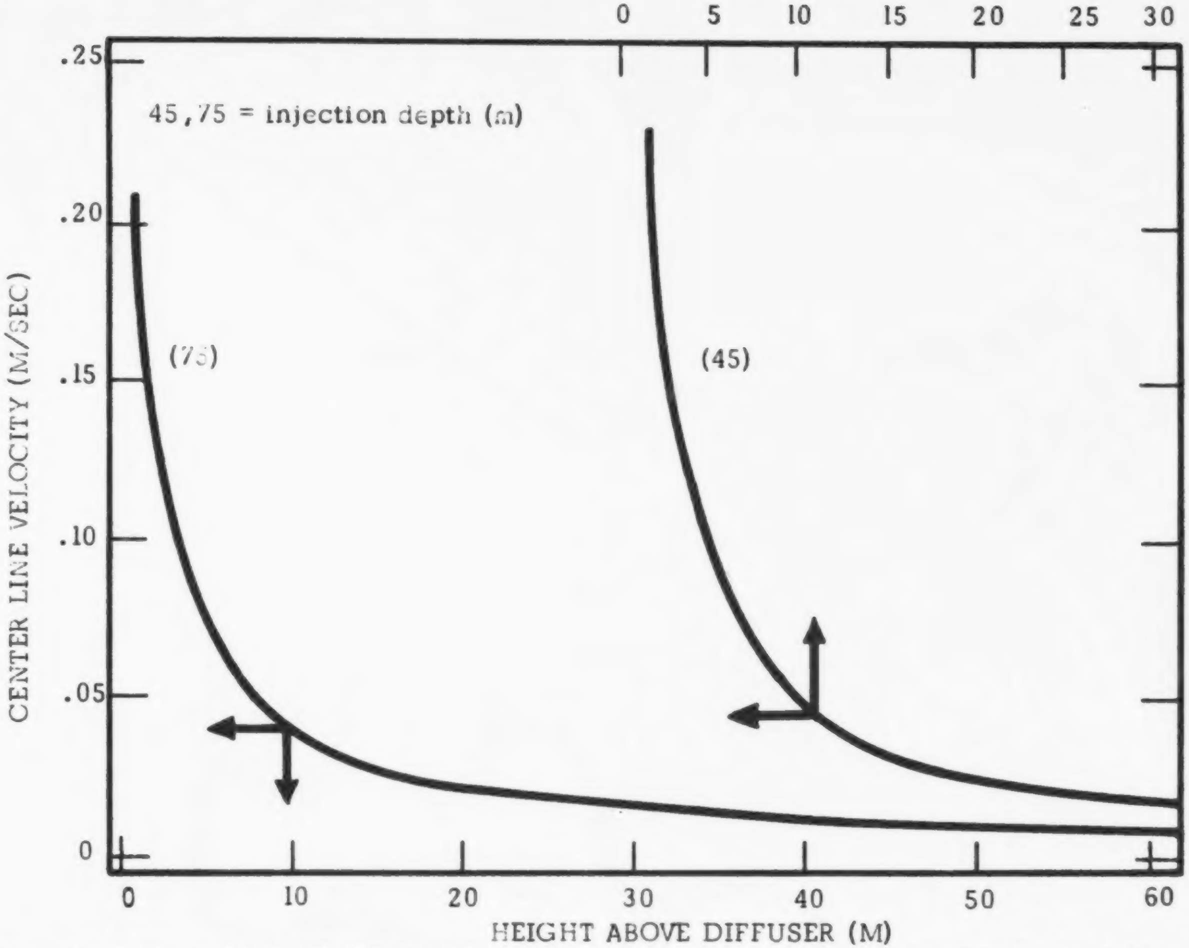

Fig. 33 CENTER LINE VELOCITY VS HEIGHT ABOVE DIFFUSER FOR INJECTION DEPTHS OF 75 AND 45 METERS AS PREDICTED BY MODEL ONE

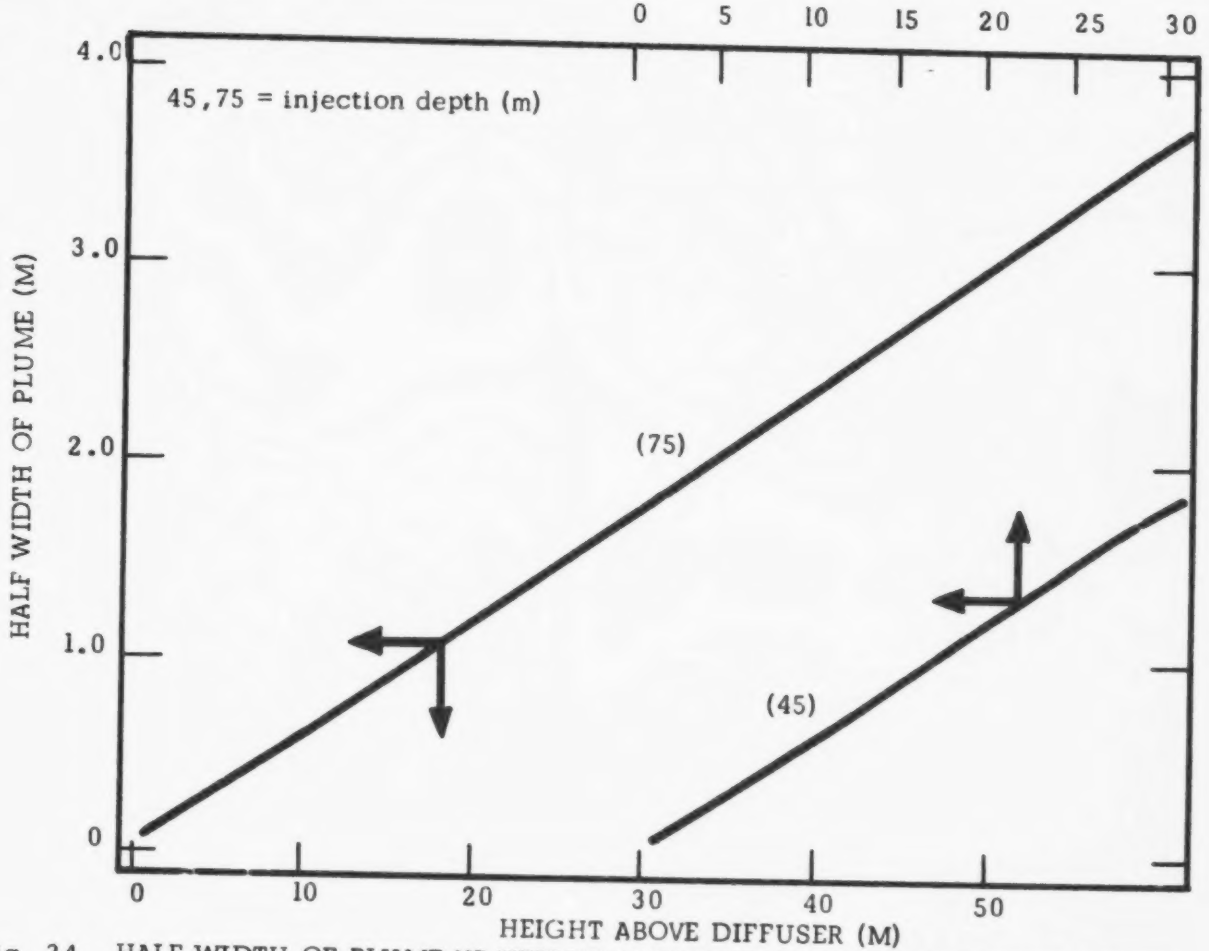

Fig. 34 HALF WIDTH OF PLUME VS HEIGHT ABOVE DIFFUSER FOR INJECTION DEPTHS OF 75 AND 45 METERS AS PREDICTED BY MODEL ONE

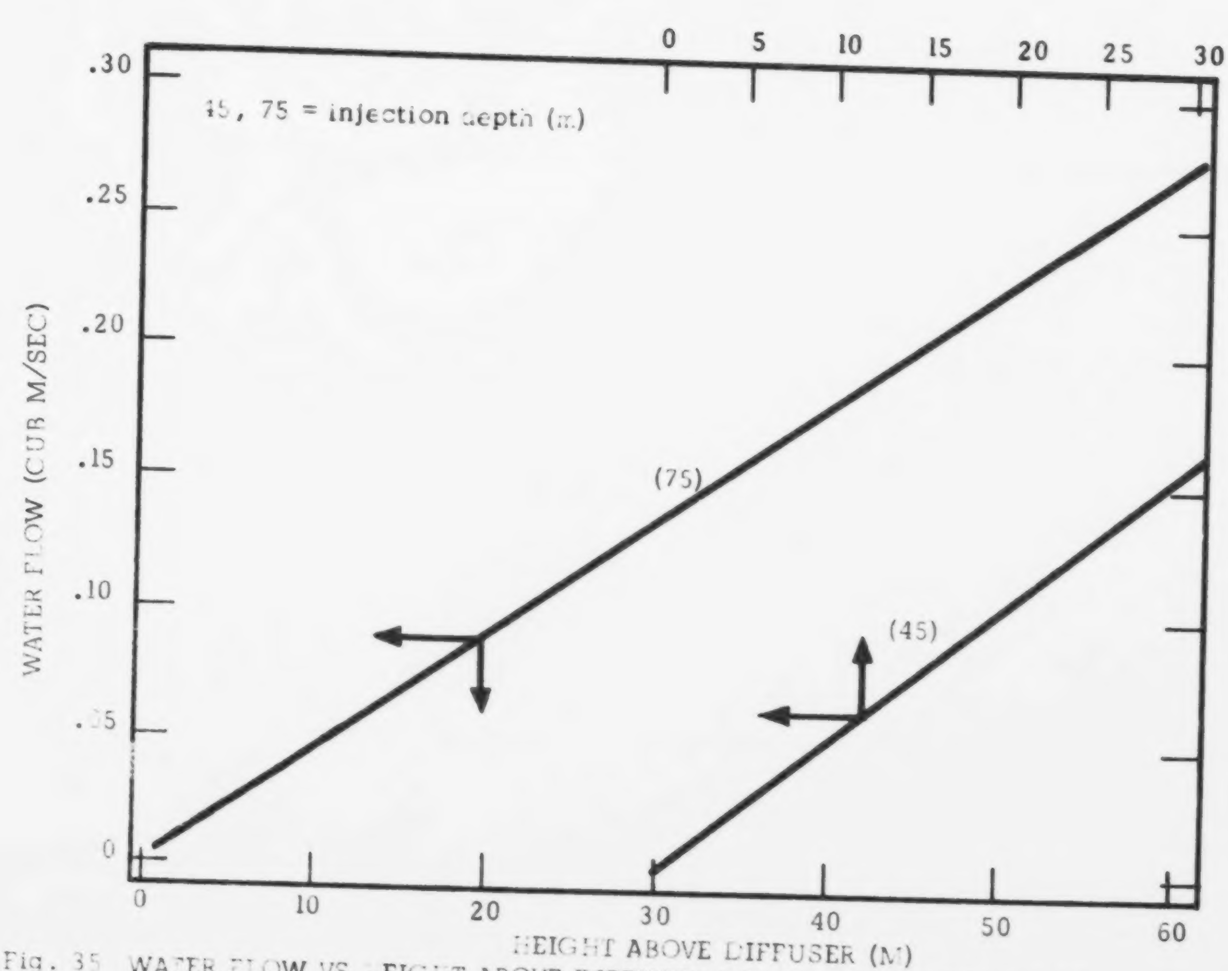

Fig. 35 WATER FLOW VS HEIGHT ABOVE DIFFUSER FOR INJECTION DEPTHS OF 75 AND 45 METERS AS PREDICTED BY MODEL ONE

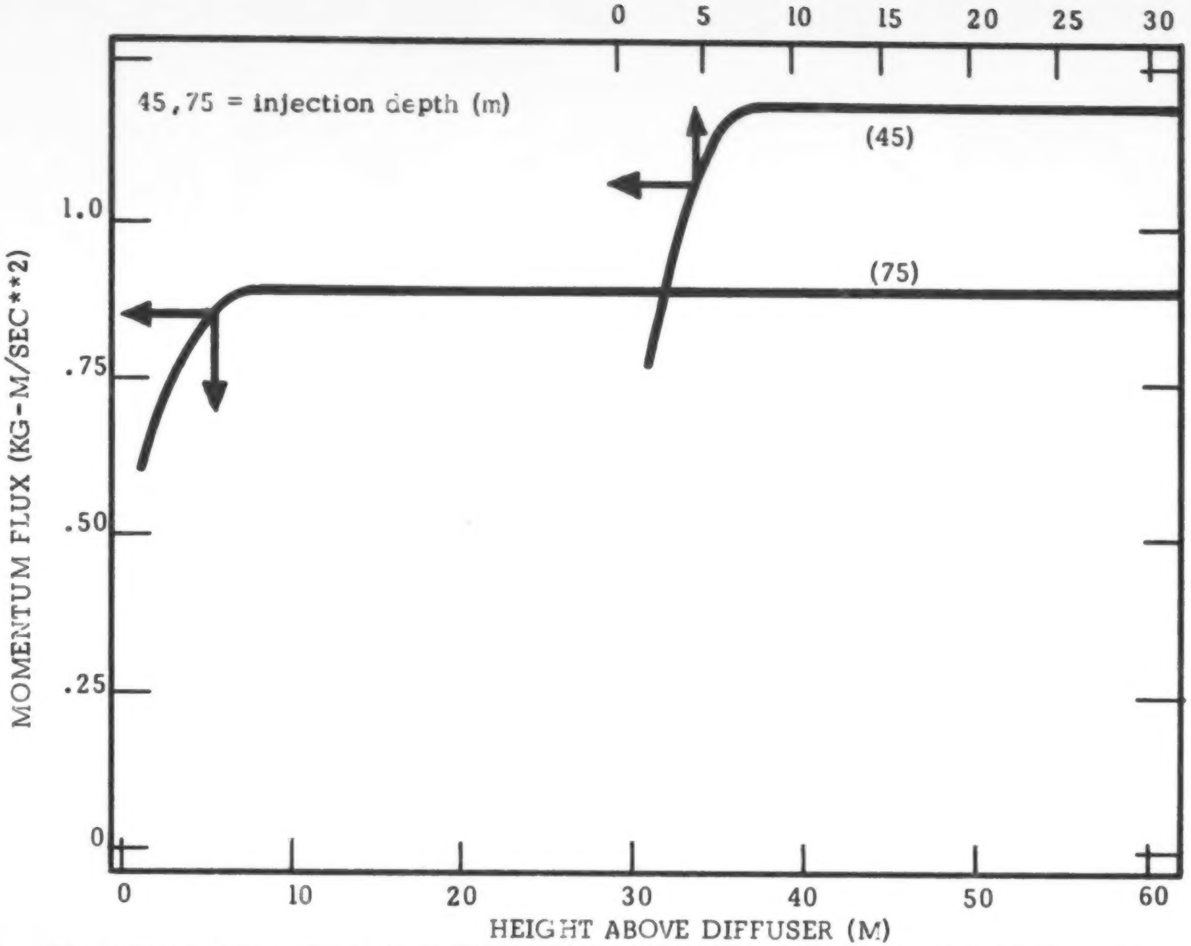

Fig. 36 MOMENTUM FLUX VS HEIGHT ABOVE DIFFUSER FOR INJECTION DEPTHS OF 75 AND 45 METERS AS PREDICTED BY MODEL ONE

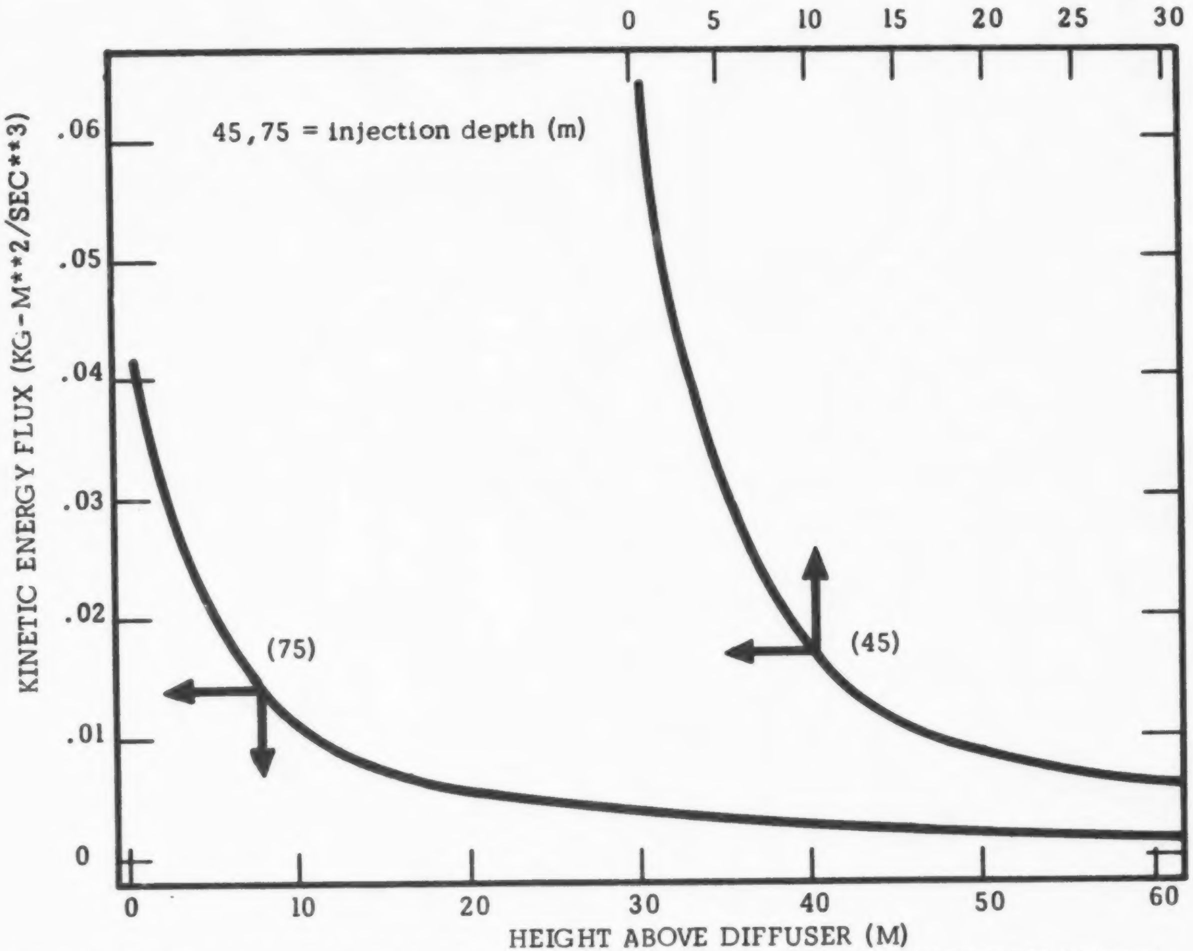

Fig. 37 KINETIC ENERGY FLUX VS HEIGHT ABOVE DIFFUSER FOR INJECTION DEPTHS OF 75 AND 45 METERS AS PREDICTED BY MODEL ONE

Effect of Flow Rate

The effect of varying the flow rate on the characteristics of the plume will be shown here for 1 and 3 l/min and an injection depth of 75 meters with a rise of 60 meters. Since the two flows are rather close in magnitude and the uncertainty of the value of the entrainment coefficient, a single value was used for both cases, namely 0.03. To demonstrate the effect of bubble size again, the output from 0.2 and 2.0 mm bubbles was considered. The initial velocity was calculated based on Equation 69 and the initial radius of the plume was assumed 0.1 meter for all cases. Consideration of Equation 57 leads to the conclusion that change in the radius of the plume with height is essentially a function of the entrainment coefficient (8). Since the same value of entrainment coefficient was used for the two cases, Figure 38 shows the half-width of the plume to be approximately the same for 1 and 3 l/min for 0.2 and 2.0 mm bubbles. The complete absorption of the 0.2 mm bubble after a short rise made the expansion of the plume a function only of the entrainment coefficient regardless of the flow rate. The 2.0 mm bubble continued to rise causing a smaller plume diameter than the 0.2 mm bubble, with a rather unnoticeable effect due to the higher flow rate.

The effect of the initial velocity of the two cases and with 0.2 and 2.0 mm bubbles is shown in Figures 39, 40. Those two variables led to the water flow rates shown in Figure 41 which indicate a higher flow rate due to 3 l/min than to 1 l/min for 0.2 and 2.0 mm bubbles. The flow rate due to the 2.0 mm bubble was higher in both cases than the 0.2 mm bubble.

Increasing the air flow rate three-fold did not cause a similar increase in the water flow rate. For the 0.2 mm bubble the increase in water flow rate was 35% while for the 2.0 mm bubble the increase was 42%.

Prediction Considering Slip Velocity

The speed of rise of a swarm of bubbles relative to the surrounding water has not been measured in this work and the literature is very conflicting on this aspect. The mathematical model with mass transfer treated it as a function of the diameter utilizing the available data in the literature (Section VII). However, the model with no mass transfer used constant slip velocity considered to be equal to 0.25 m/sec.

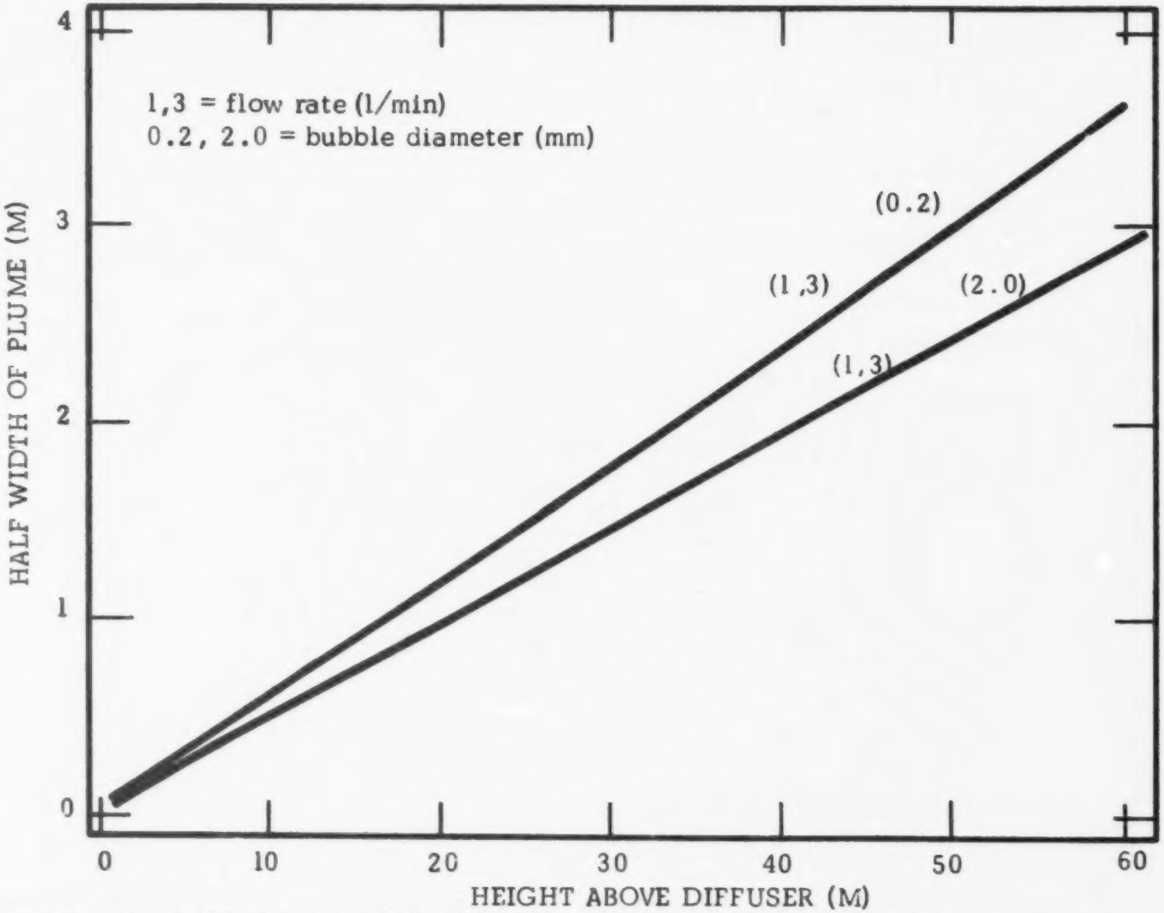

Fig. 38 HALF WIDTH OF PLUME VS HEIGHT ABOVE DIFFUSER FOR FLOW RATES OF 1 AND 3 L/MIN AND BUBBLES OF 0.2 AND 2.0 MM IN DIAMETER AT AN INJECTION DEPTH OF 75 METERS

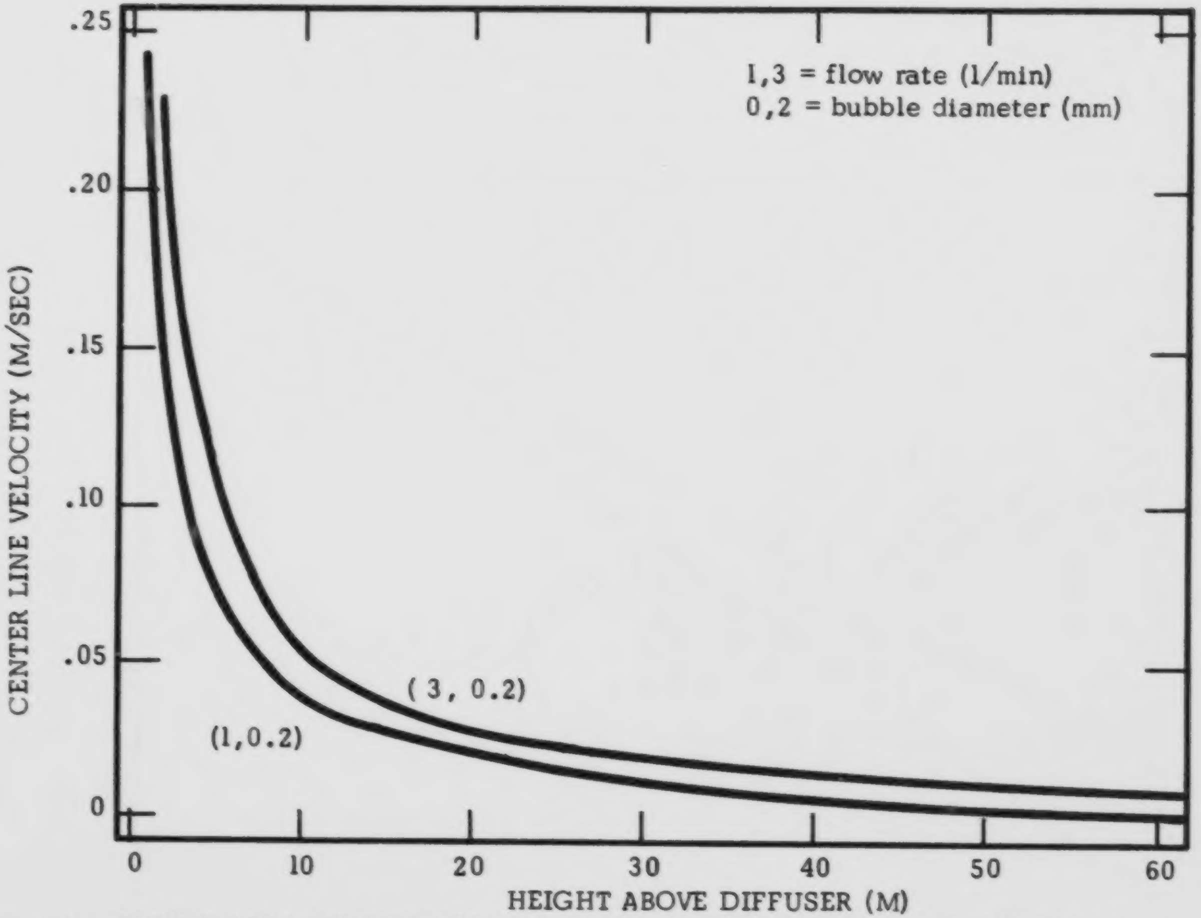

Fig. 39 CENTER LINE VELOCITY VS HEIGHT ABOVE DIFFUSER FOR FLOW RATES OF 1 AND 3 L/MIN AND BUBBLE DIAMETER OF 0.2 MM AT AN INJECTION DEPTH OF 75 METERS

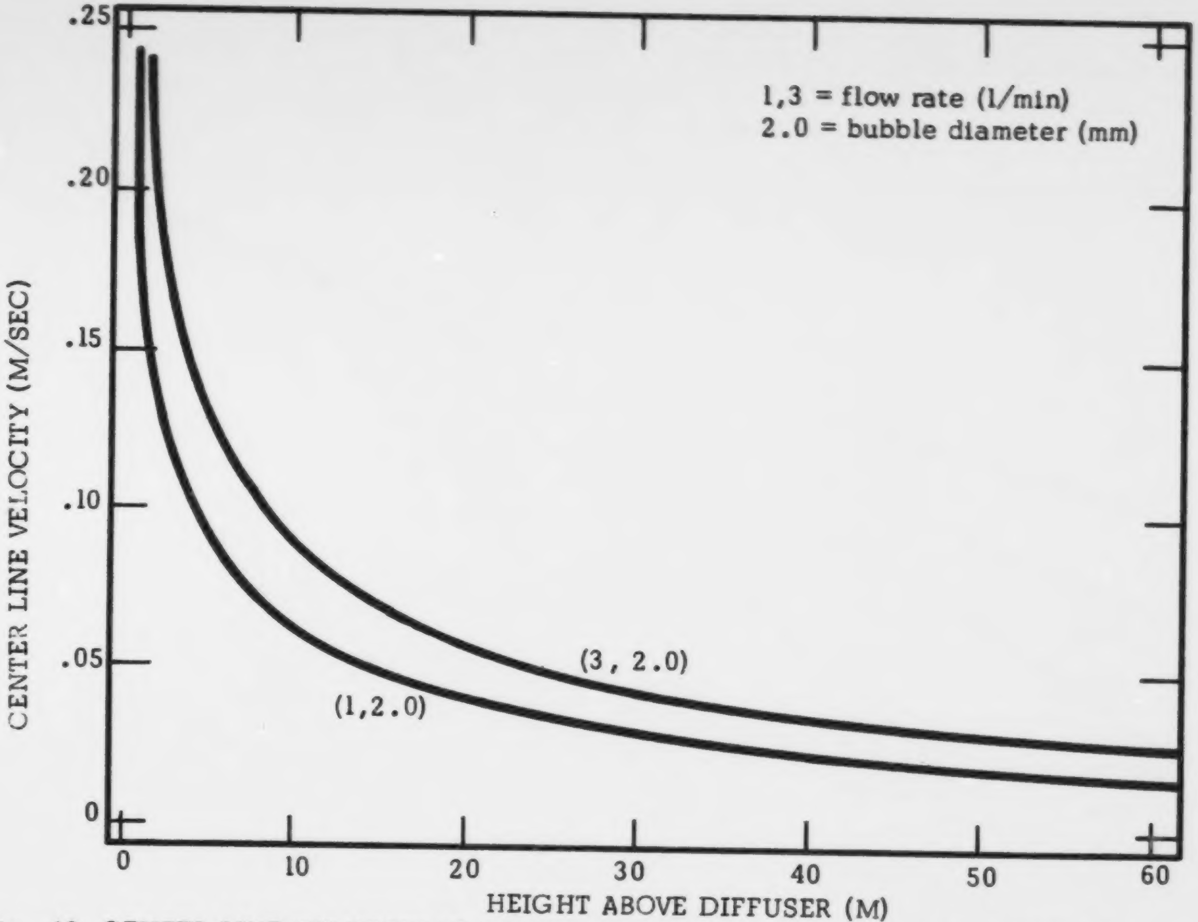

Fig. 40 CENTER LINE VELOCITY VS HEIGHT ABOVE DIFFUSER FOR FLOW RATES OF 1 AND 3 L/MIN AND BUBBLE DIAMETER OF 2.0 MM AT AN INJECTION DEPTH OF 75 METERS

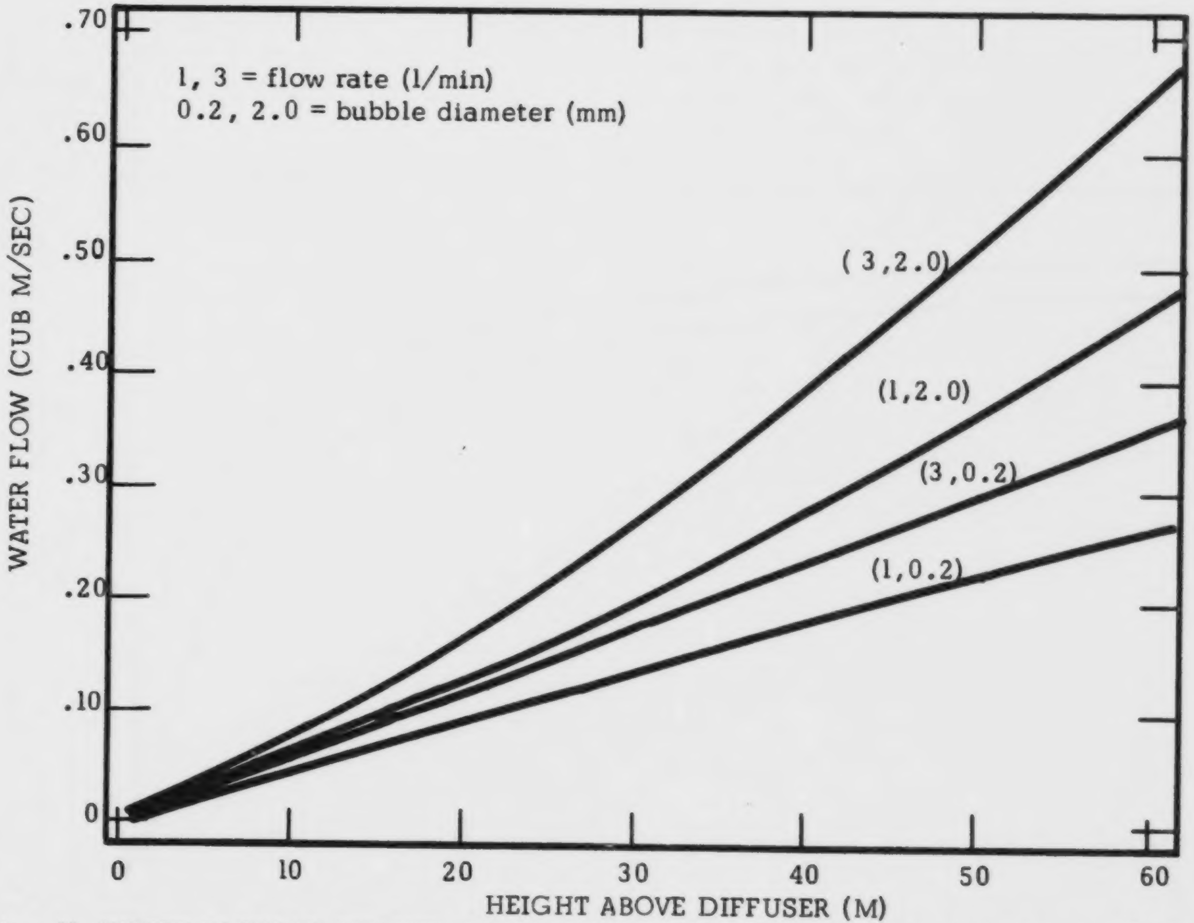

Fig. 41 WATER FLOW VS HEIGHT ABOVE DIFFUSER FOR FLOW RATES OF 1 AND 3 L/MIN AND BUBBLES OF 0.2 AND 2.0 MM IN DIAMETER AT AN INJECTION DEPTH OF 75 METERS

Figure 42 through 45 show the output of the two models and compared it to the output considering zero slip velocity. A 0.2 mm bubble has a low initial slip velocity (4 cm/sec) which continues to decrease as a function of the residual diameter until it reaches zero. This consideration caused the center line velocity of the plume to remain the same as that for zero slip velocity. However, the constant slip velocity of 0.25 m/sec used in Model Two caused a large effect on the center line velocity. The half-width of the plume remained the same for Model One while it increased with Model Two. However, the effect of the slip velocity on a 2.0 mm bubble plume is well pronounced in Figure 44 and 45. The initial slip velocity for a 2.0 mm bubble was 23 cm/sec and decreased in relation to the residual diameter. The effect of this high initial slip velocity is well demonstrated in Figure 44, and led to a larger plume as shown in Figure 45.

Although the 2.0 mm bubble plume has approximately the same initial slip velocity used for the no mass transfer case, the reduction in velocity of rise and the increase in the half-width of the plume was lesser than the no mass transfer case which demonstrated the effect of the reduction in bubble diameter and thus the slip velocity.

Other Model Predictions

The mass transfer model, in addition to solving for residual bubble diameter, velocity, radius, etc., solves for other important parameters. The program HYPO calculates for such important variables as the fraction of oxygen left, the per cent of oxygen in off gas, the oxygen to nitrogen ratio and others. Samples of such outputs are shown in the Appendix. For a certain injection rate of oxygen and with the calculated fraction of oxygen left, the amount of oxygen absorbed and thus the increase in the D.O. level in the plume is calculated. The fraction of oxygen absorbed calculated by HYPO is passed on to sub-program HYDRO which calculates the water flux caused by a known flow rate of oxygen. The increase in dissolved oxygen of the water can then be calculated. An example of such an output is shown in Figure 46 for 0.2 and 2.0 mm bubble plumes for an injection depth of 45 meters and an oxygen flow rate of 1.0 l/min. Initially, as the water flux in the plume is small and the relative amount of oxygen absorption is high, there is a positive increase in D.O. Subsequently, as the water flux rate increases and the oxygen absorption decreases, the increase in D.O. declines toward zero.

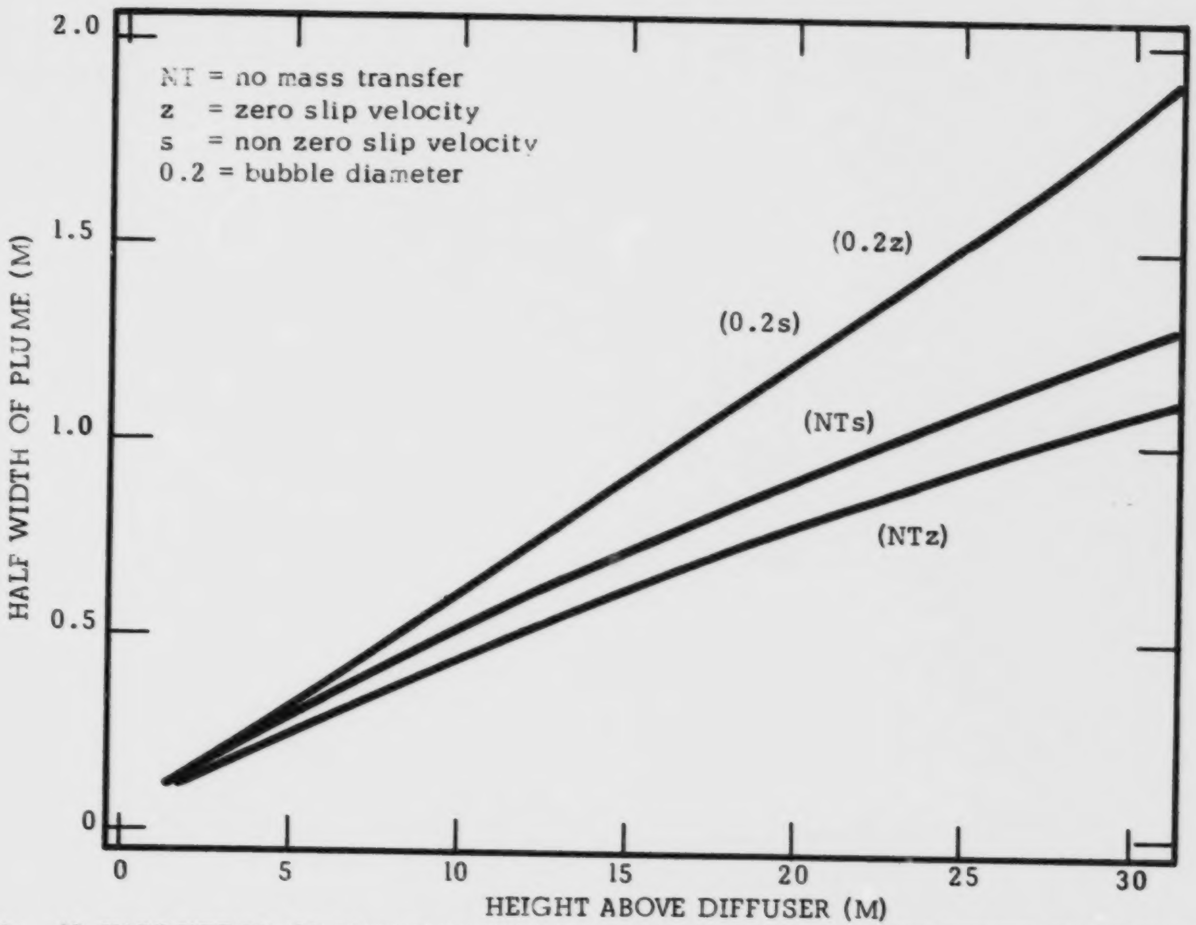

Fig. 42 HALF WIDTH OF PLUME VS HEIGHT ABOVE DIFFUSER AS PREDICTED BY MODEL ONE (0.2 MM BUBBLE) AND MODEL TWO CONSIDERING NON ZERO SLIP VELOCITY AND COMPARED TO ZERO VELOCITY

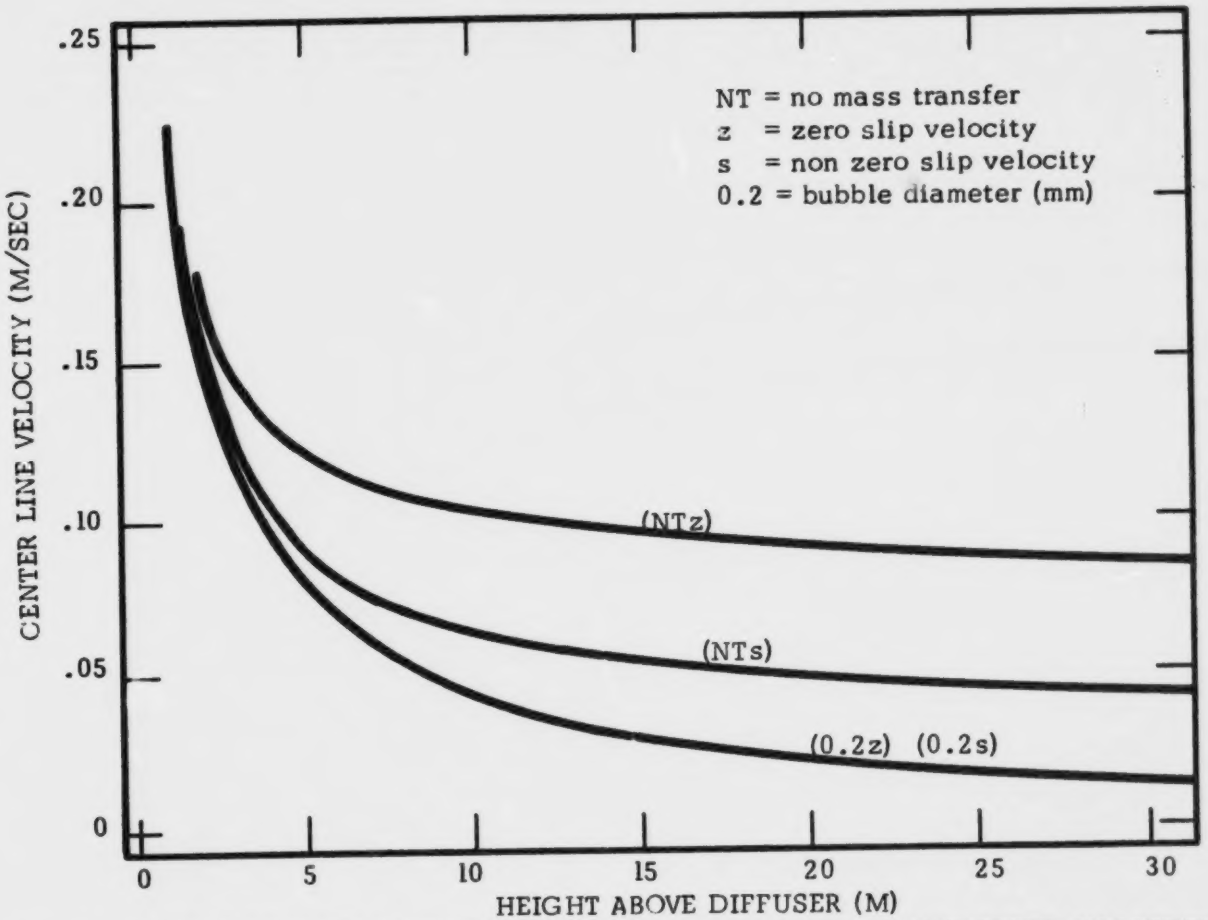

Fig. 43 CENTER LINE VELOCITY VS HEIGHT ABOVE DIFFUSER AS PREDICTED BY MODEL ONE (2MM BUBBLE) AND MODEL TWO CONSIDERING NON ZERO SLIP VELOCITY AND COMPARED TO ZERO SLIP VELOCITY

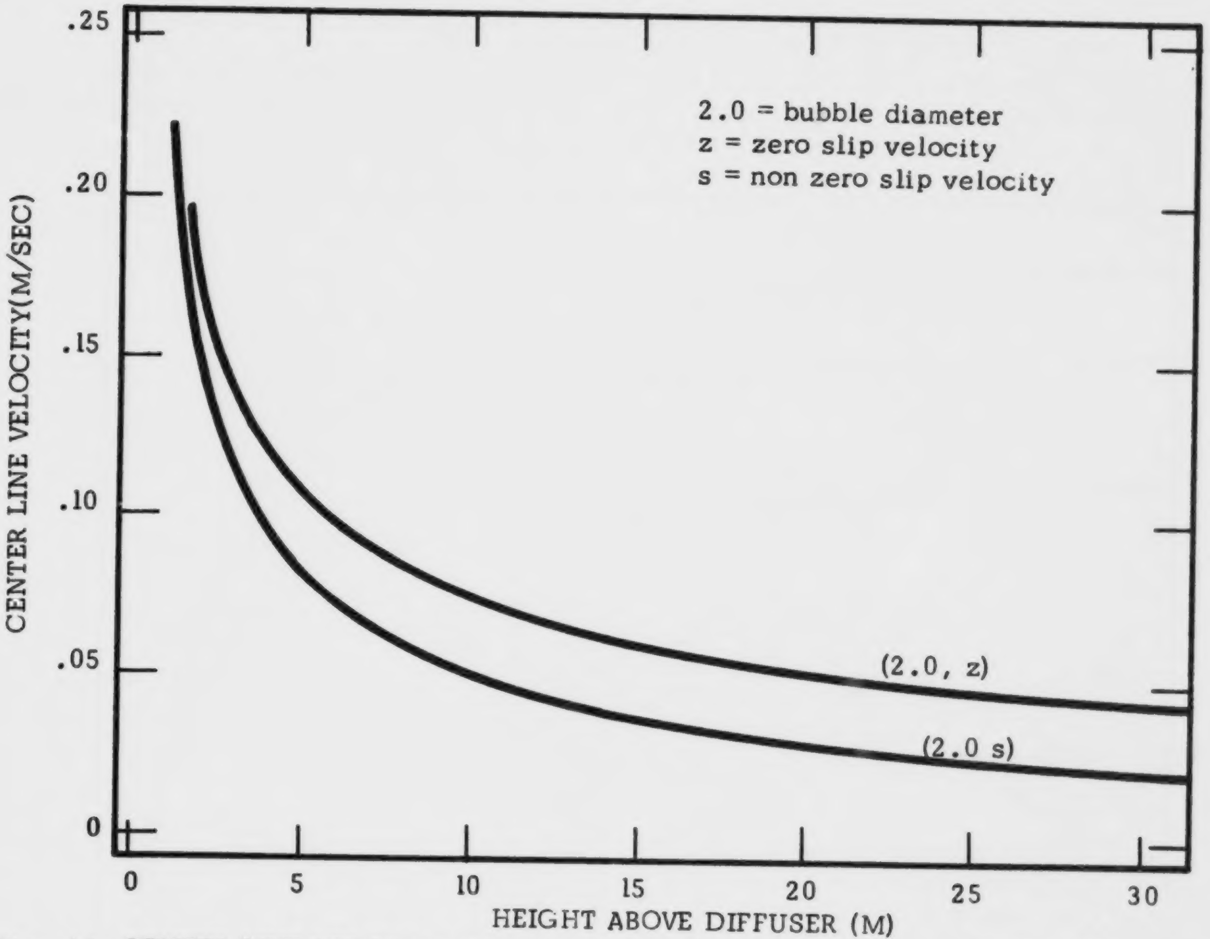

Fig. 44 CENTER LINE VELOCITY VS HEIGHT ABOVE DIFFUSER AS PREDICTED BY MODEL ONE (2.0 MM BUBBLE) AND MODEL TWO CONSIDERING NON ZERO SLIP VELOCITY AND COMPARED TO ZERO SLIP VELOCITY

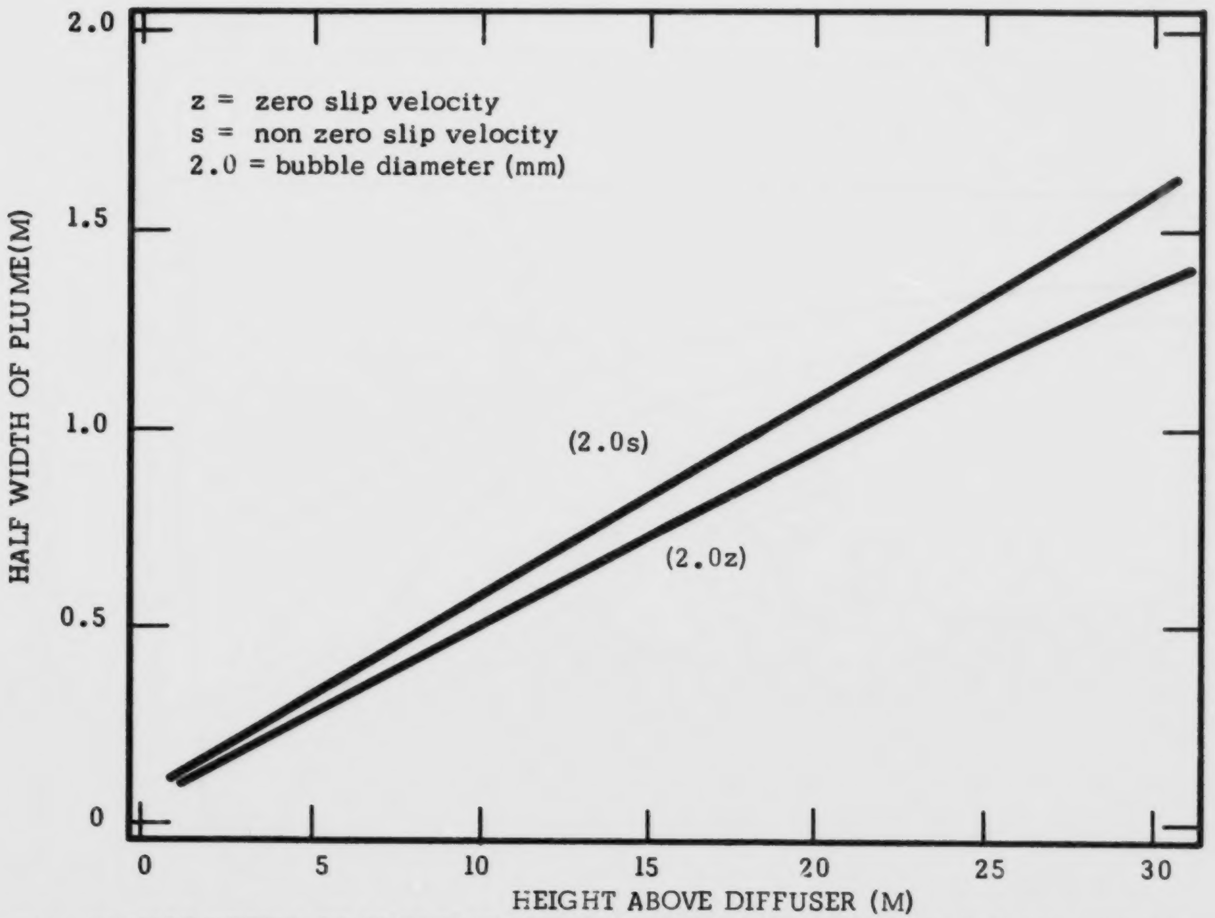

Fig. 45 HALF WIDTH OF PLUME VS HEIGHT ABOVE DIFFUSER FOR A 2.0 MM BUBBLE PLUME AS PREDICTED BY MODEL ONE CONSIDERING ZERO SLIP VELOCITY AND COMPARED TO NON ZERO SLIP VELOCITY

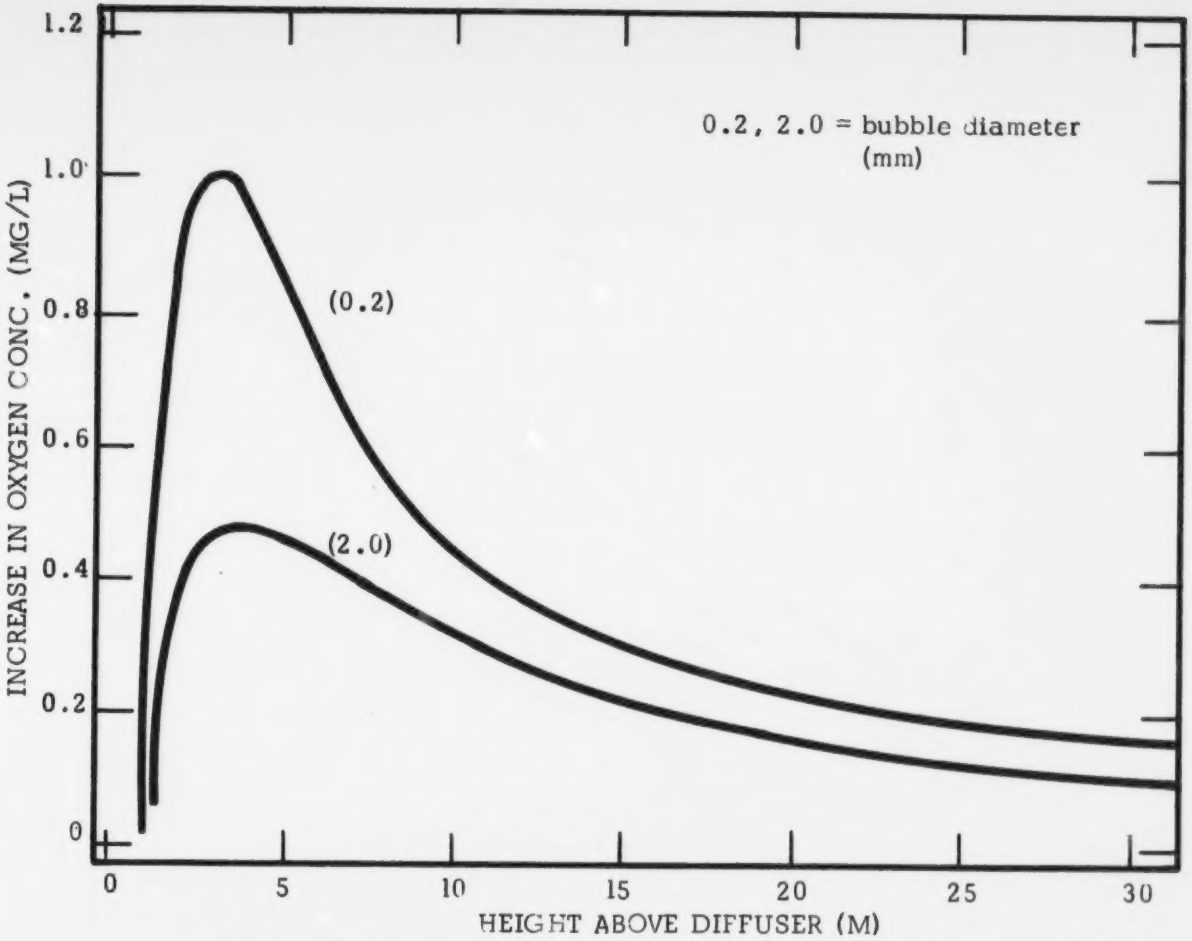

Fig. 46 INCREASE IN OXYGEN CONC. VS HEIGHT ABOVE DIFFUSER FOR A FLOW RATE OF 1 L/MIN AND BUBBLES OF 0.2 AND 2.0 MM AT AN INJECTION DEPTH OF 45M

The complete absorbance of the 0.2 mm bubbles and the lower water flow leads to a higher increase in D.O. in the plume than that caused by the 2.0 mm bubble.

General Guide

The purpose of this section is to present the prediction of the model for various conditions of injection depth, bubble diameters and oxygen flow rates to be used as a general guide for field work. The given prediction is for injection depths of 25, 50, 75, and 100 meters and oxygen flow rates of 1 and 2 l/min for diffusers that produce 0.2, 0.5, and 1.0 mm bubbles. In all cases the metalimnion is assumed at a depth of 15 meters below the surface. The prediction for the center line velocity, half-width of the plume, water flow and increase in D.O. are tabulated in Tables 3 through 6 at the quarter points of the distance from the diffuser to the metalimnion (x). The prediction is also shown graphically in the Appendix (Part C).

The following symbols are used in Tables 3 through 7:

BD = Bubble Diameter (mm)
h = Distance above diffuser (M)
X = Distance between diffuser and metalimnion (m)
V_c = Center line velocity (M/sec)
b = Half width of plume (M)
WQ = Water flux (M^3/sec)
ΔDO = Increase in plume dissolved oxygen (mg/l)

Illustrative Example of Use of Tables

To illustrate the use of those tables and graphs, let us assume a lake of approximately 90 meters in depth which is to be aerated using commercial oxygen. We would like to know the velocity, width, water flow and increase in D.O. of the plume if we used a 0.5 mm bubble diffuser at a depth of 85 meters and an oxygen flow of 2 l/min. From the tables and graphs for a depth of 75 and 100 meters the above mentioned variables can be obtained at any height above the diffuser. With these predictions we can approximate the behavior of this plume at 85 meters injection depth. This interpolation is shown in Table 7. Similar tables could be constructed for a 0.2 or 1.0 mm diffuser. Knowing these characteristics we can decide on the best diffuser to use, for a certain flow rate, to yield the highest increase in D.O. with the least disturbance to the stratification.

TABLE: 3

Model Predictions for 1. L/Min
and Depths of 25 and 50 Meters.

Oxygen Flow = 1 L/Min

		25 M X=10				50 M X=35			
BD	H	V_c	b	WQ $\times 10^2$ =	ΔD. o. $\times 10$ =	V_c	b	WQ $\times 10^2$ =	ΔD. o. $\times 10$ =
0.2	0	0.261	0.1	.82	0.0	0.22	0.1	0.69	0.0
	$\frac{X}{4}$	0.135	0.226	2.2	8.7	0.045	.59	4.9	4.8
	$\frac{X}{2}$	0.089	0.361	3.66	6.4	0.024	1.11	9.4	2.5
	$\frac{3X}{4}$	0.064	0.51	5.2	4.6	0.016	1.64	13.7	1.7
	X	0.049	0.66	6.7	3.5	0.012	2.2	18.2	1.3
0.5	0	0.261	0.1	.82	0.0	0.22	0.1	0.69	0.0
	$\frac{X}{4}$	0.15	0.216	2.2	4.1	0.072	0.5	5.5	3.6
	$\frac{X}{2}$	0.117	0.323	3.86	3.9	0.042	0.95	11.9	1.97
	$\frac{3X}{4}$	0.099	0.43	5.76	3.2	0.0276	1.46	18.5	1.3
	X	0.085	0.54	7.9	2.7	0.02	1.99	25.2	0.94
1.0	0	0.261	0.1	.82	0.0	0.22	0.1	0.69	0.0
	$\frac{X}{4}$	0.152	0.214	2.2	3.1	0.08	0.48	5.7	2.8
	$\frac{X}{2}$	0.124	0.32	3.9	3.0	0.055	0.86	12.9	1.7
	$\frac{3X}{4}$	0.108	0.42	5.9	2.6	0.042	1.26	21.3	1.1
	X	0.093	0.52	8.1	2.2	0.035	1.7	30.5	0.77

TABLE: 4

Model Predictions for 1. L/Min
and Depths of 75 and 100 Meters

Oxygen Flow = 1 L/Min

		75 M X=60				100 M X=85			
BD	H	V_c	b	WQ $\times 10^2$ =	ΔD. o. ×10 =	V_c	b	WQ $\times 10^2$ =	ΔD. o. ×10 =
	0	0.196	0.1	0.6	0.0	0.179	0.1	0.56	0.0
	$\frac{X}{4}$	0.025	0.96	7.2	3.3	0.016	1.33	9.2	2.6
0.2	$\frac{X}{2}$	0.013	1.87	13.9	1.7	0.0083	2.6	17.9	1.3
	$\frac{3X}{4}$	.0086	2.76	20.6	1.4	.0056	3.88	26.7	0.88
	X	.0065	3.67	27.4	.86	.0042	5.16	35.5	0.6
	0	0.196	0.1	0.6	0.0	0.179	0.1	0.56	0.0
	$\frac{X}{4}$	.041	0.83	8.8	2.6	0.026	1.2	11.7	2.0
0.5	$\frac{X}{2}$	0.02	1.7	18.6	1.27	0.013	2.47	24.3	.97
	$\frac{3X}{4}$	0.013	2.6	28.3	0.83	0.008	3.74	36.8	0.64
	X	0.0098	3.5	38.	.62	.006	5.02	49.4	0.4
	0	0.196	0.1	0.6	0.0	0.179	0.1	0.56	0.0
	$\frac{X}{4}$	0.052	0.76	9.4	2.2	.036	1.07	12.9	1.74
1.0	$\frac{X}{2}$	0.03	1.5	21.5	1.1	0.018	2.26	29.	0.8
	$\frac{3X}{4}$	0.02	2.35	34.6	0.68	0.012	3.5	45.4	0.52
	X	0.014	3.24	47.9	0.5	.008	4.8	61.8	0.38

TABLE: 5

Model Predictions for 2. L/Min
and Depths of 25 and 50 Meters.

Oxygen Flow = 2. L/Min

		25 M X=10				50 M X=35			
BD	H	V_c	b	WQ $\times10^2$ =	ΔD. o. $\times10$ =	V_c	b	WQ $\times10^2$ =	ΔD. o. $\times10$ =
0.2	0	0.33	0.1	1.03	0.0	0.276	0.1	0.87	0.0
	$\frac{X}{4}$	0.17	0.226	2.7	13.7	0.057	0.58	6.2	7.6
	$\frac{X}{2}$	0.11	0.36	4.6	10.0	0.03	1.11	11.8	4.
	$\frac{3X}{4}$	0.08	0.51	6.5	7.2	.021	1.64	17.3	2.7
	X	.062	0.66	8.5	5.6	0.016	2.2	22.8	2.1
0.5	0	0.33	0.1	1.03	0.0	0.276	0.1	0.87	0.0
	$\frac{X}{4}$	0.19	0.22	2.8	6.5	0.09	0.49	7.0	5.7
	$\frac{X}{2}$	0.147	0.32	4.9	6.2	0.053	0.95	15.	3.1
	$\frac{3X}{4}$	0.124	0.43	7.25	5.2	0.035	1.5	23.3	2.
	X	0.108	0.54	9.9	4.3	0.026	1.98	31.7	1.5
1.0	0	0.33	0.1	1.03	0.0	0.276	0.1	0.87	0.0
	$\frac{X}{4}$	0.192	0.21	2.8	4.9	0.10	0.476	7.2	4.5
	$\frac{X}{2}$	0.156	0.32	4.9	4.7	0.072	0.82	15.1	2.8
	$\frac{3X}{4}$	0.136	0.42	7.4	4.1	0.053	1.3	26.8	1.7
	X	0.123	0.51	10.2	3.4	0.044	1.7	38.4	1.22

TABLE: 6

Model Predictions for 2. L/Min
and Depths of 75 and 100 Meters.

Oxygen Flow = 2. L/Min

		75 M X=60				100 M X=85			
BD	H	V_c	b	WQ $\times 10^2$ =	ΔD. o. $\times 10$ =	V_c	b	WQ $\times 10^2$ =	ΔD. o. $\times 10$ =
	0	0.246	0.1	0.77	0.0	0.226	0.1	0.7	0.0
	$\frac{X}{4}$	.03	0.96	9.	5.2	0.021	1.33	11.5	4.1
0.2	$\frac{X}{2}$	0.016	1.9	17.5	2.7	0.011	2.6	22.6	2.1
	$\frac{3X}{4}$	0.011	2.8	25.9	1.8	0.0071	3.88	33.6	1.4
	X	0.008	3.7	34.4	1.4	.0053	5.2	44.7	1.1
	0	0.246	0.1	0.77	0.0	0.226	0.1	0.71	0.0
	$\frac{X}{4}$	0.052	0.83	11.1	4.2	0.033	1.2	14.8	3.2
0.5	$\frac{X}{2}$	0.025	1.71	23.4	2.	0.016	2.5	30.6	1.5
	$\frac{3X}{4}$	0.017	2.6	35.6	1.3	0.011	3.7	46.4	1.
	X	0.012	3.5	47.9	0.98	0.0078	5.02	62.2	0.76
	0	0.246	0.1	0.77	0.0	0.226	0.1	0.71	0.0
	$\frac{X}{4}$	0.065	0.76	11.8	3.5	0.045	1.07	16.3	2.8
1.0	$\frac{X}{2}$	0.038	1.51	27.1	1.7	0.023	2.26	36.6	1.3
	$\frac{3X}{4}$	0.025	2.35	43.6	1.1	0.015	3.53	57.2	0.8
	X	0.018	3.24	60.4	0.8	0.011	4.81	77.9	0.6

TABLE 7

Illustrative Example

		75 Meters	1000 Meters	Interpolated 85 Meters Diffuser Depths
V_c at	x/4	.052	.033	.042
V_c at	x/2	.025	.016	.021
V_c at	3x/4	.017	.011	.014
V_c at	x	.012	.0078	.01
b at	x/4	.83	1.2	1.0
b at	x/2	1.71	2.5	2.1
b at	3x/4	2.6	3.7	3.15
b at	x	3.5	5.02	4.25
WQ at	x/4	11.1 x 10^{-2}	14.8 x 10^{-2}	13 x 10^{-2}
WQ at	x/2	23.4 x 10^{-2}	30.6 x 10^{-2}	27 x 10^{-2}
WQ at	3x/4	35.6 x 10^{-2}	46.4 x 10^{-2}	41 x $^{10-2}$
WQ at	x	47.9 x 10^{-2}	62.2 x 10^{-2}	55 x 10^{-2}
ΔD.O. at	x/4	4.2 x 10^{-1}	3.2 x 10^{-1}	3.7 x 10^{-1}
ΔD.O. at	x/2	2 x 10^{-1}	1.5 x 10^{-1}	1.7 x 10^{-1}
ΔD.O. at	3x/4	1.3 x 10^{-1}	1 x 10^{-1}	1.15 x 10^{-1}
ΔD.O. at	x	.98 x 10^{-1}	.76 x 10^{-1}	.88 x 10^{-1}

SECTION X

ACKNOWLEDGMENTS

This study was sponsored by the Office of Research and Monitoring, Environmental Protection Agency. Grateful appreciation is extended to Richard Hiller, who was the initial Project Officer and Lowell Leach, who subsequently served as project officer for the major portion of the grant. These men took a genuine interest in the project and whole heartedly supported it. Appreciation is also extended to Dr. Curtis C. Harlin, Jr. for his support of this project as well as the general area of river and impoundment aeration.

The University of Texas at Austin staff of Environmental Health Engineering and Dr. Gus Fruh in particular are gratefully acknowledged for their consultation and encouragement. The staff and facilities of the Center for Research in Water Resources are much appreciated.

SECTION XI

REFERENCES

1. Albertson, M.L., Dai, Y.B., Jensen, R.A. and Rouse, H., Diffusion of Submerged Jets", Trans. A.S.C.E., V. 115, 1950, p. 639.

2. Baines, W.D., Hamilton, G.F., "On the Flow of Water Induced by a Rising Column of Air Bubbles", International Association for Hydraulic Research, 8th Congress, Montreal, August 24-29, 1959.

3. Barnhart, Edwin L., "Transfer of Oxygen in Aqueous Solutions", proceedings of the American Society of Civil Engineers, Sanitary Eng. Div., June 1969.

4. Batchelor, G.K., 1954 Quart. J.R. Met. Soc. 80, p. 339.

5. Bouissinesq, Comptes Rendues, 1912, 153, pp. 983, 1035, 1040, 1124.

6. Bowonder, B., Kumar, R., "Studies in Bubble Formation-IV Bubble Formation at Porous Discs", Chem. Engr. Science, 25:25, 1970.

7. Brasher, P., Contribution to Compressed Air Magazine, April 1907.

8. Cederwall, K., and Ditmars, J.D., "Analysis of Air-Bubble Plumes", Report #KH-R-24, Sept., 1970, California Institute of Tech.

9. Collins, R.J., Fluid Mech., 22, 763, 1965.

10. Datta, R.L., Napier, D.H., Newitt, D.M., "The Properties and Behaviors of Gas Bubbles Formed at Circular Orifice", Trans. Instn. Chem. Engrs., 28: 14, 1950.

11. Davies, R.M., Taylor, G.I., "The Mechanics of Large Bubbles Rising Through Extended Liquids and Through Liquids in Tubes," Proc., Royal Soc. of London, Vol. 200, Series A, 1950, p. 395.

12. DeNevers, N., "Bubble Driven Fluid Circulation", AIChE Journal, Vol. 14, No. 2, March 1968.

13. Dumitrescu, D.T., Z. Angew, Math. Mech. 23, 139, 1943.

14. Evans, J.T., "Pneumatic and Similar Breakwaters", Proc. Roy. Soc. (London), Series A, Vol. 231, 1935, p. 457.

15. Feuerstein, D.L., and R.E. Selleck (1963), "Fluorescent Tracers for Dispersion Measurements", J. of San. Engr. Div., ASCE, 89, SA 4, August.

16. Gay, F., and Hagedorn, Z., "Forced Convection in Stratified Fluid by Air Injection," M.I.T. Thesis, Jan. 1962.

17. Haberman, W.L., Morton, R.K., "An Experimental Study of Bubbles Moving in Liquids", Trans. Amer. Soc. Civil Engr., 121: 227, 1956.

18. Hadamard, Comptes Rendues, 1911, 152, 1735, and 1912, 154, 109.

19. Khurana, A.K., Kumar R., "Studies in Bubble Formation III", Chem. Engr. Sci., 24: 1711, 1969.

20. Kobus, H.E., Analysis of the Flow Induced by Air Bubble Systems", Coast. Eng. Conf. Vol. II, London, 1968.

21. Kurihara, M., "Pneumatic Breakwater, Section I, II, and III", Translated by K. Horikawa, Univ. of California, Institute of Engineering Research, Wave Research Lab., Series 104, Issues 4, 5, and 6, 1954.

22. Maneri, C.C., Mendelson, H.D., "The Rise Velocity of Bubbles in Tubes and Rectangular Channels as Predicted by Wave Theory", AIChE Journal, Vol. 14, No. 2, page 295, 1968.

23. Mathers, W.G., Winter, E.E., "Principles and Operation of an Air-Operated Mixer-Settler. The Can. J. Chem. Engr., 37:99, 1959.

24. Moore, D.W., "The Velocity of Rise of Distorted Gas Bubbles in a Liquid of Small Viscosity," J. Fluid Mech., 23 (4): 749, 11963.

25. Morton B.R., Taylor, G.I., and Turner, J.S., "Turbulent Gravitational Convection From Maintained and Instantaneous Sources," Proc. Roy. Soc., Vol. A236, (1936).

26. Murphy, D., Clark, D.S., Lentz, C.P., "Aeration in Tower Type Fermenters", The Can. J. of Chem. Engr., 37:157, 1959.

27. Nicklin, D.J., "Two-Phase Bubble Flow", Chem. Eng. Science, Vo. 17, pp. 693-702, 1962.

28. O'Brien and Gosline, Ind. Eng.Chem., 1935, 27, 1436.

29. Pattle, R.E., "Factors in the Production of Small Bubbles", Trans. Instn. Chem. Engrs., 28; 14, 1950.

30. Pritchard, D.W., and J.H. Carpenter, (1960), "Measurement of Turbulent Diffusion in Estuarine and Inshore Waters." Bull. Int. Assoc. Sci. Hydrol. No. 20.

31. Ramakrishnan, S., Kumar, R., Kuloor, N.R., "Studies in Bubble Formation I; Bubble Formation Under Constant Flow Conditions," Chem. Engg. Sci., 24, 731, 1969.

32. Reith, T., Renken, S., Israel, B.A., "Gas Hold-up and Axi l Mixing in the Fluid Phase of Bubble Columns." Chem. Engr. Sci., 23, 619, 1968.

33. Rouse, H., Yih, C.S., and Humphreys, H.W., "Gravitation Convection from Boundary Source", 1952, Tellus, 4, 201.

34. Rybczynski, Bull. Acad. Sci. Gracovie, 1911, 1, 40.

35. Satyanarayanan, A., Kumar, R., Kuloor, N.R., "Studies in Bubble Formation II: Bubble Formation Under Constant Pressure Conditions," Chem. Engg. Sci., 24: 749, 1969.

36. Schmidt, W., 1941, Z. Angew. Math. Mech. 21, 265, 351.

37. Siemes, W., Weises, W., "Mixing of Fluid in Narrow Blow Columns". Chem. Eng. Tech., 29, 727, 1957.

38. Speece, R.E., "Hypolimnion Aeration", Journal American Water Works Association, Vol. 63, No. 2, January 1971.

39. Speece, R.E., "The Use of Pure Cxygen in River and Impoundment Aeration." Presented at the 24th Purdue Industrial Waste Conference, May 8, 1969.

40. Stokes, G.G., Mathematical and Physical Papers, Cambridge University Press, 1880, Cambridge, U.K.

41. Subramanian, R., and Chi Tien, "Longitudinal Mixing in Liquid Columns Due to Bubble Motion", Department of Chem. Eng. and Metallurgy, Syracuse University, Syracuse, N.Y., Research Report #70-2

42. Tadaki, T., Maeda, S., Chem. Eng. Japan, 28: 270, 1964.

43. Turner, G.K., Associates. "Cperating and Service Manual, Model III Fluorometer."

44. Uno, Seiji, and Kintner, R.C., AIChE Journal, 2, 3, Sept. 1956.

45. Wilson, J.R., and Masch F.D., "Field Investigation of Mixing and Dispersion in a Deep Reservoir", Hydraulic Eng. Lab., University of Texas, Austin Texas, Tech. Report HYD 10-6701, June 1967.

46. Yih, C.S., 1951, Proc. 1st Nat. Cong. Appl. Mech., p. 941.

47. Zieminski, S.A., and Whittemore, R.C., "Induced Air Mixing of Large Bodies of Polluted Water." EPA Program #16080 DWP., 1970.

SECTION XII

LIST OF PUBLICATIONS

One publication, to date, has resulted from this project. It is entitled "Alternative Considerations in the Oxygenation of Reservoir Discharges and Rivers" by R. E. Speece, Fawzi Rayyan, George Murphee. It is a publication in the Conference Proceedings - Applications of Commerical Oxygen the Water and Wastewater Systems University of Texas Press (In Press).

No patents resulted from this study.

SECTION XIII

APPENDICES

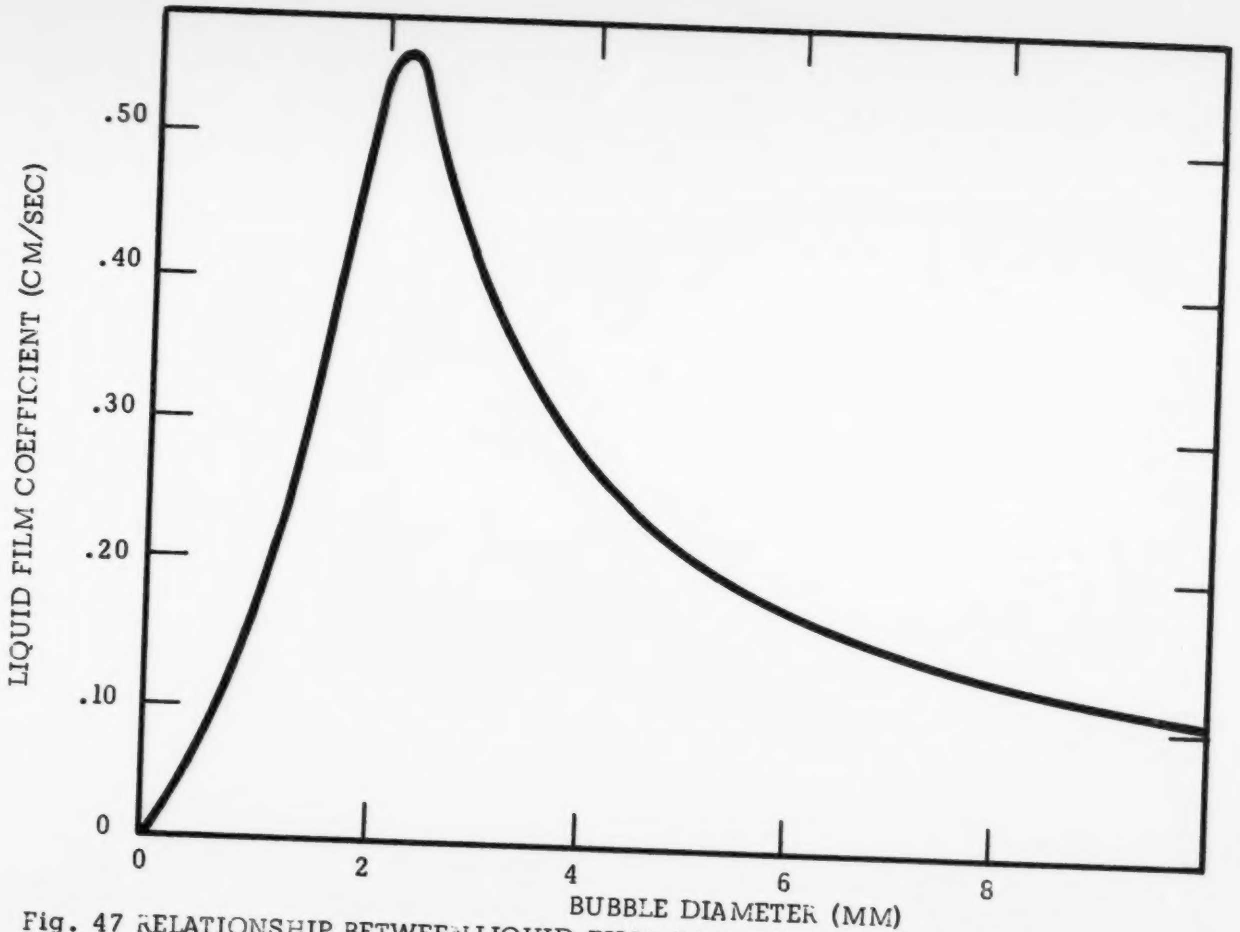

Fig. 47 RELATIONSHIP BETWEEN LIQUID FILM COEFFICIENT AND BUBBLE DIAMETER AT 20° CENTIGRADE

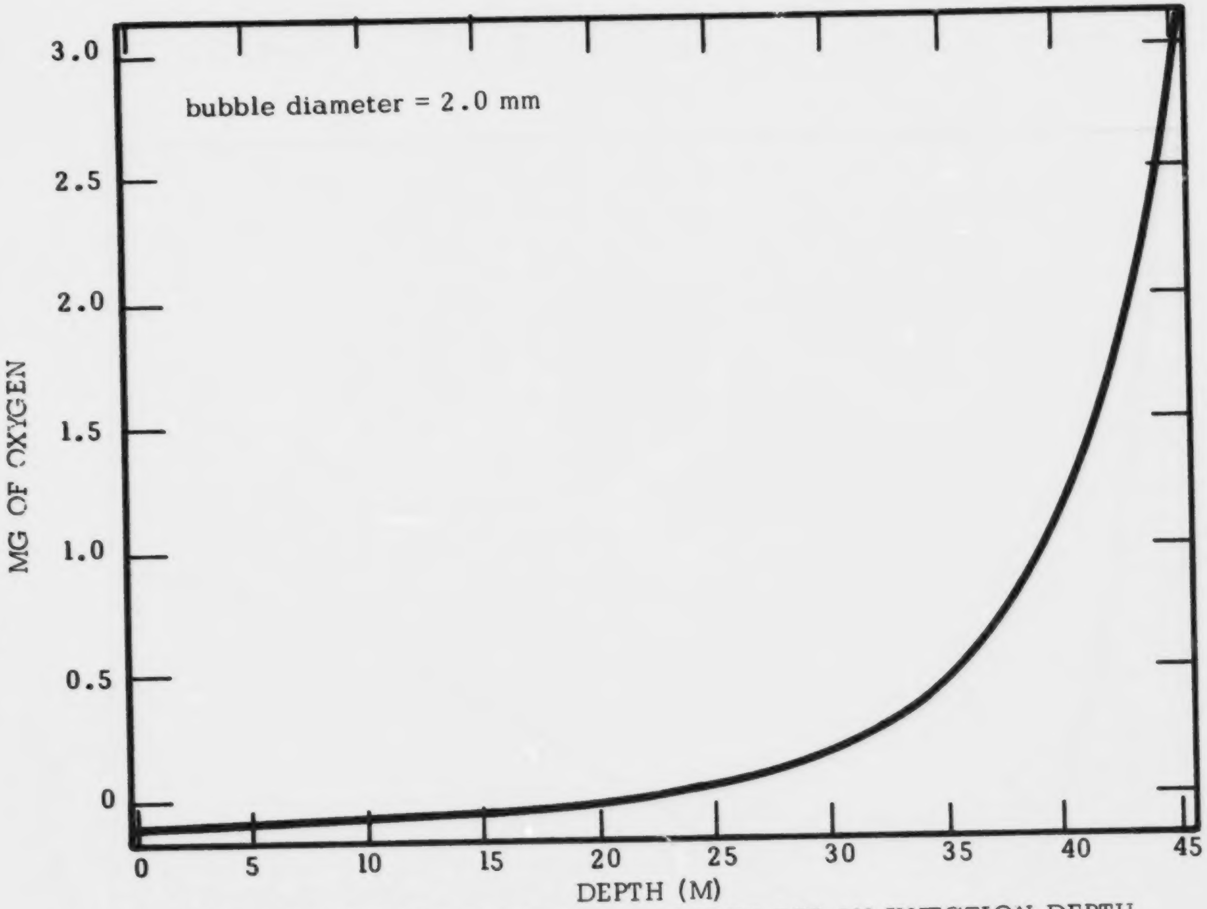

Fig. 48 MG OF OXYGEN AS A FUNCTION OF DEPTH FOR AN INJECTION DEPTH OF 45M AND A BUBBLE DIAMETER OF 2.0 MM

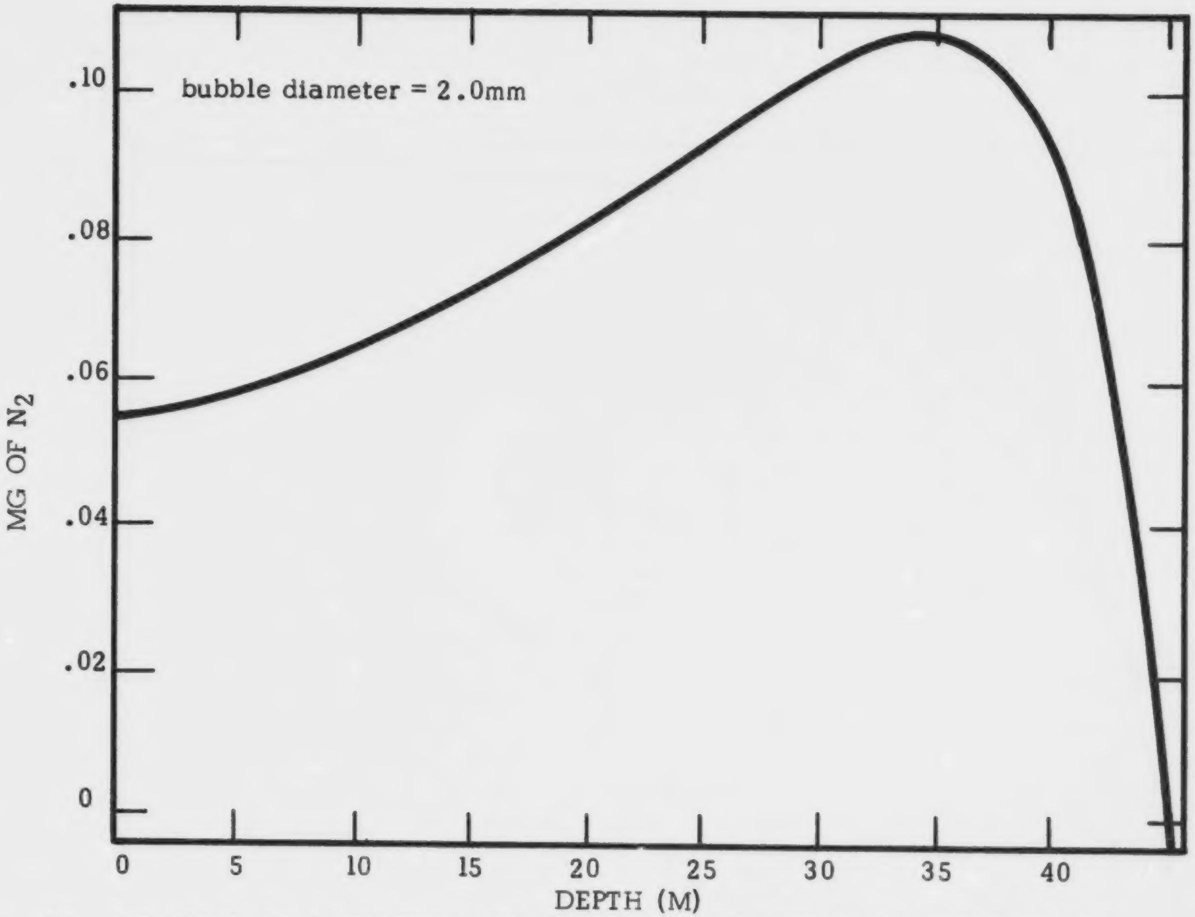

Fig. 49 MG OF N_2 AS A FUNCTION OF DEPTH FOR AN INJECTION DEPTH OF 45M AND A BUBBLE DIAMETER OF 2.0 MM

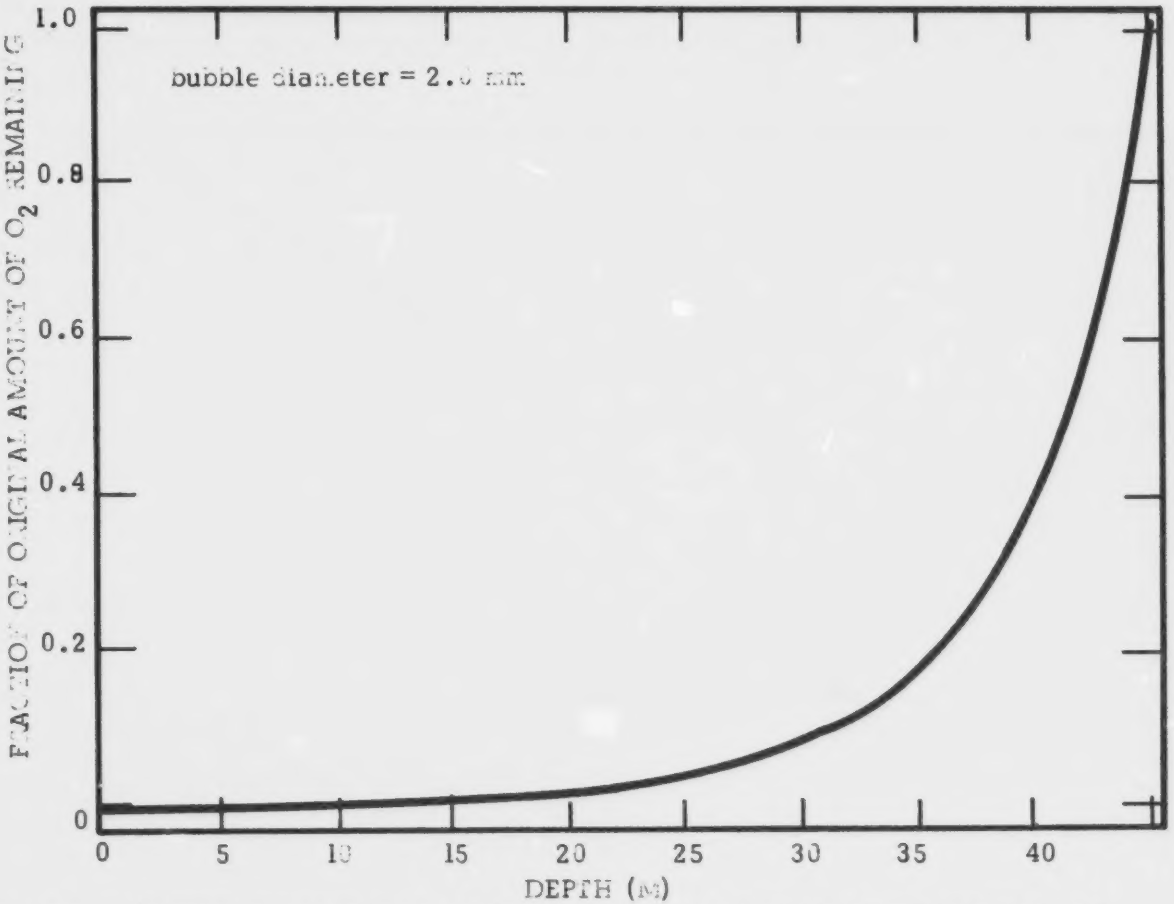

Fig. 50 FRACTION OF ORIGINAL AMOUNT OF O_2 REMAINING AS A FUNCTION OF DEPTH FOR AN INJECTION DEPTH OF 45M AND A BUBBLE DIAMETER OF 2.0MM

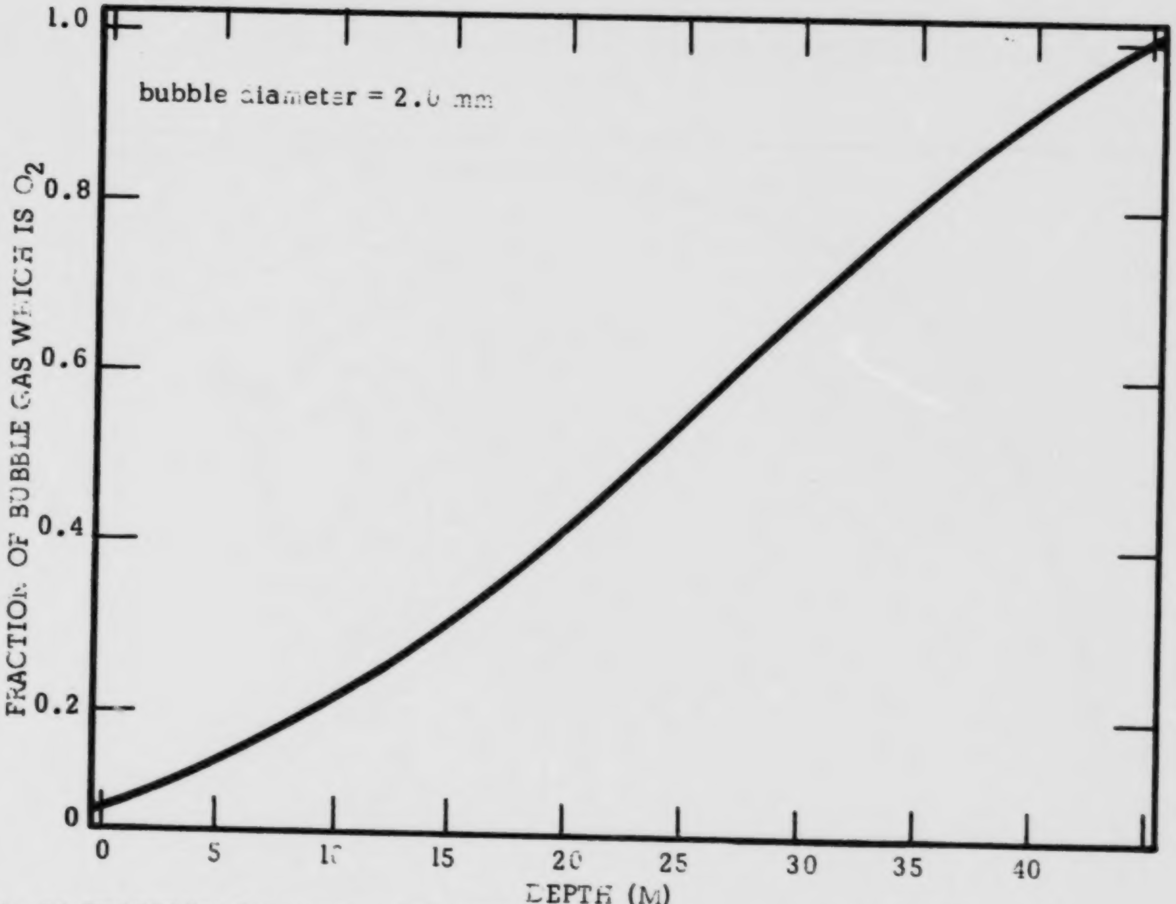

Fig.51 FRACTION OF BUBBLE GAS WHICH IS O_2 AS A FUNCTION OF DEPTH FOR AN INJECTION DEPTH OF 45M AND A BUBBLE DIAMETER OF 2.0MM

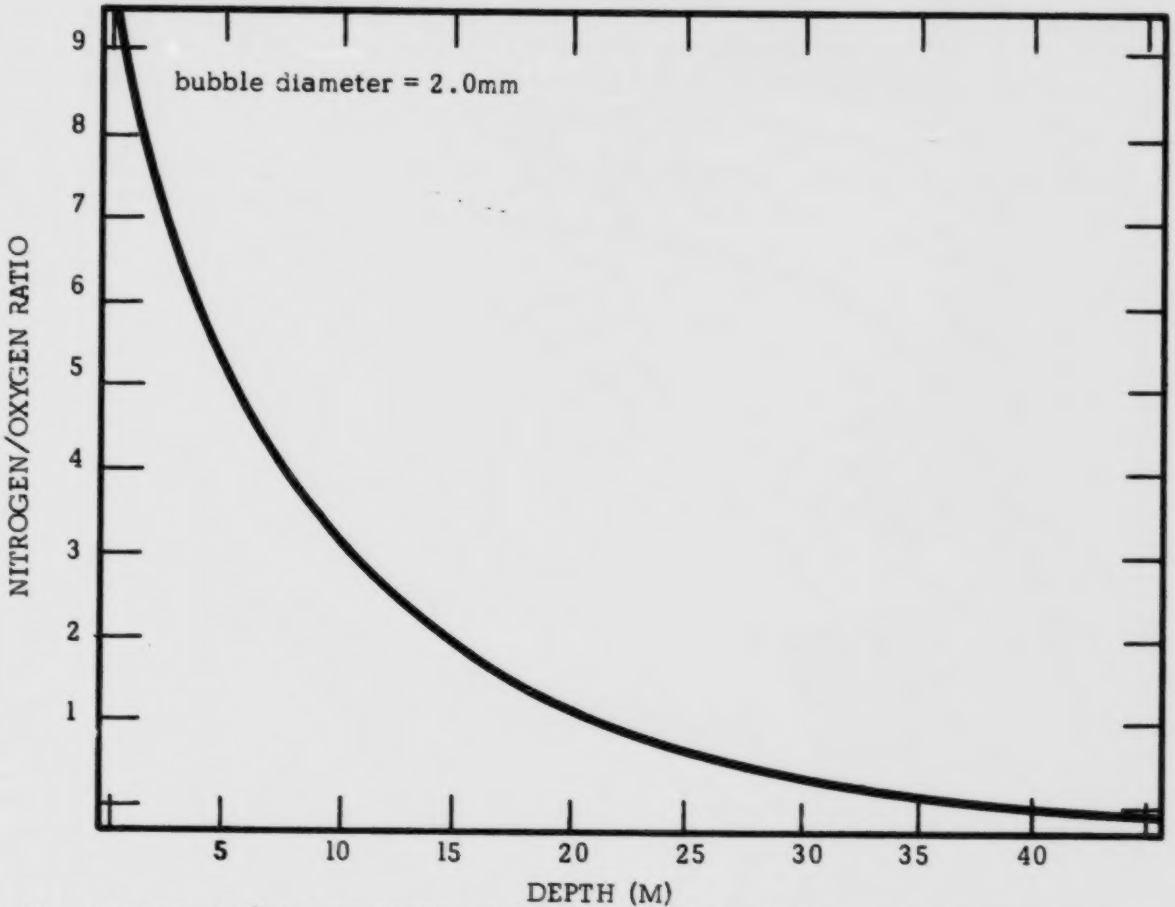

Fig. 52 NITROGEN/OXYGEN RATIO AS A FUNCTION OF DEPTH FOR AN INJECTION DEPTH OF 45 M AND A BUBBLE DIAMETER OF 2.0 MM

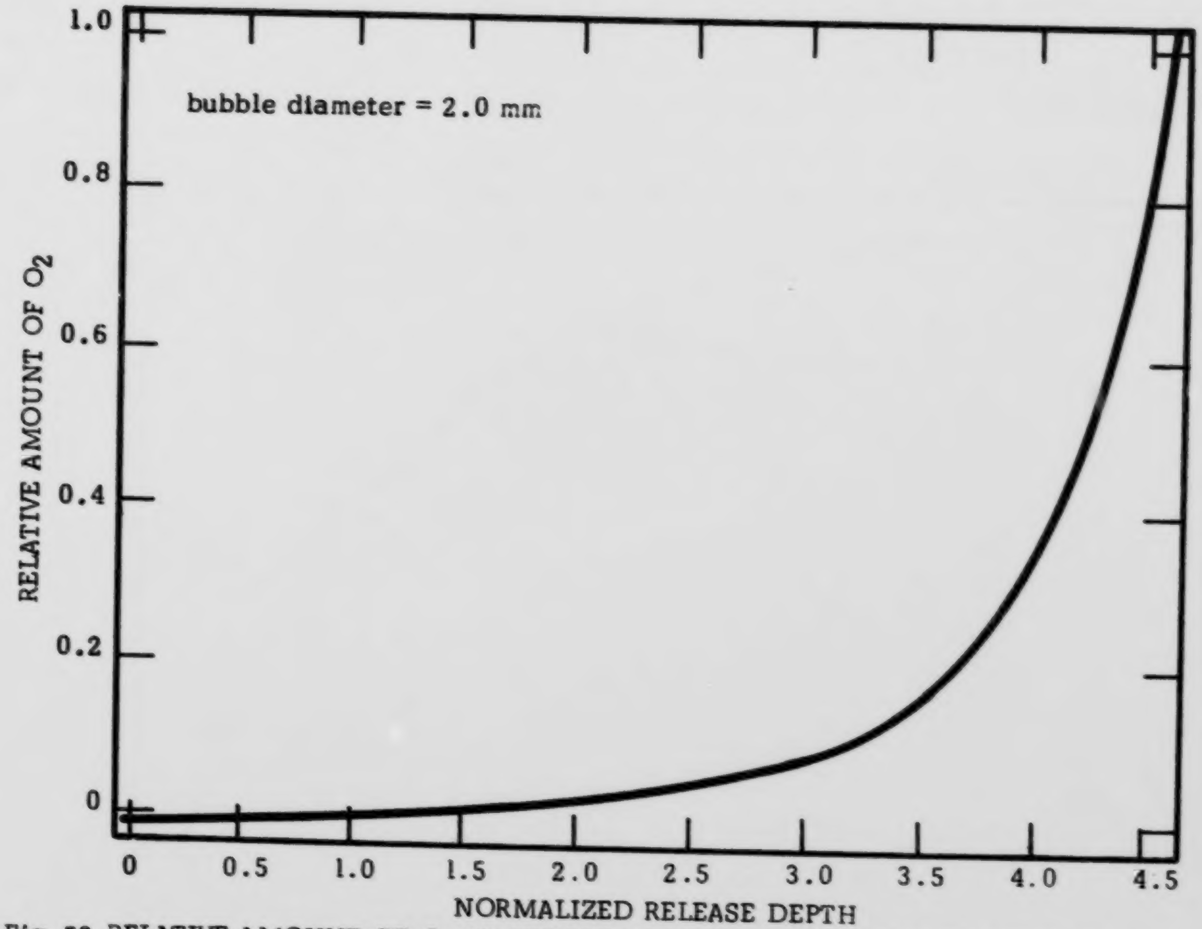

Fig.53 RELATIVE AMOUNT OF O_2 IN BUBBLE VS NORMALIZED RELEASE DEPTH FOR AN INJECTION DEPTH OF 45M AND A BUBBLE DIAMETER OF 2.0 MM

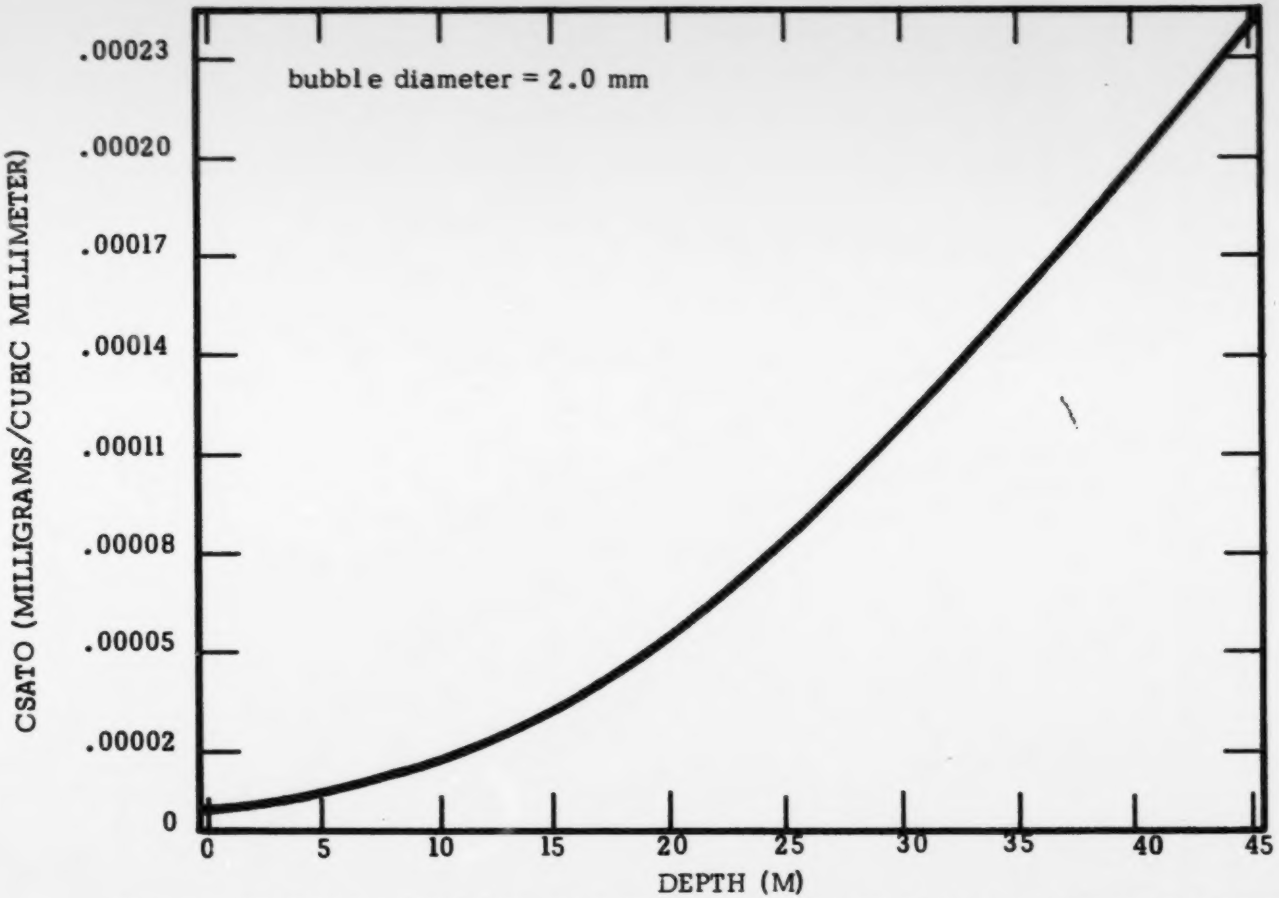

Fig. 54 CSATO VS DEPTH FOR AN INJECTION DEPTH OF 45 M AND A BUBBLE DIAMETER OF 2.0 MM

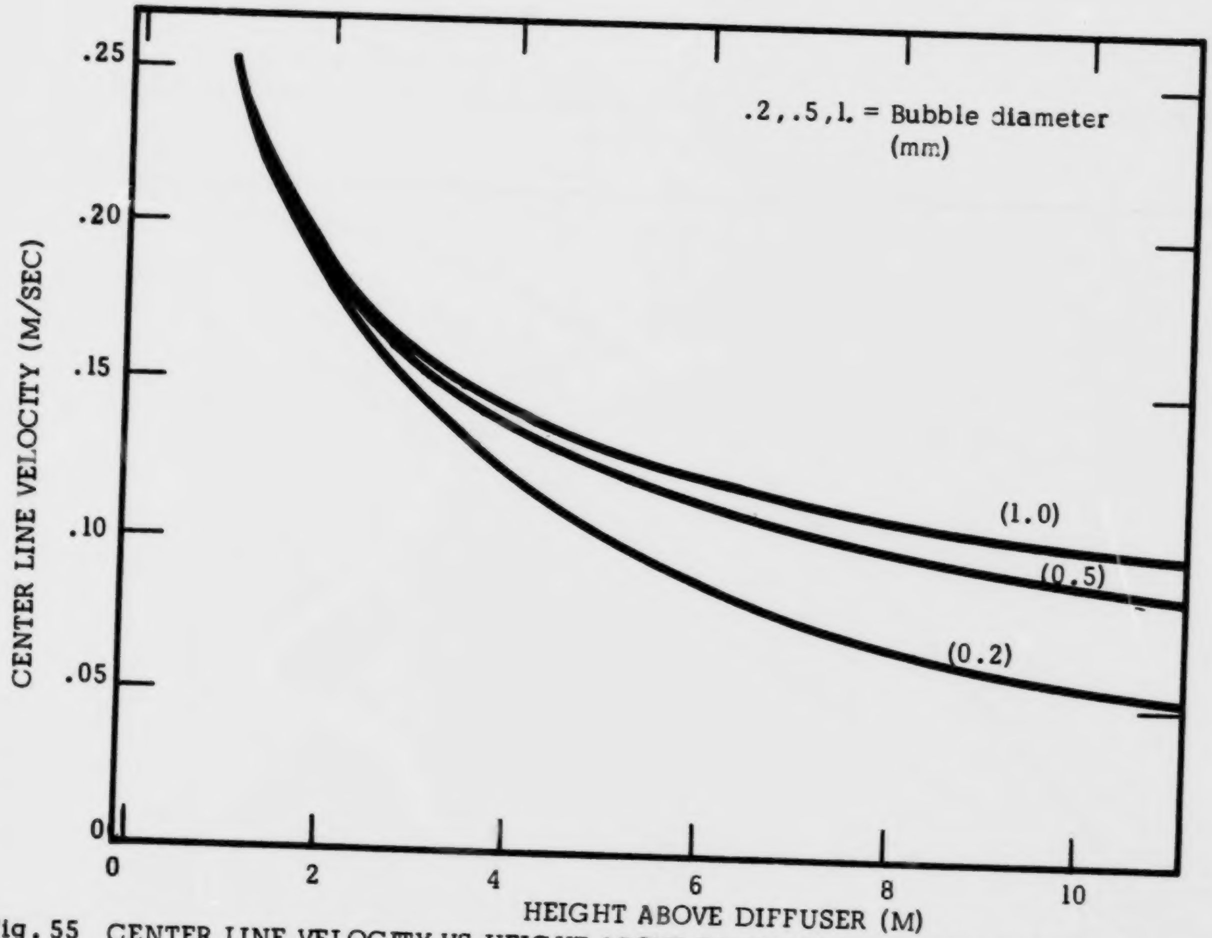

Fig. 55 CENTER LINE VELOCITY VS HEIGHT ABOVE DIFFUSER FOR A FLOW RATE OF 1 L/MIN AND BUBBLE DIAMETER OF 0.2, 0.5 AND 1.0 MM AND AN INJECTION DEPTH OF 25 M

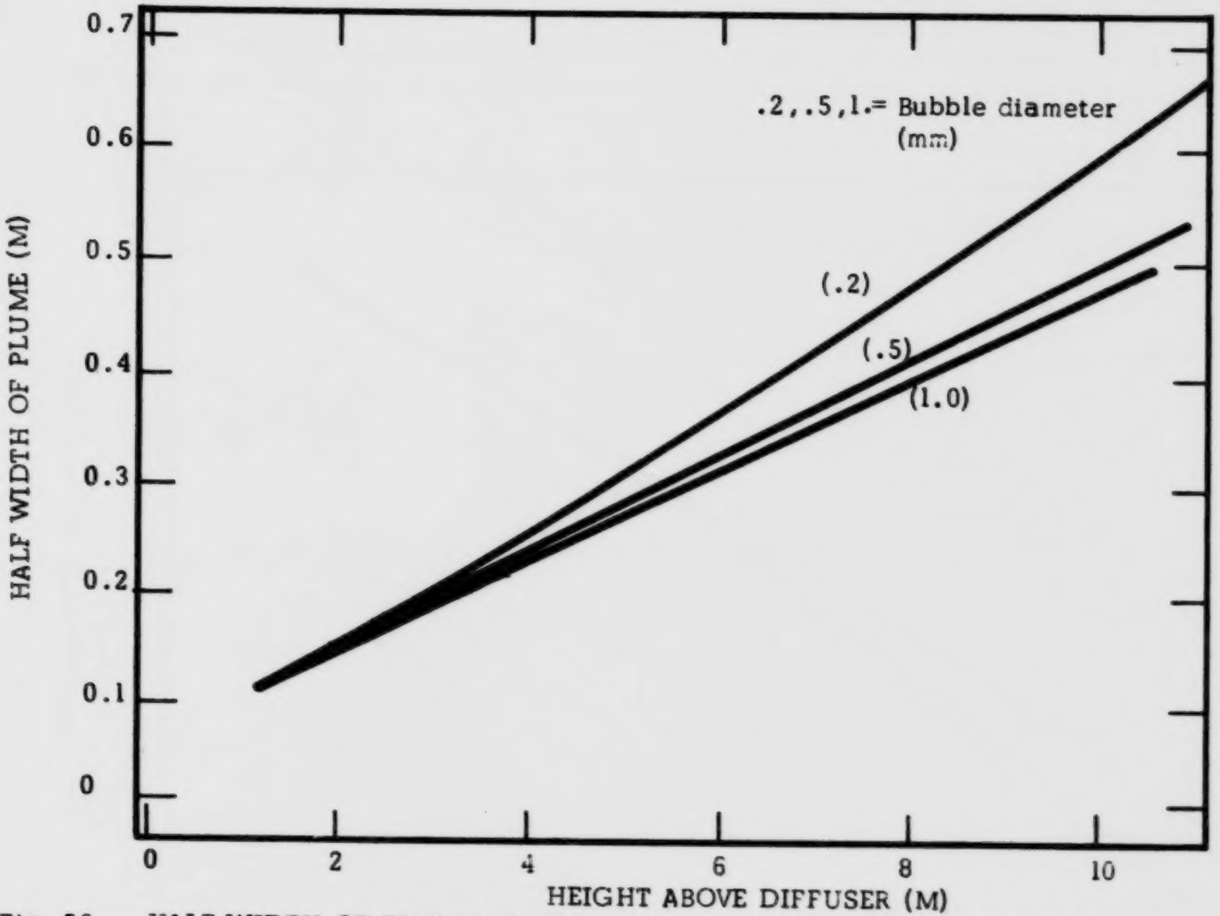

Fig. 56 HALF WIDTH OF PLUME VS HEIGHT ABOVE DIFFUSER FOR A FLOW RATE OF 1 L/MIN AND BUBBLE DIAMETER OF 0.2, 0.5, AND 1.0 MM AND AN INJECTION DEPTH OF 25 M

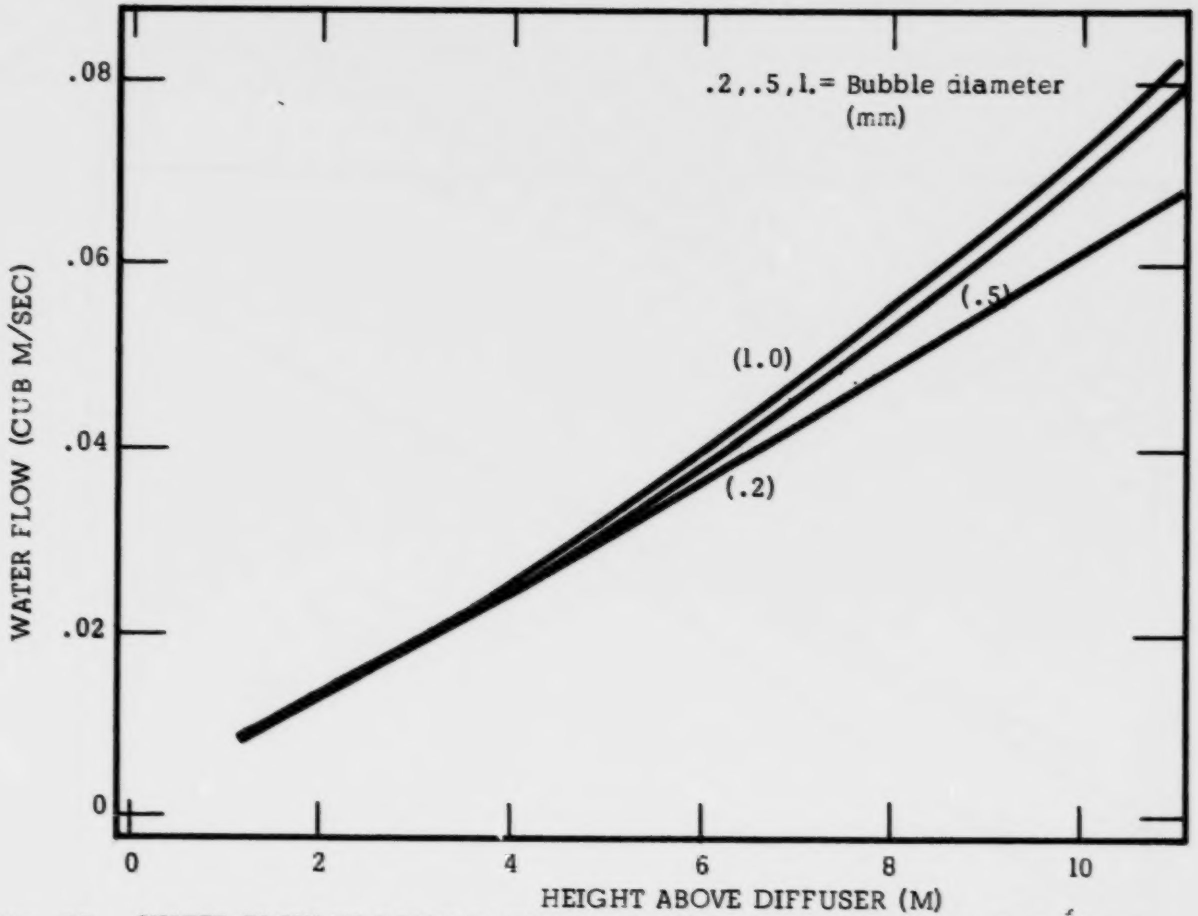

Fig. 57 WATER FLOW VS HEIGHT ABOVE DIFFUSER FOR A FLOW RATE OF 1 L/MIN AND BUBBLE DIAMETER OF 0.2, 0.5, AND 1.0 MM AND AN INJECTION DEPTH OF 25M

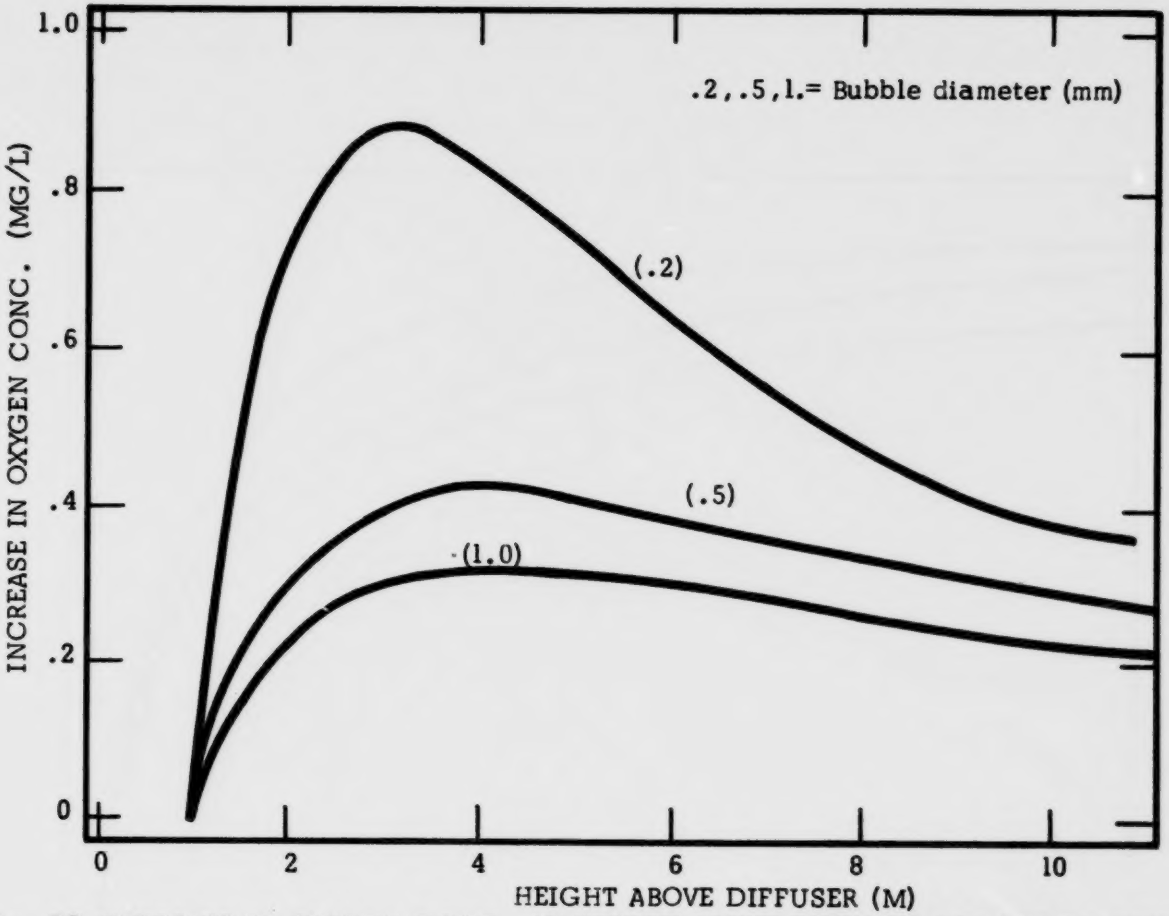

Fig. 58 INCREASE IN OXYGEN CONC. VS HEIGHT ABOVE DIFFUSER FOR A FLOW RATE OF 1. L/MIN AND BUBBLE DIAMETER OF 0.2, 0.5 AND 1.0 MM AND AN INJECTION DEPTH OF 25 M

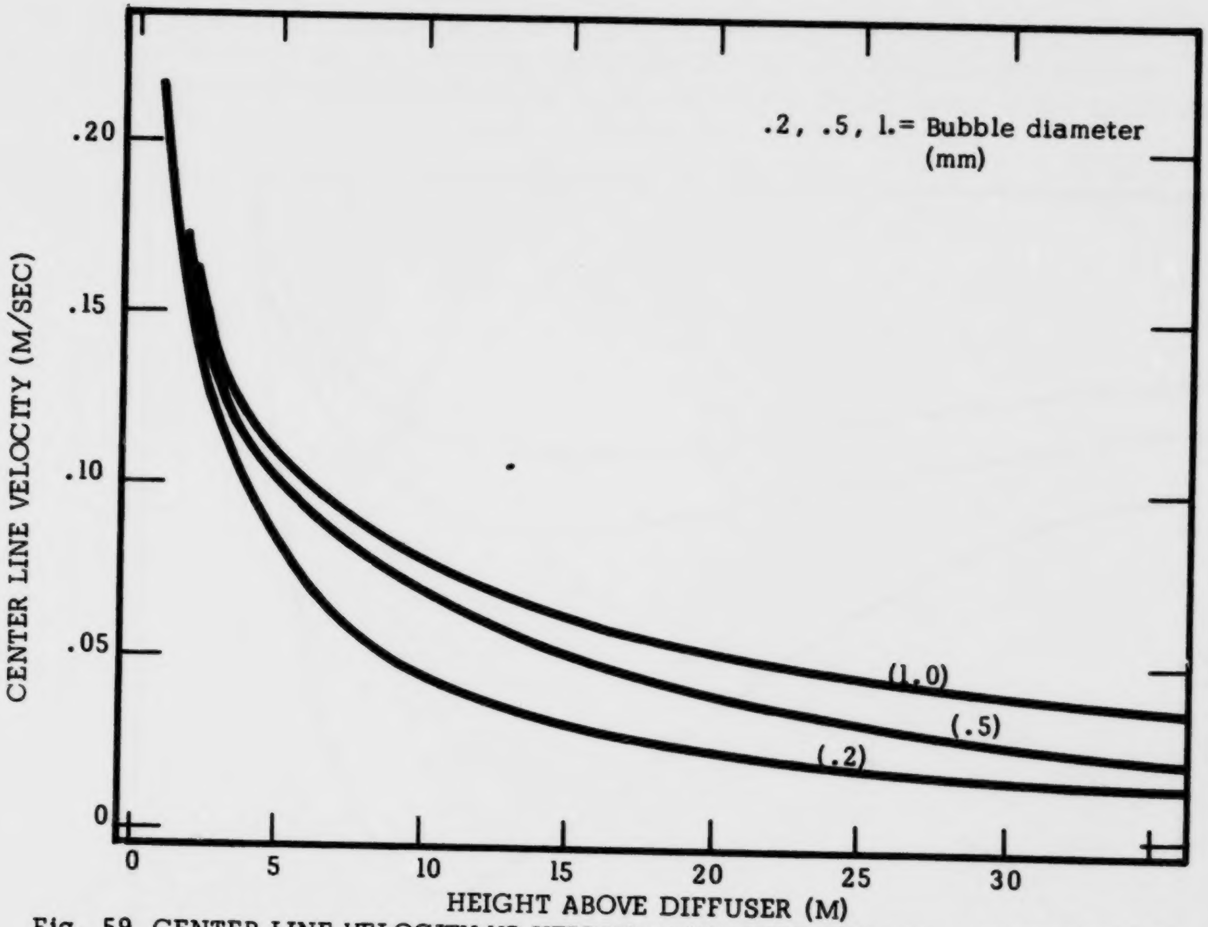

Fig. 59 CENTER LINE VELOCITY VS HEIGHT ABOVE DIFFUSER FOR A FLOW RATE OF 1 L/MIN AND BUBBLE DIAMETER OF 0.2, 0.5, AND 1.0 MM AND AN INJECTION DEPTH OF 50 M

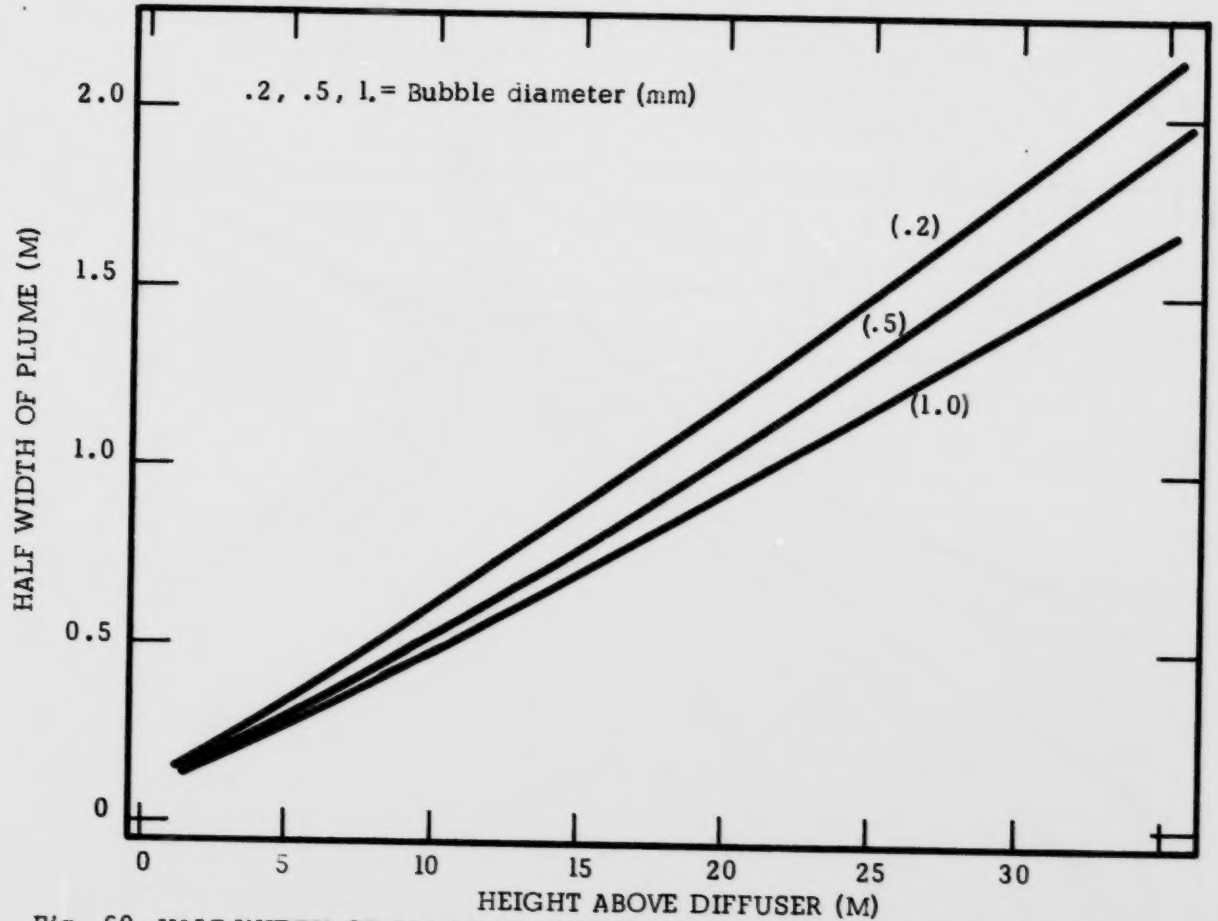

Fig. 60 HALF WIDTH OF PLUME VS HEIGHT ABOVE DIFFUSER FOR A FLOW RATE OF 1 L/MIN AND BUBBLE DIAMETER OF 0.2, 0.5 AND 1.0 MM AND AN INJECTION DEPTH OF 50 M

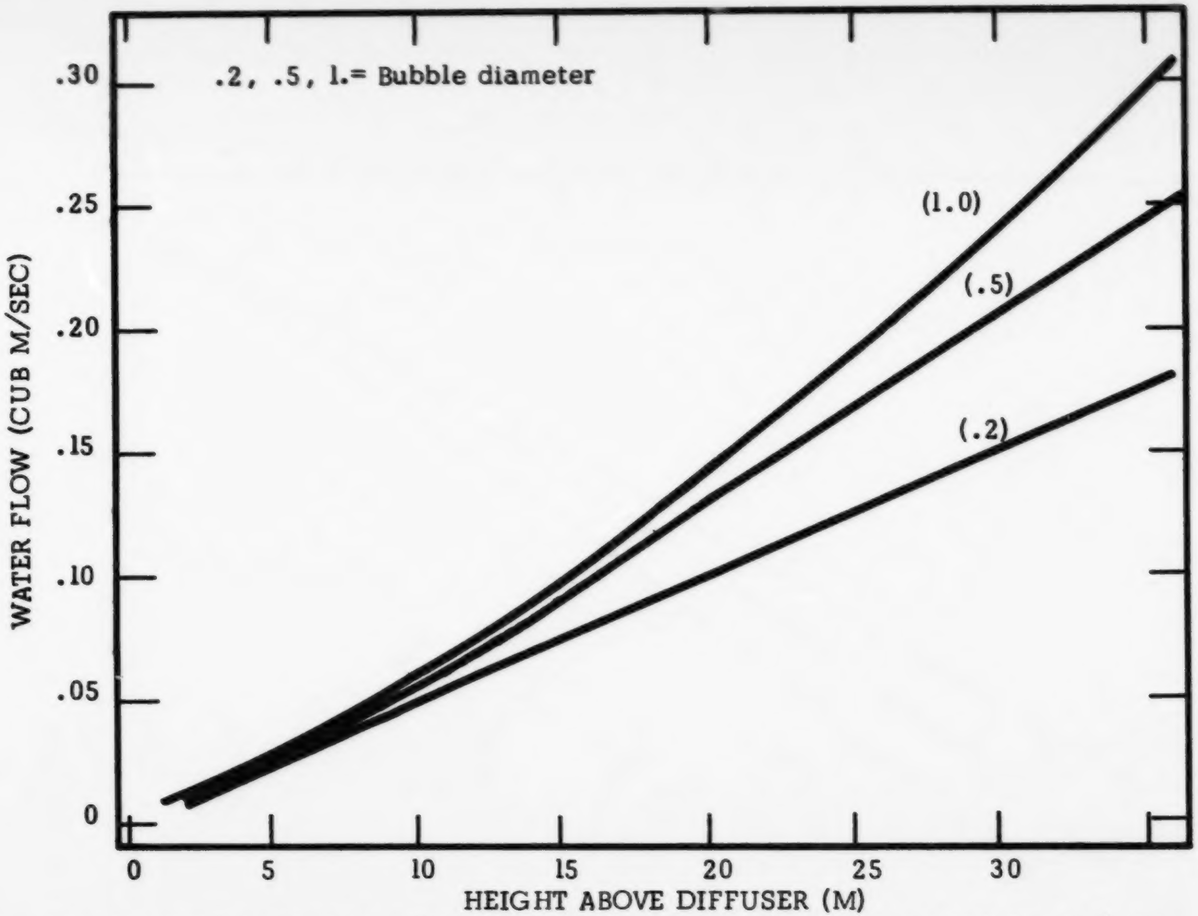

Fig. 61 WATER FLOW VS HEIGHT ABOVE DIFFUSER FOR A FLOW RATE OF 1 L/MIN AND BUBBLE DIAMETER OF 0.2, 0.5, AND 1.0 MM AND AN INJECTION DEPTH OF 50 M

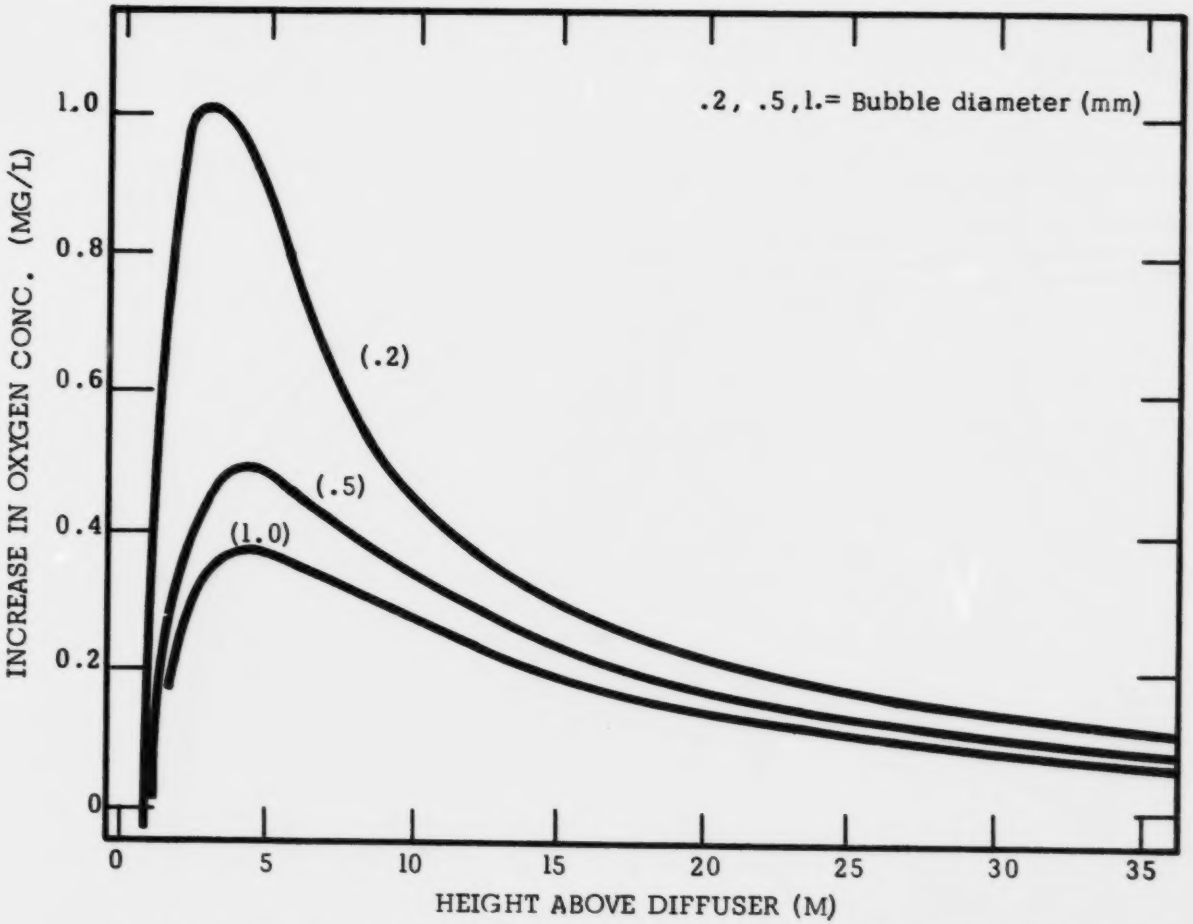

Fig. 62 INCREASE IN OXYGEN CONC. VS HEIGHT ABOVE DIFFUSER FOR A FLOW RATE OF 1. L/MIN AND BUBBLE DIAMETER OF 0.2, 0.5, AND 1.0 MM AND AN INJECTION DEPTH OF 50 M

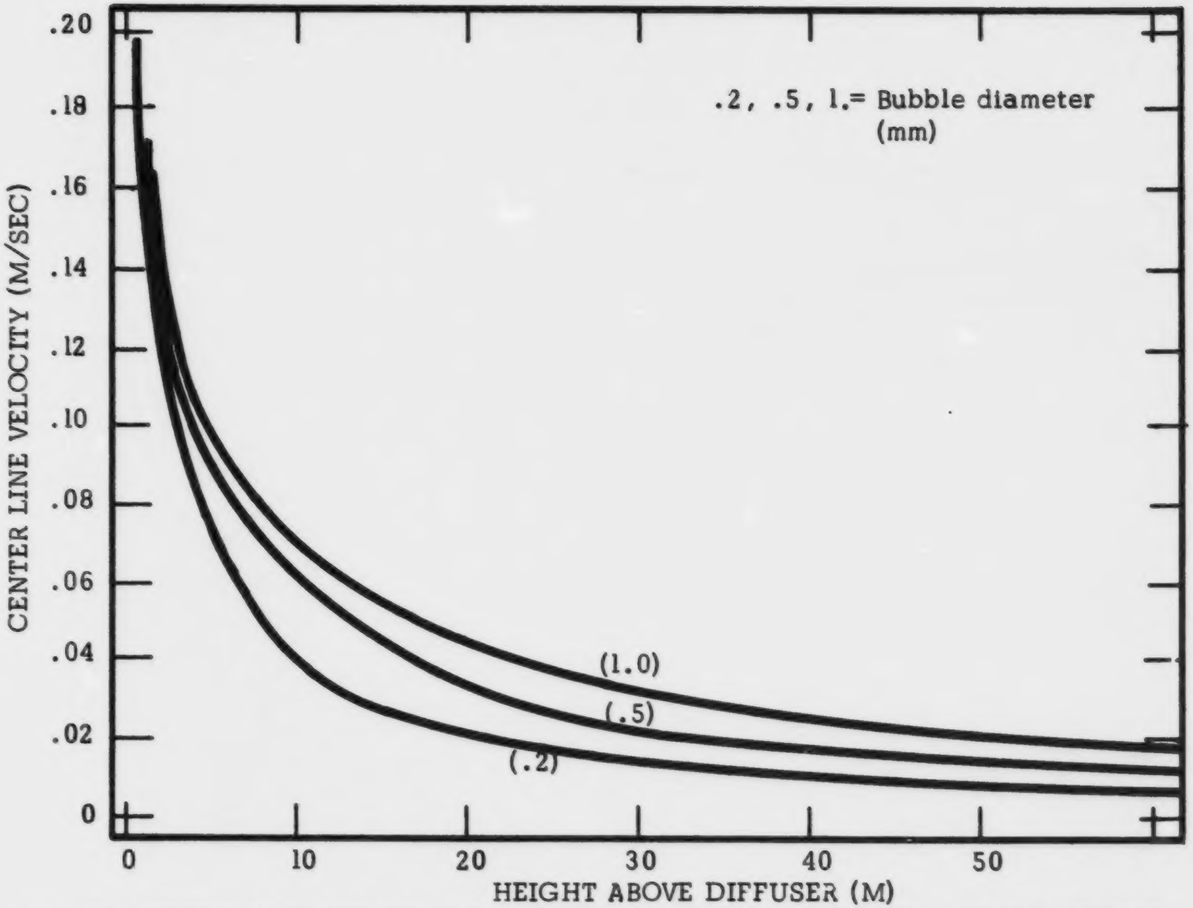

Fig. 63 CENTER LINE VELOCITY VS HEIGHT ABOVE DIFFUSER FOR A FLOW RATE OF 1 L/MIN AND BUBBLE DIAMETER OF 0.2, 0.5, AND 1.0 MM AND AN INJECTION DEPTH OF 75 M

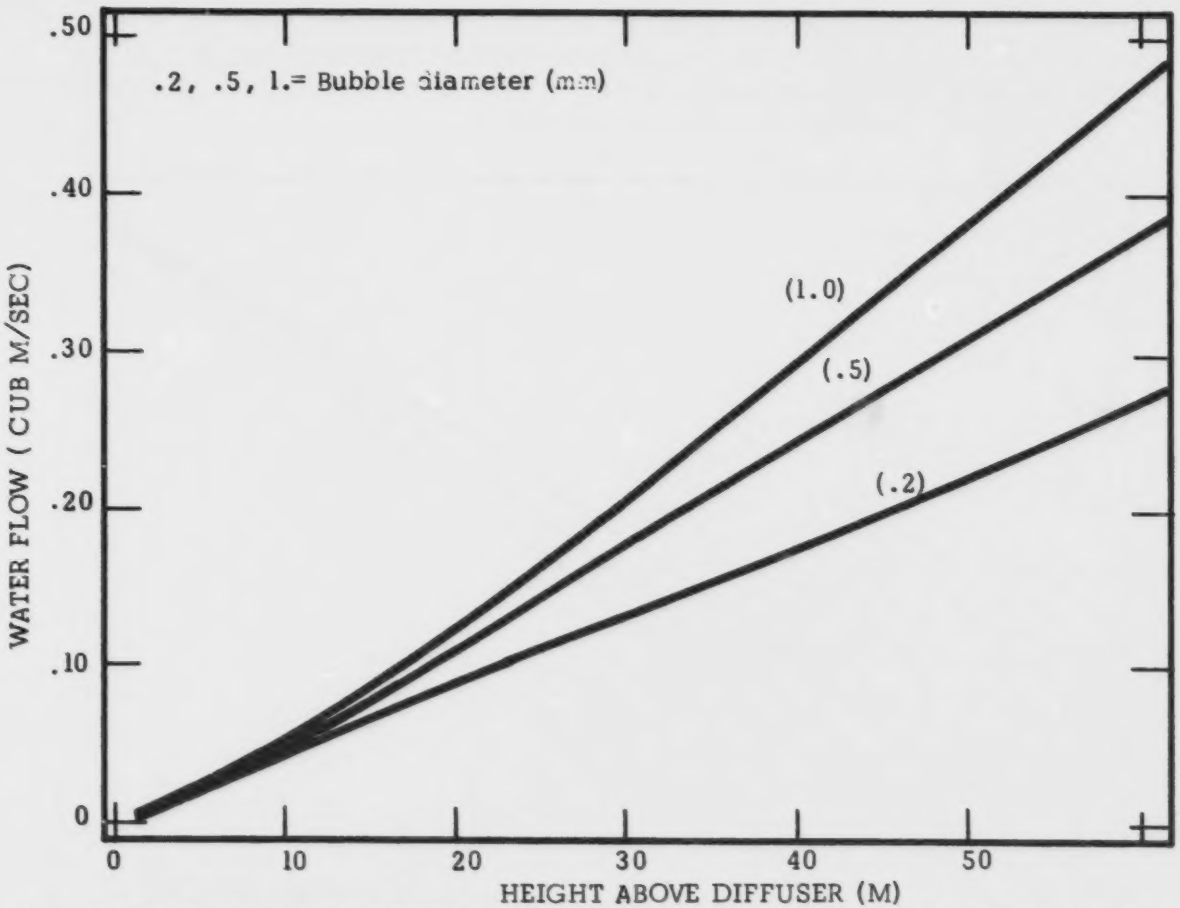

Fig. 64 WATER FLOW VS HEIGHT ABOVE DIFFUSER FOR A FLOW RATE OF 1 L/MIN AND BUBBLE DIAMETER OF 0.2, 0.5, AND 1.0 MM AND AN INJECTION DEPTH OF 75 M

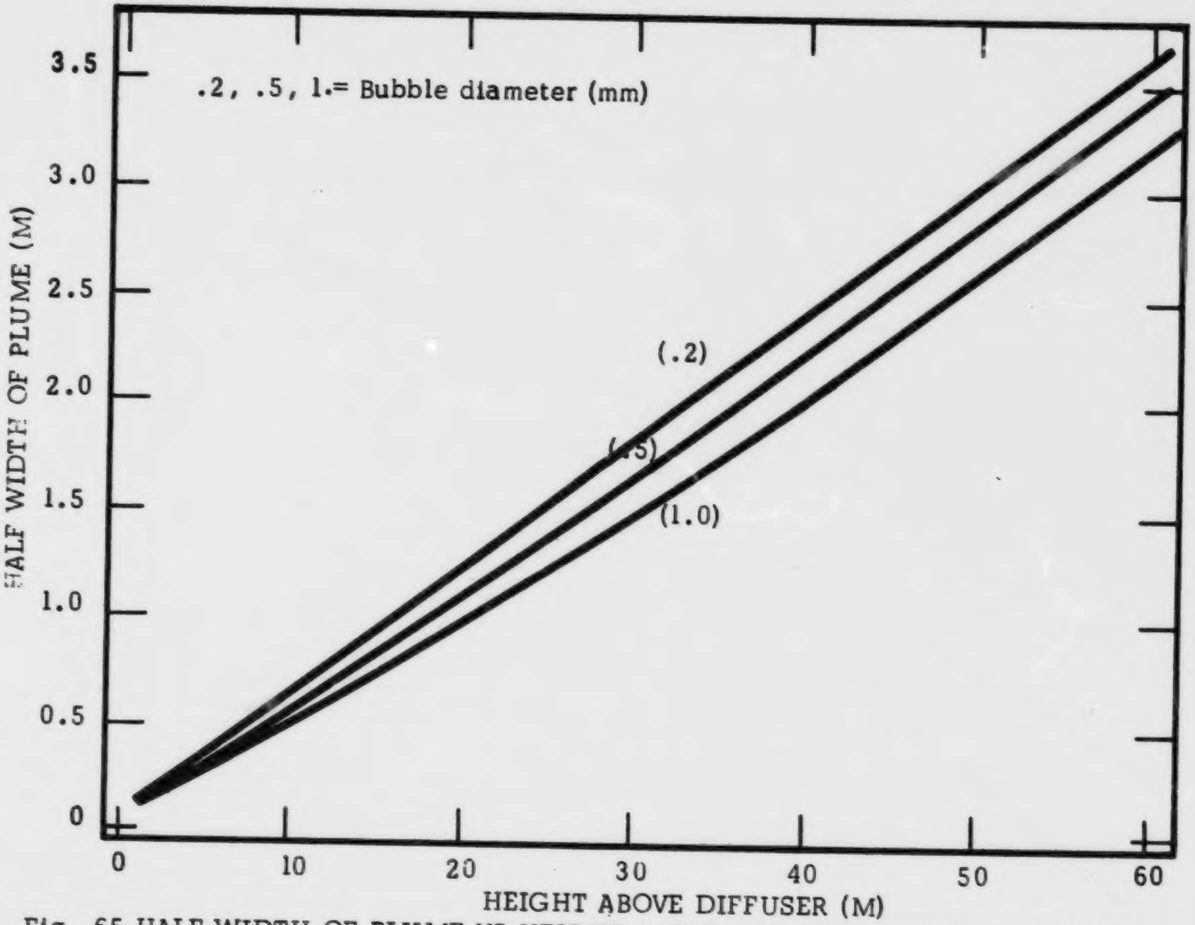

Fig. 65 HALF WIDTH OF PLUME VS HEIGHT ABOVE DUFFUSER FOR A FLOW RATE OF 1 L/MIN AND BUBBLE DIAMETER OF 0.2, 0.5 AND 1.0 MM AND AN INJECTION DEPTH OF 75 M

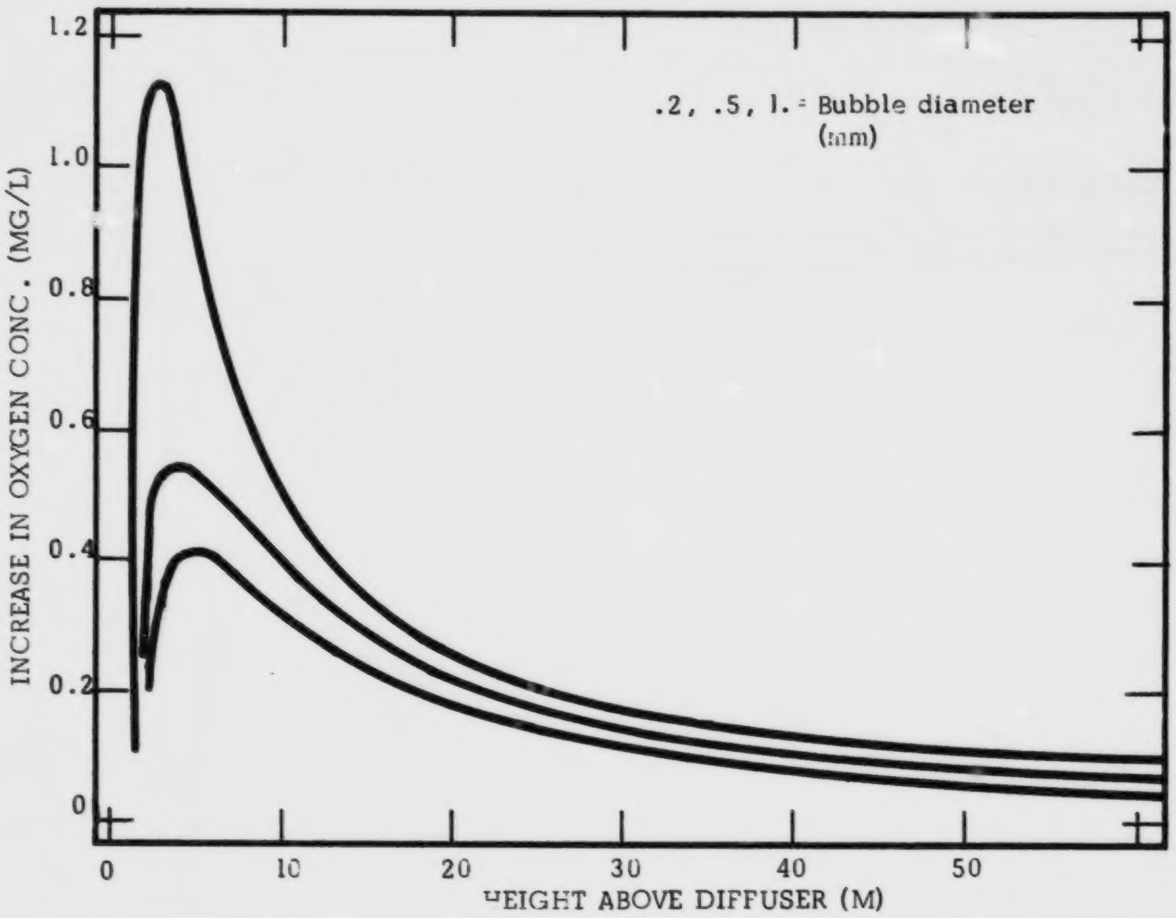

Fig. 66 INCREASE IN OXYGEN CONC. VS HEIGHT ABOVE DIFFUSER FOR A FLOW RATE OF 1. L/MIN AND BUBBLE DIAMETER OF 0.2, 0.5 AND 1.0 MM AND AN INJECTION DEPTH OF 75 M.

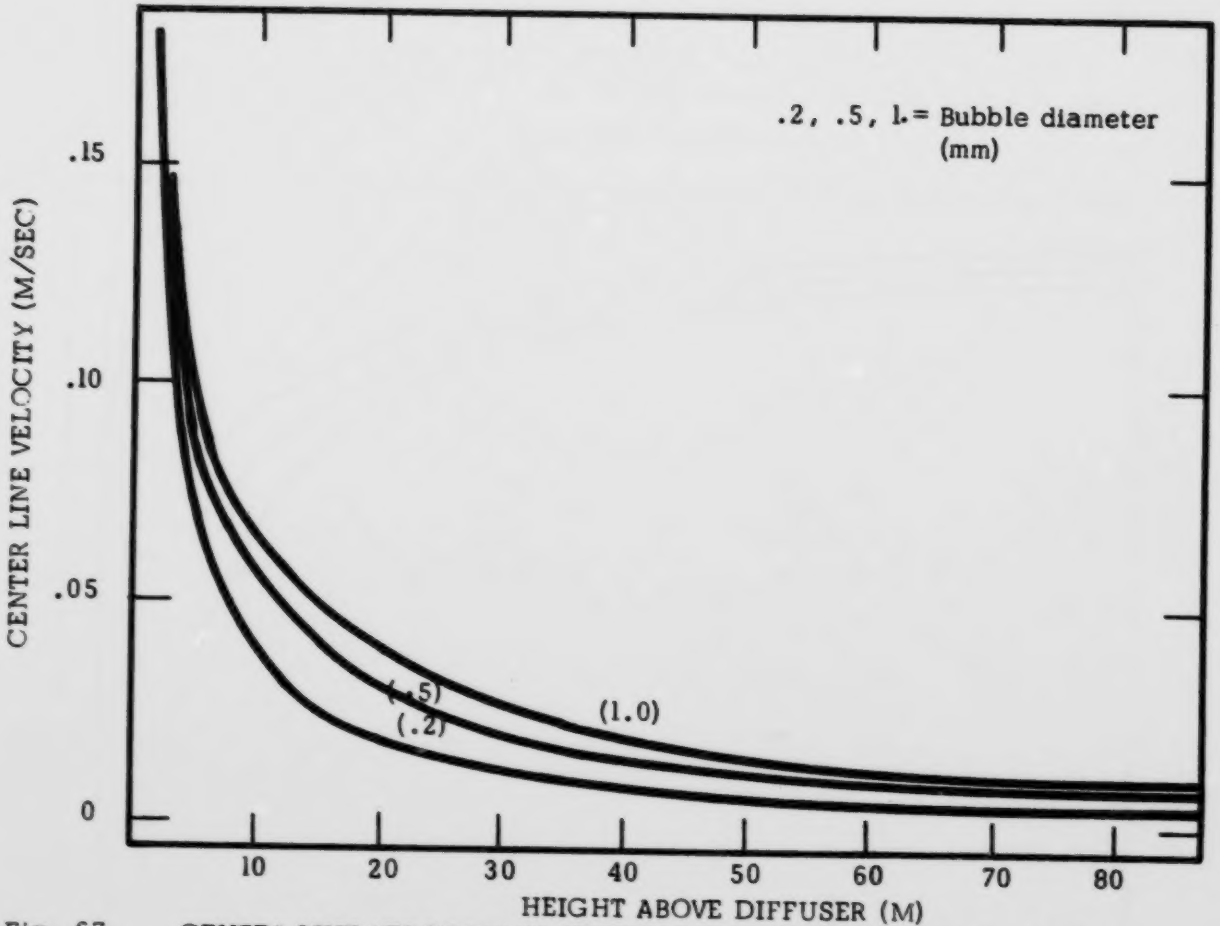

Fig. 67 CENTER LINE VELOCITY VS HEIGHT ABOVE DIFFUSER FOR A FLOW RATE OF 1 L/MIN BUBBLE DIAMETER OF 0.2, 0.5, AND 1.0 MM AND AN INJECTION DEPTH OF 100 M

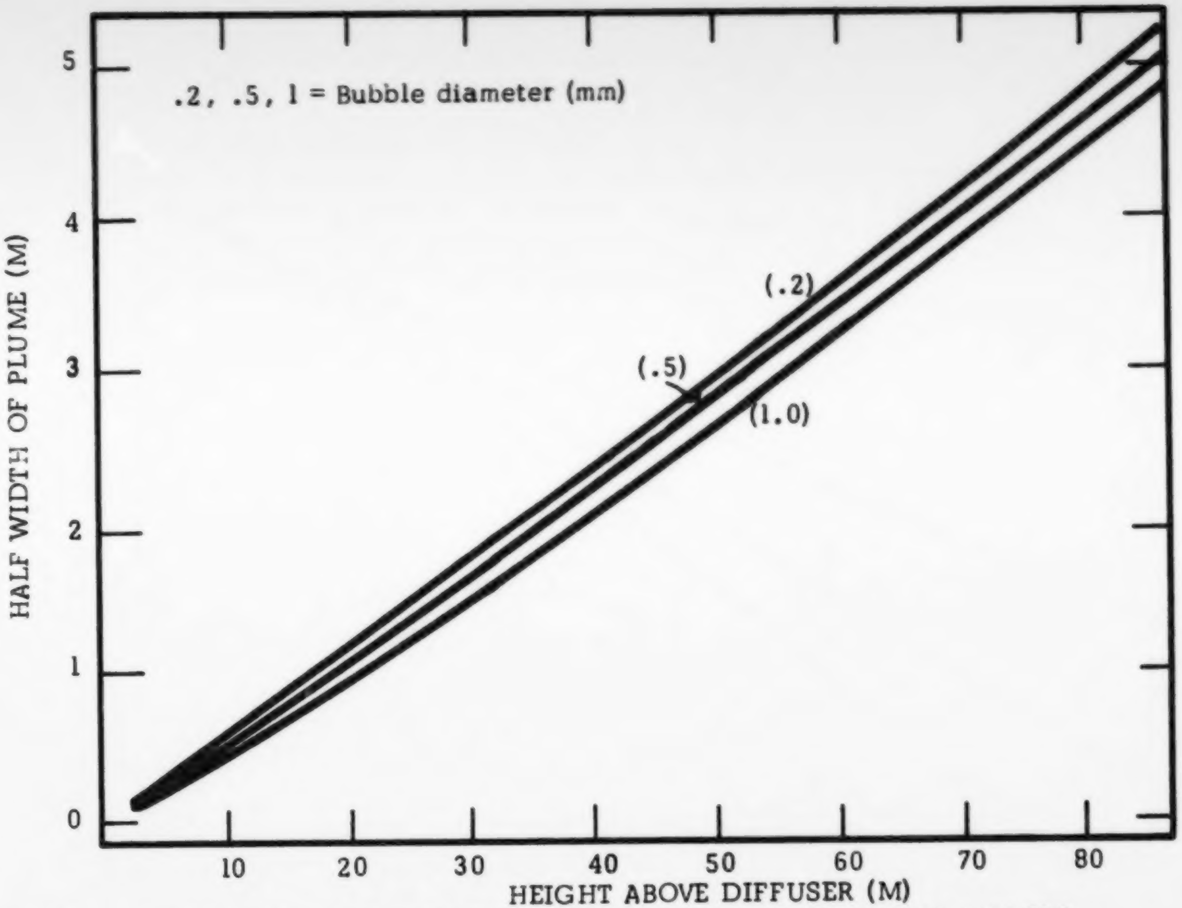

Fig. 68 HALF WIDTH OF PLUME VS HEIGHT ABOVE DIFFUSER FOR A FLOW RATE OF 1 L/MIN AND BUBBLE DIAMETER OF 0.2, 0.5 AND 1.0 MM AND AN INJECTION DEPTH OF 100 M

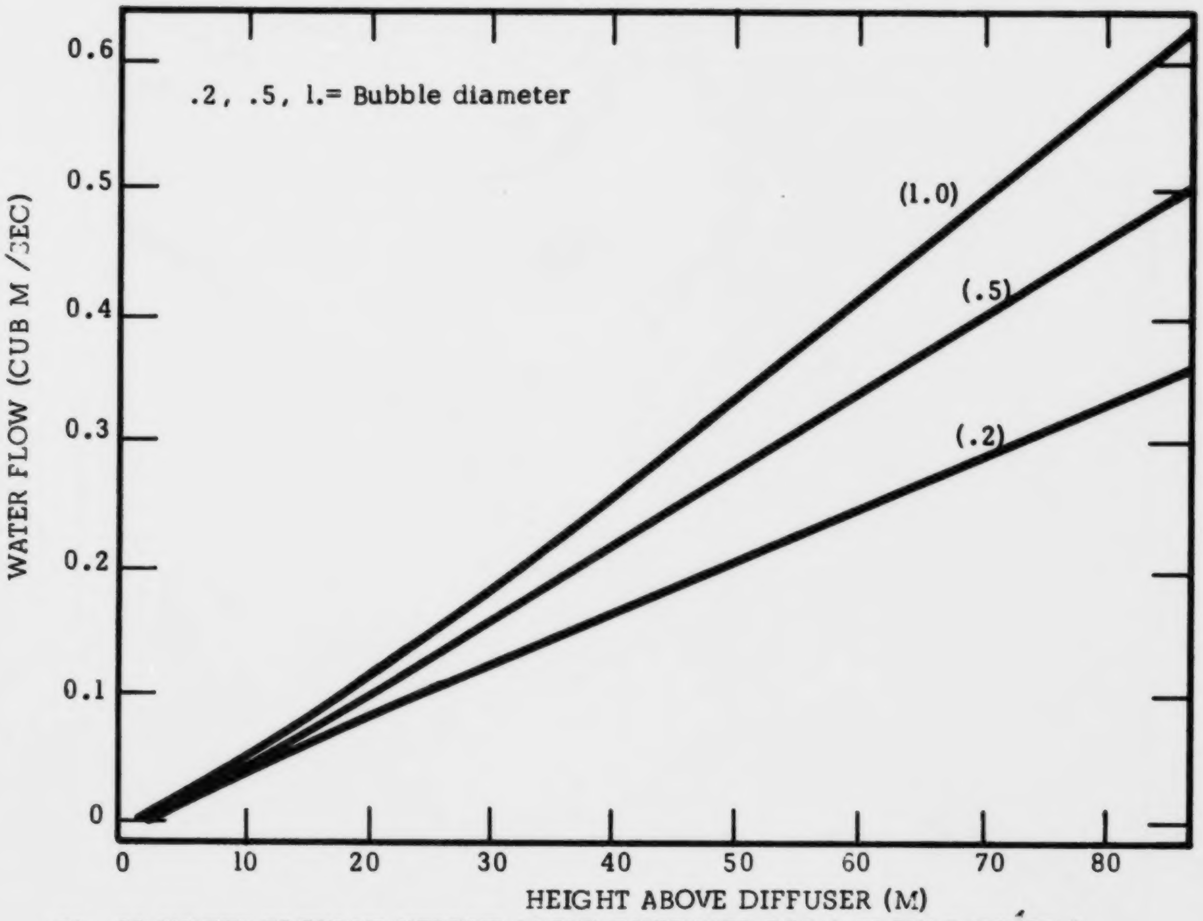

Fig.69 WATER FLOW VS HEIGHT ABOVE DUFFUSER FOR A FLOW RATE OF 1 L/MIN AND BUBBLE DIAMETER OF 0.2, 0.5 AND 1.0 MM AND AN INJECTION DEPTH OF 100 M

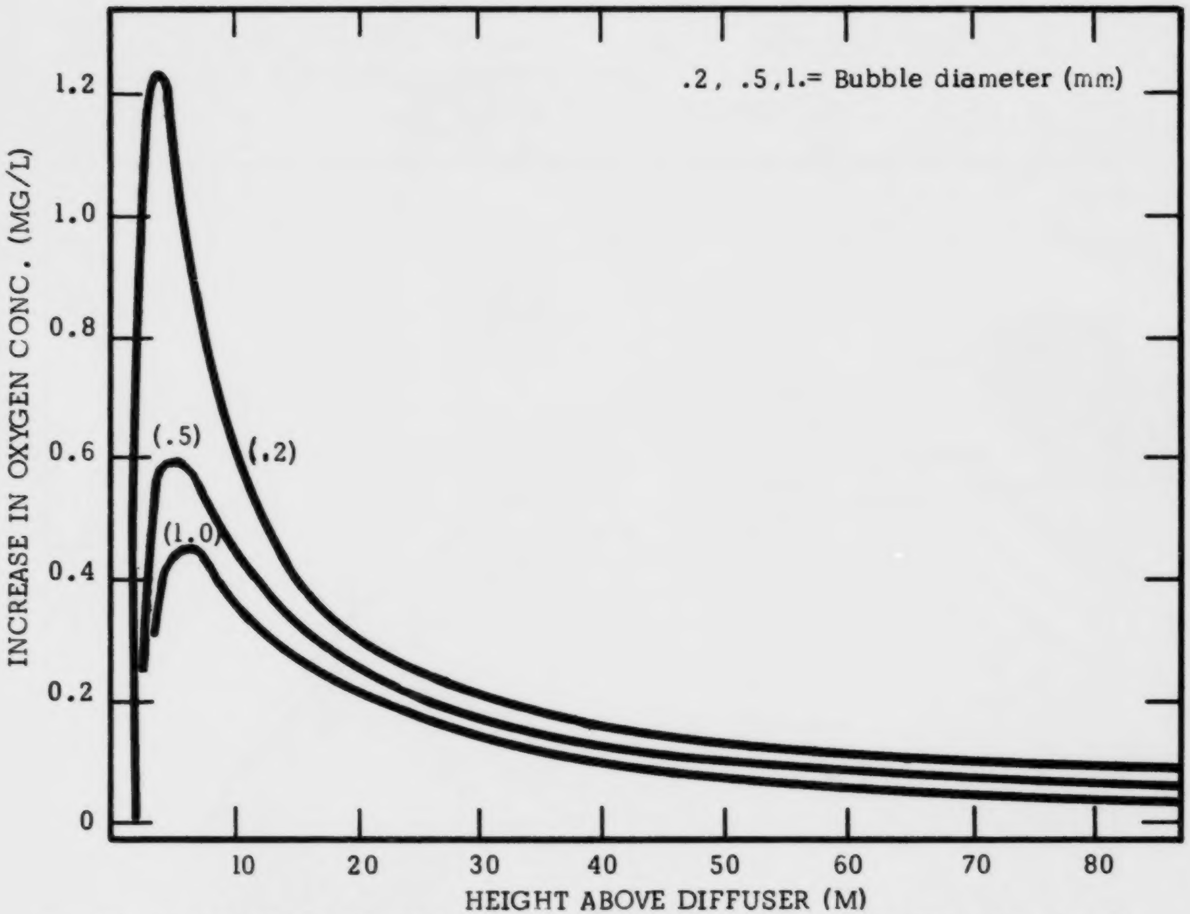

Fig. 70 INCREASE IN OXYGEN CONC. VS HEIGHT ABOVE DIFFUSER FOR A FLOW RATE OF 1. L/MIN AND BUBBLE DIAMETER OF 0.2, 0.5 AND 1.0 MM AND AN INJECTION DEPTH OF 100 M

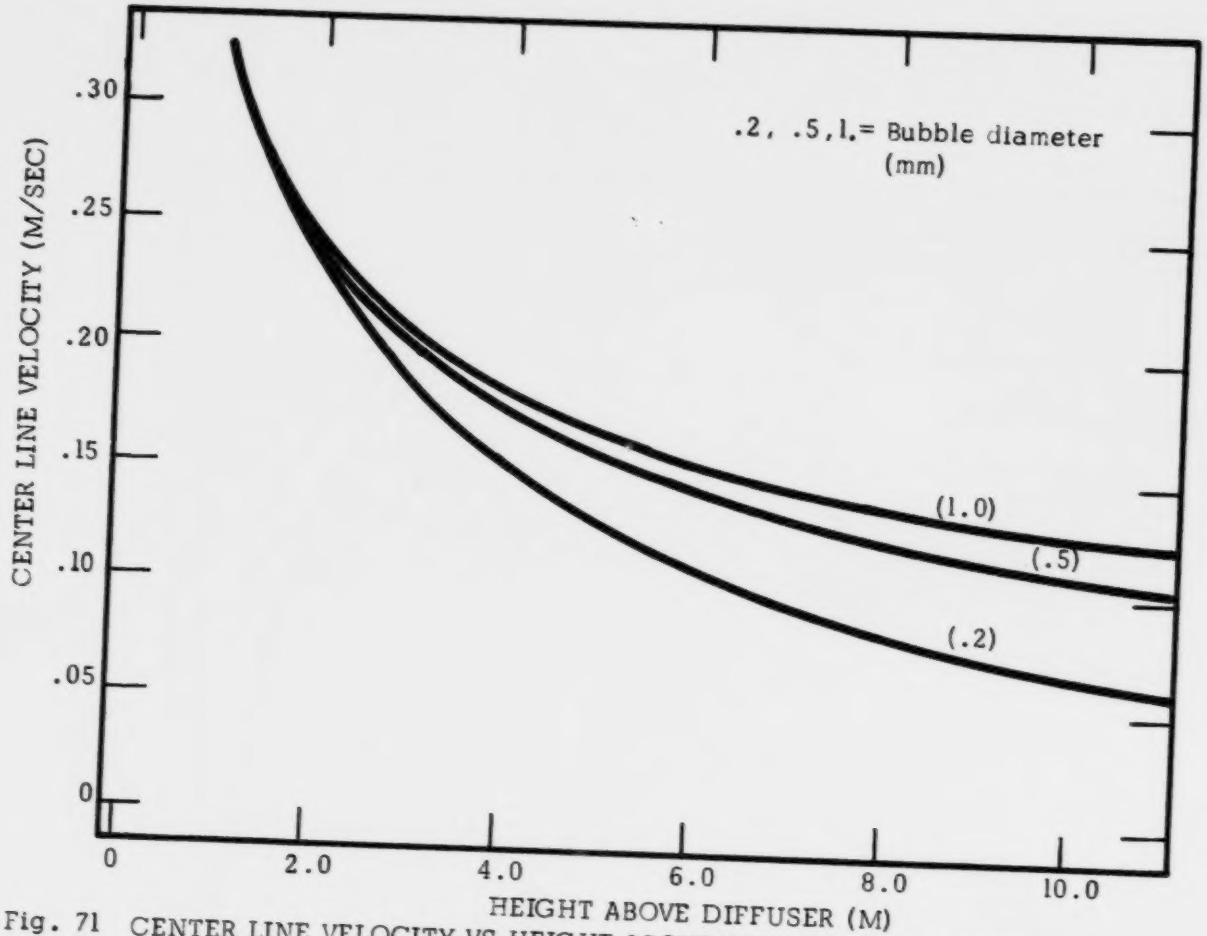

Fig. 71 CENTER LINE VELOCITY VS HEIGHT ABOVE DIFFUSER FOR A FLOW RATE OF 2 L/MIN AND BUBBLE DIAMETER OF 0.2, 0.5 AND 1.0 MM AND AN INJECTION DEPTH OF 25M

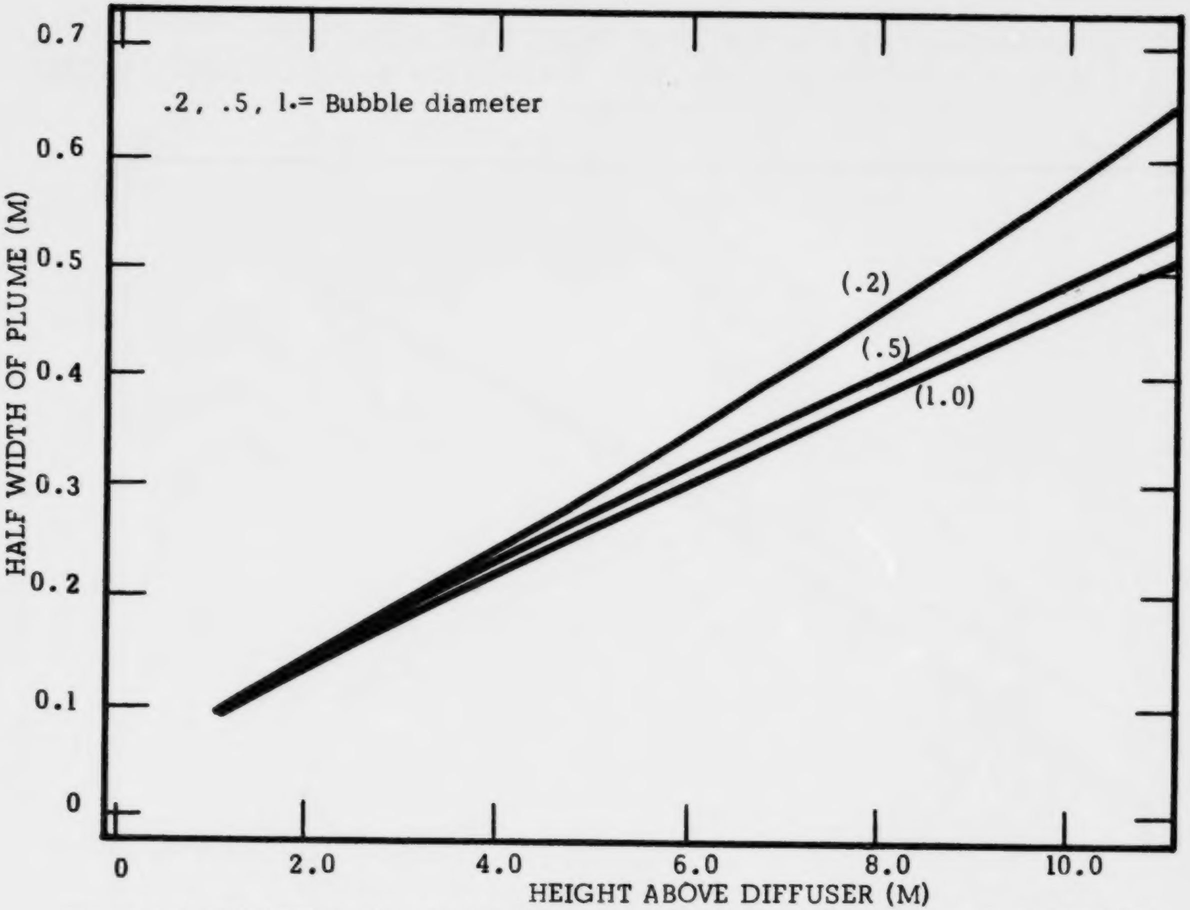

Fig. 72 HALF WIDTH OF PLUME VS HEIGHT ABOVE DIFFUSER FOR A FLOW RATE OF 2 L/MIN AND BUBBLE DIAMETER OF 0.2, 0.5 AND 1.0 MM AND AN INJECTION DEPTH OF 25M

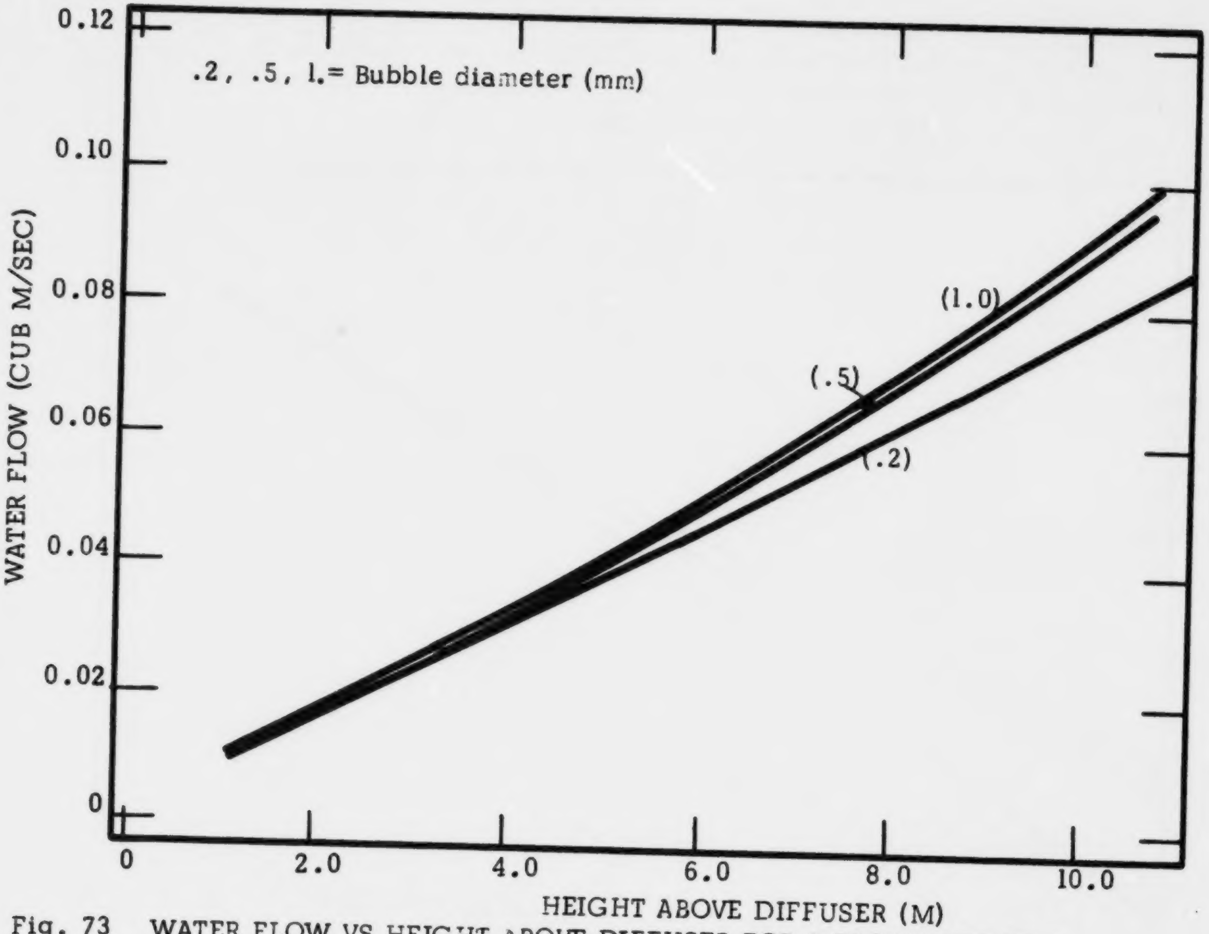

Fig. 73 WATER FLOW VS HEIGHT ABOVE DIFFUSER FOR A FLOW RATE OF 2 L/MIN AND BUBBLE DIAMETER OF 0.2, 0.5 AND 1.0 MM AND AN INJECTION DEPTH OF 25 M

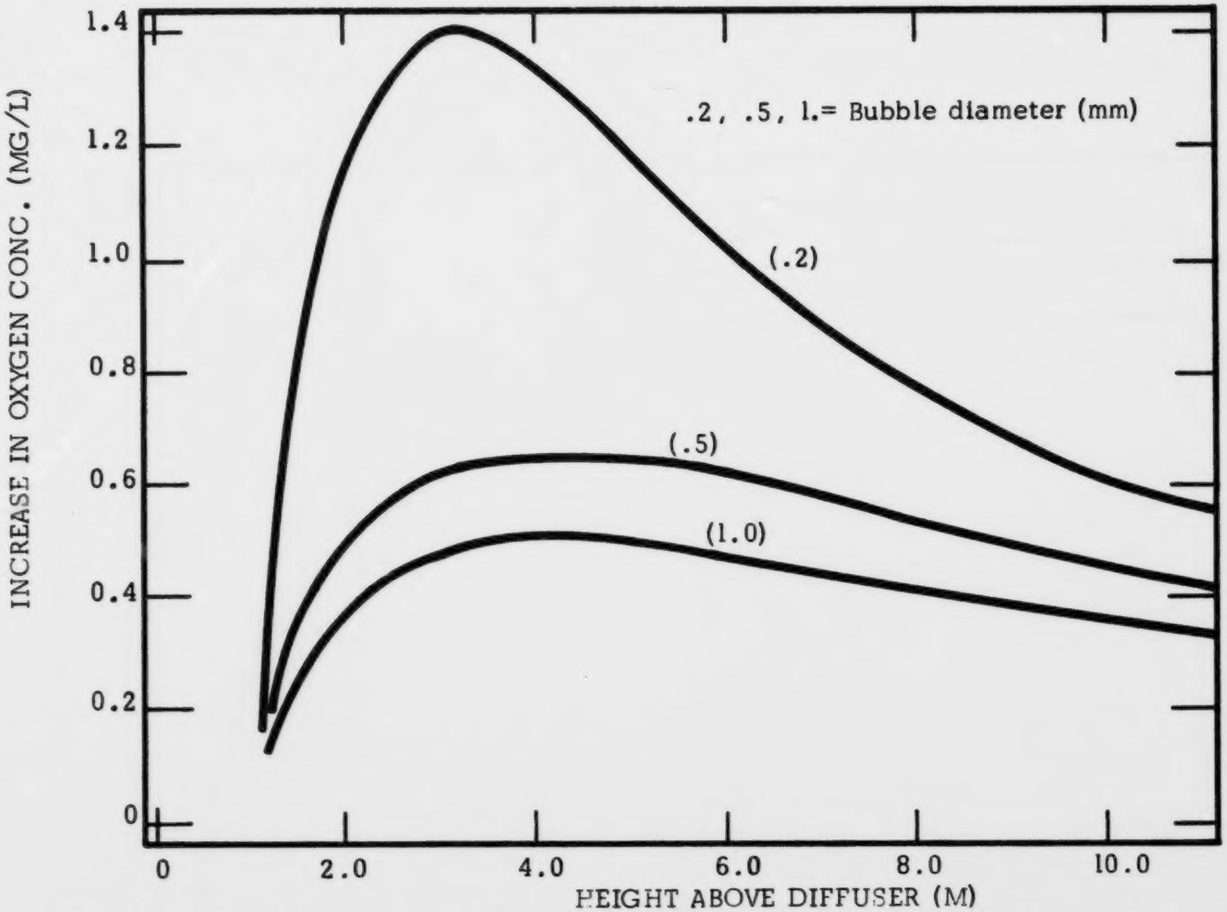

Fig. 74 INCREASE IN OXYGEN CONC. VS HEIGHT ABOVE DIFFUSER FOR A FLOW RATE OF 2. L/MIN AND BUBBLE DIAMETER OF 0.2, 0.5 AND 1.0 MM AND AN INJECTION DEPTH OF 25M

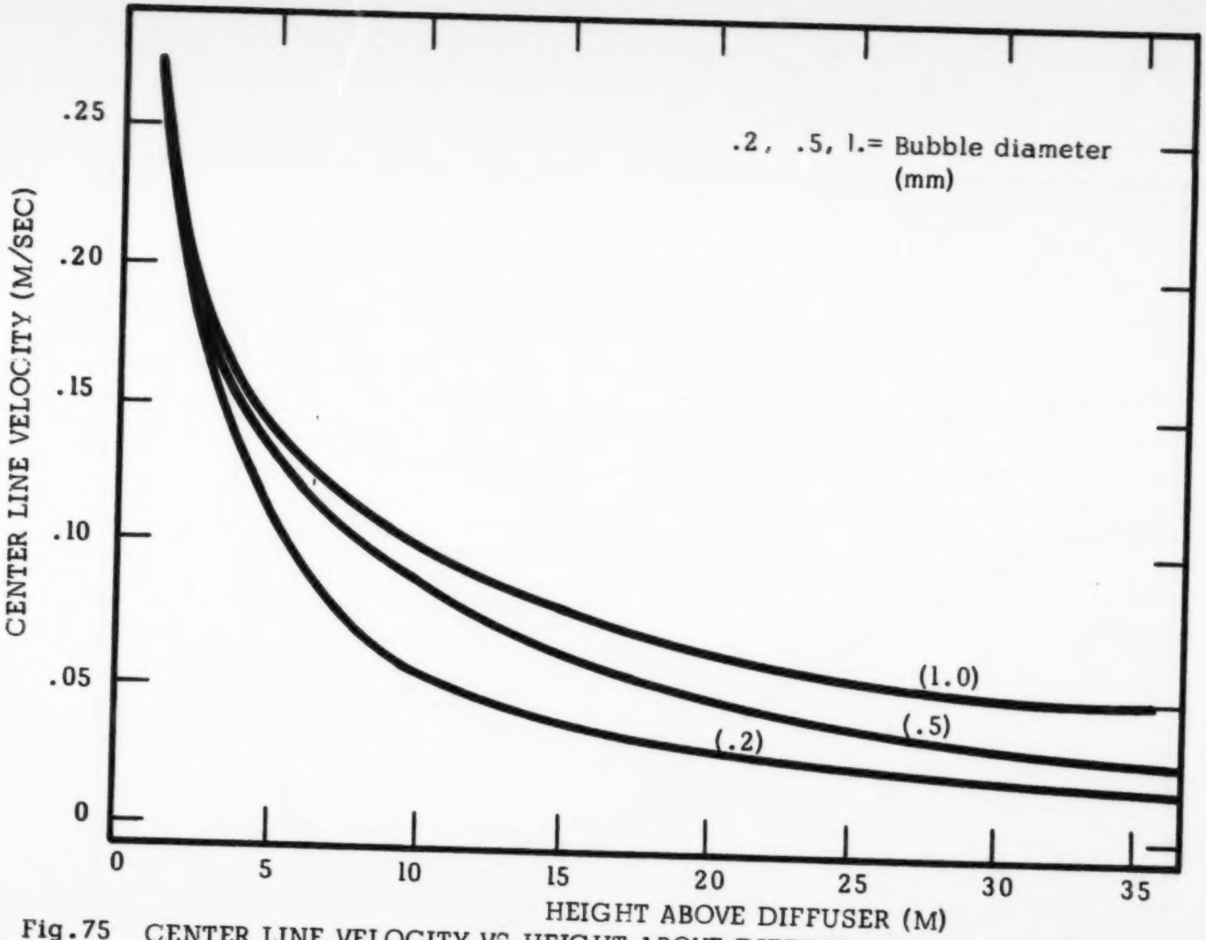

Fig. 75 CENTER LINE VELOCITY VS HEIGHT ABOVE DIFFUSER FOR A FLOW RATE OF 2 L/MIN AND BUBBLE DIAMETER OF 0.2, 0.5 AND 1.0 MM AND AN INJECTION DEPTH OF 50M

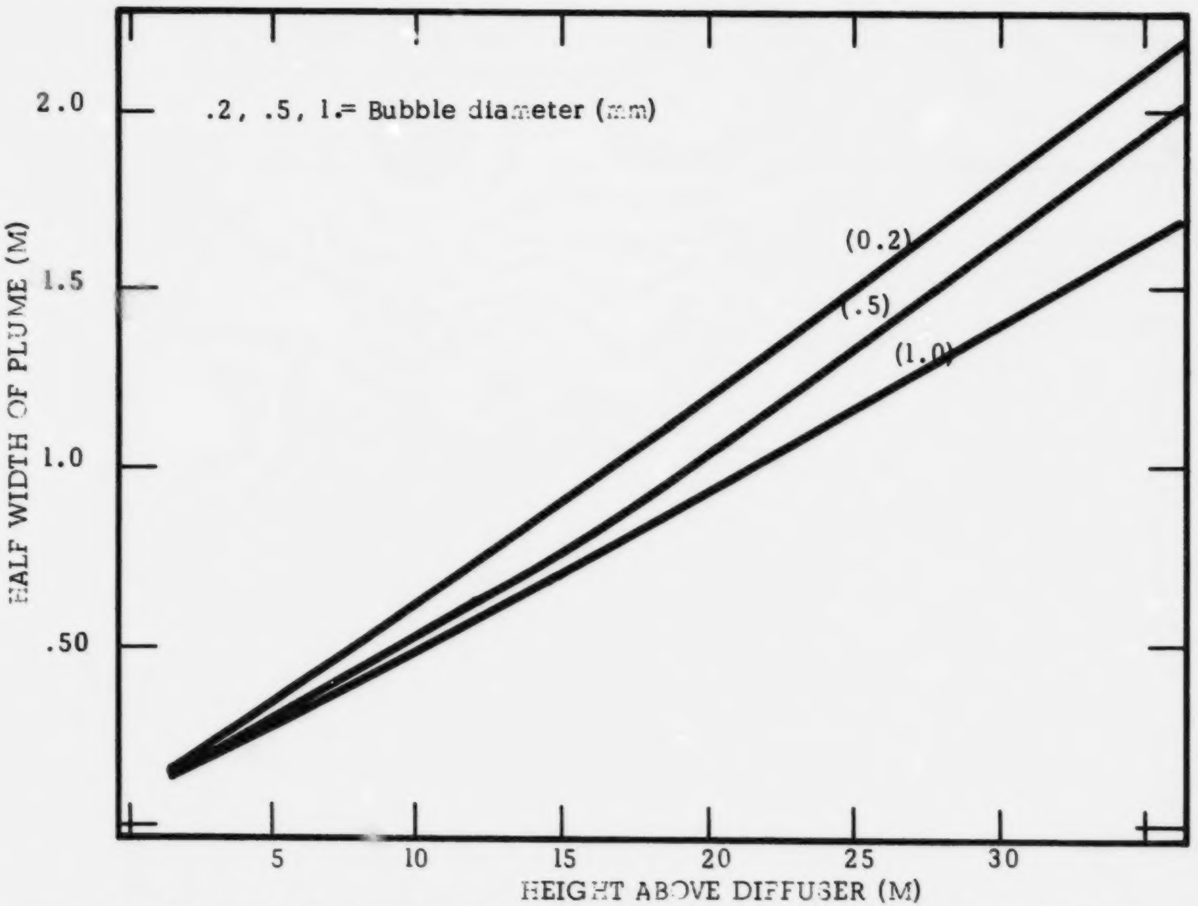

Fig. 76 HALF WIDTH OF PLUME VS HEIGHT ABOVE DIFFUSER FOR A FLOW RATE OF 2 L/MIN AND BUBBLE DIAMETER OF 0.2, 0.5 AND 1.0 MM AND AN INJECTION DEPTH OF 50 M

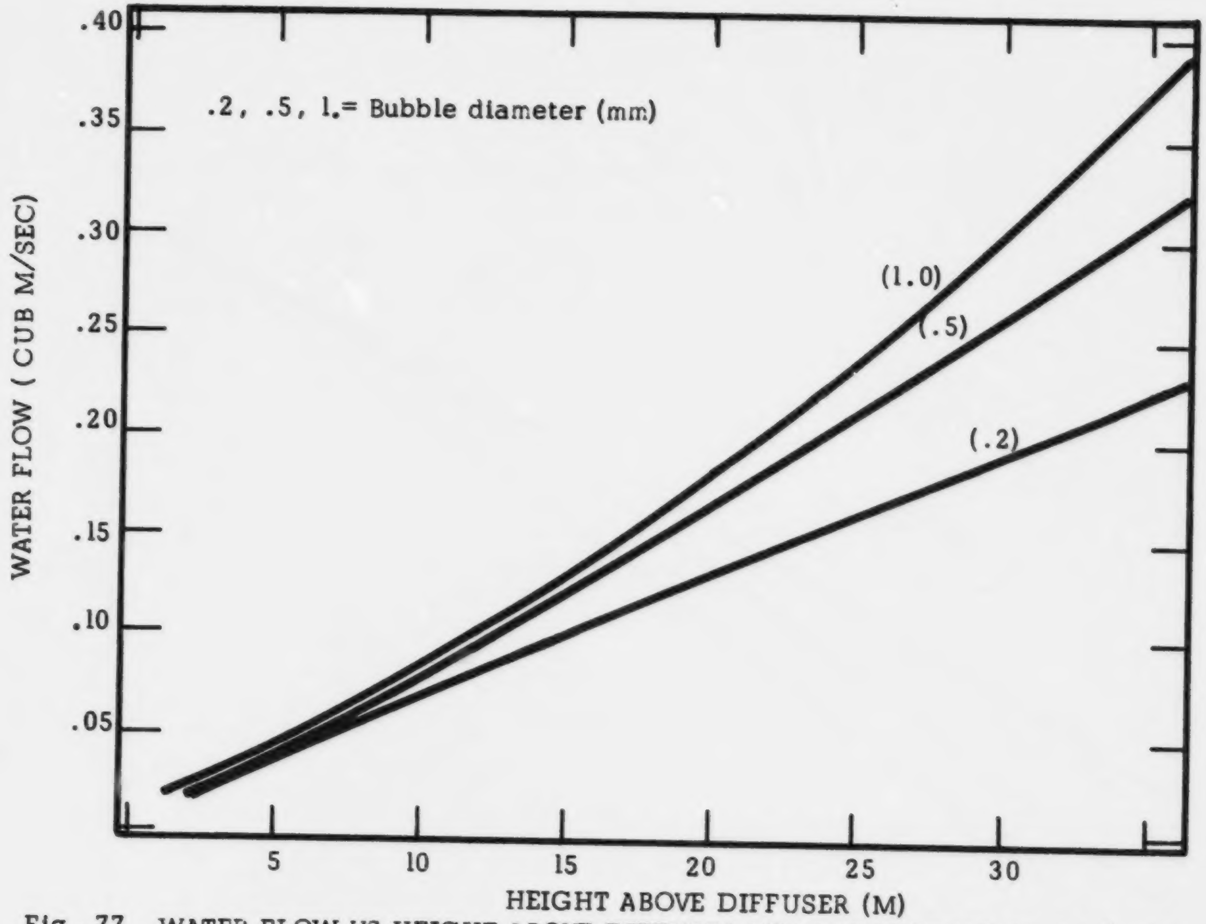

Fig. 77 WATER FLOW VS HEIGHT ABOVE DIFFUSER FOR A FLOW RATE OF 2 L/MIN AND BUBBLE DIAMETER OF 0.2, 0.5 AND 1.0 MM AND AN INJECTION DEPTH OF 50 M

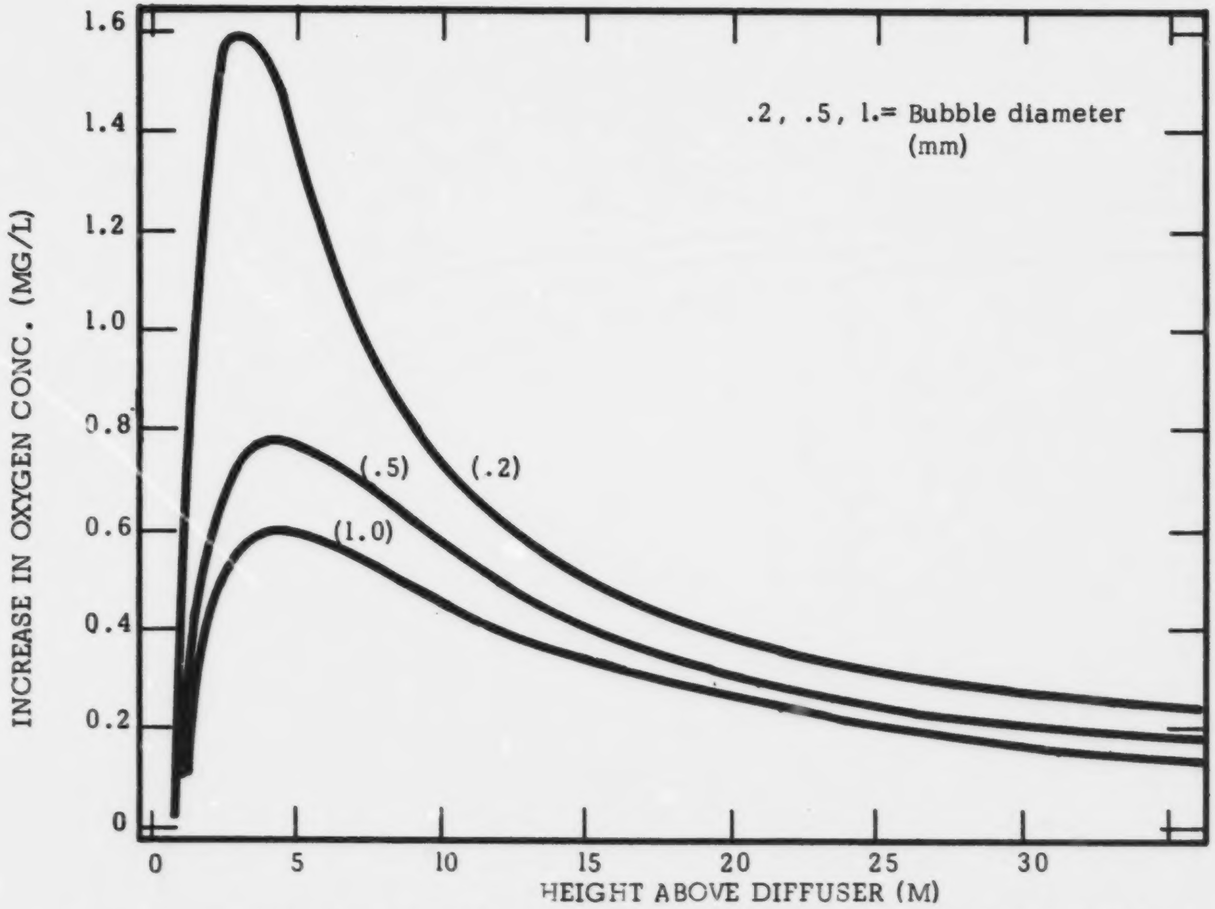

Fig. 78 INCREASE IN OXYGEN CONC. VS HEIGHT ABOVE DIFFUSER FOR A FLOW RATE OF 2. L/MIN AND BUBBLE DIAMETER OF 0.2, 0.5 AND 1.0 MM AND AN INJECTION DEPTH OF 50M

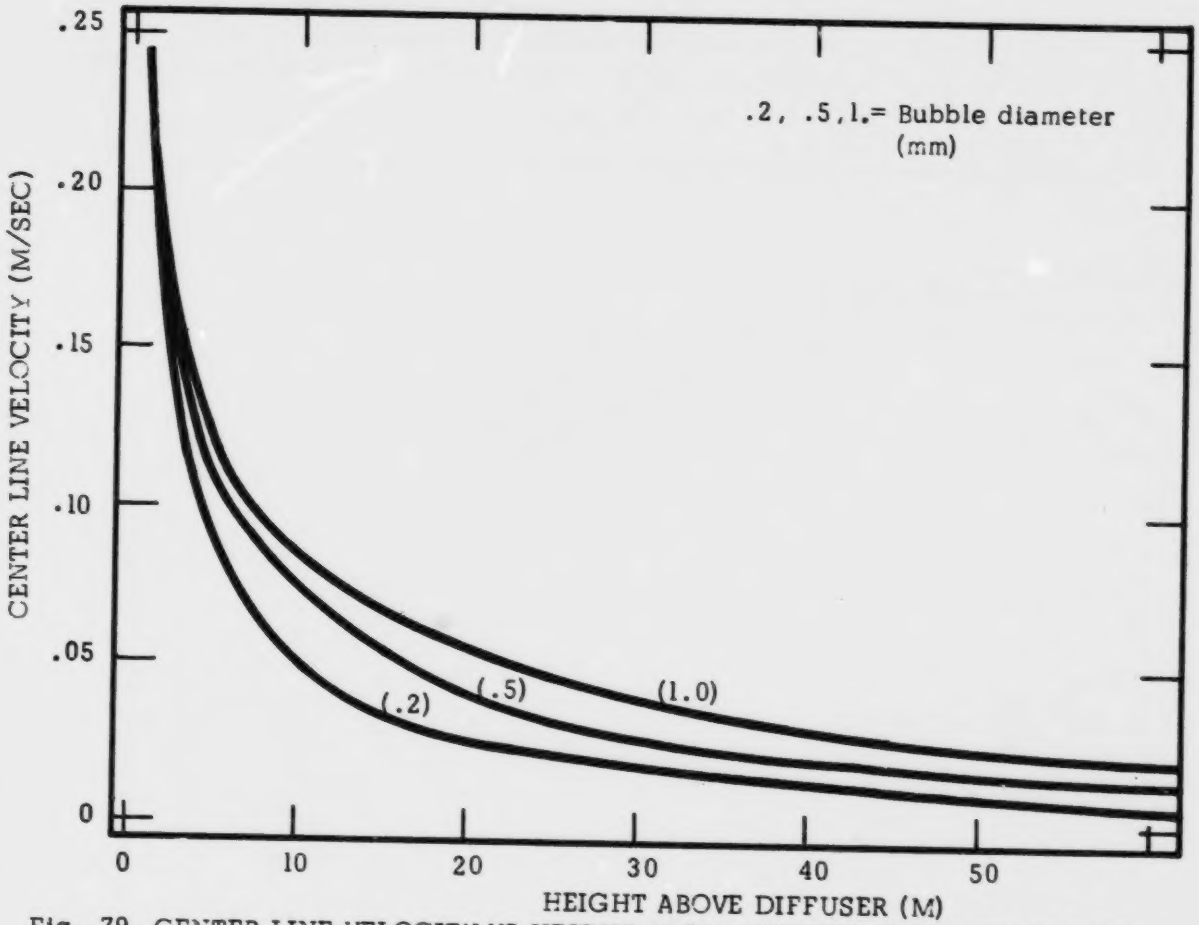

Fig. 79 CENTER LINE VELOCITY VS HEIGHT ABOVE DIFFUSER FOR A FLOW RATE OF 2 L/MIN AND BUBBLE DIAMETER OF 0.2, 0.5 AND 1.0 MM AND AN INJECTION DEPTH OF 75 M

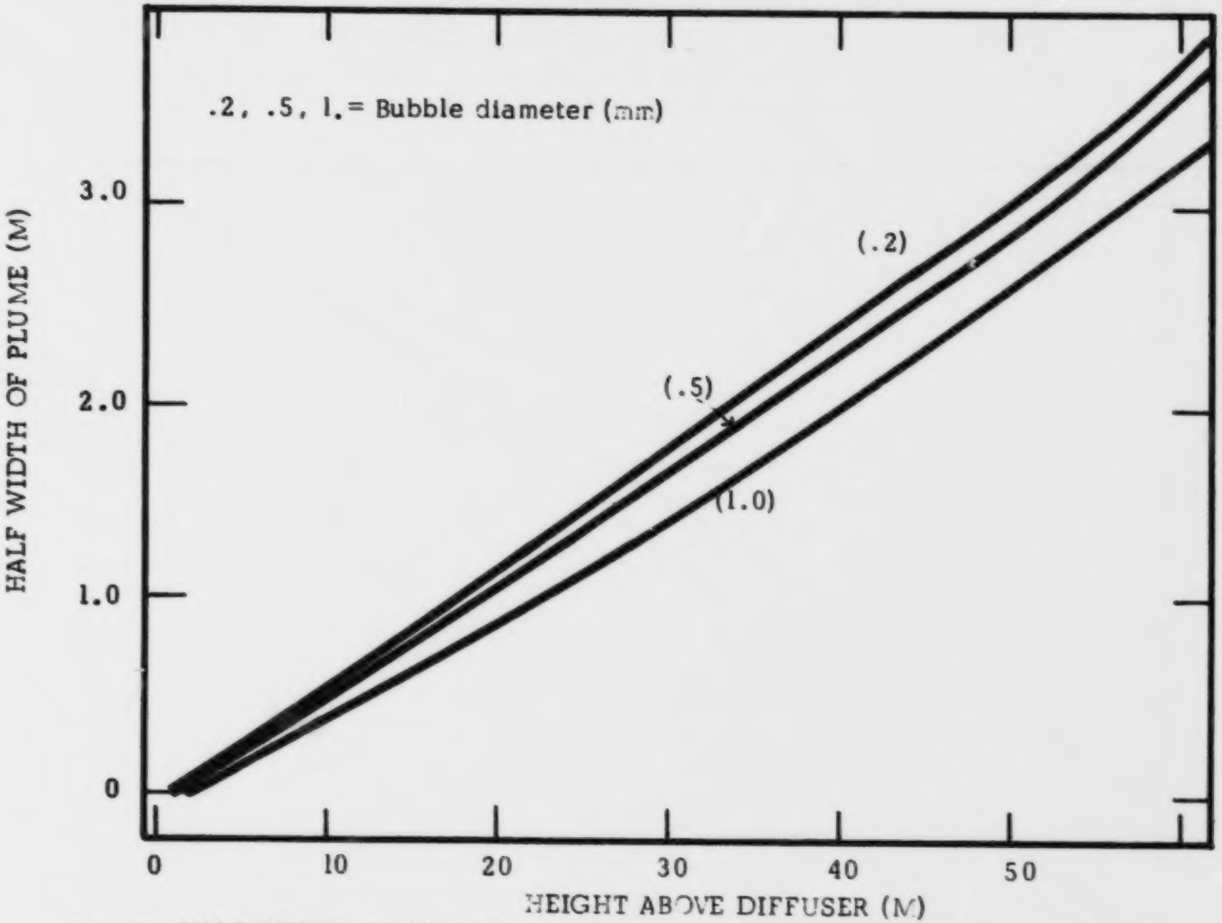

Fig. 80 HALF WIDTH OF PLUME VS HEIGHT ABOVE DIFFUSER FOR A FLOW RATE OF 2 L/MIN AND BUBBLE DIAMETER OF 0.2, 0.5, AND 1.0 MM AND AN INJECTION DEPTH OF 75 M

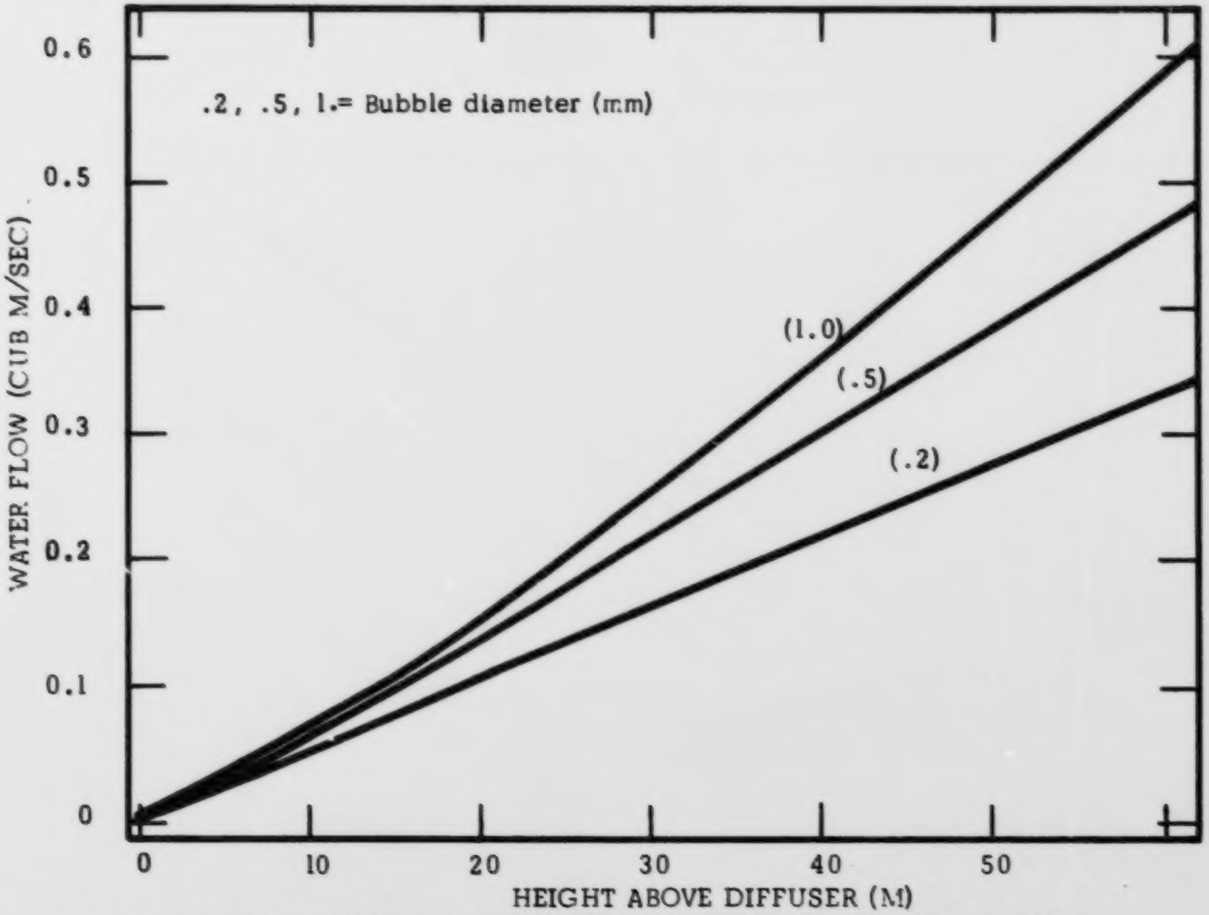

Fig. 81 WATER FLOW VS HEIGHT ABOVE DIFFUSER FOR A FLOW RATE OF 2 L/MIN AND BUBBLE DIAMETER OF 0.2, 0.5 AND 1.0 MM AND AN INJECTION DEPTH OF 75 M

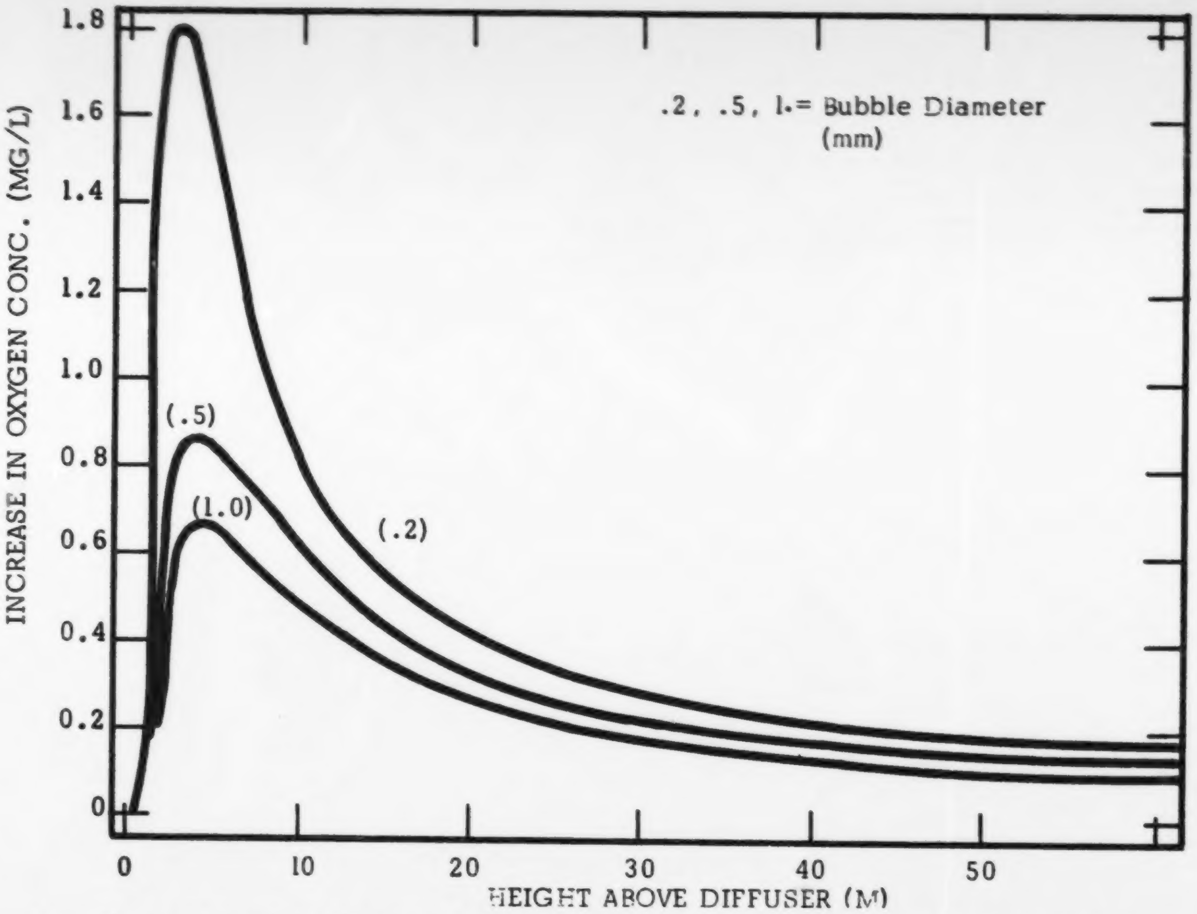

Fig. 82 INCREASE IN OXYGEN CONC. VS HEIGHT ABOVE DIFFUSER FOR A FLOW RATE OF 2. L/MIN AND BUBBLE DIAMETER OF 0.2, 0.5 AND 1.0 MM AND AN INJECTION DEPTH OF 75M

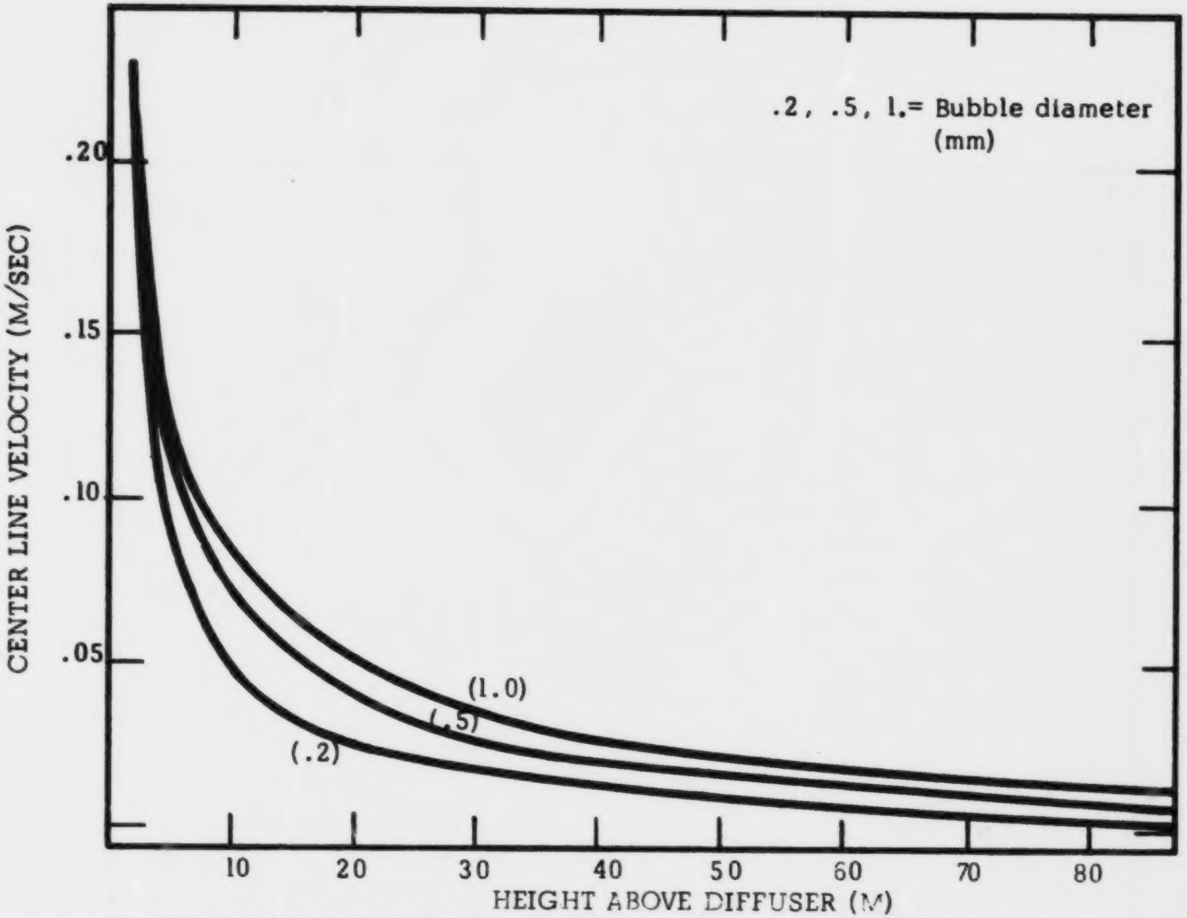

Fig. 83 CENTER LINE VELOCITY VS HEIGHT ABOVE DIFFUSER FOR A FLOW RATE OF 2 L/MIN AND BUBBLE DIAMETER OF 0.2, 0.5 AND 1.0 MM AND AN INJECTION DEPTH OF 100M

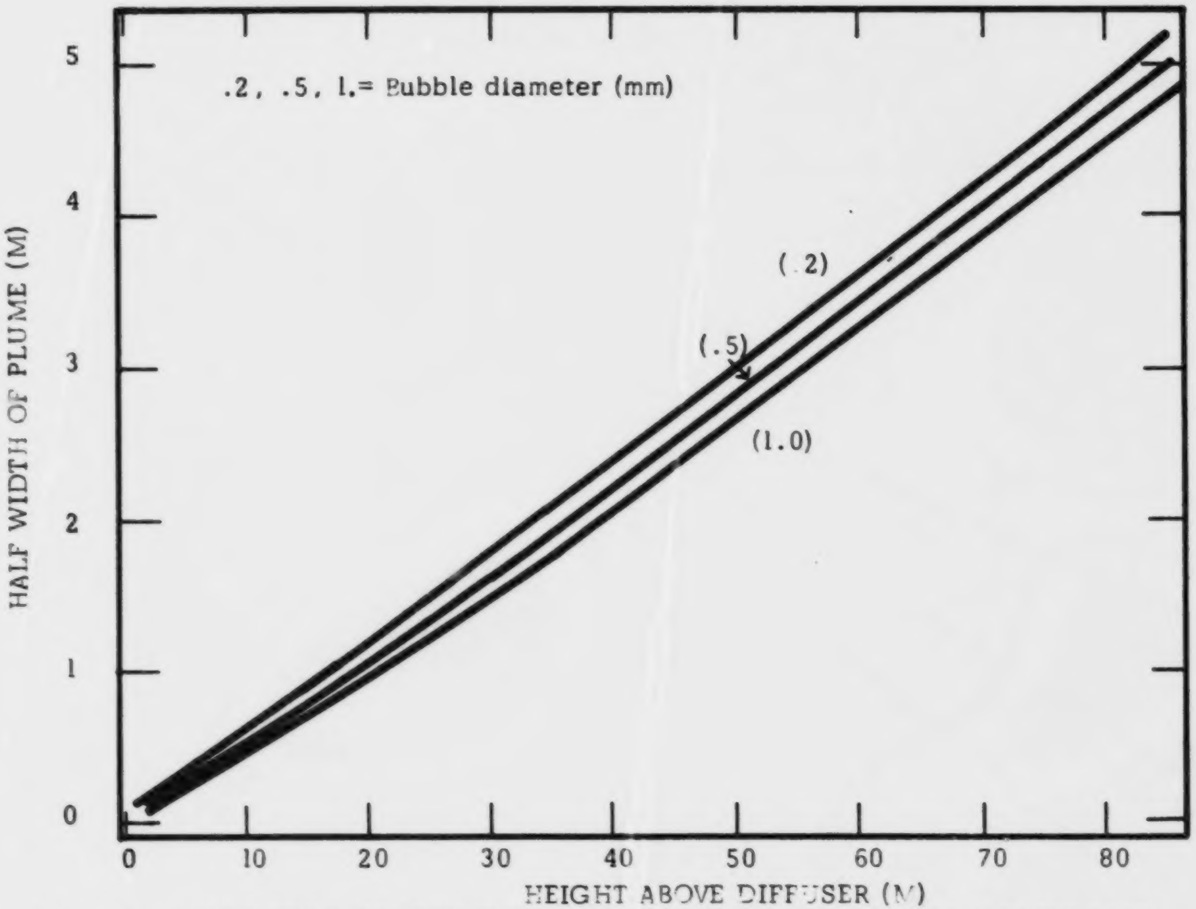

Fig. 84 HALF WIDTH OF PLUME VS HEIGHT ABOVE DIFFUSER FOR A FLOW RATE OF 2 L/MIN AND BUBBLE DIAMETER OF 0.2, 0.5 AND 1.0 MM AND AN INJECTION DEPTH OF 100 M

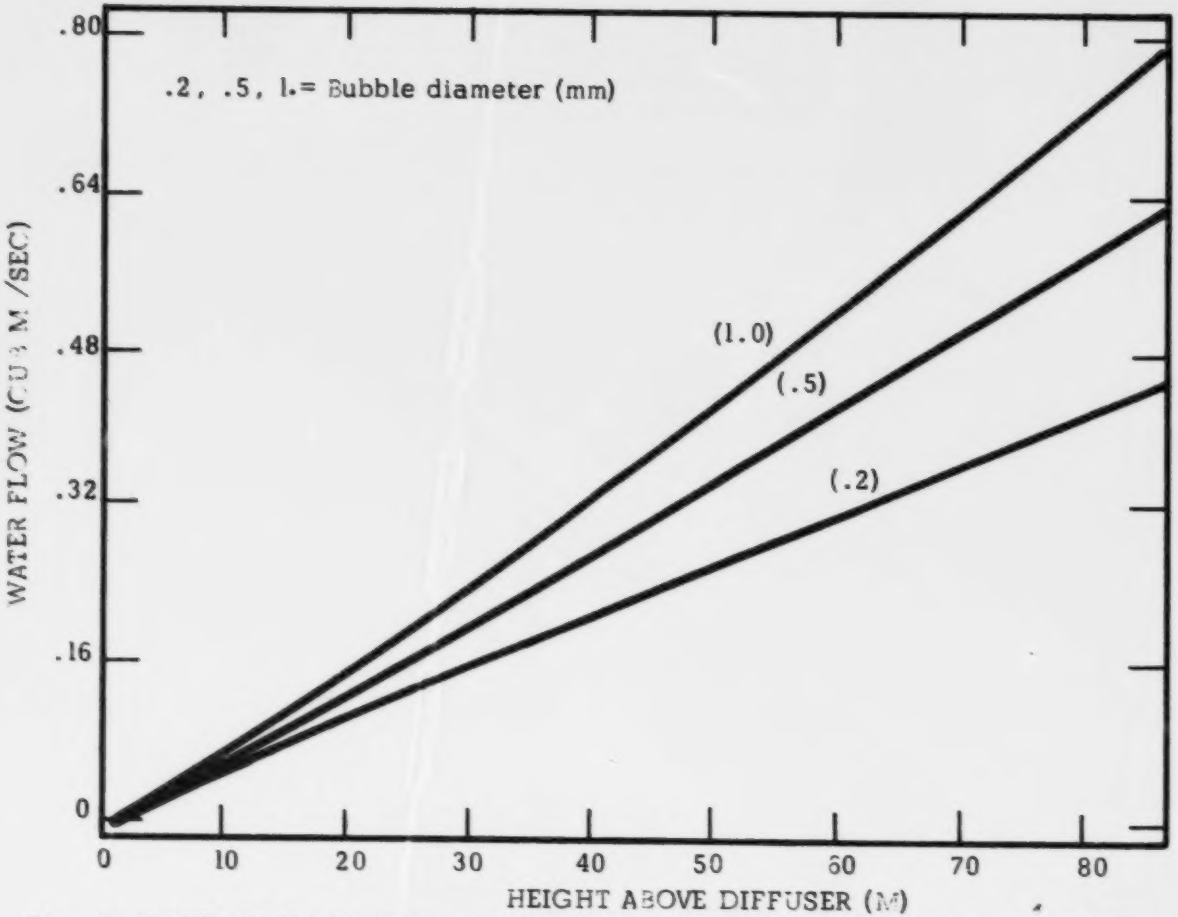

Fig. 85 WATER FLOW VS HEIGHT ABOVE DIFFUSER FOR A FLOW RATE OF 2 L/MIN AND BUBBLE DIAMETER OF 0.2, 0.5 AND 1.0 MM AND AN INJECTION DEPTH OF 100 M

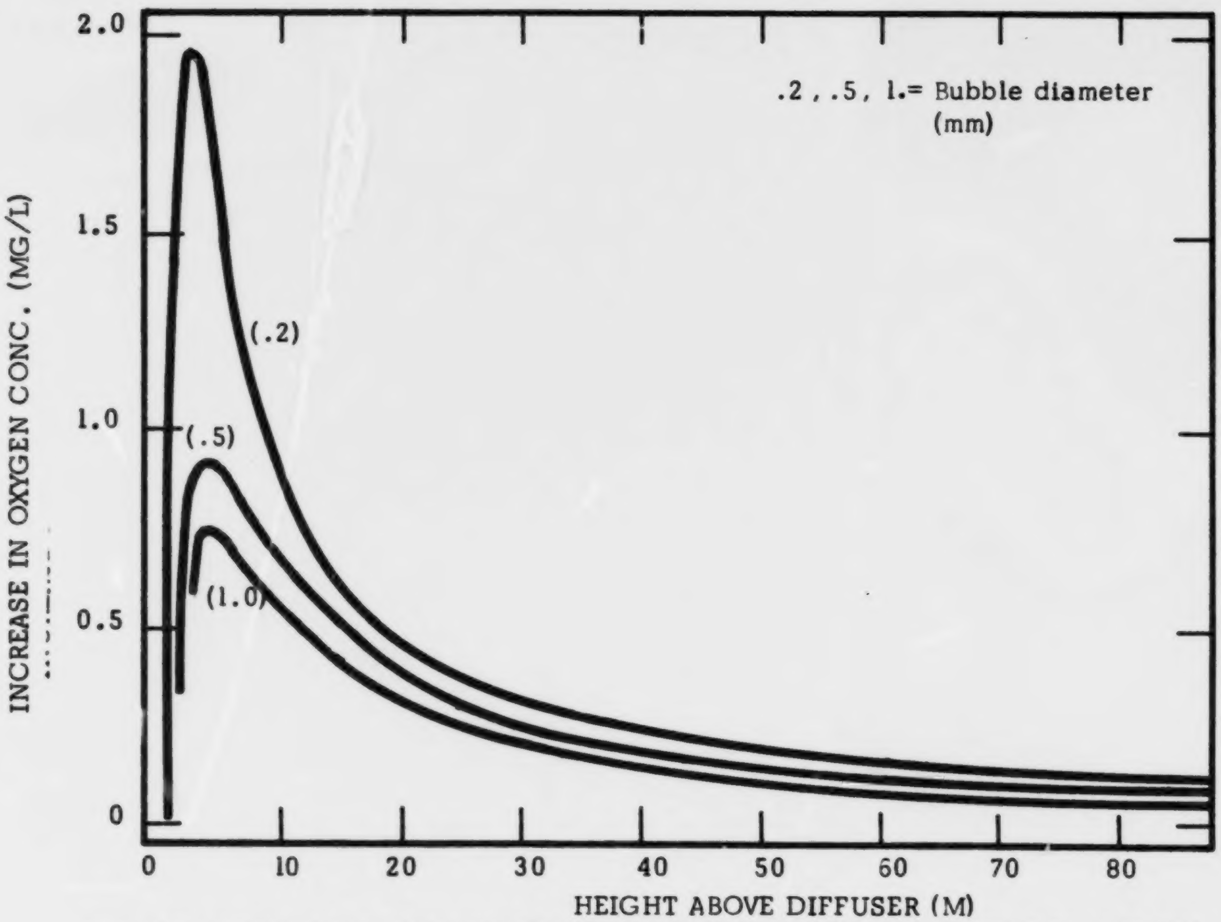

Fig. 86 INCREASE IN OXYGEN CONC. VS HEIGHT ABOVE DIFFUSER FOR A FLOW RATE OF 2/ L/MIN AND BUBBLE DIAMETER OF 0.2, 0.5 AND 1.0 MM AND AN INJECTION DEPTH OF 100 M

FIELD DATA

ON

INDUCED MIXING AND CIRCULATION

Field Data
on
Induced Mixing and Circulation

Date: 8-10-1971

Flow Rate: 2 l./min.

Diffuser Depth: 100 feet

Type of Diffuser: P.V.C.

Depth (feet)	Sampling Location in Feet from Diffuser	
	24'	
	F.R.	Temp. °F.
90	2	65
80	1	70
70	2.5	74
60	11	79
50	3	79.5
40	7.5	79.7
30	8.5	80
20	39	80
10	2	80

Remarks

1) F.R. = Fluorescence Reading

2) All readings on 30x scale unless indicated otherwise.

3) Reading taken 24 hrs. from injection time.

4) Approximate sampling interval is 2 - 3 min.

Date: 8-11-1971

Diffuser Depth: 100 ft.

Flow Rate: 2 l./min.

Type of Diffuser: P.V.C.

Depth (feet)	Sampling Location in Feet from Diffuser				Remarks
	2.0'	12'	24'	12'	
	F.R.	F.R.	F.R.	Temp. °F.	
90	4.5	6	3	65	Data collected 48 hours from injection time.
80	2.5	0.5	1.5	70	
70	0	0.5	0	74	
60	0.5	0.5	0	79	
50	1	0.5	0	79.5	
40	0.5	0.2	0	79.7	
30	0	0.4	0.5	80	
20	0.3	0.5	0.5	80	
10	0	0.5	0	80	

Date: 8-26-1972

Diffuser Depth: 100 ft.

Flow Rate: 2 l./min.

Type of Diffuser: P.V.C.

Depth (feet)	Sampling Location in Feet from Diffuser				Remarks
	2'	12'	24'		
	F.R.	F.R.	F.R.	Temp. °F.	
90	3	5	2.5	70	Data collected 24 hours after injection.
80	7	1	3	75	
70	2.5	3.5	7	78	
60	3	6	2	79	
50	3	5	9	79	
40	5	5	2	79.5	
30	7	7	16	81.5	
20	1.5	2	1	83	
10	3.5	5		83.5	

Date: 9-16-1971 | Diffuser Depth: 60'

Flow Rate: 0.75 l./min. | Type of Diffuser: P.V.C.

Depth (feet)	Sampling Location in Feet from Diffuser						
	25'L F.R.	12'L F.R.	10'R F.R.	30'R F.R.	50'R F.R.	100'R F.R.	2'R Temp.°F
60	10	55(3x)	70	58	24	7	80
50	8	37	20	3	17	11	80.2
40	4	18	8	13	60	4	80.5
30	11	6	8	7	8	5.3	80.7
20	8.5	7	2	5	4	6	81.1
10	3.5	2	1	6	3	5	81.2

Remarks:

1) L, R, = to the left and to the right of diffuser respectively.

2) F.R. = Fluorescence reading

3) Sampling started two hours after injection.

Date: 9-27-1971 **Diffuser Depth:** 60'

Flow Rate: 0.75 **Type of Diffuser:** P.V.C.

Sampling Location in Feet from Diffuser

Depth (feet)	25'L	20'R	40'R	80'R	100'R	0	30'R	Temp. °F.
60		14	14	9	19		22	77.7
50		6	2	1	4	61	32	78
40	80	2	4	2	1	83	3	78
30	26	2	1	1	0.5	50	2	78
20	6	2	1	3	1	15	1	78
10	2	12	1	0	1	6	1	78

Remarks: Sampling started two hours from dye injection.

Date: 10-1-1971 Diffuser Depth: 60 ft

Flow Rate: .75 l./min. Type of Diffuser: P.V.C.

Depth	Sampling Location in Feet from Diffuser						Temp.
(feet)	25'L	0	20'R	40'L	80'L	10'L	°.F
60		6	0.5	0	1	0	78
50		15	6	0	0	1	78
40	4	61	0	0	0	0	78.2
30	1	10	2	1	1	1	78.2
20	0	0	0	0	0	0	78.2
10	0	0	0	0	0	0	78.3

Remarks:

Sampling started two hours after dye injection.

Date: 10-13-1971 Diffuser Depth: 60 ft.

Flow Rate: 2 l./min. Type of Diffuser: P.V.C.

Depth	Sampling Location in Feet from Diffuser					
(feet)	25L	20R	40R	70R	100R	Temp. °F.
60		20	13	15	8	76
50		17	12	0	8	76
40	27	16	12	8	8	76
30	39	16	12	9	11	76
20	65	20	10	17	5	76
10	32(10x)	55	15	9	85	76

Remarks:

Sampling started 60 minutes from injection time.

Date: 10-13-1971 Diffuser Depth: 60 ft.

Flow Rate: 2 l./min. Type of Diffuser: P.V.C.

	Sampling Location in Feet from Diffuser									
Depth	20'L				40'R		20'R		0	Temp.
(feet)	10 min.	30 min.	60 min.	120 min.	40 min.	80 min.	70 min.	140 min.	130 min.	°F.
60					39	13	20	6	10	76
50					32	12	17	4	5	76
40	3	60 (3x)	27	8	30	12	16	5	7	76
30	6	75	39	31	27	12	16	4	6	76
20	5	30	65	67		10	20 (3x)	27	10	76
10			32 (10x)	10		15	55	10	6	76

Remarks:

Time (min.) from time of dye injection.

(-x) = Fluorescence scale

Date: 10-18-1971 **Diffuser Depth: 60 ft.**

Flow Rate: 2 l./min. **Type of Diffuser: P.V.C.**

	Sampling Location in Feet from Diffuser										
Depth	25'L				40'R			20R	70R	160R	
(feet)	16 min.	31 min.	45 min.	60 min.	25 min.	45 min.	60 min.	67 min.	75 min.	82 min.	Temp. °F.
60					7	5	3	36	20	5	75.8
50					6		3	23	17	4	75.8
40	8	35 (1x)	32	24	8	4	2		13	10	75.8
30	6	28 (10x)	27		5		3	23	10	4	75.8
20	7	45	30	12	5	6	3	20	13	1	75.8
10	15	78	25	41	8		7	14	6		75.8

Remarks:

Indicated time (min.) from injection of dye .

L,R = To the left or right of diffuser.

Date: 10-24-1971

Diffuser Depth: 60 ft.

Flow Rate: 1 l./min.

Type of Diffuser: Ceramic

Sampling Location in Feet from Diffuser

Depth (feet)	25'L		20'R	50'R		Temp. °F.
	10	20	15	32	45	
60		1		17	2	74.9
50	0	1	15	12	1	74.9
40	1.5	64 (3x)	4	9	9	74.9
30	1	95 (1x)	3	7	5	74.9
20	40 (10x)	75 (1x)	0			74.9
10						74.9

Typical

Date: 9-5-1972 | **Depth of Diffuser: 90 ft.**

Flow Rate: 2 l./min. | **Type of Diffuser: P.V.C.**

Start Up O_2 Flow at 12:30 | **Dye Injection at 1:45**

Distance Away (feet)	Time	Depth	F.R.
12	1:55	75	15
12	1:57	65	10
12	1:59	60	5
12	2:00	50	1
12	2:02	40	2
12	2:04	30	1
12	2:05	20	2
7	2:07	80	40*
7	2:09	70	25*
7	2:12	60	2
7	2:15	50	2
7	2:16.5	40	2
7	2:18	30	1.5
7	2:19	20	2
7	2:18.5	80	10*
7	2:20.5	70	35*
7	2:23	60	2
7	2:26	50	2
7	2:27.5	80	15*
7	2:29	70	12

cont.

Distance Away (Feet)	Time	Depth	P.R.
7	2:31	60	2.5
7	2:33	50	2
7	2:34	80	5
7	2:37	70	[illegible]
7	2:39	[illegible]	2
7	2:40	50	1.5

Note: All readings from zero to 60 were between one and two.

* went down to 2 after 15 seconds then started going up again.

Typical

Date: 14- 5-1972

Flow Rate: 2 l./min.

Start Up O_2 Flow: 2:15

Depth of Sampling: 75 ft.

Continuous Sampling Gate (30x)

Diffuser Depth: 90 ft.

Type of Diffuser: P.V.C.

Distance from Diffuser: 40 '

Dye Injection at 3:22

Time	F.R.	Time	F.R.
3:40	8	4:27	[illegible]
3:50	12	4:29	11
3:55	14	4:30	13
4:05	16	4:31	14
4:08	17	4:33	8
4:11	14	4:36	18
4:12	20	4:38	16
4:13	22	4:41	21
4:14	20	4:42	20
4:15	16	4:44	22
4:16	10	4:48	16
4:16	13	4:52	13
4:17	10	4:58	20
4:19	11	5:01	24
4:20	6	5:07	20
4:24	8	5:10	20
4:25	7	5:20	18
4:26	10	5:40	14

Note: Measurements at depths for surface to [illegible]0' were between 1 and [illegible] F.R. (Fluorescence Reading). Temp. profile is shown in Figure 5-3.

PROGRAM LISTING

AND

USER'S GUIDE

PROGRAM LISTING
and
USER'S GUIDE

The listing included hereafter is for Model One (mass transfer) with slip velocity. However, the equations for zero slip velocity consideration are also listed.

To run the program as it stands one need first (if not at U.T.) to delete those statements for the PLOTT sub-routine and include his plotting sub-routine or add a print statement to get a listing of the output. However, a listing of PLOTT sub-routine is available from U.T. Computation Center. The user needs to do the following:

1) Set the value of the depth of injection in program HYPO-DEPTH 1 - in meters.
2) Set the bubble diameter - DIAM 1 in mm.
3) Set the value of Z in HYDRO equal to DEPTH 1 + 1.0 in meters.
4) Set the value of Omega in HYDRO to whatever level needed. (Omega & Z) in meters.
5) set BD = DIAM 1.
6) Set FR - the oxygen flow rate in $m.^3$/sec.
7) Set the value of Alpha = initial value of x in meters.
8) Set YJ(1) = initial half-width of plume in meters.
9) Set YJ(2) = center line velocity in m./sec.

To run the program with zero slip condition insert the corresponding equations, DF(M,1), DF(M,2) in place of the listed equations and delete Function VELB (DIAM).

To run the program with no mass transfer, start the program with HYDRO.

This program has been run on CDC 6600 and 6400.

```
       LIST OF ABBREVIATIONS
       *********************
DIAM1 = DIAMETER OF BUBBLE (MM)
DEPTH1 = DEPTH OF INJECTION(M)
ZMGO =MG OF O2
ZMGN=MG OF N2
ZMGC=MG OF CO2
TO2L=FRACTION OF ORIGINAL AMOUNT OF O2 REMAINING
RNTO = NITROGEN/OXYGEN
XMGO = RELATIVE AMOUNT OF O2  IN BUBBLE NORMALIZED TO CONSTANT
       RELEASE DEPTH
CSTO=CSAT OF O2 (MG/L)
CSTC =CSAT OF CO2 (MG/L)
PCO2 =RELATIVE AMOUNT OF O2 IN BUBBLE NORMALIZED TO CONSTANT
      RELEASE DEPTH
TO2A =FRACTION OF O2 ABSORBED
KLOZ =OVER ALL MASS TRANSFER COEFFICIENT (O2)
BD =BUBBLE DIAMETER (MM) =DIAM1
HO =ATM PRESSURE (M)
Z = DEPTH OF INJECTION + 1. (M)
FR =O2 FLOW RATE (CUB. M./SEC.)
Q = NUMBER OF BUBBLES PRODUCED /SEC.
VEL =CENTER LINE VELOCITY OF PLUME
RAD= HALF WIDTH OF PLUME
WQ = WATER FLUX
WM = MOMENTUM FLUX
KE = KINETIC ENERGY FLUX
O2T = INCREASE IN D.O.
```

```
      PROGRAM HYPO (INPUT,OUTPUT)
C
C     THIS PROGRAM CALCULATES THE TRANSFER OF OXYGEN OUT OF AND THE
C     TRANSFER OF NITROGEN INTO A BUBBLE INJECTED AT THE BOTTOM OF
C     A RESERVOIR  ---  INITIALLY THE BUBBLE IS PURE OXYGEN
C       THE UNITS FOR THE DEPTH AND THE DIAMETER ARE METERS AND MILLIMET
C       RESPECTIVELY
C
C
      REAL KLCZ
      REAL MGCZ
      REAL MGCZ1
      REAL KLOZ
      REAL MGOZ1
      REAL MGOZ
      REAL KLNZ
      REAL MGNZ
      REAL MGNZ1
      COMMON /1/ TEMP
      DIMENSION DPTH(1000),DYAM(1000),ZMGO(1000),ZMGN(1000)
      DIMENSION TO2L(1000),PCO2(1000),RNTO(1000),DPTN(1000)
      DIMENSION XMGO(1000),ZMGC(1000),CSTO(1000),CSTC(1000)
      DIMENSION AREA(13,51),YSCALE(51),TO2A(1000)
      ISYMBL=1H1
      NFMAX=1
      NF=1
      MY=0
      MX=0
      MM = 1
      YLINE=0.0
      XLINE=0.0
      LL = 1
      NLS = 36
      NCL = 80
      NDMAX=450
      NDMAX=100
      NCTP =0
      NDATA=100
      TEMP=20.
      DIAM = 0.0
      DO 1 I = 1, 100
      DIAM = DIAM+.1
      ZMGO(I)=KLOZ(DIAM)
    1 DPTH(I)=DIAM
      PRINT 14
      CALL PLOTT (DPTH, ZMGO, NDATA, NDMAX, ISYMBL, NF, XLINE, MX, YLINE
     1, MY, NLS, NCL, MM, LL, AREA, YSCALE, NFMAX)
      PRINT 21
      PRINT 14
      TEMP=20.
      TO = (TEMP*(.0161*TEMP-1.6088)+69.528)/1000000.
      TN = (TEMP*(.01189*TEMP-.87461)+30.533)/1000000.
      TC = (TEMP*(1.2043*TEMP-106.2314)+3319.657)/1000000.
      T = 273./(273.+TEMP)
      PI = 3.1416
      CWATO = 0.0*28.3
      CWATN = 15.5E-6
      CWATC=0.00
      BICNO2 = 1.0
      BICNN2 = 0.0
      BICNCO2 = 1.-BICNO2-BICNN2
      DEPTH1 = 45.0
      PRINT 13
      DEPTH = DEPTH1
      DIAM1=2.
      DIAM =DIAM1
      STEP =0.1
      PRINT 23, I, DEPTH, DIAM, TEMP
      PRINT 14
      KTKNT = DEPTH/2.0
      IF (KTKNT .EQ. 0) KTKNT = 1
    2 NCTP=0
      DEEP1 = DEPTH
      DEPTH =DEPTH1
      DIAM =DIAM1
      ATM = 1.+DEPTH/10.3632
      VOLB= ((1./6.)*PI*(DIAM**3))*100.
      MGOZ = VOLB*ATM*BICNO2*T*1.4285E-3
      MGOZ1 = MGOZ
      MGNZ = VOLB*ATM*BICNN2*T*1.2500E-3
      MGNZ1 = MGNZ
      MGCZ = VOLB*ATM*BICNCO2*T*1.9642E-3
      MGCZ1 = MGCZ
      VOLOZ = VOLB*BICNO2
      VOLNZ = VOLB*BICNN2
      VOLCZ = VOLB*BICNCO2
      PCOZ = BICNO2
      PCCZ=BICNCO2
      PCNZ=BICNN2
      CSATO = ATM*PCOZ*TO
      CSATC = ATM*PCCZ*TC
      VOL1B =VOLB/100.
      IF (DIAM .GT. 2.0) GO TO 3
      ARE =PI*(DIAM**2)*100.
      GO TO 4
3     E = .125*DIAM-.25
      A=EXP(ALOG(3.*VOL1B/(4.*PI*SQRT(1.-E**2)))/3.)
      ARE = ((PI*A**2) *(2.+(1.-E**2)*ALOG((1.+E)/(1.-E))/E))*100.
4     CONTINUE
      IF(NCTP.LT.NDMAX)GO TO 5
      KTKNT = 2*KTKNT
      GO TO 2
    5 CONTINUE
      IF(DIAM.GE. 0.0 .AND. DIAM .LE. .72) VEL=24.4*DIAM*0.01
      IF(DIAM .GE. .72.AND.DIAM .LE. 5.) VEL=(17.6+(( DIAM-0.72)*1000.)
     1/(30.+156.*(DIAM-0.72)))*0.01
 34   CONTINUE
      STEP =0.1
C
 7    DO 9 KT = 1, KTKNT
      NCTP =NCTP+1
      OLEFT = MGOZ/MGOZ1
      O2AB=1.-OLEFT
      PCOZ = VOLOZ/VOLB
      PCNZ = VOLNZ/VOLB
      PCCZ = VOLCZ/VOLB
      RNZOZ = MGNZ/MGOZ
      DPTH(NCTP)=DEPTH
      DYAM(NCTP)=DIAM
      TO2L(NCTP)=OLEFT
      TO2A(NCTP)=O2AB
      ZMGO(NCTP)=MGOZ
      CSTO(NCTP)=CSATO
      CSTC(NCTP)=CSATC
      ZMGN(NCTP)=MGNZ
      PCO2(NCTP)=PCOZ
      RNTO(NCTP)=RNZOZ
      XMGO(NCTP)=MGOZ/MGOZ1
      DPTN(NCTP)=DEPTH/DEEP1
      ZMGC(NCTP)=MGCZ
      CSATO = ATM*PCOZ*TO
      CSATN = ATM*PCNZ*TN
      CSATC = ATM*PCCZ*TC
      DMOZ = KLOZ(DIAM)*ARE*(CSATO-CWATO)*(STEP/VEL)
      MGOZ = MGOZ-DMOZ
      IF (MGOZ .LE. 0.0) GO TO 10
      KLNZ = .89*KLOZ(DIAM)
      KLCZ=KLOZ(DIAM)
      DMNZ=KLNZ*ARE*(CSATN-CWATN)*STEP/VEL
      DMCZ=KLCZ*ARE*(CSATC-CWATC)*STEP/VEL
      MGNZ = MGNZ-DMNZ
      MGCZ = MGCZ-DMCZ
      DEPTH =DEPTH - STEP
      IF (DEPTH .LE. 0.0) GO TO 10
      ATM = 1.+DEPTH/10.3632
      VOLOZ = MGOZ/(ATM*T*1.4285E-3)
      VOLNZ = MGNZ/(ATM*T*1.2500E-3)
      VOLCZ = MGCZ/(ATM*T*1.9642E-3)
      VOLB = VOLOZ+VOLNZ+VOLCZ
      VOL1B=VOLB/100.
      IF (VOL1B.LE. 0.0) GO TO 10
      IF (VOL1B.LE. 4.1555) DIAM=((6.*VOL1B)/PI)**0.3333
      IF (VOL18.GT. 4.1555) DIAM=EXP(ALOG(6.*VOL18/PI)/3.)
      IF (DIAM .GT. 2.0) GO TO 8
      ARE =PI*(DIAM**2)*100.
      GO TO 9
8     E = .125*DIAM-.25
      A=EXP(ALOG(3.*VOL18/(4.*PI*SQRT(1.-E**2)))/3.)
      ARE = ((PI*A**2) *(2.+(1.-E**2)*ALOG((1.+E)/(1.-E))/E))*100.
9     CONTINUE
      GO TO 4
   10 DO50 J=NCTP,1000
      DYAM(J)=0.0
      TO2A(J)=TO2A(NCTP)
   50 CONTINUE
      NDATA=NCTP-1
      CALL PLOTT (DPTH, DYAM, NDATA, NDMAX, ISYMBL, NF, XLINE, MX, YLINE
     1, MY, NLS, NCL, MM, LL, AREA, YSCALE, NFMAX)
      PRINT 18
      PRINT 14
      CALL PLOTT (DPTH, ZMGO, NDATA, NDMAX, ISYMBL, NF, XLINE, MX, YLINE
     1, MY, NLS, NCL, MM, LL, AREA, YSCALE, NFMAX)
      PRINT 15
      PRINT 14
      CALL PLOTT (DPTH, ZMGN, NDATA, NDMAX, ISYMBL, NF, XLINE, MX, YLINE
     1, MY, NLS, NCL, MM, LL, AREA, YSCALE, NFMAX)
      PRINT 16
      PRINT 14
      CALL PLOTT (DPTH, TO2L, NDATA, NDMAX, ISYMBL, NF, XLINE, MX, YLINE
     1, MY, NLS, NCL, MM, LL, AREA, YSCALE, NFMAX)
      PRINT 17
      PRINT 14
      CALL PLOTT (DPTH, PCO2, NDATA, NDMAX, ISYMBL, NF, XLINE, MX, YLINE
     1, MY, NLS, NCL, MM, LL, AREA, YSCALE, NFMAX)
      PRINT 19
      PRINT 14
      CALL PLOTT (DPTH, RNTO, NDATA, NDMAX, ISYMBL, NF, XLINE, MX, YLINE
     1, MY, NLS, NCL, MM, LL, AREA, YSCALE, NFMAX)
      PRINT 20
      PRINT 14
      CALL PLOTT (DPTN, XMGO, NDATA, NDMAX, ISYMBL, NF, XLINE, MX, YLINE
     1, MY, NLS, NCL, MM, LL, AREA, YSCALE, NFMAX)
      PRINT 24
      PRINT 14
      CALL PLOTT (DPTH, CSTO, NDATA, NDMAX, ISYMBL, NF, XLINE, MX, YLINE
     1, MY, NLS, NCL, MM, LL, AREA, YSCALE, NFMAX)
      PRINT 32
      PRINT 14
      CALL PLOTT (DPTH, ZMGC, NDATA, NDMAX, ISYMBL, NF, XLINE, MX, YLINE
     1, MY, NLS, NCL, MM, LL, AREA, YSCALE, NFMAX)
      PRINT 26
      PRINT 14
      CALL PLOTT (DPTH, CSTC, NDATA, NDMAX, ISYMBL, NF, XLINE, MX, YLINE
     1, MY, NLS, NCL, MM, LL, AREA, YSCALE, NFMAX)
      PRINT 31
      CALL HYDRO(DYAM,TO2A)
C     *****************
 13   FORMAT   (2X*LABEL*,7X*RELEASE DEPTH*,10X*DIAMETER*,10X*TEMPERATUR
     1E*)
 14   FORMAT    (*1*)
   15 FORMAT(30X*MG OF O2 AS A FUNCTION OF DEPTH IN METERS*)
   16 FORMAT(30X*MG OF N2 AS A FUNCTION OF DEPTH IN METERS*)
   17 FORMAT(20X*FRACTION OF ORIGINAL AMOUNT OF O2 REMAINING AS A FUNCTI
     1ON OF DEPTH IN METERS*)
   18 FORMAT (30X*DIAMETER,IN MILLIMETER,OFBUBBLE AS A FUNCTION OF DEPTH
     1*)
   19 FORMAT (30X*FRACTION OF BUBBLE GAS WHICH IS O2*)
   20 FORMAT(30X*NITROGEN/OXYGEN RATIO AS A FUNCTION OF DEPTH*)
   21 FORMAT(20X*RELATIONSHIP BETWEEN LIQUID FILM COEFFICIENT AND BUBBLE
     1 DIAMETER*)
 23   FORMAT    (I5,3E20.3)
   24 FORMAT (20X *RELATIVE AMOUNT OF O2 IN BUBBLE NORMALIZED TO CONSTAN.
     1T RELEASE DEPTH*)
   26 FORMAT (30X* MGOF CO2 IN BUBBLE AS AFUNCTION OF DEPTH(M.)*)
   31 FORMAT(30X*CSATC VS, DEPTH(M)*)
   32 FORMAT (30X*CSATO (MILLIGRAMS/CUBIC MILLIMETER) VS, DEPTH*)
      END
      FUNCTION KLOZ (DIAM)

      REAL KLOZ
      COMMON /1/ TEMP
      IF (DIAM .GT. 0.0) GO TO 1
      KLOZ=0.013
      RETURN
1     T = 1.028**(TEMP-20.)
      IF (DIAM .GT. 2.2) GO TO 2
      KLOZ=0.013+DIAM*(0.04088+0.0962*DIAM)*T
      RETURN
2     IF (DIAM .GT. 2.5) GO TO 3
      KLOZ = .5555*T
      RETURN
3     KLOZ = (400./(432.*DIAM-360.))*T
      RETURN
      END
```

```
SUBROUTINE HYDRO (DYAM,TO2A)


DIMENSION YJ(10)
DIMENSION TO2A(1000),O2T(1000),DYAM(1000)
DIMENSION AREA(13,51),YSCALE(51)
COMMON G, Q, HO, PI, S, Z, C
DIMENSION RAD(1000),VEL(1000),WQ(1000),WM(1000),KE(1000)
COMMON/CSAVE/SAVE(2000)
DOUBLE SAVE
COMMON/XSAV/DEPT(1000)
REAL KE
EXTERNAL F
NDATA=301
NDMAX=301
ISYMBL=1H1
XLINE=0.0
YLINE=0.0
NF=1
MY=0
MX=0
NCL=80
NLS=36
NF=1
LL=1
MM=1
ALPHA=1.
G=9.815
BD=2.
FR=0.0000166
PI=3.1414
Q=FR/((PI*(BD)**3/6.)*1.0E-9)
HO=10.362
OMEGA=31.
Z=46.
S=0.2
C=0.03
H=0.1
YJ(1)=0.1
YJ(2)=0.2233
HMIN=1.0E-6
IPR=0
HMAX=1.0
EMAX=1.0E+6
EMIN=0.

CALL RKAM(F,YJ,ALPHA,OMEGA,H,IPR,HMIN,HMAX,EMIN,EMAX,DYAM)
```

```
      K=2*NDATA-1
      II =1
      DO 300 I=1,K,2
      RAD(II) =SAVE(I)
      VEL(II)= SAVE(I+1)
  300 II =II+1
      DO 500 I=1,NDATA
      WQ(I)=PI*(VEL(I))*(RAD(I))**2
      WM(I)=(PI*(RAD(I)**2)*(VEL(I)**2)*1000.)/2.
      KE(I)=(PI*(RAD(I)**2)*(VEL(I)**3)*1000.)/6.
      O2T(I)=TO2A(I)*FR*1420./WQ(I)
  500 CONTINUE
      PRINT 100
      CALL PLOTT(DEPT,RAD,NDATA,NDMAX,ISYMBL,NF,XLINE,MX,YLINE,MY,NLS,
     1NCL,MM,LL,AREA,YSCALE)
      PRINT 700
      PRINT 100
      CALL PLOTT(DEPT,VEL,NDATA,NDMAX,ISYMBL,NF,XLINE,MX,YLINE,MY,NLS,
     1NCL,MM,LL,AREA,YSCALE)
      PRINT 600
      PRINT 100
      CALL PLOTT(DEPT, WQ,NDATA,NDMAX,ISYMBL,NF,XLINE,MX,YLINE,MY,NLS,
     1NCL,MM,LL,AREA,YSCALE)
      PRINT 800
      PRINT 100
      CALL PLOTT(DEPT, WM,NDATA,NDMAX,ISYMBL,NF,XLINE,MX,YLINE,MY,NLS,
     1NCL,MM,LL,AREA,YSCALE)
      PRINT 200
      PRINT 100
      CALL PLOTT(DEPT, KE,NDATA,NDMAX,ISYMBL,NF,XLINE,MX,YLINE,MY,NLS,
     1NCL,MM,LL,AREA,YSCALE)
      PRINT 400
      PRINT 100
      CALL PLOTT(DEPT,O2T,NDATA,NDMAX,ISYMBL,NF,XLINE,MX,YLINE,MY,NLS,
     1NCL,MM,LL,AREA,YSCALE)
      PRINT 150
  150 FORMAT(30X*INCREASE IN OXYGEN CON. ,MG/LT*)
  600 FORMAT(30X*CENTER LINE VELOCITY(M./SEC.)VS. HEIGHT ABOVE DIFFUSER
     1(M.)*)
  700 FORMAT(30X*HALF WIDTH OF PLUME(M.) VS. HEIGHT ABOVE DIFFUSER(M.)*)
  800 FORMAT(30X*WATER FLOW (CUB.M./SEC.)VS. HEIGHT ABOVE DIFFUSER(M.)*)
  400 FORMAT(25X*KINETIC ENERGY FLUX(KG.-M.*3H**2*/SEC.*3H**3*)VS. HEIGH
     1T ABOVE DIFFUSER(M.)*)
  200 FORMAT(30X*MOMENTUM FLUX(KG.-M./SEC.*3H**2*)VS. HEIGHT ABOVE DIFFU
     1SER(M.)*)
  100 FORMAT (*1*)
      RETURN
      END
      SUBROUTINE RKAM (F, YJ, ALPHA, OMEGA, H, IPR, HMIN, HMAX, EMIN, EM
     1AX,DYAM)


C************** ADAMS-MOULTON PROCEDURE WITH RUNGE-KUTTA STARTER ********
C* PARAMETER LIST ******************************************************
C*    F -- USER-SUPPLIED SYSTEM                                         *
C*    ALPHA -- INITIAL VALUES OF INDEPENDENT VARIALBE                   *
C*             EXIT POINT SINGLE-STEP ERROR                             *
C*    OMEGA -- TERMINAL (EXIT) VALUE OF INDEPENDENT VARIABLE            *
C*    H -- INITIAL (EXIT) VALUE OF STEP SIZE                            *
C*   IPR -- PRINTING INDEX(EVERY IPR-TH STEP PRINTED)                   *
C* ERROR ANALYSIS PARAMETERS                                            *
C*    HMIN -- MINIMUM STEP SIZE                                         *
C*    HMAX -- MAXIMUM STEP SIZE                                         *
C*    EMIN -- MINIMUM SINGLE-STEP ERROR                                 *
C*    EMAX -- MAXIMUM SINGLE-STEP ERROR                                 *
C*   SET HMIN = HMAX FOR NO ERROR ANALYSIS                              *
C*   SET EMIN = 0. FOR NO DOUBLING OF STEP SIZE                         *
C*   SET EMAX = A LARGE VALUE  FOR NO HALVING OF STEP SIZE              *
C* PARAMETER LIST ******************************************************
      DIMENSION X(7), Y(7,10), YJ(10), D(7,10), DF(7,10), XS(7), W(4), B
     1(4,4), A(4), BP(4), BC(4), PHI(10), YS(7,10)
      DIMENSION DYAM(1000)
      COMMON/CSAVE/SAVE(2000)
      DOUBLE SAVE
      COMMON/XSAV/DEPT(1000)
      DOUBLE PRECISION Y, PHI, YS
      JJ=3
      II=1
      SAVE(1)=0.1
      SAVE(2)=0.2233
      IF (EMIN .GT. EMAX .OR. HMIN .GT. HMAX) 20,10
 10   IF (HMIN .EQ. HMAX) GO TO 30
      IF (HMIN .GT. H .OR. HMAX .LT. H) 20,30
 20   PRINT 520
      PRINT 540, HMIN, HMAX, EMIN, EMAX
      PRINT 550, ALPHA, OMEGA, H
      RETURN
C -------  COEFFICIENTS
 30   W(1) = W(4) = 1./6.
      W(2) = W(3) = 1./3.
      KK = 4
      A(2) = A(3) = .5
      A(4) = 1.
      B(2, 1) = B(3, 2) = .5
      B(3, 1) = B(4, 1) = B(4, 2) = 0.
      B(4, 3) = 1.
      IQ = 4
      FCT = 19./270.
      BP(1) = -9./24.
      BP(2) = 37./24.
      BP(3) = -59./24.
      BP(4) = 55./24.
      BC(1) = 1./24.
      BC(2) = -5./24.
      BC(3) = 19./24.
      BC(4) = 9./24.
C ------- RKAM ENTRY POINT
      CALL F (ALPHA,YJ,1,DF,N,DYAM(II))
      IF (IPR) 40,70,40
 40   PRINT 530
      IF (HMIN .EQ. HMAX) 60,50
 50   PRINT 540, HMIN, HMAX, EMIN, EMAX
 60   PRINT 550, ALPHA, OMEGA, H
      PRINT 560, (YJ(I), I = 1, N)
 70   ITC = 1
      IQM1 = IQ-1
      IQP1 = IQ+1
      IQP = 2*IQ-1
      ISTP = 0
      SIGN = 1.
      IF (H .LT. 0.) SIGN = -1.
      X(1) = ALPHA
      DEPT(1)  =ALPHA
      DO 80 I = 1, N
 80   Y(1, I) = YJ(I)
 90   MM = 1
      IFLG = 0
 100  KCOUNT = 0
 110  M = MM
      MM = M+1
      II=II+1
      IF (MM .GT. IQP) MM = 1
      X(MM) = X(M)+H
      DEPT(II) =X(MM)
      IF (ABS(OMEGA-X(MM)) .LE. SIGN*H) 120,150
 120  IF (ABS(OMEGA-X(MM)) .EQ. SIGN*H) 140,130
 130  H = OMEGA-X(M)
      IFLG = 0
      X(MM) = X(M)+H
      DEPT(II)=X(MM)
 140  ISTP = 1
 150  XJ = X(M)
      DO 160 I = 1, N
 160  YJ(I) = Y(M, I)
      IF (IFLG .NE. 0) GO TO 270
C -------  RUNGE-KUTTA PROCEDURE

      DO 220 K = 1, KK
      IF (K .EQ. 1) GO TO 200
      XJ = X(M)+H*A(K)
      DO 170 I = 1, N
 170  PHI(I) = 0.0D0
      KM1 = K-1
      DO 190 I = 1, N
      DO 180 J = 1, KM1
 180  PHI(I) = PHI(I)+H*B(K, J)*D(J, I)
 190  YJ(I) = Y(M, I)+PHI(I)
  200 CALL F(XJ,YJ,K,D,N,DYAM(II))
      IF (K .NE. 1) GO TO 220
      DO 210 I = 1, N
 210  DF(M, I) = D(1, I)
 220  CONTINUE
      DO 230 I = 1, N
 230  PHI(I) = 0.0D0
      DO 250 I = 1, N
      DO 240 K = 1, KK
 240  PHI(I) = PHI(I)+H*W(K)*D(K, I)
      Y(MM,I)=Y(M,I)+PHI(I)
      SAVE(JJ)=Y(MM,I)
      JJ=JJ+1
  250 CONTINUE
      IF (MM .EQ. IQ) IFLG = 2
      IF (ITC-ITC/IPR*IPR .NE. 0) GO TO 260
      PRINT 570, X(MM), H
      PRINT 580, (Y(MM, I), I = 1, N)
 260  ITC = ITC+1
      IF (ISTP .EQ. 1) GO TO 510
      GO TO 110
C -------  ADAMS PREDICTOR-CORRECTOR PROCEDURE
  270 CALL F(XJ,YJ,M,DF,N,DYAM(II))
      DO 280 I = 1, N
 280  PHI(I) = 0.0D0
      DO 290 K = 1, IQ
      J = K+KCOUNT
      IF (J .GT. IQP) J = J-IQP
      DO 290 I = 1, N
 290  PHI(I) = PHI(I)+H*BP(K)*DF(J, I)
      DO 300 I = 1, N
 300  YJ(I) = Y(M, I)+PHI(I)
      XJ = X(MM)
      CALL F(XJ,YJ,MM,DF,N,DYAM(II))
      DO 310 I = 1, N
 310  PHI(I) = 0.0D0
      DO 320 K = 1, IQ
      J = K+KCOUNT+1
      IF (J .GT. IQP) J = J-IQP
      DO 320 I = 1, N
 320  PHI(I) = PHI(I)+H*BC(K)*DF(J, I)
      DO 330 I = 1, N
      Y(MM,I)=Y(M,I)+PHI(I)
      SAVE(JJ)=Y(MM,I)
      JJ=JJ+1
  330 CONTINUE
```

```
C ------ SINGLE-STEP ERROR
      IF (HMIN .EQ. HMAX) GO TO 500
      DLTMX = 0.
      DO 340 I = 1, N
      YMM = Y(MM, I)
      DLT = ABS(YMM-YJ(I))
      IF (DLT .LE. DLTMX) GO TO 340
      DLTMX = DLT
      IDLT = I
 340  TEST = DLTMX/Y(MM, IDLT)
      IF QUOTIENT OVERFLOW 350,360
 350  SSE = ABS(FCT*DLTMX)
      GO TO 370
 360  SSE = ABS(FCT*TEST)
 370  IF (ITC-ITC/IPR*IPR .NE. 0) GO TO 380
      PRINT 590, X(MM), H, SSE
      PRINT 580, (Y(MM, I), I = 1, N)
 380  ITC = ITC+1
C -------  ERROR ANALYSIS
      IF (EMIN .LT. SSE .AND. SSE .LT. EMAX) GO TO 500
      IF (SSE .GT. EMAX) 390,420
 390  H = H/2.
      IF (SIGN*H .LT. HMIN) 490,400
 400  IF (IFLG .EQ. 2) GO TO 90
      M = M-1
      IF (M .EQ. 0) M = IQP
      X(1) = X(M)
      DO 410 I = 1, N
 410  Y(1, I) = Y(M, I)
      GO TO 90
 420  IF (ISTP .EQ. 1) GO TO 510
      H = 2.*H
      IF (SIGN*H .GT. HMAX) 490,430
 430  IF (IFLG .EQ. 2) GO TO 90
      L = 0
      DO 470 K = 1, IQ
      J = IQP1-K
      M = MM-L
      IF (M .LE. 0) 440,450
 440  M = M+IQP
      L = 0
      MM = M
 450  IF (X(M) .LT. ALPHA) GO TO 90
      XS(J) = X(M)
      DO 460 I = 1, N
      D(J, I) = DF(M, I)
 460  YS(J, I) = Y(M, I)
 470  L = L+2
      DO 480 K = 1, IQ
      X(K) = XS(K)
      DO 480 I = 1, N
      DF(K, I) = D(K, I)
 480  Y(K, I) = YS(K, I)
      MM = IQ
      IFLG = 1
      GO TO 100
 490  PRINT 600, H
      PRINT 540, HMIN, HMAX, EMIN, EMAX
      GO TO 510
 500  IF (ISTP .EQ. 1) GO TO 510
      IFLG = 1
      KCOUNT = KCOUNT+1
      IF (KCOUNT .EQ. IOP) KCOUNT = 0
      GO TO 110
C -------  RKAMSUB EXIT POINT
 510  OMEGA = XJ
      IF (HMIN .NE. HMAX) ALPHA = SSE
      RETURN
C
 520  FORMAT ( *0     RKAM  --   INITIAL PARAMETERS INCORRECT*)
 530  FORMAT (*0          --  RKAM  --*)
 540  FORMAT (*0   HMIN=*E15.8,2X,*HMAX=*E15.8,2X,*EMIN=*E15.8,2X,*EMAX=
     1*E15.8)
 550  FORMAT (*    ALPHA=*E15.8,2X,*OMEGA=*E15.8,2X,*H=*E15.8)
 560  FORMAT (*    YJ ARRAY * /(2X,7(2X,E15.8)))
 570  FORMAT (*0   X = *E15.8,5X,*H = *E15.8)
 580  FORMAT (*    YJ ARRAY * /(2X,7(2X,D15.8)))
 590  FORMAT (*0   X = *E15.8,5X,*H = *E15.8,5X,*SSE = *E15.8)
 600  FORMAT (*0     RKAM  --  STEP SIZE OUT OF BOUNDS  -- H=*E15.8)
      END
 SUBROUTINE F(X,YJ,M,DF,N,DYAM)

 COMMON G, Q, HO, PI, S, Z, C
 DIMENSION DF(7,10),YJ(10)
 N=2
 DF(M,1)=(2.*C)-(G*HO*G*((PI*(DYAM)**3)*(1.E-9)/6.)/(PI*(YJ(2)**2)*
1YJ(1)*(HO+Z-X)*((YJ(2)/(1.+S**2))+VELB(DYAM))))
 DF(M,2)=(2.*G*HO*Q*((PI*(DYAM)**3)*(1.E-9)/6.)/(PI*YJ(2)*(YJ(1)**2
1)*(HO+Z-X)*((YJ(2)/(1.+S**2))+VELB(DYAM))))-(2.*C*YJ(2)/YJ(1))
 RETURN
 END
```

```
      FUNCTION VELB(DYAM)

      IF(DYAM.GE. 0.72 .AND. DYAM .LE. 5.)GO TO 10
      VELB =24.4*DYAM*0.01
      RETURN
   10 VELB=(17.6+((DYAM-0.72)*1000.)/(30.+156.*(DYAM-0.72)))*0.01
      RETURN
      END
```

*U.S. GOVERNMENT PRINTING OFFICE: 1974 546-314/208 1-3